UNIVERSITY OF CALIFORNIA,
IRVINE

# Trace Gas Emissions from California Landfills and Dairies: The Impact on Disadvantaged Communities and the Environment

DISSERTATION

submitted in partial satisfaction of the requirements
for the degree of

DOCTOR OF PHILOSOPHY

in Chemistry

by

Brenna Crawford Biggs

Dissertation Committee:
Professor Donald R. Blake, Chair
Professor Barbara J. Finlayson-Pitts
Professor James N. Smith

2021

# DEDICATION

To my family and friends,

old and new

for constantly supporting me

on this adventure called “life”

and

for inspiring me to be more

than I thought possible.

# TABLE OF CONTENTS

# LIST OF FIGURES

# LIST OF TABLES

# LIST OF ABBREVIATIONS

| | |
|---|---|
| AB | Assembly Bill |
| ADC | Alternative Daily Cover |
| AGAGE | Advanced Global Atmospheric Gases Experiment |
| AMMP | Alternative Manure Management Program |
| AR | Assessment Report |
| CalEPA | California Environmental Protection Agency |
| Cal Poly SLO | California Polytechnic State University, San Luis Obispo |
| CARB | California Air Resources Board |
| CDFA | California Department of Food and Agriculture |
| CFC | Chlorofluorocarbon |
| DDRDP | Dairy Digester Research and Development Program |
| ECD | Electron Capture Detector |
| EF | Emission Factor |
| EPA | Environmental Protection Agency |
| FID | Flame Ionization Detector |
| GC | Gas Chromatograph |
| GHG | Greenhouse Gas |
| GHGRP | Greenhouse Gas Reporting Program |
| GWP | Global Warming Potential |
| HFC | Hydrofluorocarbon |
| HYSPLIT | Hybrid Single-Particle Lagrangian Integrated Trajectory |
| IPCC | International Panel on Climate Change |
| LFG | Landfill Gas |
| LULUCF | Land-Use Change and Forestry |
| MCF | Methane Conversion Factor |
| MDP | Management and Design Practices Factor |
| MIR | Maximum Incremental Reactivity |
| MS | Mass Spectrometer |
| MSW | Municipal Solid Waste |
| NAAQS | National Ambient Air Quality Standards |
| NASA | The National Aeronautics and Space Administration |
| NMHC | Non-Methane Hydrocarbon |
| NOAA | The National Oceanic and Atmospheric Administration |
| OEHHA | Office of Environmental Health Hazard Assessment |
| OFP | Ozone Formation Potential |
| PBL | Planetary Boundary Layer |
| PDT | Pacific Daylight Time |
| PFC | Perfluorocarbon |
| PGM | Processed Green Material |

| | |
|---|---|
| PM | Particulate Matter |
| POCP | Photochemical Ozone Creation Potential |
| RCNG | Renewable Compressed Natural Gas |
| RCP | Representative Concentration Pathway |
| SARP | Student Airborne Research Program |
| SB | Senate Bill |
| SJV | San Joaquin Valley |
| SOA | Secondary Organic Aerosol |
| TCD | Thermal Conductivity Detector |
| VOC | Volatile Organic Compound |
| VS | Volatile Solid |
| WAS | Whole Air Sampling |

# ACKNOWLEDGEMENTS

I would like to sincerely thank my committee chair, Professor Donald Blake, for demonstrating the power of storytelling, humility, and curiosity. Thank you for believing in me over the years. Traveling the world with you to do impactful airborne science has been the highlight of my graduate career. I have enjoyed every moment in your group.

I would like to thank my committee members, Professor Barbara Finlayson-Pitts, for her incredible wisdom and for creating space for women in this field, and Professor Jim Smith, whose class inspired me and who brought joy to my daily commute when we often passed in the hallway.

To the past and present Rowland-Blake group members, Simone, Gloria, Brent, Barbara B., Barb C., Alex, Nicola, and Isobel, it has been a pleasure working, flying, and prepping snakes with you. The weird hours, heavy lifting, and blurry-eyed modifying were worth it because of your positivity, humor, and collaborative spirit. You have taught me that science is a team sport. Thank you for your dedication and your behind-the-scenes efforts to make the lab run smoothly.

A big thank you to Rock City Climbing Gym, my home away from home, for bringing a sense of community to my life. You gave me confidence and taught me that falling is normal; it is your attitude when you land—and whether you choose to try again—that makes all the difference. I have so much love for the owner and all the friends I have made there.

I would also like to thank my family. Mom, you inspired me to completely change career paths from Communications to Chemistry—simply with the power of your words. You are a force of a woman and I am so in awe of you. Thank you for your phone calls, your support, and your love—now and always. Bradley, my little buppo, come get your Ph.D. with me so we can pass each other in the halls! Thank you for your silliness, for loving fiercely, and for speaking honestly. And to Cassandra, I could not be happier with my future sister! You are a light in a dark world.

To Dad: thank you for showing me the wonder of flying and the purity of science. You have shaped the way I view the world. To my grandparents: thank you for the countless celebrations and for giving me a sense of identity. Thank you for sharing your humor, stories, and petits fours.

A huge thank you to the Gallardo family: Mirza, Ruben, Marco, and Melissa. Thank you for supporting me as I navigated graduate school. I am especially grateful for the dinners, board game nights, and hilly runs we have shared.

I would like to acknowledge the UCOP Lab Fees Project, the NASA Student Airborne Research Program, the UCI Carbon Neutrality Initiative Applied Research Working Group, the Newkirk Center for Science and Society, The Loh Down on Science, and the Ridge to Reef NSF Research Traineeship, award DGE-1735040 for their financial support and training.

Finally, I want to thank my best friend, Ceasar Gallardo. You are my person, and there will never be enough space on a page to describe how incredible you are. Starting a relationship with someone who is starting their Ph.D. is crazy, but we have blossomed into the most amazing team over the last five years. From our movie nights, late fast-food runs, and video games to roller skating, traveling, and rock climbing, I cherish every second I spend with you. Thank you.

# VITA

**Education**

**University of California, Irvine** — **2016 – Present**
Doctor of Philosophy in Chemistry — March 2021
Master of Science in Chemistry — June 2020

**California State University, Fullerton** — **2010 – 2015**
Bachelor of Science in Chemistry — May 2015

**Awards**

Dynamic Womxn of the Year Award — June 2020
1st Place, UCI Elevator Pitch Competition — April 2020
2nd Place, UCI "Grad Slam" Finals — February 2020
NASA Group Achievement Award — June 2019
Science in Action Ambassador Award — June 2019
Michael E. Gebel Award for Environmental Excellence and Community Service — May 2019
Special Commendation, UC Center Sacramento STEM Solutions in Public Policy — February 2019
CSUF Outstanding Senior Honors Project — May 2015
2nd Place, CSU Statewide Research Competition — May 2015
American Chemical Society Outstanding Achievement Award — April 2015
Special Recognition for Mathematics Research — April 2015
Mathematical Association of America Achievement Award — March 2015
Îndrumator al Elevilor Rezolvitori la Gazeta Matematica — March 2015
1st Place, CSUF Student Research Competition — February 2015
Achievement in Analytical Chemistry Award — April 2014

**Certificates**

Unconscious Bias and Identity — November 2020
Research Justice & Community-based Research, Newkirk Center for Science and Society — September 2020
Modern World Ethics, UCI Graduate Resource Center — June 2019
Public Speaking by Activate to Captivate — May 2019
Mentoring Excellence, UCI Graduate Resource Center — May 2019

**Research Experience**

**Graduate Researcher, Rowland-Blake Group** — **2017 – Present**
**Department of Chemistry, UC Irvine**

- Measure greenhouse gases and pollution at California dairy farms and landfills to help meet reduction goals
- Evaluate how pollution could affect communities of disadvantage in California
- Train other students how to use a variety of gas chromatography equipment
- Fly and collect air samples on various NASA airborne missions: ATom, SARP, OWLETS, and FIREX-AQ
- Created and presented results as 2 posters and 13 talks to diverse audiences

**Community-Based Research Initiative Fellow** — **2019 – 2020**
**The Newkirk Center for Science and Society**

- Facilitated collaborative meetings between a community organization and academic partners using Team Science techniques
- Completed 4 grant reports for a community air monitoring project for the California Air Resources Board
- Educated residents on air quality, advocacy, and environmental justice
- Hosted a bilingual workshop online to empower residents to advocate for cleaner air

**Bonnie Reiss Carbon Offsets Fellow** **2019 – 2020**
**Carbon Neutrality Initiative, UC Irvine**
- Communicated importance of carbon offsets to faculty, students, and staff
- Recommended next steps for UC Irvine by writing executive summaries
- Delivered 3 presentations about carbon offsets in classroom and administrative settings both in-person and online

**Undergraduate Researcher, Haan Group** **2013 – 2015**
**Department of Chemistry, CSU Fullerton**
- Developed a solar-powered device to convert carbon dioxide to fuel
- Optimized formate quantification methods using UV-Vis spectrometry
- Presented research to policymakers and staffers on Capitol Hill (2016)
- Created and presented results in 5 posters and 7 talks at local and regional conferences

**Undergraduate Researcher, Grudpan Group** **2014**
**Chiang Mai University, Thailand**
- Developed a method to quantify protein using an Apple iPhone digital camera
- Contributed chemistry experience to a multicultural group of graduate students
- Communicated results as talks at 2 local conferences

**Science Communication**

***The Loh Down on Science* Radio Show** **2019 – Present**
**Writer and Managing Editor**
- Edit 8 science radio scripts monthly for clarity, scientific content, and fun
- Wrote and edited 12 radio scripts summarizing current scientific research for the general audience, which reached 4 million listeners nationwide
- Manage and upload scripts and writer bios to WordPress website monthly
- Increased accessibility to include translated scripts into Spanish and alt text for listeners with vison impairment

***Special Pandemic Edition* Reporter** **2020**
- Wrote and recorded 14 scripts about the science and history behind past and current pandemics
- Released episodes on various platforms including Spotify, PRX, Apple Podcasts, Blubrry, and Stitcher
- Shared the science of pandemics as a panelist on *Pandemonium U* to an international audience of 80 attendees

**Brews and Brains** **2019 – 2021**
**Outreach Coordinator**
- Coached 33 graduate students and post-docs to present their research to a general audience in-person and via Zoom
- Recorded, edited, and uploaded student talks to online platforms

**The National Aeronautics and Space Administration** **2019**
**Science Mentor, Student Airborne Research Program**
- Mentored 7 undergraduates to collect air samples aboard the NASA DC-8
- Taught students to analyze air samples in the lab using gas chromatography
- Facilitated workshops, discussion, and scientific project execution daily
- Coached 28 undergraduate students to communicate effectively as scientists

**Mathematics Teacher and Facilitator** **2015**
**CSUF "Fullerton Math Circle"**
- Prepared middle school students for national mathematical competitions
- Empowered students to solve problems from the Romanian mathematical publication *Gazeta Matematica*

**Publications**

Wofsy, S. C., Afshar, S., Allen, H. M., Apel, E., Asher, E. C., Barletta, B., Bent, J., Bian, H., Biggs, B.C. ... & Wennberg, P. (2018). ATom: Merged atmospheric chemistry, trace gases, and aerosols, ORNL DAAC, Oak Ridge, Tennessee, USA.

Saric, S. R., Haan, J. L., Biggs, B., Janbahan, M., Mayoral, S., & Nguyen, C. (2016). Formate: An Energy Storage Alternative. Poster presented by S. Saric at SoCal Conference for Undergraduate Research. Fullerton, CA.

Saric, S., Biggs, B., Janbahan, M., Hamilton, R., Do, H. K., Mayoral, S., & Haan, J. L. (2016). An integrated device to convert carbon dioxide to energy. *Applied energy, 183,* 1346-1350.

Vo, T., Purohit, K., Nguyen, C., Biggs, B., Mayoral, S., & Haan, J. L. (2015). Formate: an energy storage and transport bridge between carbon dioxide and a formate fuel cell in a single device. *ChemSusChem, 8*(22), 3853-3858.

**Languages**

English
French

# ABSTRACT OF THE DISSERTATION

Trace Gas Emissions from California Landfills and Dairies:
The Impact on Disadvantaged Communities and the Environment

by

Brenna Biggs

Doctor of Philosophy in Chemistry

University of California, Irvine, 2021

Professor Donald Blake, Chair

Many California regulations try to decelerate climate change by mitigating emissions from various industries. Greenhouse gases (GHGs) such as methane, carbon dioxide, and nitrous oxide must be fully understood to meet these strict reduction goals. Landfills release GHGs during decomposition and active dumping, while dairy farms release GHGs enterically (i.e., from cows) and from manure management. This study aims to better understand these GHGs at active and closed Orange County landfills as well as at a Visalia dairy farm in California. All samples were collected using whole air sampling techniques and analyzed using gas chromatography to identify and quantify many trace gases. Select oxygenates (i.e., methanol, ethanol, and acetaldehyde), dimethyl sulfide, and carbonyl sulfide were also a focus at these locations. Unexpected and novel sources of these gases were revealed, which have possible implications for pollution and the global sulfur budget.

Samples were collected at the landfills seasonally during four campaigns: Spring 2018, Summer 2018, Fall 2018, and Winter 2019 and at the dairy farm during five campaigns: September 2018, March 2019, June 2019, September 2019, and January 2020. Samples from both industries were compared to airborne and remote air samples to determine their

enhancements relative to background concentrations. This research establishes previously unexplored or misrepresented sources of various gases, which is important for the success of the state's reduction efforts, the environment, and the health of surrounding communities.

California's San Joaquin Valley, an extremely productive agricultural area, also contains many disadvantaged communities. Residents typically experience low socioeconomic status and a disproportionate amount of air pollution, which can lead to health problems. In addition to GHGs, this study also explores how direct emissions from dairy farms may affect these communities living downwind throughout the San Joaquin Valley. Orange County is more affluent but is often a nonattainment area for several pollutants including ozone and particulate matter, which affect the people living there. This study explores the contribution of trace gases from dairy farms and landfills in California to the formation of pollution and odor in these surrounding communities. Solutions for decreasing trace gas emissions from these sources are also proposed.

# 1. INTRODUCTION

## 1.1 Air Quality of the United States and Relevant Federal Legislation

Concern regarding the effects of air pollution in the United States has increased as population steadily rises over time. As the United States develops, contributing sources of air pollution have become more prevalent: industrial factories and manufacturing, vehicular emissions, waste management, agriculture and farming, and fires. These sources are often more prominent in areas of higher population. They emit gases and particulate matter (PM) into the atmosphere and surrounding areas, which can potentially affect the health of humans and the natural environment: trees, animals, plants, crops, and bodies of water. Numerous important federal and statewide laws have been passed as a direct result of the country's growth and subsequent air quality concerns. Select laws relevant to this work are presented in detail below.

### 1.1.1 Montreal and Kyoto Protocols

The United States is not alone in its growth. As countries around the world develop simultaneously, increased air pollution poses three major global issues: stratospheric ozone depletion and tropospheric ozone generation, climate change, and health concerns. Sherwood Rowland and Mario Molina first recognized chlorofluorocarbons (CFCs) as a potential cause of this ozone depletion in the mid-1970s (Molina & Rowland, 1974). They showed that chlorofluoromethanes, $CF_2Cl_2$ and $CFCl_3$, first break down in the atmosphere at high altitude (20 – 40 km) as shown in Reactions 1-1 and 1-2.

$$CF_2Cl_2 \rightarrow CF_2Cl\bullet + Cl\bullet \qquad \text{Reaction 1-1}$$

$$CFCl_3 \rightarrow CFCl_2\bullet + Cl\bullet \qquad \text{Reaction 1-2}$$

These reactions free up chlorine atoms to deplete stratospheric ozone, shown in Reactions 1-3 and 1-4. Reaction 1-4 also regenerates the chlorine radical, which can go on to react with ozone again and again.

$$Cl\bullet + O_3 \rightarrow ClO\bullet + O_2 \qquad \text{Reaction 1-3}$$

$ClO\bullet + O \rightarrow Cl\bullet + O_2$ Reaction 1-4

The discovery of the Antarctic ozone hole confirmed Molina and Rowland's suspicions a decade later (Farman et al., 1985). Subsequently, regulations were put in place to decrease the use of ozone-depleting substances, particularly CFCs and other, similarly behaving, halogen-containing species.

The Montreal Protocol, introduced in 1987, is perhaps the most important of these regulations. It required that the production and use of ozone-depleting substances be phased out by the year 2000 (Velders et al., 2007). The Protocol itself was amended six times, typically to encourage future mitigation efforts. The Montreal Protocol has been widely regarded as a success, as CFC emissions have declined as a direct result. Tropospheric ozone generation is discussed in greater detail in Chapter 1.1.2.

As mentioned previously, large-scale globalization poses another major threat: climate change. Climate change is exacerbated by the greenhouse effect. Many molecules, known as greenhouse gases (GHGs), do not absorb the sun's incoming radiation. Instead, they absorb and redirect Earth's *outgoing* infrared radiation (Finlayson-Pitts & Pitts, 1999). This keeps heat close to the planet, like a natural insulator, helping its inhabitants enjoy comfortable living temperatures. But, when extra GHGs are emitted, they heat up the earth and can cause the climate to change. Some of the most common GHGs include carbon dioxide ($CO_2$), ozone ($O_3$), methane ($CH_4$), water ($H_2O$), and nitrous oxide ($N_2O$) (Finlayson-Pitts & Pitts, 1999).

The Kyoto Protocol, introduced in the late 1990s, aimed to decrease GHG emissions, particularly in developed nations. The Kyoto Protocol recognizes 1) that global warming is occurring, and 2) that anthropogenic carbon emissions are likely predominantly responsible. It targeted the following gases and compound categories: $CO_2$, $CH_4$, $N_2O$, sulfur hexafluoride ($SF_6$), hydrofluorocarbons (HFCs) and perfluorocarbons (PFCs). The first Kyoto Protocol commitment period lasted from 2008 until 2012, when the Doha Amendment was introduced with additional

commitment targets. The 36 countries that completed the first commitment period saw success. However, GHG emissions still increased *globally* during that time, so the Kyoto Protocol's overall success has been questioned. It may be used as a segue to stricter future requirements (UNEP 2012, 2012).

### 1.1.2 Clean Air Act and the National Ambient Air Quality Standards

The concerns surrounding air pollution do not end with stratospheric ozone concentrations and climate change. Industrialization and increased emissions can lead to long-term exposure to air pollution, which can impact human health. Health effects can be chronic or acute. They include respiratory issues like lung irritation or disease, asthma, bronchitis, and cancer, as well as cardiovascular issues like heart disease. Exposure to air pollution has also been linked to reduced life expectancy and mortality (Kampa & Castanas, 2008). To combat these possible negative health impacts, the United States Environmental Protection Agency (EPA) has compiled a list of "criteria pollutants" that are monitored nationwide. These are compounds that are dangerous to humans and the environment.

This idea for a list of "criteria pollutants" began with the Clean Air Act, a federal law passed in the United States in 1963 and amended over the decades. Originally, the law was designed to better research, monitor, and control air pollution (Clean Air Act of 1963, 1963). One of the more recent amendments, in 1990, required the EPA to develop and implement standards for measuring and monitoring "criteria pollutants" nationwide. These standards, known as the National Ambient Air Quality Standards (NAAQS), are periodically revised according to current scientific recommendations and discoveries. The NAAQS were last updated in 2015 (NAAQS, 2015).

The NAAQS address the following six "criteria pollutants": carbon monoxide (CO), lead (Pb), ozone ($O_3$), nitrogen dioxide ($NO_2$), PM, and sulfur dioxide ($SO_2$). They have a Primary and Secondary standard level. Primary standards aim to protect human health, particularly the health

of vulnerable populations like children and the elderly. Secondary standards protect public welfare by improving visibility and decreasing damage to animals, crops, plants, and buildings (NAAQS, 2015). The NAAQS at their Primary and Secondary levels, as well as their time averages, are summarized in Table 1.1.

**Table 1.1** U.S. EPA National Ambient Air Quality Standards (NAAQS, 2015)

| Pollutant | | Primary/Secondary | Averaging Time | Level | Form |
|---|---|---|---|---|---|
| CO | | Primary | 8 hours | 9 ppm | ≤ once/year |
| | | | 1 hour | 35 ppm | |
| Pb | | Both | Rolling 3-month average | 0.15 $\mu g/m^3$ | Maximum |
| $NO_2$ | | Primary | 1 hour | 100 ppb | $98^{th}$ percentile of 1-hour daily maximum concentrations, averaged over 3 years |
| | | Primary and Secondary | 1 year | 53 ppb | Annual mean |
| PM | $PM_{2.5}$ | Primary | 1 year | 12.0 $\mu g/m^3$ | Annual mean, averaged over 3 years |
| | | Secondary | 1 year | 15.0 $\mu g/m^3$ | Annual mean, averaged over 3 years |
| | | Primary and Secondary | 24 hours | 35 $\mu g/m^3$ | $98^{th}$ percentile, averaged over 3 years |
| | $PM_{10}$ | Primary and Secondary | 24 hours | 150 $\mu g/m^3$ | Not to be exceeded more than once per year on average over 3 years |
| $SO_2$ | | Primary | 1 hour | 75 ppb | 99th percentile of 1-hour daily maximum concentrations, averaged over 3 years |
| | | Secondary | 3 hours | 500 ppb | Not to be exceeded more than once per year |
| $O_3$ | | Primary and Secondary | 8 hours | 0.070 ppm | Annual fourth-highest daily maximum 8-hour concentration, averaged over 3 years |

Although these standards are generally successful in keeping air pollution in check, they are not all-encompassing. Many other pollutants and trace gases, including potent GHGs, are not included on this list. However, reducing them is important to keep the air quality healthy and clean for the environment. These additional gases are addressed more specifically at the statewide level and are presented in detail below in Chapter 1.2.

## 1.2 California Air Quality and Relevant Statewide Legislation

Despite all the rules and regulations passed federally over the years, California still has some of the worst air quality in the nation because of its population and productivity. Pollution and GHG emissions from various industries and activities negatively impact people and the environment. Select laws at the state level attempt to mitigate these issues and are presented here. Statewide laws pertaining to waste management and dairy farms are of special relevance, as much of the research presented in this document focuses on the air pollution contribution from those industries.

### 1.2.1 Global Warming Solutions Act

California's leaders aim to reduce the amount of GHGs that the state emits. In 2006, California passed Assembly Bill (AB) 32, the Global Warming Solutions Act, leading the country in GHG reductions. The Global Warming Solutions Act was enacted in response to Governor Schwarzenegger's Executive Order S-3-05 from June 2005, which states that California must decrease its GHG emissions to 2000 levels by the year 2010, 1990 levels by 2020, and 80% below 1990 levels by 2050 (Global Warming Solutions Act of 2006, 2006).

The Global Warming Solutions Act developed a program to decrease GHGs statewide from all sources, known as the Cap-and-Trade Program, and gave the program's implementation authority to the California Air Resources Board (CARB) (Hanemann, 2007). CARB was designated as the state agency in charge of monitoring and regulating sources of GHGs (Global Warming Solutions Act of 2006, 2006). Gases targeted under the Global Warming Solutions Act

are the same as those targeted under the federal-level Kyoto Protocol: $CO_2$, $CH_4$, $N_2O$, $SF_6$, HFCs and PFCs (California Global Warming Solutions Act of 2006: emissions limit, 2016).

The Global Warming Solutions Act also set up the Greenhouse Gas Reduction Fund, which collects money from the State's Cap-and-Trade program to further California's climate-related goals. In 2016, Governor Jerry Brown signed Senate Bill (SB) 32, which expanded upon AB-32. Under SB-32, California is required to reduce its GHG emissions to 40% below 1990 levels by the year 2030 (California Global Warming Solutions Act of 2006: emissions limit, 2016). This is meant to keep the state on track to reach reductions of 80% below 1990 levels by 2050, as required by AB-32.

### 1.2.2 Disadvantaged Community Designation and Zoning Laws

To further direct the activities of the Cap-and-Trade program, California passed SB-535 in 2012. This requires that 25% of the proceeds from the Greenhouse Gas Reduction Fund go to projects that benefit "disadvantaged" communities (California Global Warming Solutions Act of 2006: Greenhouse Gas Reduction Fund, 2012). It was initially unclear how these communities should be designated, and what parameters should be included in the decision. California's Environmental Protection Agency (CalEPA) became responsible for identifying those communities. Although the term "disadvantaged" has been defined in many ways, it was important that this designation follow SB-535 guidelines, which means it must identify disadvantaged communities based on geographic, socioeconomic, public health, and environmental hazard parameters (OEHHA, 2017).

Recent interest in defining "disadvantaged" has led to the introduction of tools like the California Office of Environmental Health Hazard Assessment (OEHHA) CalEnviroScreen, which calculates a score (0 to 100%) for California communities using the categories defined by SB-535. CalEnviroScreen synthesizes twenty different parameters to determine the score for each census tract. Seven parameters represent Exposure: ozone concentrations, $PM_{2.5}$

concentrations, diesel PM concentrations, drinking water contaminants, pesticide use, toxic release from facilities, and traffic density. Five indicators represent Environmental Effects: cleanup sites, groundwater threats, hazardous waste generators and facilities, impaired water bodies, and solid waste sites and facilities. Three parameters represent the presence of Sensitive Populations: asthma rates, cardiovascular disease, and low birth weight of infants. Lastly, five parameters represent Socioeconomic Factors: educational attainment, housing burden, linguistic isolation, poverty, and unemployment.

Each of these indicators is assigned an individual score for each California census tract based on current and applicable data. Scores are weighted and added together to calculate a "Pollution Burden" score, which includes the parameters in the Exposure and Environmental Effects categories, and a "Population Characteristics" score, which includes the parameters from the Sensitive Populations and Socioeconomic Factors categories. The Pollution Burden and Population Characteristics scores are multiplied together to give a final CalEnviroScreen score between 0 and 100%. The higher the score, the worse the conditions, and the more disadvantaged the community.

The scores numerically highlight the disparity between different standards of living. Disadvantaged communities, which are regularly communities of color, often experience a higher environmental burden. The disproportionate exposure of these communities and low-income families to pollution is termed *environmental injustice*. Many of these communities are built near heavy-hitting emitters, such as waste disposal services, dairy farms, roads, and manufacturing facilities. This is partly due to the zoning laws laid out in the cities' General Plans.

This research deals primarily with emissions from landfills and dairy farms in California, both of which can affect disadvantaged communities built near—and unfortunately sometimes *in*—areas zoned for these industries. Cities' zoning maps indicate that the zones are also not always consistently, transparently, or accurately labelled. For example, the city of Irvine's zoning

map shows one of the largest landfills in Orange County, Frank R. Bowerman landfill, is built in a zone labelled “preservation.” Although this might be technically true, this label is misleading and does not accurately reflect activities occurring in that zone. Zoning areas containing “medium and high density residential” buildings were built less than half of a mile away from this landfill (City of Irvine, 2018). This issue persists statewide.

In California’s region known as the *Central Valley*, dairy farms are built in zones typically labelled “agriculture” (Tulare County Resource Management Agency, 2012). However, in many of its counties, like Tulare County, these zones allow for homes to be built within this “agriculture” zone, exposing residents to emissions from these industries with no buffer region (Tulare County Resource Management Agency, 1947). Overall, the General Plans are often a bit opaque. Therefore, it is important to better understand, monitor, and improve the air in these areas to empower and bring resilience to the communities living in them. This work attempts this by better understanding the emissions from point sources in these areas, particularly landfills and dairy farms. The following laws discussed in Chapters 1.2.3 and 1.2.4 are relevant to emissions at those industries.

### 1.2.3 Assembly Bill 1594 for California Landfills

Although landfills were first built in California in the 1930s, it was not until California’s Integrated Waste Management Act of 1989 that the state created stricter regulatory agencies, inspections, and permits to monitor water and air quality at landfills. Since then, over 300 landfill-related bills have also been passed.

At California landfills, waste must now be covered after each daily disposal to reduce emission, odor, dust, and trash pollution. Recent laws like AB-1594 have pushed landfill operators to continually update these management practices. AB-1594 specifically affects what goes on the surface of the landfills rather than what goes inside. Although soil is often used for daily cover, the environmental and monetary costs of collecting and hauling soil have led to 11 approved

alternative daily cover (ADC) materials including shredded tires, green material, and compost (A.B. 1594, 2014).

As part of AB-1594, which started in 2020, using green material as ADC now constitutes “disposal” instead of “diversion.” This means that green material is now included in the strict 50% per capita maximum disposal rate and should no longer be used as daily cover (A.B. 1594, 2014). To avoid fines, landfill operators chose to either 1) accept less solid waste or 2) determine another way to divert green material. Because using compost as ADC still constitutes “diversion” and not “disposal,” and does not count towards the maximum disposal rate, some California landfills started composting on-site to prepare for 2020. To appease AB-1594, green and organic components of municipal solid waste (MSW) could also be converted to compost and diverted as ADC (California Department of Resources Recycling and Recovery, 2015). This means the amount of compost at landfill sites has increased, and may continue to increase, over time.

### 1.2.4 Senate Bill 1383 Methane Targets at Landfills and Dairy Farms

The final law relevant to this work is Governor Brown’s SB-1383, passed in 2016. SB-1383 introduced specific targets for methane at landfills and dairy farms. It requires that methane emissions, regardless of source, be reduced to 40% below 2013 levels by 2030. It also required California landfills to reduce the disposal of organic waste to 50% of 2014 levels by 2020. This law provided more motivation for landfills to compost MSW and divert it as ADC so that it would not count towards their disposal limit. SB-1383 also established the Short-Lived Climate Pollutant Reduction Strategy (CARB, 2017), which created a path to decrease GHG emissions and decrease dependence on natural gas derived from fossil fuels. SB-1383 strategies specifically target not only landfill emissions, but dairy farms as well (S.B. 1383, 2016).

Per SB-1383, California will adopt regulations to reduce methane emissions from dairy farms starting on January 1, 2024. One proposed solution is to use the methane produced at dairy farms as a renewable form of natural gas for the transportation and energy sectors (S.B. 1383,

2016). State leaders plan to develop and encourage the installation of biomethane infrastructure to push dairy farmers to change their management styles before the mandatory methane restrictions of SB-1383 begin in 2024. This work discusses this in more detail in Chapter 8.5.2.

### 1.3 Geography and Exports of California's Central Valley

Nestled in the center of the state of California is the Central Valley, which is approximately 450 miles long and between 40 and 60 miles wide (American Museum of Natural History, 2019). Figure 1.1 shows a map of the Central Valley (Trump, 2004). The Central Valley's climate is created from a combination of oceanic and continental influences. California is in a zone of prevailing westerly winds and is located near a persistent high-pressure area of the Pacific Ocean. However, the Central Valley is in a thermal low-pressure area. Because of these conditions, air typically flows from the west or northwest regardless of season (Western Regional Climate Center, 2008).


**Figure 1.1** Map of the Central Valley. Sacramento Valley is in the North, San Joaquin Valley is in the South (Trump, 2004).

The Central Valley is located between the Pacific coastline and Sierra Nevada mountain range. Western areas closer to the coast are strongly influenced by the Pacific Ocean. Residents enjoy warm winters, cool summers, high relative humidity, and low seasonal variation (Western Regional Climate Center, 2008). Eastern areas closer to the Sierra Nevada range are more strongly influenced by the continent and have more extreme weather variations: warmer summers, cooler winters, lower relative humidity, and more seasonal variations (Western Regional Climate Center, 2008).

Because of the mountains, the area is prone to inversions. Inversions occur when the air temperature increases with altitude, rather than its typical decrease with altitude. During an

inversion, the warm air above the cool air prevents vertical mixing. This can lead to concentrated levels of pollution near the surface as the air is confined to a smaller mixing volume. The Central Valley's inversions tend to be stronger during the night and are worse in winter as nights get longer. This phenomenon is incredibly important to the Central Valley because of the vast number of emission sources (Berg, 2011). Many gases are emitted as a direct result of the Central Valley being an extremely productive agricultural area. Its main exports include nuts, cereal grains, citrus, grapes, and vegetables (USGS, n.d.). The most valued exports are almonds, pistachios, and dairy products, which grossed $4.5 billion, $1.7 billion, and $1.7 billion respectively in 2018 (CDFA, 2019a).

### 1.3.1 Counties and Dairies in the San Joaquin Valley

The Central Valley can be further divided into the northern Sacramento Valley and the southern San Joaquin Valley (SJV), as was shown in Figure 1.1. The Sacramento Valley contains all or some of ten different counties: Butte, Placer, Colusa, Glenn, Sacramento, Shasta, Sutter, Tehama, Yolo, Solano, and Yuba. The SJV contains some or all of eight different counties that are also, coincidentally, the state's top milk-producers as of 2015. In order from least to most productive, the counties are as follows: Madera, San Joaquin, Fresno, Kern, Kings, Stanislaus, Merced, and Tulare (CDFA, 2016a). Nearly 90% of California's dairy cows live in the San Joaquin Valley (CDFA, 2018).

According to the California Department of Food and Agriculture's Agricultural Reports, there are approximately 1.5 million milk cows in the San Joaquin Valley as of 2019 (CDFA, 2019b; CDFA, 2018). The breakdown of cows per SJV county is shown in Table 1.2. Tulare County contains more milk cows than any other county in California, with nearly half of a million cows in 2019. Tulare County also contains the most dairies in the region, with over 250 active dairy farms in 2017. However, dairies in Kern county have more cows per dairy than the other counties.

Dairies in Kern county contain an average of over three thousand cows, while some counties, like Stanislaus and San Joaquin, contain approximately only one thousand cows per dairy in 2017.

**Table 1.2** Milk cows and dairies by county in the San Joaquin Valley

| County | Milk Cow Total (2019) | Number of Dairies (2017) | Avg. Number of Cows per Dairy (2017) |
|---|---|---|---|
| Fresno | 99,000 | 70 | 1,600 |
| Kern | 115,000 | 48 | 3,300 |
| Kings | 170,000 | 107 | 1,700 |
| Madera | 66,000 | 37 | 2,200 |
| Merced | 270,000 | 206 | 1,300 |
| San Joaquin | 105,000 | 101 | 1,000 |
| Stanislaus | 185,000 | 185 | 1,000 |
| Tulare | 495,000 | 258 | 1,800 |
| **Total** | **1,505,000** | **1,012** | **Avg. 1,700** |

In total, the Central Valley produces over twenty percent of the nation's dairy and dairy products, with most of the products coming from the San Joaquin Valley (House Committee on Natural Resources, 2014). This productivity compounded by the terrain means that the San Joaquin Valley unfortunately has some of the worst air quality in California. As of August 2020, part (or all) of the eight San Joaquin Valley counties (Madera, San Joaquin, Fresno, Kern, Kings, Stanislaus, Merced, and Tulare) were nonattainment areas for multiple NAAQS criteria pollutants. All counties were nonattainment areas for $PM_{2.5}$ and 8-hour ozone concentrations, and parts of Kern County were nonattainment areas for $PM_{10}$. Counties south of the SJV, including Orange County, where much of this study also took place, was also a nonattainment area for $PM_{2.5}$ and 8-hour ozone (EPA, 2020a).

### 1.3.2 Dairy Farm Emissions, Management, and Logistics in California

The high concentration of cows in the Central Valley, particularly in the San Joaquin Valley, clearly has its drawbacks. Cows and associated livestock management methods produce high amounts of greenhouse gases such as $CH_4$ and $N_2O$ (California Environmental Protection Agency Air Resources Board, 2014). CARB has identified the agricultural sector, most of which is concentrated in the Central Valley, as a source of GHGs. In 2017, the sector accounted for

about 8% of the statewide GHG emissions. Within the agricultural sector, livestock is said to account for about 70% of these emissions, primarily as methane from enteric fermentation (nearly 11 million tons of $CO_2e$ per year) and manure management strategies (nearly 12 million tons of $CO_2e$ per year) (CARB, 2019). Dairy facilities specifically account for > 3% of California's GHG emissions according to CARB's GHG inventory in 2017. Additionally, over a decade ago, the San Joaquin Valley Air Pollution Control District identified dairy farms as a main source of the area's smog-causing volatile organic compounds (VOCs) and particulate matter (Goodrich et al., 2003; Crow, 2005).

GHGs at dairy farms are emitted directly from the animals, in the form of enteric fermentation, as well as from manure management. According to CARB's 2017 Methane Inventory, $CH_4$ emitted from enteric fermentation and manure management at dairy farms account for over 50% of the statewide methane emissions (CARB, 2019). There has been a 12% and 30% increase in enteric fermentation emissions and manure management, respectively, from 2000 to 2017 (CARB, 2019).

Emissions are dependent on the animal housing and manure management strategies that dairy farmers prefer. Factors such as herd size, temperature, and available space often inform these decisions. There are three types of common housing options for dairy cows: dry lots, free stalls, and tie-stalls. In dry lots, cows are separated into pens and are free to roam around. Cows share feed and water in long troughs. Although exposed to the elements, dry lots also typically feature shaded structures and bedding areas to increase comfortability.

Free stall dairies, on the contrary, provide more protection from high temperatures and heavy rainfall. Cows are free to move around, and food and water are brought to them regularly. Free stall barns allow for easier collection of manure, which can be used as a natural fertilizer for crops. Lastly, some dairies, typically with small herd sizes, use tie-stalls. In a tie-stall setup, cows each have their own pen where they are fed, watered, and milked (Undeniably Dairy, 2018). In

Tulare County, the highest milk-producing county in California, free stalls are commonly chosen for animal housing (Meyer et al., 2011). Most dairy farmers in the SJV use settling basins and lagoons as a general manure management practice. Manure is typically flushed or scraped from the feeding areas and is also often reused later for cow bedding (Meyer et al., 2011). These choices affect the emissions that come from the manure.

### 1.3.3 Disadvantaged Communities in the San Joaquin Valley

Greenhouse gases are not the only compounds that are enhanced in the SJV. Emissions from industry, traffic, waste management, agriculture, and livestock have led to very poor air quality, which disproportionately affects residents living in the area. As mentioned in Chapter 1.2.2, CalEPA introduced CalEnviroScreen, which assigns a score to census tracts in California based on parameters such as low income and educational attainment, high ozone and pollution levels, poor drinking water quality, pesticide use, hazardous waste, linguistic isolation, or poor cardiovascular and respiratory health. The score is used to designate areas as “disadvantaged,” and is often used as a proxy for environmental injustice. Areas with a low CalEnviroScreen score typically have high income, low air and water pollution, and relatively better health.

For example, Newport Coast, California, an affluent coastal neighborhood, has a low score between 1 – 5% and is therefore not labelled “disadvantaged.” Comparatively, many counties in the SJV are as high as 95% and are labelled “disadvantaged” (OEHHA, 2017). Figure 1.2 shows CalEnviroScreen scores for most census tracts within the states.

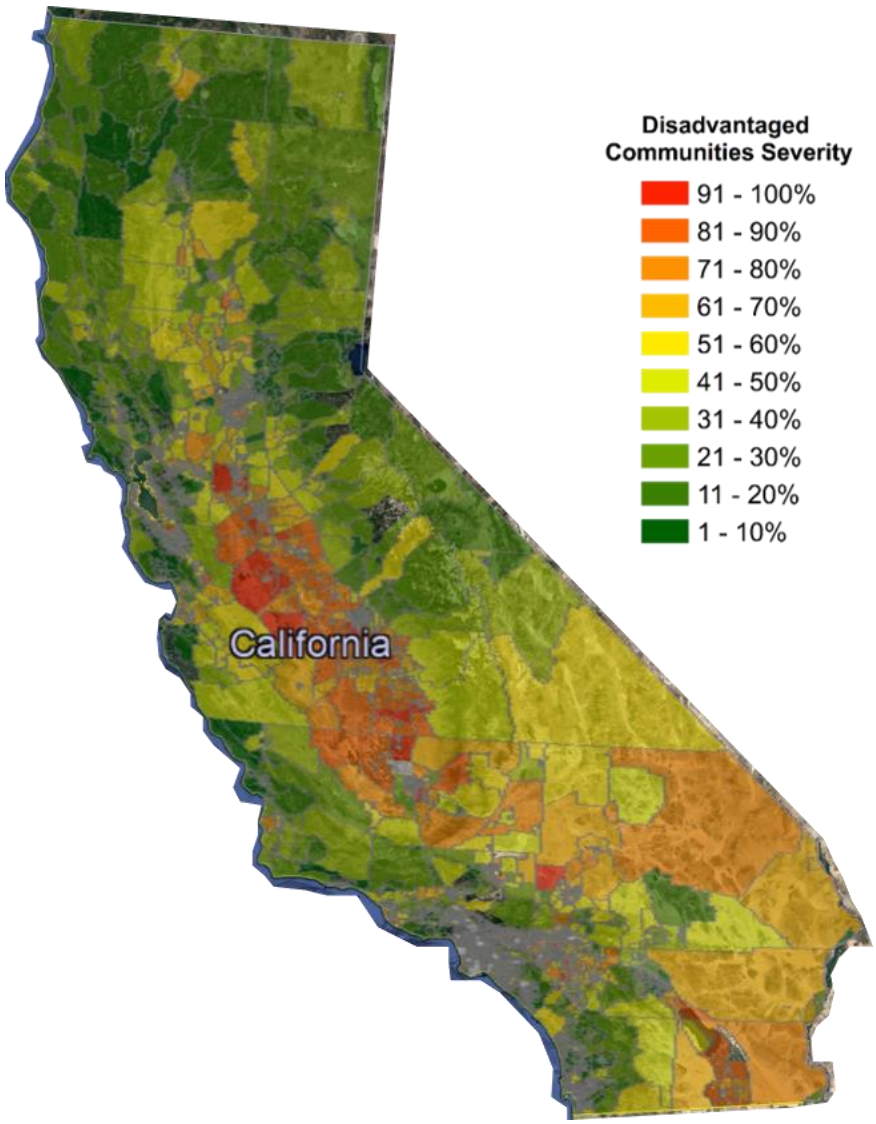


**Figure 1.2** Map of California showing CalEnviroScreen scores (OEHHA, 2017). The higher the score, the more the area is considered "disadvantaged" based on parameters surrounding health, water quality, air quality, and socioeconomics.

Census tracts within the SJV have predominantly high scores of at least 70%, showing that most of the counties in the SJV are designated as "disadvantaged." The high severity seen in the SJV is part of why this region was chosen as a study area for this research.

### 1.4 Landfill Infrastructure in Orange County, California

Californians dispose of 30 million tons of trash per year in landfills, specially engineered plots of land designed to collect waste while attempting to protect the environment (California

Department of Resources Recycling and Recovery, 2015). The research presented in this document primarily focuses on landfills in Orange County, California. Contrary to the outdated open dump, these landfills attempt to render the deposited waste inert by controlling landfill gas (LFG) emissions. However, even with these mitigation efforts in place, landfills are a constant target for GHG reduction efforts. An overview of the components found at Orange County landfills is shown in Figure 1.3 from Orange County Waste & Recycling (OCWR, 2020a).

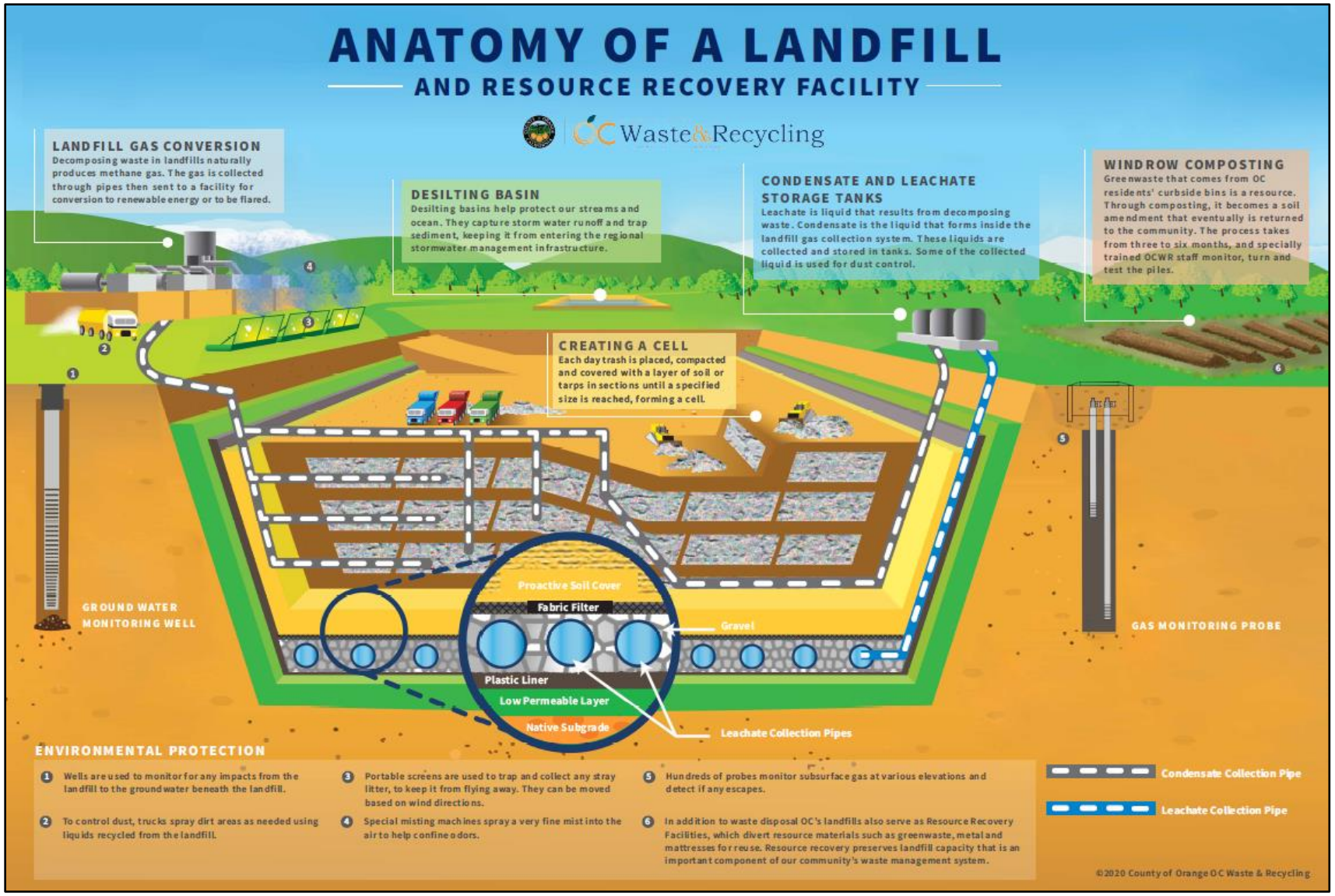


**Figure 1.3** Anatomy of a landfill in Orange County, California (OCWR, 2020a).

The base of modern landfills is lined with a combination of low permeability liners, plastic liners, fabric filters, and soil covers all to prevent contaminated liquid, or leachate, from seeping into the groundwater system from the decomposing waste. These liners also have collection pipes installed, which bring the leachate to above-ground collection tanks. The interior of the landfill also has additional pipes to bring the condensate, the contaminated liquid that condenses out of landfill gas, to the collection tanks as well. Some of this water is recycled and sprayed onto the landfill surface to control dust levels.

On top of the series of liners, waste is placed in cells. A cell continues to receive trash until it is full. Areas receiving trash must be covered daily. The gases produced in the landfill as waste decomposes underground are monitored. Pipes also collect this gas and either flare it or convert it to usable energy. Parts of the pump system are exposed on the surface of the landfill for easy monitoring. One such exposed pump is shown in Figure 1.4.

**Figure 1.4** Exposed landfill gas collection pump infrastructure at Prima Deshecha landfill. Photo taken by Brenna Biggs during April 2018.

The landfill also contains a desilting basin, which is responsible for trapping runoff water and silt from storms, protecting oceans and streams. A photo of this basin at an Orange County landfill is shown in Figure 1.5.

**Figure 1.5** Filled water runoff and desilting basin at Prima Deshecha landfill in Orange County. Photo by Brenna Biggs in April 2018.

Landfills in Orange County all typically engage in a composting program, where green waste and other MSW piles are turned, monitored, and tested for 3 to 6 months while they decompose. After this period, clean piles are sometimes returned to the community as good quality compost, but they are also often used as daily cover for the trash.

Lastly, Orange County landfills also have additional methods in place to lower trash and odor contamination for surrounding communities. Landfills spray a fine chemical mist into the air to try to prevent odor from escaping active dumping areas. They also use portable screens to prevent trash from being picked up and carried by the wind. Unfortunately, wind is not the only method through which trash can escape. Birds often flock to the landfill—likely for the free food. They can cause quite a problem for surrounding neighborhoods by dropping the gross remnants they have picked up on people, cars, and other belongings.

Therefore, Orange County landfills have been using a bird abatement program since 2013. Specially trained hawks and falcons patrol the skies, frightening off other birds that show up to

the landfill hoping for an easy meal. In the late 1990s, nearly 4,500 sea gulls were observed at an Orange County landfill in a single day. With the bird abatement program, however, that number has decreased to less than 50 gulls per day (OCWR, n.d.). A photograph showing a falconer with one of the landfills' trained raptors is shown in Figure 1.6.

**Figure 1.6** Falconer with a raptor specially trained for bird abatement at Orange County landfills. Photo taken at Frank R. Bowerman landfill in February 2018 by Brenna Biggs.

According to the falconer, this technique works incredibly well to scare away scavenging birds, such as seagulls and crows. Local birds have even started recognizing the falconer's special truck. They leave the landfill when he arrives, before the falcons even make their appearance.

California landfills are no longer just a “hole in the ground” where waste is piled with no purpose or regulations. They are specially engineered and heavily monitored plots of land designed to store waste effectively while also attempting to protect the surrounding environment and communities.

### 1.4.1 Landfill Gas Composition and Emission Pathways

Regardless of how many abatement and mitigation efforts landfills have in place, decomposing waste will create gas. This LFG is produced within a landfill during four stages of waste decomposition summarized in Table 1.3 (Lisk, 1991; Crawford & Smith, 2016; Farquhar & Rovers, 1973). First, emissions are produced during an aerobic stage, when aerobic bacteria consume oxygen and emit $CO_2$ as a main product. Then, during the anaerobic non-methanogenic stages, anaerobic bacteria convert products from the aerobic stage and emit $H_2$ and $CO_2$ as primary products. In the third step, anaerobic bacteria neutralize waste as methanogenic bacteria finally begin producing $CH_4$. Finally, during the last step, bacteria continue to emit gases for a long time, and the LFG composition remains constant.

**Table 1.3** Waste decomposition stages and descriptions (Lisk, 1991; Crawford & Smith, 2016; Farquhar & Rovers, 1973)

| Stage | Description |
|---|---|
| I. Aerobic | Aerobic bacteria consume oxygen and break down long-chained molecules, emitting $CO_2$ |
| II. Anaerobic Non-Methanogenic | Anaerobic bacteria convert Stage I products into an acrid mixture of acids and alcohols, emitting $H_2$ and $CO_2$ |
| III. Anaerobic Methanogenic Unsteady | Anaerobic bacteria neutralize the waste, while methanogenic bacteria begin thriving and produce $CH_4$ |
| IV. Anaerobic Methanogenic Steady | LFG composition (typically 45-70% $CH_4$, 30-60% $CO_2$, and 0-9% trace gases) and production rate are constant |

It is important to mention that the landfill cells are layered, so multiple stages can occur simultaneously. Stage IV may continue for up to 50 years (Crawford & Smith, 2016; Farquhar & Rovers, 1973). Landfill engineering has accelerated rapidly over the years since the first landfill

was built in 1937 in Fresno, California. Now, LFG is typically collected, filtered, and flared or used as energy (Lisk, 1991). LFG composition varies due to several factors: temperature, moisture, age, geology, and landfill management. However, LFG commonly consists of the same six classes of compounds: 1) saturated and unsaturated hydrocarbons, 2) acidic hydrocarbons and organic alcohols, 3) aromatic hydrocarbons, 4) halogenated compounds, 5) sulfur compounds, and 6) inorganic compounds (Brosseau & Heitz, 1994).

Trace gases at landfills significantly contribute to toxicity, odor, and secondary pollutants (Allen et al., 1997). They are released through two main pathways: 1) volatilization and 2) waste decomposition (Giess et al., 1999). Occasionally, gases are released from both pathways; these gases exhibit constant background levels from decomposition and elevated levels during volatilization (Young & Parker, 1983). This ambiguity of sources, combined with factors like temperature, humidity, location, and pH, make trace gas emissions at landfills rather heterogenous. Summarizing LFG trace gas trends is challenging due to the variability of LFG sitewide and regionally, which explains the large range of concentrations and trends reported in the literature (Brosseau & Heitz, 1994; Giess et al., 1999; Chiavarini et al., 1993).

According to the literature, LFG odor is primarily produced by esters, sulfur compounds, solvents, alkyl benzenes, and limonene (Giess et al., 1999). Persistent odors, while not a direct threat to human health, are an occupational nuisance and possibly overwhelming to nearby communities. Studies have shown that raw LFG under the landfill surface can require as much as a $10^6$ dilution to bring gases below the odor threshold (Young & Parker, 1983).

To reduce the amount of escaped LFG, modern landfills are typically lined and covered. The liner, along with the leachate and condensate holding tanks, prevent the spread of contaminated liquid into the groundwater (Lisk, 1991). In the 1980s, raw LFG was flared to reduce odor, but flaring untreated LFG can generate atmospheric contaminants and corrode the combustion system (Lisk, 1991; Brosseau & Heitz, 1994). Instead, modern California landfills use

daily cover material to trap odor and control emissions (Closure and Post-Closure Maintenance Requirements for Solid Waste Landfills, 1997). These cover materials are discussed further in the following Chapter 1.4.2.

### 1.4.2 Cover Materials at Modern California Landfills

At modern Orange County landfills, waste is piled on the liner and covered with daily, intermediate, or final cover materials to reduce the emissions of disposed and decomposing waste. In California, waste must be covered daily with at least 6 inches of compacted earthen material, usually soil, to prevent erosion and gas diffusion (Closure and Post-Closure Maintenance Requirements for Solid Waste Landfills, 1997). Methanotrophic oxidation by soil microbes is also a methane sink, which further prevents $CH_4$ from seeping out of the landfill (Spokas & Bogner, 2011). As mentioned in Chapter 1.2.3, there are also eleven ADC materials that California landfills could use in place of soil, which can be expensive and damaging to collect and haul. Inactive areas of the landfill receive at least 12 inches of intermediate cover, and closed parts of the landfill require final cover consisting of a 24-inch foundation layer, a 12-inch permeability layer, and a 12-inch erosion resistant layer. Completely closed landfills are monitored for an additional 30 years (Closure and Post-Closure Maintenance Requirements for Solid Waste Landfills, 1997).

Daily, intermediate, and final cover also help to reduce rogue emissions and thereby decrease LFG on the surface. This is highly beneficial and important, as LFG commonly contains irritants absorbed by various human organs. If repeated exposure and accumulation occur, these gases can cause cell mutation and eventually cancer (Brosseau & Heitz, 1994). The most notorious gases responsible for landfill-related health concerns are $H_2S$, vinyl chloride, xylene, benzene, and toluene (Giess et al., 1999; Brosseau & Heitz, 1994).

Much of the literature regarding landfills focuses on underground LFG that will be flared, transported, or is otherwise blocked by the cover material. Instead, this research mostly focuses

on gases that escape during active dumping or *through* the cover material. These emissions could directly impact occupational and residential communities, many of which work or live very close to the landfills.

### 1.4.3 Waste Disposal Trends in California

Waste disposal in California declined from 2005–2012 before a steady increase into the present. Although the annual amount of waste deposited has generally increased over time, the amount of methane released into the atmosphere has *declined* as a direct result of LFG collection and control systems prompted by CARB's Landfill Methane Control Measure, which requires monitoring and capturing fugitive emissions (CARB, 2019). Municipal solid waste landfills in the United States accounted for over 15% of human-related methane emissions in 2018 (EPA, 2020b). These emissions not only signify a large source of anthropogenic GHGs, but also a missed chance to capture and use a prevalent source of energy in much of the country.

All active Orange County landfills have implemented modern landfill gas-to-energy projects. This infrastructure converts LFG, which at its longest stages consists of mostly $CH_4$ and $CO_2$, to energy, powering thousands of surrounding homes and sometimes the landfills themselves. Although Orange County has been a quick adopter of landfill gas-to-energy projects, the rest of the state has been slower to follow. According to CARB, emissions from the recycling and waste sector account for over 2% of the state's GHG inventory in 2017. This is only 1% less than the emission contribution from dairy farms in California. Emissions from the recycling and waste sector have grown by 20% since the year 2000. Within this sector, which includes landfills and commercial-scale composting, landfill emissions account for 96% of the overall emissions (CARB, 2019).

## 1.5 Motivation and Goals for This Work

Many laws and mitigation efforts have been put in place to try to improve the air quality for California residents, workers, infrastructure, and environment. Most of the regulations, particularly

those that target landfills and dairy farms, rely on reducing GHG emissions. However, these laws do not, and cannot, target all the harmful emissions that these industries in California can emit. While GHGs such as $CH_4$, $CO_2$, and $N_2O$ do indeed pose a nontrivial threat to our environment, other gases are often not included in scientific studies. These gases, including oxygenates, sulfur-containing compounds, and non-methane volatile organic compounds, can still have a big impact.

For California to be able to achieve its ambitious reduction goals, as well as clean up the other pollutants, the state needs to accurately account for emission sources and amounts. This work primarily focuses on a broader range of emitted gases from dairy farms and landfills and explores how they might impact surrounding communities. This endeavor was entirely new for Orange County landfills, which have not been comprehensively studied. Although dairy farms have been studied in the past, this work gives special attention to the southern half of California's Central Valley, a resilient hub of agriculture, industry, farming, and traffic against a backdrop of poverty, air pollution, water pollution, and socioeconomic issues.

Sampling at dairy farms and at Orange County landfills was funded by the University of California Office of the President. Dairy farm campaigns were hosted by the University of California, Riverside, while sampling and analysis was completed entirely by the author in the Rowland-Blake lab at University of California, Irvine. Sampling for the landfill campaigns was conducted entirely by graduate students in the Rowland-Blake lab, including the author.

This work compares the data from dairy farms, which are slow to adopt new engineering techniques, to landfills in Orange County, which are touted as being highly engineered. Regional airborne data were also considered to explore the effects of landfills and dairy farms on the surrounding communities. As dairy farms and landfills can face fines for excess emissions starting in 2024, this is an important time to explore mitigation options and strategies.

Although sampling strategies at dairy farms and Orange County landfills were different, both campaigns maintained similar goals: determine emissions from various on-site sources and

explore how they may impact their surroundings. Specific goals motivating the landfill studies in this work were as follows:

1. Compare active dumping emissions at the active landfills to areas that have been covered with daily, intermediate, and final cover material to determine if any rogue emissions escape through the surface of the landfill.
2. Collect samples upwind, downwind, and near on-site areas of interest, such as composting pilot programs, potentially leaky infrastructure, and near surrounding neighborhoods to determine point sources of above-ground emissions.
3. Compare emissions at closed landfills to emissions at active landfills in Orange County.
4. Consider how the communities living near and downwind of the landfills might be affected by the air produced by the landfill.
5. Explore reduction strategies to improve air quality and decrease GHG emissions.

These goals were achieved by sampling at a variety of landfills, at different areas around the landfill, and across different seasons. This work also compares the emissions of select GHGs, oxygenates, sulfuric gases, and other non-methane volatile organic compounds emitted at Orange County landfills to a dairy farm in the SJV. Additionally, these data were also compared to regional and remote air quality data in California, when applicable.

The overarching goal of the dairy campaign was to collect and analyze air at different areas around the dairy site. Samples were collected at the dairy farm with the following goals in mind:

1. Collect samples upwind, downwind, and around point sources to better understand source-specific emissions at California dairy farms and their contributions to regional emissions.
2. Determine whether the sources of on-site emissions can be separated.
3. Consider how air from dairy farms may affect disadvantaged communities.

4. Determine whether the emissions change seasonally over time.
5. Explore methane reduction strategies to prevent possible fines starting in 2024.

Similar to the landfill campaigns, regional airborne and remote data were used to infer more information about SJV air quality on a regional scale and to pick out trends over time.

## 1.6 References


A.B. 1594, 2013-2015 Biennium, 2014 Reg. Sess. (Cal. 2014).

Allen, M. R., Braithwaite, A., & Hills, C. C. (1997). Trace organic compounds in landfill gas at seven UK waste disposal sites. *Environmental Science & Technology, 31*(4), 1054-1061.

American Museum of Natural History. (2019). California Central Valley. Retrieved from www.amnh.org/learn-teach/curriculum-collections/grace/grace-tracking-water-from-space/california-central-valley

Berg, N. (2011). Why Does California's Central Valley Have Such Bad Air Pollution?. *Bloomberg City Lab*. Retrieved from https://www.bloomberg.com/news/articles/2011-09-28/why-does-california-s-central-valley-have-such-bad-air-pollution

Brosseau, J., & Heitz, M. (1994). Trace gas compound emissions from municipal landfill sanitary sites. *Atmospheric Environment*, 28(2), 285-293.

California Air Resources Board (CARB). (2017). The 2017 Climate Change Scoping Plan Update the Proposed Strategy for Achieving California's 2030 Greenhouse Gas Target. Retrieved from https://ww3.arb.ca.gov/cc/scopingplan/scoping_plan_2017.pdf

California Air Resources Board (CARB). (2019). Greenhouse Gas Emissions Inventory Summary [2000 - 2017]. Retrieved from https://www.arb.ca.gov/app/ghg/2000_2017/ghg_sector_data.php

California Department of Food and Agriculture (CDFA). (2016a). California's Top 10 Milk Producing Counties, Percent Share of California Milk Production, January-December 2015. Retrieved from https://www.cdfa.ca.gov/dairy/uploader/docs/DataChartsGraphs/Top_10_Counties_Milk_Production_2015.pdf

California Department of Food and Agriculture (CDFA). (2018). California Agricultural Statistics Review 2017-2018. Retrieved from https://www.cdfa.ca.gov/statistics/PDFs/2017-18AgReport.pdf

California Department of Food and Agriculture (CDFA). (2019a). California Agricultural Exports 2018-2019. Retrieved from https://www.cdfa.ca.gov/Statistics/PDFs/AgExports2018-2019.pdf

California Department of Food and Agriculture (CDFA). (2019b). California Agricultural Statistics Review 2018-2019. Retrieved from https://www.cdfa.ca.gov/Statistics/PDFs/AgExports2018-2019.pdf

California Department of Resources Recycling and Recovery. (2015). 2014 Disposal-Facility Based Characterization of Solid Waste in California (DRRR-2015-1546). Retrieved from https://www2.calrecycle.ca.gov/Publications/Details/1546

California Environmental Protection Agency Air Resources Board. (2014). California's 2000-2012 Greenhouse Gas Emissions Inventory Technical Support Document. Retrieved from https://ww3.arb.ca.gov/cc/inventory/doc/methods_00-12/ghg_inventory_00-12_technical_support_document.pdf

California Office of Environmental Health Hazard Assessment (OEHHA). (2017). CalEnviroScreen 3.0. Retrieved from https://oehha.ca.gov/calenviroscreen/sb535

California Global Warming Solutions Act of 2006: emissions limit, H.S.C. § 38566 (2016).

California Global Warming Solutions Act of 2006: Greenhouse Gas Reduction Fund, H.S.C. § 39711, 39713, 39715, 39721, and 39723 (2012).

Chiavarini, C., Cremisini, C., Morabito, R., Caricchia, A. M., & De Poli, F. (1993). GC/MS Characterisation of Main and Trace Organic Constituents of Gaseous Emissions from a MSW Landfill. In *Fourth International Landfill Symposium* (pp. 617-621).

City of Irvine. (2018). Irvine Zoning Map. Retrieved from http://gis.cityofirvine.org/pdf/Map%20Gallery/Zoning-Map_36x36_20190401.pdf

Clean Air Act of 1963, 42 U.S.C. § 7401 (1963).

Closure and Post-Closure Maintenance Requirements for Solid Waste Landfills, 27 C.C.R. § 21090 (1997).

Crawford, J. F., & Smith, P. G. (2016). *Landfill technology*. Elsevier.

Crow, D., 2005. Air Pollution Control Officer's Determination of VOC Emission Factors for Dairies. *San Joaquin Valley Air Pollution Control District*. Retrieved from https://www.valleyair.org/busind/pto/dpag/APCO%20Determination%20of%20EF_August%201_.pdf

Environmental Protection Agency (EPA). (2020a). Current Nonattainment Counties for All Criteria Pollutants. Retrieved from https://www3.epa.gov/airquality/greenbook/ancl.html

Environmental Protection Agency (EPA). (2020b). Landfill Methane Outreach Program (LMOP): Basic Information about Landfill Gas. Retrieved from https://www.epa.gov/lmop/basic-information-about-landfill-gas

Farman, J. C., Gardiner, B. G., & Shanklin, J. D. (1985). Large losses of total ozone in Antarctica reveal seasonal ClO x/NO x interaction. *Nature*, *315*(6016), 207-210.

Farquhar, G. J., & Rovers, F. A. (1973). Gas production during refuse decomposition. *Water, Air, and Soil Pollution*, 2(4), 483-495.

Finlayson-Pitts, B. J., & Pitts, J. N. (1999). *Chemistry of the upper and lower atmosphere: theory, experiments, and applications*. Elsevier.

Giess, P., Bush, A., & Dye, M. (1999). Trace gas measurements in landfill gas from closed landfill sites. *International Journal of Environmental Studies*, *57*(1), 65-77.

Global Warming Solutions Act of 2006, H.S.C. § 38500 (2006).

Goodrich, L. B., Parnell Jr, C. B., Mukhtar, S., Lacey, R. E., & Shaw, B. W. (2003). A Science-Based PM10 Emission Factor for Freestall Dairies. In *2003 Annual International Meeting of the American Society of Agricultural Engineers.* Paper (No. 034115).

Hanemann, W. M. (2007). How California Came to Pass AB 32, the Global Warming Solutions Act of 2006.

House Committee on Natural Resources. (2014). California's Central Valley: Producing America's Fruits and Vegetables. Retrieved from https://web.archive.org/web/20150623012337/http:/naturalresources.house.gov/news/documentsingle.aspx?DocumentID=368934

Kampa, M., & Castanas, E. (2008). Human health effects of air pollution. *Environmental pollution*, *151*(2), 362-367.

Lisk, D. J. (1991). Environmental effects of landfills. *Science of the total environment*, 100, 415-468.

Meyer, D., Price, P. L., Rossow, H. A., Silva-del-Rio, N., Karle, B. M., Robinson, P. H., ... & Fadel, J. G. (2011). Survey of dairy housing and manure management practices in California. *Journal of dairy science*, *94*(9), 4744-4750.

Molina, M. J., & Rowland, F. S. (1974). Stratospheric sink for chlorofluoromethanes: chlorine atom-catalysed destruction of ozone. *Nature*, *249*(5460), 810-812.

National Primary and Secondary Ambient Air Quality Standards (NAAQS), 40 C.F.R. § 50 (2015).

Orange County Waste and Recycling (OCWR). (2020a). Anatomy of a Landfill. Retrieved from https://www.oclandfills.com/landfills/anatomy-landfill

Orange County Waste and Recycling (OCWR). (n.d.). Abatement Programs. Retrieved from https://www.oclandfills.com/environmental-programs/abatement-programs

S.B. 1383, 2015-2016 Biennium, 2016 Reg. Sess. (Cal. 2016).

Spokas, K. A., & Bogner, J. E. (2011). Limits and dynamics of methane oxidation in landfill cover soils. *Waste management*, *31*(5), 823-832.

Trump, M. (2004). Map California Central Valley. *Wikipedia*. Retrieved from https://commons.wikimedia.org/wiki/File:Map_california_central_valley.jpg

Tulare County Resource Management Agency. (1947). Section 9.7: "AE-40" Exclusive Agricultural Zone 40 Acre Minimum. *Tulare County Zoning Ordinance*. Retrieved from https://tularecounty.ca.gov/rma/index.cfm/rma-documents/planning-documents/tulare-county-zoning-ordinance/chapter-3-section-9-7-ae40/

Tulare County Resource Management Agency. (2012). Tulare County Planning Areas. Retrieved from: http://generalplan.co.tulare.ca.us/documents/GP/002Board%20of%20Supervisors%20Materials/001BOS%20Agenda%20Items%20-%20Public%20Hearing%20August,%2028%202012/008Attachment%20G.%20Public%20Comment,%20%20Staff%20Matrix,%20and%20Responses/004Item%204.%20GPU%20AMUS/10-Page%204-5%20(FOLD%20OUT)%201-Planning%20Area.PDF

Undeniably Dairy. (2018). Where Do Cows Live? The Strategy Behind Dairy Barns. Retrieved from https://www.usdairy.com/news-articles/where-do-cows-live

UNEP 2012. The Emissions Gap Report 2012. United Nations Environment Programme (UNEP), Nairobi.

United States Geological Survey (USGS). (n.d.). California's Central Valley. Retrieved from https://ca.water.usgs.gov/projects/central-valley/about-central-valley.html

Velders, G. J., Andersen, S. O., Daniel, J. S., Fahey, D. W., & McFarland, M. (2007). The importance of the Montreal Protocol in protecting climate. *Proceedings of the National Academy of Sciences*, *104*(12), 4814-4819.

Western Regional Climate Center (2008). Climate of California. Retrieved from https://wrcc.dri.edu/Climate/narrative_ca.php, accessed May 20th, 2009.

Young, P. J., & Parker, A. (1983). The identification and possible environmental impact of trace gases and vapours in landfill gas. *Waste Management & Research*, *1*(3), 213-226.

# 2. Experimental Design

Seasonal samples were collected at closed and active Orange County landfills and at a dairy site in Visalia, California. Mixing ratios of select GHGs and other trace gases were compared between sources and across time. Trace gases at the landfills and dairy farm were also compared to regional airborne samples, particularly from above the SJV, as well as to ambient remote samples collected near the California coastline. This work synthesizes these samples to better determine how air from landfills and dairy farms affects California's air quality, greenhouse gas footprint, and the health of surrounding communities.

## 2.1 NASA Student Airborne Research Program (SARP)

This work uses airborne data collected during various Student Airborne Research Program (SARP) summer campaigns to determine the mixing ratios of select trace gases at the regional scale in the SJV. The Rowland-Blake group has been a part of National Aeronautics and Space Administration (NASA) SARP since its inception in 2009. About thirty senior undergraduates with various academic backgrounds from around the country are selected to participate each year. They spend weeks learning atmospheric science and executing projects with graduate student mentors and faculty mentors representing four different universities.

As part of the program, they fly on a NASA airplane, collect samples, and analyze samples in the Rowland-Blake lab at University of California, Irvine to use for their projects. SARP has occurred every summer since 2009, and the dataset collected can be useful to track atmospheric trace gas trends in California over time. Most of the flights departed from the NASA Armstrong Flight Research Center (formerly the NASA Dryden Flight Research Center) in Palmdale, California or from other local airports in Southern California. Most flights occurred aboard the NASA DC-8 airplane, shown in Figure 2.1.


**Figure 2.1** The NASA DC-8 airplane used for most of the SARP flights. Photo taken during the NASA and National Oceanic and Atmospheric Administration **(**NOAA) Fire Influence on Regional to Global Environments and Air Quality campaign in 2019 by Brenna Biggs.

The plane typically seats a few dozen students, scientists, and flight crew. Students assist with sample collection and have an opportunity to chat with other scientists or learn about the instruments aboard the airplane. Although most of the SARP flights occurred on the DC-8, there were two exceptions: SARP 2012 used the P-3 airplane and SARP 2017 used the NASA C-23 “Sherpa” airplane. A photo of the “Sherpa” outside of the hangar at NASA Armstrong Flight Research Center’s Building 703 in Palmdale, California can be seen in Figure 2.2.

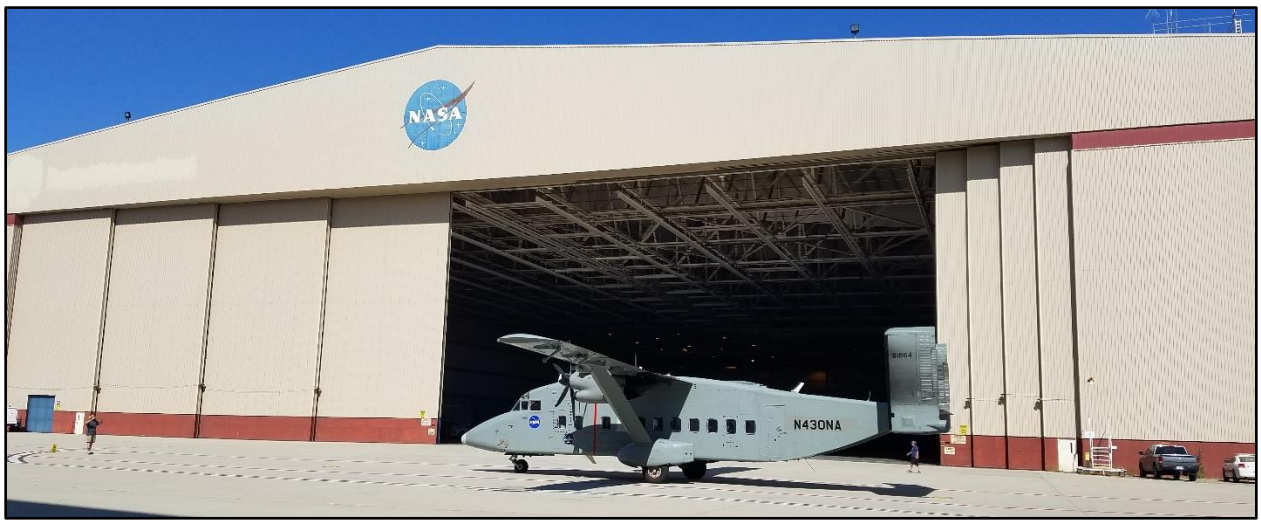


**Figure 2.2** The NASA C-23 “Sherpa” airplane used for SARP 2017 flights. Photo taken at NASA Armstrong Flight Research Center during SARP 2017 by Brenna Biggs.

Samples were collected by various instruments, including the Rowland-Blake lab’s Whole Air Sampling (WAS) equipment, which allowed researchers to draw in and collect air from outside

of the fuselage of the plane as it flew. Details about this sample collection can be found in Chapter 3.1.3. SARP samples were collected throughout Southern California, with an emphasis on the air above the LA Basin, Santa Barbara, Catalina Island, and the SJV.

Out of all the SARP flights, 2011 had one flight, 2013 had three flights, 2014 had three flights, 2015 had one flight, 2017 had three flights, and 2019 had one flight at low altitude within SJV counties. Previous data has shown that the typical planetary boundary layer (PBL) in the SJV during summer is 3,000 feet (Day et al., 2008). This was assumed to be true for all SARP samples in the SJV, and all samples chosen for this analysis had been collected below a pressure altitude of 3,000 feet. The flight tracks at low altitude (< 3,000 feet) through the SJV for 2011, 2013, 2014, 2015, and 2017 are shown in Figure 2.3.

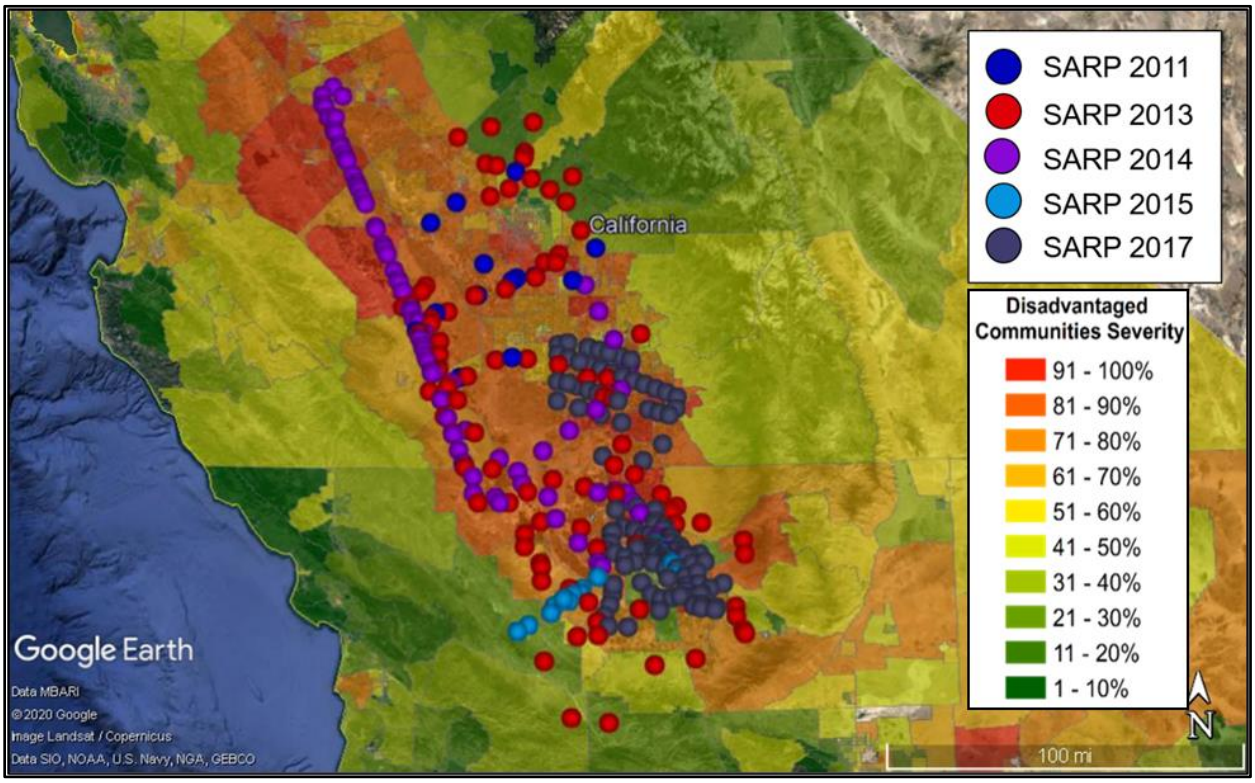


**Figure 2.3** SARP flights through the disadvantaged communities in the San Joaquin Valley at a pressure altitude of 3,000 feet or lower.

This figure also shows that the SARP flight tracks traveled through many disadvantaged communities of the SJV, many of them as high as the 91-100% range. Table 2.1 shows the SARP flights by year, time, and date.

**Table 2.1** SARP flights by date and local time

| SARP Year | Flight Number | Date | Local Start Time (PDT) | Local End Time (PDT) |
|---|---|---|---|---|
| 2011 | 2 | June 29 | 10:38:12 | 13:04:40 |
| 2013 | 2 | June 17 | 13:21:40 | 16:32:10 |
| 2013 | 4 | June 18 | 13:50:41 | 16:01:28 |
| 2013 | 5 | June 18 | 13:46:21 | 18:03:54 |
| 2014 | 2 | June 23 | 15:47:59 | 18:20:15 |
| 2014 | 3 | June 24 | 09:06:53 | 12:13:20 |
| 2014 | 4 | June 24 | 14:40:05 | 16:30:47 |
| 2014 | 5 | June 25 | 07:55:56 | 14:38:10 |
| 2015 | 3 | June 23 | 13:55:25 | 16:22:50 |
| 2017 | 4 | June 27 | 08:35:42 | 10:37:20 |
| 2017 | 5 | June 27 | 11:34:32 | 13:14:05 |
| 2017 | 6 | June 27 | 15:05:42 | 16:36:58 |

Only the samples collected at a pressure altitude under 3,000 feet over SJV counties during these flight times were included in this analysis. All flights occurred in the month of June of their respective years, with varying start times between morning and afternoon, Pacific Daylight Time (PDT).

### 2.2 Quarterly Trips to the Remote California Coast

The Rowland-Blake lab completes quarterly trips to several locations along the Pacific Ocean to measure “remote” air quality: Alaska, the Pacific Northwest, California and Baja California, Mexico, Central America, Central Pacific (Guam, Saipan, Hawaii), and Southern Pacific (New Zealand, Cook Islands). Trips are funded by NASA and have occurred from the late 1970s through the present. The original goal was to track changes in CFC-11, CFC-12, carbon tetrachloride, methyl chloroform, and methane at different locations seasonally over the years, but additional trace gases have since been added. For this analysis, 512 samples collected on the coast of California (34.5 – 40.0 °N) have been used to track changes in methane background

levels from 1980 until present. A map showing the location for points used in this work is shown in Figure 2.4.


**Figure 2.4** Samples collected for quarterly trips on the California coastline (34.5 – 40.0 °N). Samples collected prior to 2015 are marked with a blue triangle, and samples collected in 2015 or later are marked with a green ring.

Other trace gases were added to this analysis in later years. For example, $CO_2$, dimethyl sulfide, and carbonyl sulfide were measured starting in the year 2015 and were used in this analysis. The locations corresponding to samples collected in 2015 onward are marked on Figure 2.4 with a green ring. Background mixing ratios of $CO_2$ and carbonyl sulfide were determined using 64 samples collected in remote coastal areas of California. Dimethyl sulfide was measured in 58 of these 64 samples, which were used to determine its levels at California's remote coastline locations.

### 2.3 Active and Closed Landfills in Orange County, California

The Rowland-Blake lab received funding from the University of California Office of the President to study landfills in Orange County. Orange County landfills are much different than those in the rest of the country because California has strict laws in place to prevent rogue emissions from escaping the landfills. Orange County is also one of the most affluent counties in

the State, so the way that they handle their waste is often touted as an example for the rest of California. These factors all make it an interesting area to study landfill emissions.

Orange County contains three active landfills (Olinda Alpha, Prima Deshecha, and Frank R. Bowerman), two closed landfills that are nearing the end of their 30-year monitoring period (Santiago Canyon and Coyote Canyon), and eighteen closed landfills that are no longer monitored (including Vista Grande Park, formerly known as La Habra landfill) (OCWR, 2020b). All samples at the Orange County landfills were collected and analyzed by the author in the Rowland-Blake laboratory at the University of California, Irvine. Two other landfills outside of Orange County (Chiquita Canyon and Santa Maria Regional) have also been used as a comparison for parts of this analysis. These samples were collected by members of California Polytechnic University, San Luis Obispo (Cal Poly SLO) and they were analyzed by members of the Rowland-Blake lab, including the author.

These landfills are classified according to the waste they accept. Table 2.2 shows the landfills used for this study grouped by their class designation and type of collected waste (Identification and Listing of Hazardous Waste, 2012; California Water Code, 2012). All the landfills used for this analysis are classified as Class III, meaning they only accept nonhazardous materials, but the variety of accepted waste is expected to change their emissions. Vista Grande Park (formerly La Habra landfill) was built before regulations were in place and did not receive a class designation.

**Table 2.2** Landfill class and accepted waste (Identification and Listing of Hazardous Waste, 2012; California Water Code, 2012)

| Landfill | Class | County | Waste Accepted |
|---|---|---|---|
| Frank R. Bowerman | III | Orange | Mixed municipal, construction/demolition, industrial |
| Olinda Alpha | III | Orange | Mixed municipal, construction/demolition, industrial, agricultural, tires, wood waste |
| Prima Deshecha | III | Orange | Mixed municipal, construction/demolition, industrial |
| Chiquita Canyon | III | Los Angeles | Mixed municipal, green materials, construction/demolition, industrial, inert |
| Santa Maria Regional | III | Santa Barbara | Mixed municipal, green materials, construction/demolition, industrial, agricultural, tires, metals |
| Santiago Canyon | III | Orange | Mixed municipal, construction/demolition, industrial, agricultural, tires, other designated |
| Coyote Canyon | III | Orange | Mixed municipal, construction/demolition, agricultural, tires, other designated, sludge |
| Vista Grande Park | n/a | Orange | Pre-regulation |

Olinda Alpha is the only Orange County landfill that accepts green waste (i.e., agricultural, wood waste) and tires for disposal. The rest accept a mix of mixed municipal, construction, demolition, and industrial wastes. Table 2.3 summarizes the status, closure dates, waste footprints, and disposal rates of each landfill (CalRecycle, 2020). Of the active Orange County landfills, Frank R. Bowerman can accept the most waste per day, and Prima Deshecha can accept the least. Santiago Canyon, Coyote Canyon, and Vista Grande Park landfills have been closed for decades and no longer accept waste. Coyote Canyon landfill is nearing the end of its 30-year monitoring period, which is set to end sometime in 2021. Plans have been made to repurpose the landfill's surface into a golf course and boutique hotel (Davis, 2019).

**Table 2.3** Status, waste footprint, and disposal rate of active and closed landfills in Orange County and other counties used in this analysis

| Landfill | City | Status | Opened | Planned Closure | Waste Footprint (acres) | Disposal Rate (tons/day) |
|---|---|---|---|---|---|---|
| Frank R. Bowerman (FRB)[1] | Irvine | Active | 1990 | 2053 | 534 | 8,500 |
| Olinda Alpha[1] | Brea | Active | 1960 | 2021 | 420 | 7,000 |
| Prima Deshecha[1] | San Juan Capistrano | Active | 1976 | 2067 | 698 | 1,400 |
| Chiquita Canyon[2] | Castaic | Active | 1972 | 2019 | 257 | 1,874 |
| Santa Maria Regional[2] | Santa Maria | Active | ~1970 | 2022 | 247 | < 858 |
| Santiago Canyon[1] | Silverado | Closed | 1968 | 1996 | 113 | N/A |
| Coyote Canyon[1] | Newport Beach | Closed | 1963 | 1991 | 395 | N/A |
| Vista Grande Park[1] | La Habra | Closed | 1949 | 1958 | 19 | N/A |

1. Samples collected and analyzed by the Rowland-Blake lab.
2. Samples collected by Cal Poly SLO and analyzed by the Rowland-Blake lab.

Only one sample was collected at Vista Grande Park, as it has been closed since 1958 and has not been monitored for decades. Located in a heavily trafficked area of La Habra, California, it was deemed likely unrepresentative of true landfill emissions so additional samples were not collected. Olinda Alpha is set to close in December 2021. The upcoming closure dates are subject to change, but Orange County has no plans to build another landfill even after Prima Deshecha closes in 2067. Instead, waste will be transported to other counties for disposal, greatly increasing traffic, road degradation, and incoming trash at other landfills. Although Orange County landfills are supposedly some of the best in the country, it is important to understand their rogue emissions and how they compare to other heavy-hitting trace gas emitters, such as dairy farms.

One hundred thirteen samples were collected and analyzed from the Orange County landfills. These campaigns were collected during all four seasons: Spring 2018, Summer 2018, Fall 2018, and Winter 2019. The author has also helped the Rowland-Blake group analyze 205

samples collected by Cal Poly SLO from additional landfills in other counties. The location, status, and number of samples collected at each landfill is shown in Table 2.4.

**Table 2.4** Landfill location, status, and number of samples collected

| Landfill | City | County | Status | Number of Samples |
|---|---|---|---|---|
| Frank R. Bowerman[1] | Irvine | Orange | Active | 31 |
| Olinda Alpha[1] | Brea | Orange | Active | 29 |
| Prima Deshecha[1] | San Juan Capistrano | Orange | Active | 28 |
| Chiquita Canyon[2] | Castaic | Los Angeles | Active | 103 |
| Santa Maria Regional[2] | Santa Maria | Santa Barbara | Active | 102 |
| Santiago Canyon[1] | Silverado | Orange | Closed | 12 |
| Coyote Canyon[1] | Newport Beach | Orange | Closed | 12 |
| Vista Grande Park[1] | La Habra | Orange | Closed | 1 |

1. Samples collected and analyzed by the Rowland-Blake lab.
2. Samples collected by Cal Poly SLO and analyzed by the Rowland-Blake lab.

The Rowland-Blake lab's method of sample collection was seasonally similar. At each of the active landfills, samples around the active dumping area, upwind, and downwind were always collected. Extra samples were collected in areas of interest: near potentially leaky or exposed infrastructure, above the aged trash areas, or near daily cover materials, for example. At the closed landfills, samples were collected in similar areas across each season, typically spread out throughout the landfill itself.

The locations of samples collected at Frank R. Bowerman landfill in Irvine, California across all four seasons are shown in aerial view in Figure 2.5. Duplicate samples were often collected in a single location, for example, at different heights above an aged area. Duplicate samples are shown overlapped because they have the same coordinates.


**Figure 2.5** Frank R. Bowerman landfill with samples marked for the Spring 2018 (blue rings), Summer 2018 (green rings), Fall 2018 (yellow rings), and Winter 2019 (red rings) campaigns.

Trained landfill engineers drove samplers off road to each location using 4x4 pickup trucks. Roads constantly change at active landfills as waste cells become full and the active dumping area shifts to fill up different cells.

A top-down view of the landfill roads at Frank R. Bowerman landfill is shown in Figure 2.6. Someday, before Frank R. Bowerman closes in 2053, the entire area will be completely filled with waste.

**Figure 2.6** View of select landfill roads at Frank R. Bowerman landfill in Irvine, California. Photo taken by Brenna Biggs in February 2018.

During all four seasons at Frank R. Bowerman landfill, a brief height study was conducted. Samples were collected about 6 inches, 3 feet, 5 feet, and 7 feet above the ground to determine if the distance from a source would create a noticeable change in trace gas enhancements. These studies were typically conducted over aged trash areas that had been covered with intermediate cover materials. Samples were also collected near active dumping and on-site compost areas.

The locations of the samples collected at Prima Deshecha landfill in San Juan Capistrano, California across all four seasons are shown in aerial view in Figure 2.7. Duplicate samples appear as a single point, as they have the same coordinates.


**Figure 2.7** Prima Deshecha landfill with samples marked for the Spring 2018 (blue rings), Summer 2018 (green rings), Fall 2018 (yellow rings), and Winter 2019 (red rings) campaigns.

Engineers at Prima Deshecha landfill were very interested in using mulch and compost as alternative daily cover. Like the other active Orange County landfills, they had started an on-site composting program. Air samples were collected near these compost piles and near their mulch ADC along with the typical samples collected upwind, downwind, and at the active dumping area.

Samples collected at Olinda Alpha landfill across all four seasons are shown in aerial view in Figure 2.8. Again, duplicate samples appear as the same point because of their identical coordinates.


**Figure 2.8** Olinda Alpha landfill with samples marked for the Spring 2018 (blue rings), Summer 2018 (green rings), Fall 2018 (yellow rings), and Winter 2019 (red rings) campaigns.

Olinda Alpha landfill in Brea, California was also experimenting with compost and mulch as daily cover, and samples were taken in these areas in addition to the usual samples collected upwind, downwind, and at active dumping areas. Additionally, some samples were collected on their “wet deck,” which is an alternative active dumping area that is paved with concrete or broken asphalt. This area was used when it was raining so that the heavy dump trucks would be able to handle the terrain.

Samples collected at Coyote Canyon landfill in Newport Beach, California across all four seasons are shown in aerial view in Figure 2.9.

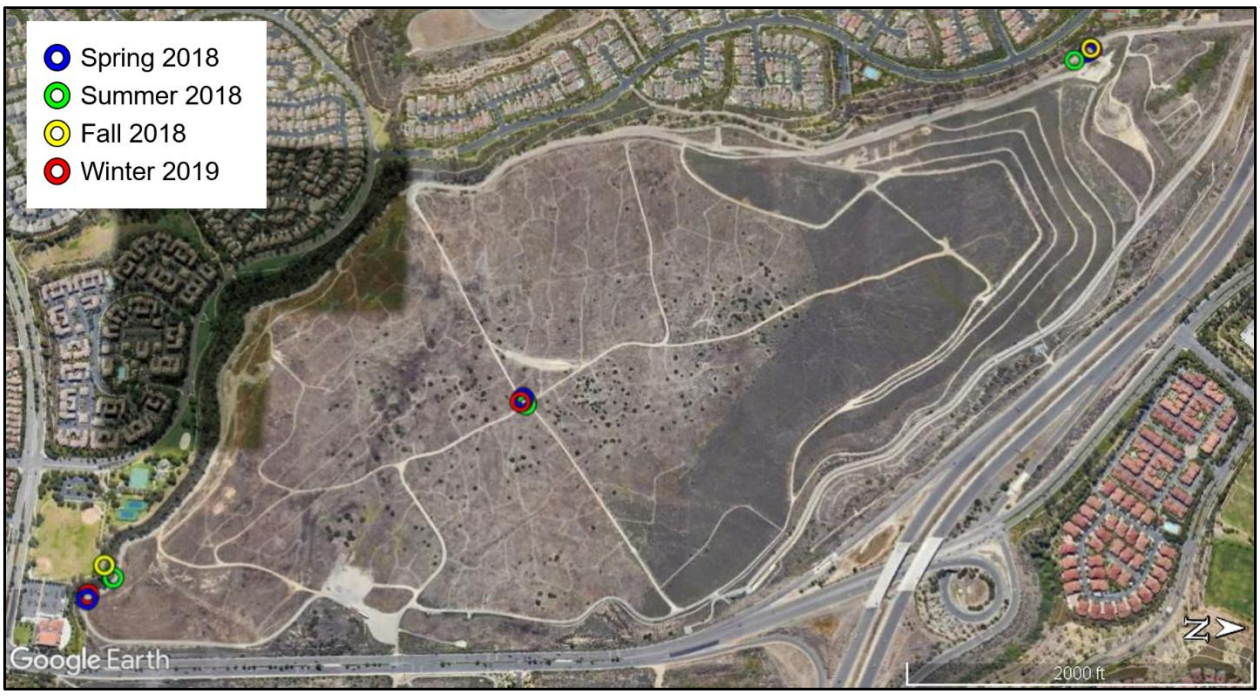


**Figure 2.9** Coyote Canyon landfill with samples marked for the Spring 2018 (blue rings), Summer 2018 (green rings), Fall 2018 (yellow rings), and Winter 2019 (red rings) campaigns.

These samples were collected in the same three general areas during each campaign. One sample was always collected near a condensate tank and siltation basin. One sample was always collected in the middle of the landfill, and one sample was always collected near the fence by a community center, which was consistently a downwind sample. Samples collected at Santiago Canyon landfill, in Silverado, CA across all four seasons are shown in aerial view in Figure 2.10.


**Figure 2.10** Santiago Canyon landfill with samples marked for the Spring 2018 (blue rings), Summer 2018 (green rings), Fall 2018 (yellow rings), and Winter 2019 (red rings) campaigns.

The sample collection locations were similar across all four campaigns. One sample was always collected near the entrance to the landfill. One sample was always collected in the middle of the landfill, and one sample was always collected near the desilting pond next to the edge of the landfill. The combination of variety and consistency throughout the sample collection process at each Orange County landfill revealed some interesting trace gas trends that are presented in this document.

### 2.3.1 Disadvantaged Communities Near Orange County Landfills

Although many landfills in California are generally located near disadvantaged communities, the landfills in Orange County were built in surprisingly affluent areas. A map of the landfills sampled in Orange County in relation to designated disadvantaged communities is shown in Figure 2.11.

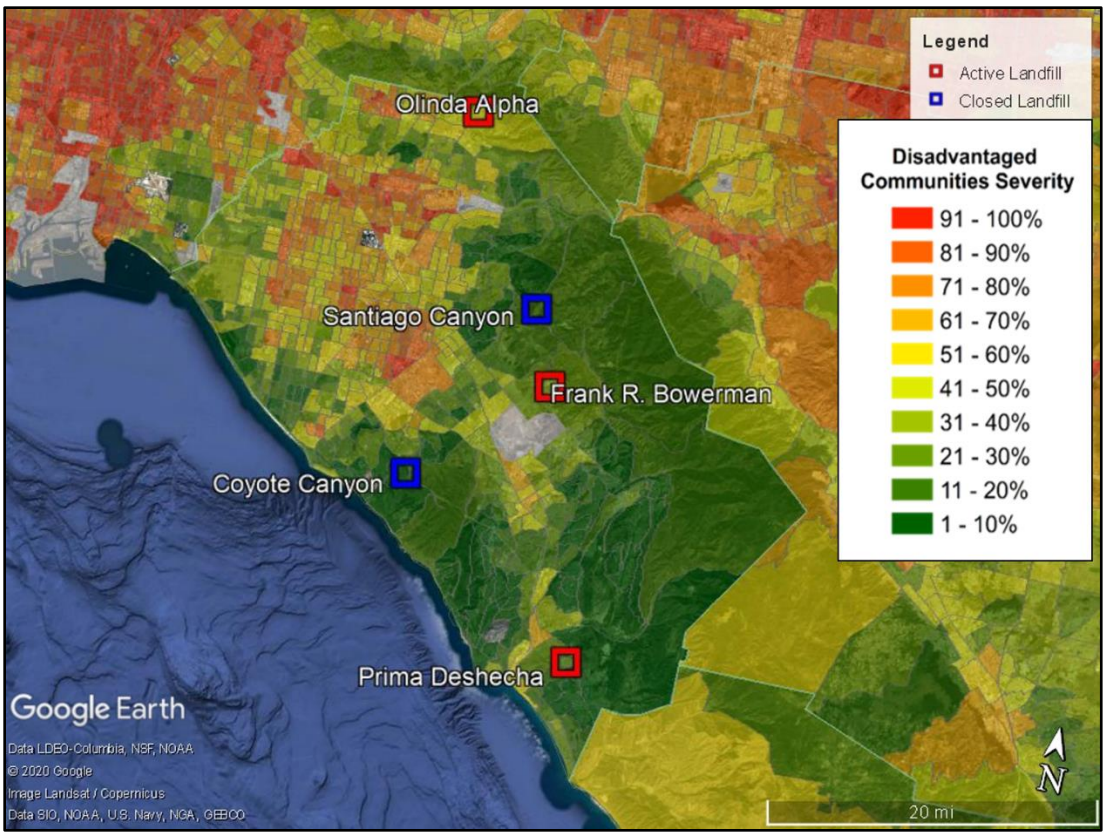


**Figure 2.11** A map of active (red square) and closed (blue square) landfills in Orange County in relation to designated disadvantaged communities.

Landfills are marked as either active (Frank R. Bowerman, Prima Deshecha, and Olinda Alpha) or closed (Santiago Canyon, Coyote Canyon). All landfills are in primarily “green” regions according to CalEnviroScreen 3.0, indicating that they are not located in areas of disadvantage. This means that residents usually enjoy higher socioeconomic statuses and typically experience less air and water pollution. Coyote Canyon is in an area scored by CalEnviroScreen 3.0 as 5 to 10%, Santiago Canyon is in an area scored as 15 to 20%. Frank R. Bowerman is in a 20 to 25% region, Prima Deshecha is in a 10 to 15% region, and Olinda Alpha is in a 40 to 45% region (OEHHA, 2017). This is much lower than the 70% minimum CalEnviroScreen 3.0 score that most of the San Joaquin Valley experiences.

These cities’ low relative scores make Orange County an interesting place to study landfills. Although landfills are still waste disposal sites, they were built in affluent areas with

stricter regulations than the rest of the state (and country). This had led to more stringent guidelines, consistent monitoring, modern infrastructure, and odor and bird abatement programs.

### 2.4 Dairy Farm Selection

Out of the thousands of potential dairy farms in California, the dairy site was selected based on the following parameters: location, typical wind direction, dairy farm layout, owner interest, maneuverability, and manure management strategy. The SJV, or the southern half of California's Central Valley, was selected as a general study region because it contains the most cows and dairies in California. The city of Visalia in Tulare County was chosen as a narrower region of interest because Tulare is the most active dairy-producing county in California (CDFA, 2016a). Eventually, a dairy site was selected in Visalia to be studied for this work. The section examines the selection parameters (e.g., number of cows, manure management style, farm cooperation and accessibility) and it also examines the eight SJV counties in more detail to better determine Visalia's representativeness as a study area.

#### 2.4.1 Manual Dairy Database

Although estimates for the number of dairies and cows are annually reported, there is currently no comprehensive public database of dairies in the SJV. However, manually analyzing satellite imagery revealed the coordinates and sizes of dairies and manure management practices, which were used for this project to understand more about the potential site's location. Combined satellite imagery via Google Earth Pro was used to manually find and measure the surface areas of bovine-containing areas and their manure management strategies, where applicable, within the SJV. A map identifying probable dairies and areas outdoors where cows are held and managed is shown in Figure 2.12. Although there is no guarantee that every point represents a separate dairy, each point does represent an area where cows are clearly kept and managed.

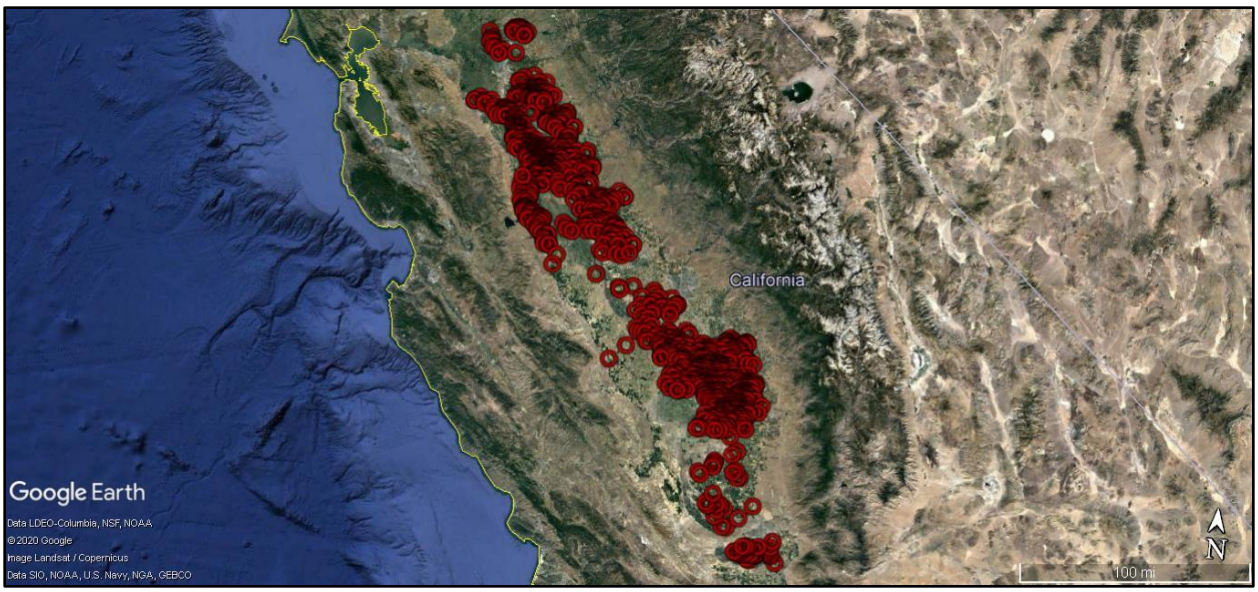


**Figure 2.12** A map identifying bovine-containing areas in California. This map was constructed manually using satellite photography of the SJV in Google Earth.

These bovine-containing areas are widely distributed throughout the SJV, with concentrated clumps in Tulare, Merced, and Stanislaus Counties. Figure 2.13 shows the surface areas of the bovine-containing areas in each county. For the dairies that use settling basins and holding ponds for their manure management, the area of those is shown as well. These dairies were all located manually using satellite imagery of the San Joaquin Valley.

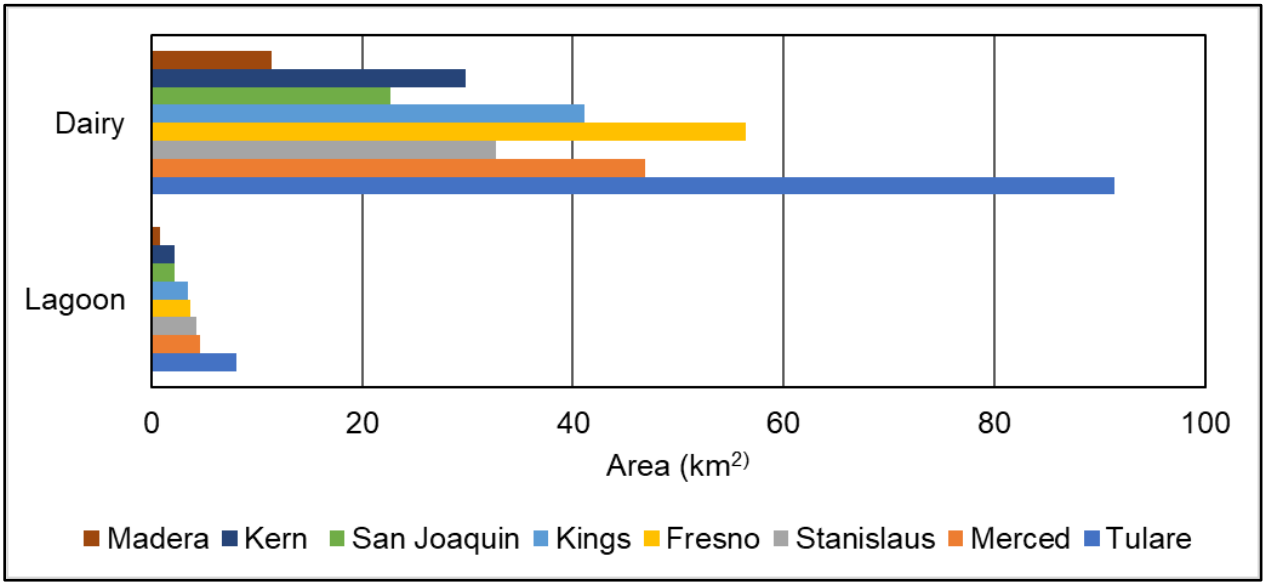


**Figure 2.13** Dairy and manure management surface area in the counties of the SJV. For the purposes of labelling this figure, all manure management areas are included in “Lagoon.”

It has been shown that most of the emissions at dairy farms come from enteric fermentation and manure. Therefore, it was important to determine which county contained the most cows and manure management operations. Based on the manual analysis of satellite imagery, it became apparent that Tulare County contained the highest surface area of dairies and lagoons. This implies that the dairy site studied in this work is located within a dense dairy region. According to the manually analyzed satellite imagery, dairies and bovine-containing areas comprise over 90 $km^2$ of Tulare County. About 8 $km^2$ of the area is composed of lagoons and settling basins used for manure management. Madera County contains the smallest surface area of dairies and wet manure management. Dairies comprise nearly 12 $km^2$ and less than 1 $km^2$ of that area is composed of manure lagoons and slurries.

### 2.4.2 Dairy Trends in Annual Agricultural Reports

The dairy site used for this analysis is in Visalia, Tulare County, California. The trends for the number of dairy cows and dairies were examined for Tulare County along with the other counties in the SJV using data from the Central Valley's annual agricultural reports over the last several years (CDFA, 2007a-b, 2009, 2011, 2015, 2016b, 2017, 2018). Figure 2.14 shows the number of dairy cows per county in the SJV from 2004 through 2017.

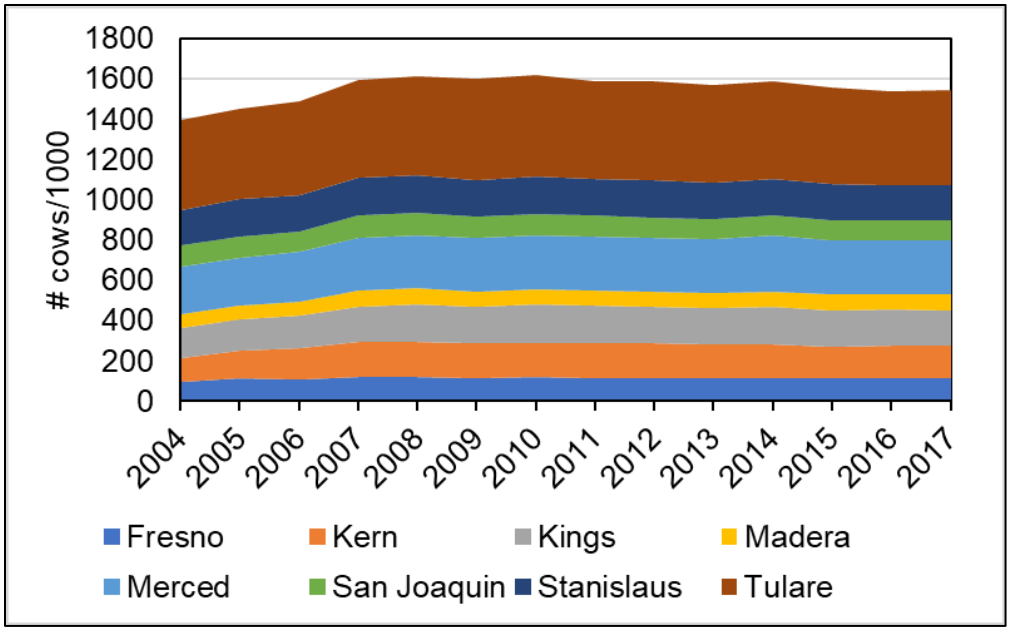


**Figure 2.14** Number of dairy cows per county in the SJV from 2004 to 2017.

The number of dairy cows fluctuates greatly over time, with totals varying between 1.4 and 1.6 million. However, Tulare County contained the highest number of dairy cows throughout all the years, while Madera County consistently contained the least number of dairy cows. Tulare County fluctuated between having approximately 443,000 dairy cows to 502,000 dairy cows, while Madera County fluctuated between having approximately 64,000 dairy cows to 81,000 dairy cows. The number of dairy cows in the SJV has fluctuated over time, and so has the number of dairies. The number of dairies in the SJV from 2004 through 2017 is shown in Figure 2.15.

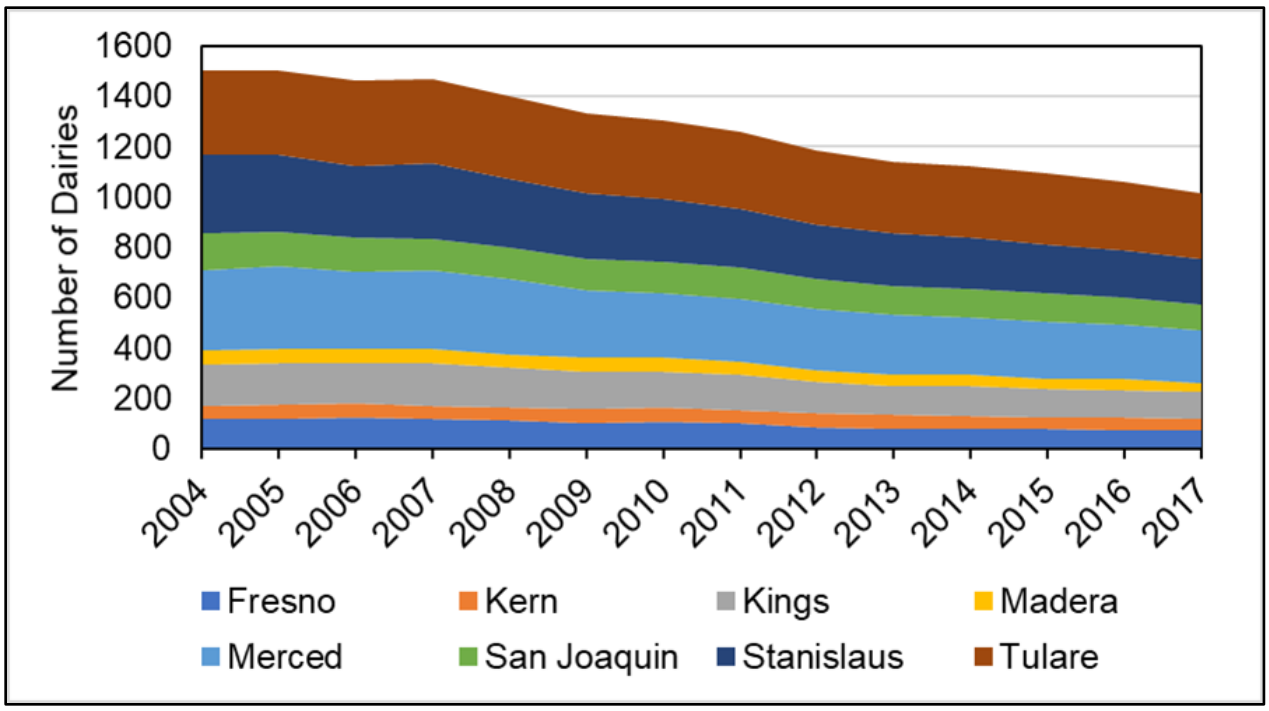


**Figure 2.15** The number of dairies in SJV counties from 2004 to 2017.

Overall, the number of dairies in the area has decreased over the last two decades for all counties. This could be a result of tighter restrictions, the decline in milk sales, or the combination of both. Currently, Tulare County is thought to contain about 250 dairy farms, the highest amount of any SJV county (CDFA, 2018).

Even though the total number of dairies generally declined, the change in the number of dairy cows per dairy in the SJV generally increased. The average number of dairy cows per dairy for SJV counties from 2004 – 2017 is shown in Figure 2.16.

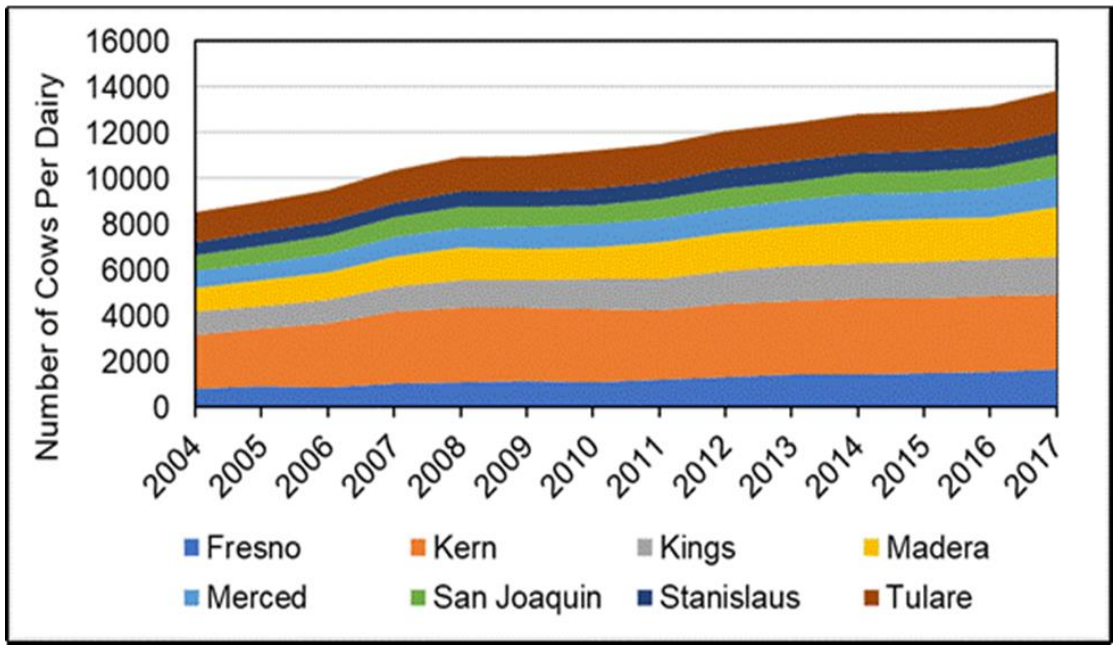


**Figure 2.16** The average number of dairy cows per dairy in the SJV from 2004 until 2017.

Over the years, Kern County typically has had the highest average number of dairy cows per dairy, with over 3,000 dairy cows at each dairy. Tulare County, where the selected dairy is located, maintained on average nearly 2,000 cows over this same period. The selected dairy maintained, on average, over 3,000 dairy cows throughout this project, and is therefore regarded as a large dairy for the region.

Based on Figure 2.16, it may appear now that the number of dairy cows per dairy is increasing again into the present. However, the fallout from the SARS-CoV-2 pandemic that started in 2019 could decrease these numbers yet again. Exports of milk products overseas and even nationwide were limited during the pandemic and could force shutdowns of dairy farms around the state. Additionally, many dairy farmers were forced to slaughter their dairy cows to support the beef industry during shortages, resulting in a possibly lower number of dairy cows in future years (Finch II, 2020; O'Neill, 2020).

### 2.4.3 Dairy Farm Logistics and Representativeness

Other factors impacting dairy farm selection included geographical location and orientation, owner interest and permission, and manure management strategy. The physical

location of the dairy farm was less important than its orientation and accessibility. The wind direction played an important role in further narrowing down a dairy location in Visalia that could be studied. The ideal dairy would be oriented such that the manure management areas would be located upwind from the rest of the dairy. This way, they could be easily and accessibly measured while minimizing the contamination of samples by other emission sources. As previously mentioned, the typical wind direction year-round in the SJV is from the northwest, meaning this is where manure management would ideally occur to isolate those emissions (Western Regional Climate Center, 2008).

Fortunately, the selected dairy site does manage its manure in the northwest corner of the farm and matched this ideal layout; it was also surrounded by drivable roads throughout the property, making sample collection easier. Importantly, the dairy owner was very interested in understanding regional trace gases and in the potential to learn more about his dairy farm, and he gave us permission to complete multiple seasonal campaigns. Lastly, the dairy site uses slurries and lagoons as its manure management strategy. This strategy, as opposed to a different method such as dry management, is most representative of Tulare and the other counties in the SJV.

Figure 2.17 shows a Google Earth satellite image of the dairy site with points of interest labelled. Heifers (i.e., young female cows that have not yet borne a calf), calves, and dry cows (i.e., dairy cows in a stage of their lactation cycle when milk production stops before giving birth) spend much of their time in corrals in a separate area of the farm north of the milk cows. The dairy has several feed hutches, known as free stalls, where the milk cows eat and spend much of their time when they are not being milked. The cows' waste is flushed from the free stalls and the milk parlor—where the cows are milked—into a processing pit, where the solid waste is separated from the liquid waste.

Liquid waste is further diluted and flushed to two subsequent open slurry ponds, Slurries 1 and 2. These act as settling basins to further separate out the sludge from the liquid. This sludge is usually mechanically removed at least once each year. Following the slurries, the liquid waste travels into two lagoons, Lagoon 3 and Lagoon 4, where it is further diluted. The final lagoon is drained to irrigate agriculture, as the liquid contains many nutrients from the manure to replenish the land and nourish crops. Silage and bedding change location around the dairy depending on the quantity and time of the year but are labelled in Figure 2.17 according to the time the satellite image was taken.

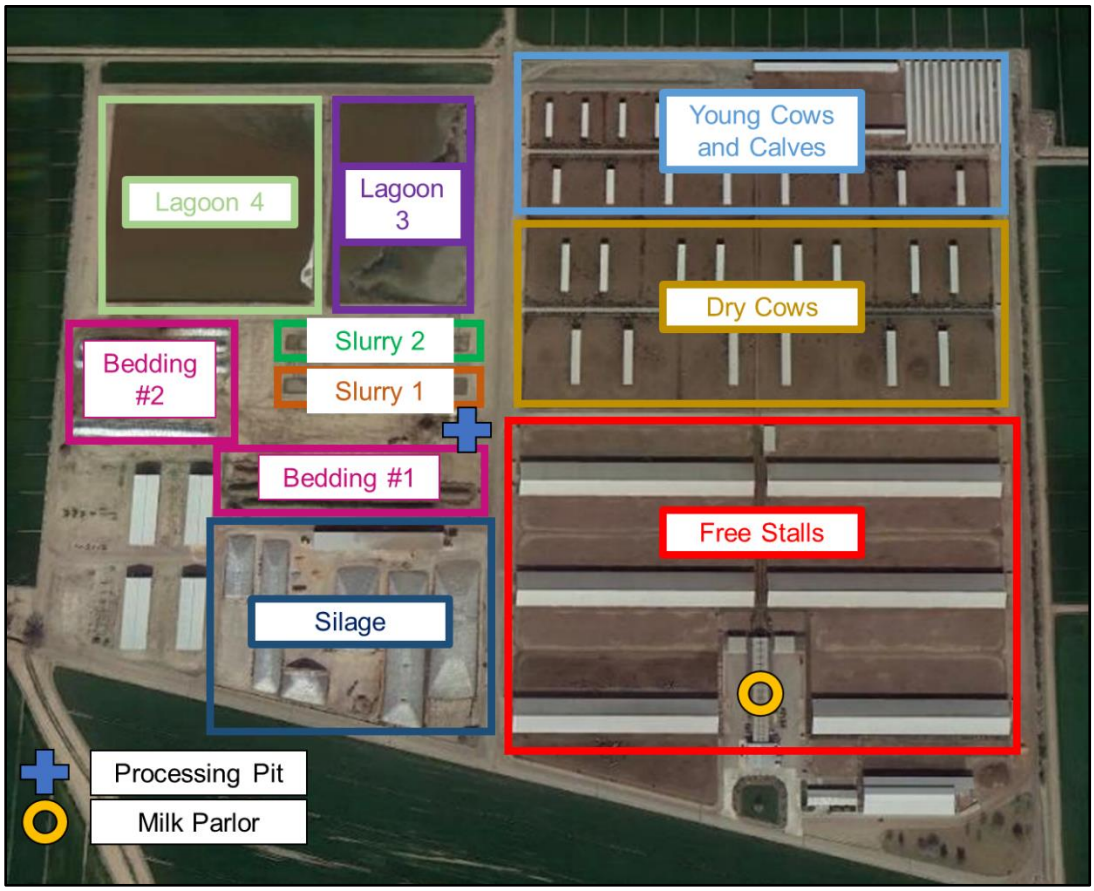


**Figure 2.17** Satellite image of the dairy farm with free stalls, dry cows, young cows (i.e., heifers), silage, bedding, slurries, lagoons, processing pit and milk parlor labelled.

As shown in Figure 2.17, the selected dairy site is mostly a free stall facility, with some corral areas for the dry cows and heifers. This dairy site follows the typical Tulare County manure management practices by flushing and scraping waste that is then separated and stored in wet

manure management systems (i.e., lagoons and slurries). Nearly 75% of the dairy farms in Tulare County separate out solid waste from liquid waste in the manure, and this dairy is no different (Meyer et al., 2011). Nearly all dairies in Tulare report using some sort of storage or treatment ponds, where diluted liquid waste is left to outgas and decompose (Meyer et al., 2011). An overview of the studied dairy site's manure management process is shown in Figure 2.18.

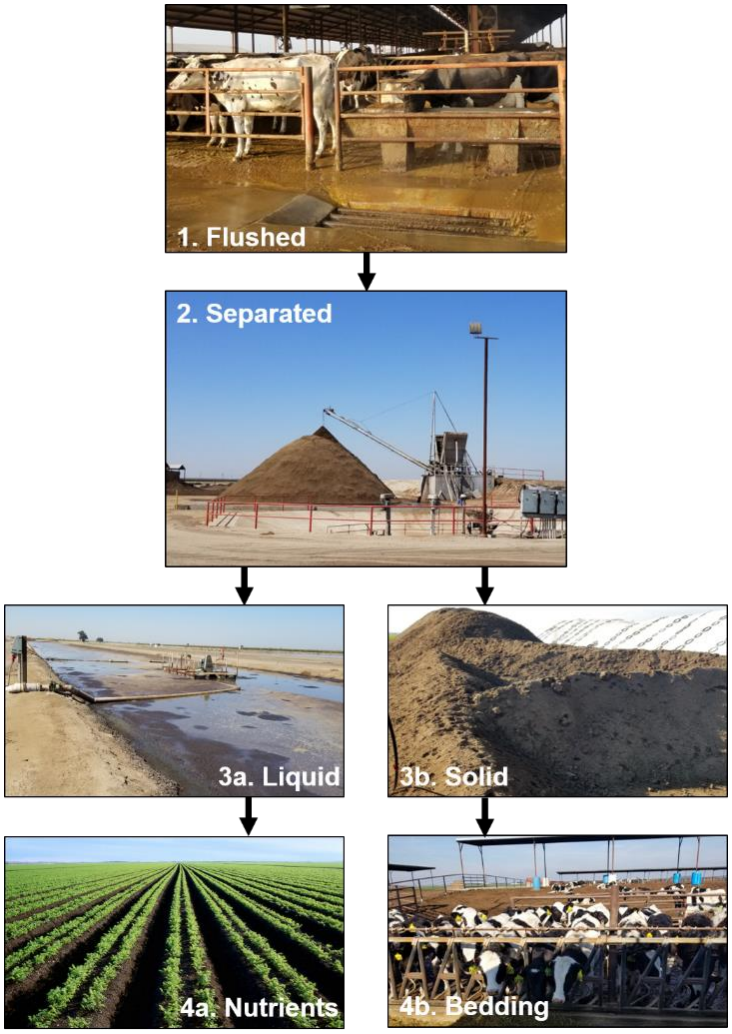


**Figure 2.18** Manure flow chart at the dairy farm in Tulare County, California.

Cows first excrete waste as urine and feces inside the free stall areas, typically while they eat and ruminate. The waste from the heifers, calves, and dry cows in the corral areas is scraped and composted separately as solid waste. However, the waste from the cows in the free stalls is

seldom scraped and is always flushed out of the free stalls, as shown in Figure 2.18.1. A similar process occurs within the milking parlor (not pictured): cows excrete waste, which is flushed.

All flushed waste is pumped to an underground collection chamber, where it is sent to the processing pit and separated into liquid and solid waste. This is shown in Figure 2.18.2. From the separator, the liquid waste makes its way sequentially through into a series of two settling basins (or slurries) and two lagoons as shown in Figure 2.18.3a. The slurry ponds are about 3,200 $m^2$, while the third holding pond, or lagoon, is approximately 29,190 $m^2$. The final lagoon is nearly 43,500 $m^2$. All basins and lagoons are about 4 meters deep. Slurry 1, 2, and Lagoon 3 are dredged typically at least once each year to mechanically remove additional solid waste, which accumulates at the bottom over time.

The solid waste that had been separated at the processing pit is mixed with other organic material and is laid out for solar drying, typically during summer, as shown in Figure 2.18.3b. After drying, it is then recycled and used as bedding for the cows, as shown in Figure 2.18.4b. The liquid waste from the lagoons is full of nutrients by the time it reaches Lagoon 4. This liquid waste is used to irrigate crops in the nearby fields. This is shown in Figure 2.18.4a.

### 2.4.4 Disadvantaged Communities and the Visalia Dairy Site

Visalia is located within the heart of the disadvantaged counties of the SJV. It is crucial that the air in these areas is better studied, understood, and cleaned up to support the residents living there. The studied dairy site, which is in Census tract 6107000900, has a CalEnviroScreen 3.0 score in the 85-90% range and is objectively designated as “disadvantaged” using the calculation described in Chapter 1.2.2 (OEHHA, 2017). Detailed CalEnviroScreen 3.0 scores in order of maximum score to minimum score for various parameters can be found in Table 2.5. Most of the parameters at the selected dairy’s census tract had a high score, indicating a higher level of disadvantage.

**Table 2.5** CalEnviroScreen 3.0 scores for the studied dairy site

| Parameter | Score (%) |
|---|---|
| Drinking Water Contaminants | 100 |
| $PM_{2.5}$ Concentration | 97 |
| Groundwater Threats | 93 |
| Solid Waste Sites | 92 |
| Educational Attainment | 91 |
| Poverty | 90 |
| Cleanup Sites | 88 |
| Pesticide Use | 86 |
| Ozone Concentration | 85 |
| Linguistic Isolation | 81 |
| Unemployment | 74 |
| Low Birth Weight | 61 |
| Housing Burden | 47 |
| Toxic Release from Facilities | 45 |
| Asthma | 44 |
| Cardiovascular Disease | 35 |
| Impaired Water Bodies | 29 |
| Traffic Density | 27 |
| Diesel PM | 17 |
| Hazardous Waste | 16 |

CalEnviroScreen 3.0 also provides demographic information. In the dairy site's census tract, 71% of people identify as Hispanic, 24% as White, 2% as African American, 2% as Asian American, 1% as Native American and 1% as Other (OEHHA, 2017).

### 2.4.5 Samples Collected at the Dairy Farm

A total of 359 canisters were collected at the dairy site over five different campaigns: September 2018, March 2019, June 2019, September 2019, and January 2020 to capture seasonal and temporal trends. Samples were collected at higher frequency near manure management areas (e.g., lagoons and slurries) and near the cows in the free stalls. Other areas, such as cows' breath, flush lanes, and silage, were sampled less frequently. A summary of the sample types collected during each campaign is found in Table 2.6.

**Table 2.6** A summary of campaigns and number of samples collected at the dairy site

| Sample Location | Sep. 2018 | March 2019 | June 2019 | Sep. 2019 | Jan. 2020 |
|---|---|---|---|---|---|
| Cows | 6 | 6 | 7 | 10 | 6 |
| Free Stalls | 8 | 4 | 9 | 15 | 3 |
| Cow Breath | 0 | 0 | 0 | 0 | 21 |
| Lagoons | 48 | 31 | 19 | 27 | 10 |
| Silage | 0 | 2 | 6 | 6 | 2 |
| Bedding | 0 | 0 | 9 | 12 | 12 |
| Flush Water | 2 | 3 | 0 | 0 | 6 |
| Processing Pit | 2 | 5 | 2 | 0 | 0 |
| Milk Parlor | 1 | 0 | 1 | 0 | 0 |
| Upwind/Downwind | 2 | 3 | 4 | 5 | 3 |
| Crops | 4 | 5 | 1 | 0 | 0 |
| Office | 2 | 0 | 1 | 0 | 1 |
| Other Dairies | 1 | 0 | 16 | 0 | 0 |
| Visalia Landfill | 1 | 5 | 4 | 0 | 0 |
| **Total** | **77** | **64** | **79** | **75** | **64** |

Samples collected near “cows” can be further broken down into the various locations around the farm: near dry cows, near heifers, and near calves. All samples collected at the main dairy site (not including other regional measurements such as at the Visalia landfill or other dairies nearby) across all campaigns are shown on the map in Figure 2.19. Duplicate samples collected in a single location appear as one point because the coordinates are identical.

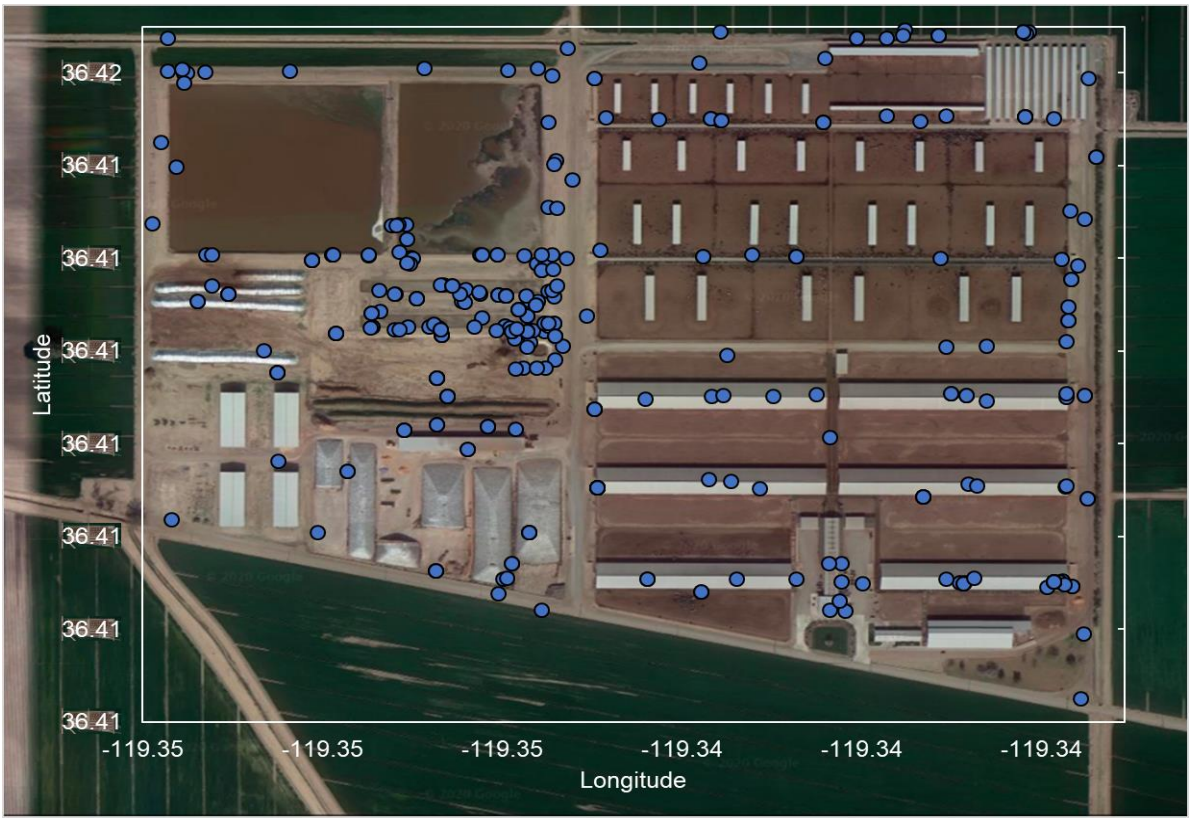


**Figure 2.19** Map of all samples collected at the dairy site across all campaigns. Samples collected elsewhere (at the Visalia landfill or other dairies) were not included in this image.

As shown in Figure 2.19, samples were collected at a variety of locations around the dairy farm, with a special emphasis on comprehensively sampling the settling basins and cow-containing areas.

## 2.5 References


California Department of Food and Agriculture (CDFA). (2007a). California Agricultural Resource Directory 2006. Retrieved from http://www.cdfa.ca.gov/files/pdf/card/AgResDirEntire06.pdf

California Department of Food and Agriculture (CDFA). (2007b). California Agricultural Statistics 2006 Crop Year. Retrieved from https://www.cdfa.ca.gov/plant/fcm/pdfs/publications/2006cas-all.pdf

California Department of Food and Agriculture (CDFA). (2009). California Agricultural Resource Directory 2008–2009. Retrieved from https://www.cdfa.ca.gov/Statistics/PDFs/ResourceDirectory_2008-2009.pdf

California Department of Food and Agriculture (CDFA). (2011). California Agricultural Resource Directory 2010–2011. Retrieved from http://www.cdfa.ca.gov/statistics/PDFs/AgResourceDirectory_2010-2011/2AgOvStat10_WEB.pdf

California Department of Food and Agriculture (CDFA). (2015). California Agricultural Resource Directory 2014–2015. Retrieved from https://www.cdfa.ca.gov/Statistics/PDFs/2015Report.pdf

California Department of Food and Agriculture (CDFA). (2016a). California's Top 10 Milk Producing Counties, Percent Share of California Milk Production, January-December 2015. Retrieved from https://www.cdfa.ca.gov/dairy/uploader/docs/DataChartsGraphs/Top_10_Counties_Milk_Production_2015.pdf

California Department of Food and Agriculture (CDFA). (2016b). California Agricultural Resource Directory 2015–2016. Retrieved from https://www.cdfa.ca.gov/Statistics/PDFs/2015Report.pdf

California Department of Food and Agriculture (CDFA). (2017). California Agricultural Statistics Review 2016–2017. Retrieved from https://www.cdfa.ca.gov/Statistics/PDFs/2016-17AgReport.pdf

California Department of Food and Agriculture (CDFA). (2018). California Agricultural Statistics Review 2017–2018. Retrieved from https://www.cdfa.ca.gov/Statistics/PDFs/2017-18AgReport.pdf

California Office of Environmental Health Hazard Assessment (OEHHA). (2017). CalEnviroScreen 3.0. Retrieved from https://oehha.ca.gov/calenviroscreen/sb535

California Water Code § 13173 (2012).

CalRecycle. (2020). Solid Waste Facilities, Sites, and Operations. Retrieved from https://www.calrecycle.ca.gov/SWFacilities/

Day, D. A., P.J. Wooldridge, and R.C. Cohen. (2008). Observations of the effects of temperature on atmospheric $HNO_3$, ΣANs, ΣPNs, and $NO_x$: evidence for a temperature-dependent $HO_x$ source. *Atmos. Chem. Phys., 8*, 1867-1879.

Davis, H. (2019). Golf course and hotel plan gets county's go-ahead for former Newport Beach landfill. *LA Times*. Retrieved from https://www.latimes.com/socal/daily-pilot/news/story/2019-10-15/golf-course-and-hotel-plan-gets-countys-go-ahead-for-former-newport-beach-landfill

Finch II, M. (2020). Widespread shutdown order slams California dairy farmers, 'You can't turn off the cows.' *The Sacramento Bee.* Retrieved from https://www.sacbee.com/news/california/article241896861.html

Identification and Listing of Hazardous Waste, 40 C.F.R. § 261.3 (2012).

Meyer, D., Price, P. L., Rossow, H. A., Silva-del-Rio, N., Karle, B. M., Robinson, P. H., ... & Fadel, J. G. (2011). Survey of dairy housing and manure management practices in California. *Journal of dairy science*, *94*(9), 4744-4750.

O'Neill, N. (2020). Farmers slaughter dairy cows amid coronavirus-fueled beef shortage. *New York Post.* Retrieved from https://nypost.com/2020/05/08/farmers-slaughter-dairy-cows-amid-coronavirus-beef-shortage/

Orange County Waste and Recycling (OCWR). (2020b). Landfills. Retrieved from http://www.oclandfills.com/landfills/closed-landfill-sites

Western Regional Climate Center (2008). Climate of California. Retrieved from https://wrcc.dri.edu/Climate/narrative_ca.php, accessed May 20th, 2009.

# 3. Analysis Methods

## 3.1 Preparation and Techniques

Samples were collected for every campaign (i.e., SARP, quarterly California coastline trips, dairy campaigns, and landfill campaigns) using 2-liter stainless steel canisters that had been specially fabricated, prepared, and maintained for air sampling. All samples were analyzed using gas chromatography and a variety of detectors, which are discussed below in more detail.

### 3.1.1 Canister Fabrication, Preparation, and Maintenance

All canisters used in this study were made of electropolished stainless steel and could hold a volume of two liters. Detailed canister fabrication methods can be found in Sive (1999). Each canister was fitted with a Nupro SS-4BG metal bellows valve that allowed it to be opened to collect air and closed to trap air. A photograph of a canister used for this work is shown in Figure 3.1.

**Figure 3.1** A photograph of a 2-liter stainless steel canister used for air sampling. Photograph by Brenna Biggs in 2018.

Before assembly, each valve was cleaned using distilled water, sonicated for 20 minutes, rinsed again with distilled water, and dried for 24 hours. Swagelock fittings connected the valves to the canisters. Each canister went through a series of leak checks. They were all checked for short-term leaks in the $10^{-2}$ torr range. For more long-term leak checks, canisters were evacuated to $10^{-2}$ torr and allowed to sit for 2 weeks prior to each sampling period. After two weeks, each canister was tested to ensure that it still maintained the vacuum.

Canisters are frequently conditioned to prevent the loss, isomerization, and growth of gases that could occur after samples are collected. They are baked at 150 °C overnight in humidified ambient air, which forms an oxidative layer on the canister's inner walls. This coating helps prevent the growth of gases within the canisters, particularly alkenes. This process is repeated every two years to renew the oxidative layer.

Samples in the canisters are typically analyzed within a month after collection. Gases reported are stable in the canisters during this time. After the samples are analyzed, the canisters are first evacuated and then flushed with ultra-high purity helium gas, which is flowed through stainless-steel tubing filled with a molecular sieve 5A and activated charcoal prior to its introduction to the canister. The tubing is immersed in liquid nitrogen, which ensures that the helium is pure before it flushes out the canisters. Following the helium flush, the canisters are re-evacuated to about $10^{-2}$ torr. After 2 weeks, they are checked for leaks and then they are ready for the next campaign.

**3.1.1a Special Note about Airborne Samples**

Canisters that will be used for airborne campaigns (e.g., SARP) undergo an additional step after being helium flushed and evacuated. The higher altitude associated with airborne campaigns means that samples are typically collected in conditions of lower relative humidity and lower temperature. To ensure consistency and precision in sample analysis, 18 torr of purified water vapor is added to each canister prior to airborne deployment. This extra step quenches

active sites within the canisters (Baker, 2008). Canisters used for source sampling at the ground level (i.e., at dairy farms, landfills, and the remote California coast) did not undergo this extra water-addition step.

### 3.1.2 On-Site Ambient Sampling Methods

All samples from quarterly coastline trips and at Orange County landfills were collected during the daytime under ambient conditions; no pump was used to pressurize the air and all samples were collected as single canister samples. To collect a sample, the researcher opened a canister's valve to let the air inside. Canisters took between 25 and 30 seconds to fill. The inlet was always faced away from the researcher and towards the wind during collection so that the sample would accurately reflect the composition of the air at that location.

All the Orange County landfill samples were collected above the landfill surface at a range of heights. Some of the samples used for this analysis were collected by Cal Poly SLO and were analyzed by Rowland-Blake group members. They also collected their samples using the Rowland-Blake group's 2-liter stainless steel canisters. They occasionally sampled raw LFG directly from the LFG transport tubes, and some of these samples were used in this analysis.

At the dairy farm, a mixture of ambient and pressurized air samples was collected. Both sample types were collected during the daytime using the same type of evacuated 2-liter stainless steel canisters. Ambient samples were collected on foot without using a pump. The dairy farm campaigns also utilized a mobile lab—a retrofitted Sprinter van owned and operated by University of California, Riverside—to collect pressurized samples. These pressurized samples were collected using a pump that was set up inside the mobile lab, whose exterior is shown in Figure 3.2.

**Figure 3.2** The mobile lab owned by University of California, Riverside. Used by the author to collect pressurized samples around the dairy farm using 2-liter stainless steel canisters. Photo by Brenna Biggs.

Among other instruments, the van also contained a Picarro Cavity Ringdown Spectrometer, which measured methane mixing ratios in real time. Knowing when methane was elevated helped inform when to collect a sample using the canisters. Samples were collected when methane was elevated as well as when methane was not very enhanced to proportionately capture all areas of the dairy. Pressurized samples at the dairy farm were collected by connecting thirty-two canisters as a “snake,” as shown in Figure 3.3A and 3.3B.

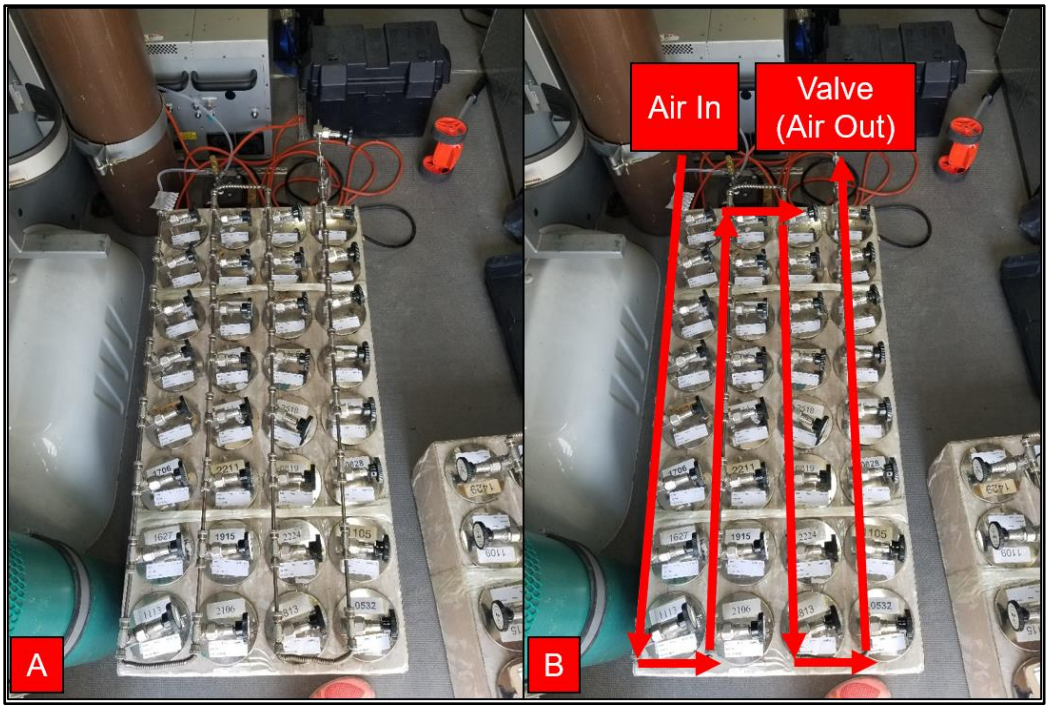


**Figure 3.3** A) Thirty-two canisters "snaked" up with tubing in the mobile lab and B) the "snake" labelled to show the direction of air. Photo by Brenna Biggs during the September 2019 dairy campaign.

Tubing from the inlet of the pump was inserted through the roof of the mobile lab, about 2.8 meters above the ground. As shown in Figure 3.3B, the outlet of the pump was connected to the snake tubing so that air from outside the van could be pumped through the snake. A valve and gauge were connected to the other end of the snake tubing. When the valve was closed, pressure built up within the snake. Once a canister was opened, the air rushed in to fill up a sample. Once the sampling period was complete (typically 30 to 45 seconds), the canister was closed, and the snake was reopened to let fresh air inside. For some samples, such as cow breath, the outside tubing was brought down from the mobile lab's roof and moved closer to the source to collect a sample. These samples were generally collected 3 to 6 inches away from the source.

### 3.1.3 Regional Airborne Sampling

Regional airborne data were obtained from low altitude flights, particularly over the SJV, from NASA SARP campaigns. Figure 3.4 shows four of the "snakes" locked upright during a NASA

DC-8 flight during SARP 2019. A similar configuration was used for most SARP campaigns. The DC-8 held, at most, seven “snakes” consisting of 24 evacuated 2-liter canisters each, for a potential total of 168 pressurized samples per flight.

**Figure 3.4** The author collecting a sample during SARP 2019 on the NASA DC-8 airplane. Photo by Megan Schill.

The “snake” tubing was connected to a forward-facing inlet mounted on the plane’s window frame. This inlet was attached to a pump, which brought in air from outside the plane to fill up one canister at a time. Like the mobile lab sampling strategy, the valve to the outlet was closed when the researcher was ready to collect a sample. Then, a canister was opened. The fill time varied by altitude, with a longer time (i.e., a minute or more) to fill up high and a shorter time (i.e., twenty seconds) to fill down low. Once the researcher was done collecting a sample, the canister was closed, and the outlet was reopened to let the “snake” flush. SARP flights from 2011, 2013, 2014, 2015, and 2017 with samples below 3,000 feet over the SJV were used for this research and were outlined in more detail in Table 2.1.

### 3.2 Trace Gas Analysis

Trace gases in ambient samples from the California coastline trips, landfills, and dairies as well as in pressurized samples from the dairy and NASA SARP were analyzed and interpreted for this study. All samples were analyzed using three different gas chromatography systems to quantify and identify trace gases. One gas chromatography system was used for the $CH_4$ analysis, one system was used for CO and $CO_2$ analysis, and a third system analyzed a variety of other non-methane hydrocarbons (NMHCs). Canisters were always first analyzed for $CH_4$, then CO and $CO_2$, and finally for NMHCs. These systems are described in more detail below. Samples analyzed for quarterly trips, which were typically collected at very remote and clean locations, were cooled prior to analysis by placing the canisters on a bed of dry ice to ensure that the amount of water vapor injected across all locations was equivalent.

#### 3.2.1 System for Methane Analysis

Methane was analyzed using a Hewlett Packard HP-5890 gas chromatograph (GC). To analyze a sample, a canister was attached to the system manifold, which was subsequently evacuated to $10^{-2}$ torr with the canister still closed. Typically, an aliquot of at least 400. torr was loaded onto the evacuated manifold and into a stainless-steel loop. For samples with extremely high concentrations of methane, a smaller aliquot was loaded to prevent overloading the system. The pressure was measured using a WIKA 1500 hi-precision-gauge-line pressure gauge (F.N. Cuthbert Inc., Toledo, OH). Excess sample was released in the manifold to bring the pressure of the aliquot to exactly 400. torr. The loop was then isolated, and the 400. torr sample was manually injected using a switching valve. When injected, nitrogen carrier gas flowed through the loop, bringing the sample into the GC where it entered the 0.9-meter, 80/100 mesh Spherocarb packed molecular sieve column. A photograph of the methane analysis system is shown in Figure 3.5.

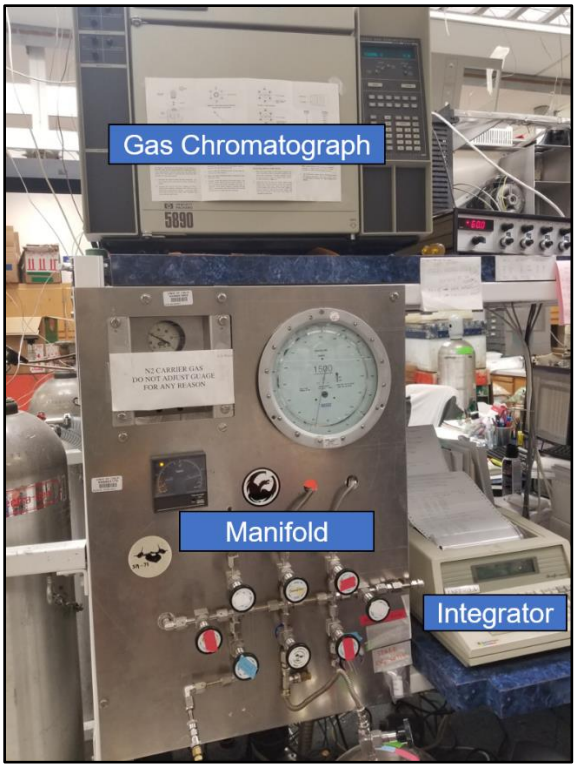


**Figure 3.5** The methane analysis system, including the gas chromatograph, manifold, and integrator in the Rowland-Blake laboratory at the University of California, Irvine. Photograph taken in 2020 by Brenna Biggs.

The GC temperature was kept at a constant 85 °C. Methane eluted quickly, after about one minute, and was detected by a flame ionization detector (FID). Peaks were integrated by a Spectra-Physics Chromjet Integrator, which reported peak height and peak area. The integrator is labelled in Figure 3.5. These values were recorded by hand. Methane mixing ratios were calculated by comparing the average peak height and area to those of a known working standard of 1.771 ppmv. For a more detailed description about the methane system, interested readers are directed to Blake (1984).

The methane analysis began with two “junk” runs. Then, a standard was injected and analyzed, followed by four canisters, followed by another standard, and so on until complete. Each “junk,” standard, and sample on the methane system was injected and analyzed twice in a row. If the peak height of the same sample differed by more than a response of 50 units (~0.2%) between the two runs, the sample was rerun.

### 3.2.2 System for Carbon Monoxide and Carbon Dioxide Analysis

Two GCs, each equipped with their own detector, were used for CO and $CO_2$ analysis. However, they were connected to the same manifold, which is shown in Figure 3.6.

**Figure 3.6** Manifold used for analysis of CO and $CO_2$ in the Rowland-Blake laboratory at the University of California, Irvine. Photograph taken in 2020 by Brenna Biggs.

To analyze a sample for CO and $CO_2$, a canister was attached to the manifold. While the canister remained closed, the manifold was evacuated to $10^{-2}$ torr. A WIKA 1500 hi-precision-gauge-line pressure gauge (F.N. Cuthbert Inc., Toledo, OH) was used to determine how much sample was loaded for analysis. Typically, a sample aliquot of at least 500. torr (occasionally less if mixing ratios were extremely elevated to prevent overloading the system) was introduced from the canister into the manifold, where it was then loaded into the CO and $CO_2$ loops and pumped down to exactly 500. torr. These loops were then isolated from the rest of the manifold before the sample was injected into both GCs. Run time for both CO and $CO_2$ systems was 7.6 minutes total.

This was then followed by a backflush period of about 2 minutes before the next sample was analyzed. More information about the CO and $CO_2$ analyses can be found in Chapter 3.2.2a and 3.2.2b, respectively.

**3.2.2a Carbon Monoxide Analysis**

The analysis of CO was performed using a Hewlett Packard HP-5890 GC. As detailed above in Chapter 3.2.2, the sample was loaded into the manifold and isolated. Pressure was released to trap a 500. torr aliquot, which was then injected into a 3-meter 80/100 mesh 5-angstrom molecular sieve column and carried through the column by helium gas to an FID. During the 7.6-minute runtime, the oven temperature ramped up from 60 °C to 110 °C. The atmospheric levels of CO are too low to be detected directly by an FID, so CO was reduced to $CH_4$ before reaching the detector. Methane is combusted more efficiently than CO in an FID flame. To reduce CO to $CH_4$, the outflow of the column was mixed with hydrogen gas and passed over a hot (365 °C) nickel catalyst. Thompson and Wood (1981) reported that the reduction efficiency is 100% at this temperature. During this process, the carbon monoxide was converted into methane gas in the following Reaction 3-1:

$$CO + 3H_2 \text{ (with Ni catalyst)} \rightarrow CH_4 + H_2O \qquad \text{Reaction 3-1}$$

After this reaction, the sample reached the detector, where CO (as $CH_4$) was detected by the FID. To prevent oxygen in the samples from deactivating the nickel catalyst, a switching valve was attached to the end of the column to divert oxygen back into the laboratory rather than send it to the catalyst. The same switching valve also let additional helium carrier gas to flow over the catalyst and the detector while oxygen eluted. Once oxygen had finished eluting, the switching valve was turned to redirect the column outflow over the catalyst and to the FID. The response of CO (as $CH_4$) was recorded using Thermo Dionex Chromeleon software on a computer. The peak corresponding to CO on the chromatogram was manually inspected and integrated to determine the area, which was both manually recorded and saved digitally on the computer. After a sample

was detected, helium carrier gas was backflushed through the column to push any $CO_2$ back out into the laboratory, which prevented elution of carbon dioxide from the column. Carbon dioxide could also be reduced by the nickel catalyst to $CH_4$, so it was important that $CO_2$ did not have an opportunity to reach the catalyst. Backflushing for two minutes prevented this from occurring.

At the start of an analysis day, two “junk” samples were injected first to ensure the system was working properly. These “junk” samples were loaded from the same cylinder as the standard but were not used for the analysis. Following the “junks,” a standard with a known amount of CO, 204 ppbv, was analyzed first before sample analysis began. Once the standard was injected and inspected, eight canisters were subsequently injected before another standard was analyzed, and then eight more samples, another standard, and so on. This process continued until canister analysis was completed for the day, always ending on a standard. Unknown mixing ratios of CO in the samples were determined through comparison to the standards. At the end of analysis, the oven temperature was raised to 150 °C to remove any possible $CO_2$ that accumulated on the column.

**3.2.2b Carbon Dioxide Analysis**

To analyze the amount of $CO_2$ present in a sample, an aliquot from the canister was loaded and isolated from the rest of the CO/$CO_2$ manifold in an 1/8-inch stainless steel loop. Pressure was released to trap a 500. torr aliquot, which was then injected into a Hewlett Packard HP-5890 GC equipped with a 2-meter 80/100 Carbosphere packed column. During the 7.6-minute runtime, the oven temperature ramped up from 150 °C to 220 °C. Once eluted from the column, $CO_2$ was detected by a thermal conductivity detector (TCD). The TCD compared the thermal conductivity of the sample to a reference, the helium carrier gas. When the resistance changed as the analyte passed over the filament, the voltage changed. This voltage change was converted to a signal and reported as a peak on the chromatogram. Similar to the CO analysis, the $CO_2$ peak was

manually inspected and integrated using Thermo Dionex Chromeleon software on the same computer.

As previously mentioned, the GC for CO analysis and the GC for $CO_2$ analysis were controlled from the same manifold. This means that the connected "junk," standard, or sample was sent to both systems simultaneously and only needed to be loaded once to be analyzed on both GCs. Therefore, the $CO_2$ analysis also began with two "junk" runs followed by one standard, eight samples, one standard, eight samples, one standard, and so on until complete, always ending on a standard. To determine mixing ratios of $CO_2$, the $CO_2$ peak on the sample's chromatogram was compared to the $CO_2$ peak on the standard's chromatograms. The standard contained either 364 ppmv or 375 ppmv of $CO_2$, depending on when the sample was analyzed; a different standard was used for more recent samples than for less recent samples.

### 3.2.3 System for Non-Methane Hydrocarbon (NMHC) Analysis

The Rowland-Blake lab has two identical NMHC analysis systems, "System 1" and "System 2." System 1 was used for source samples collected at locations expected to have very enhanced mixing ratios, like the dairy farm and landfill. System 2 was used for cleaner airborne sample analysis and the remote California coastline trip samples. Both systems contained three Hewlett-Packard 6890 GCs. Each GC had different detection methods, columns, and compounds measured. A diagram outlining the three gas chromatographs used for System 1 and 2 is shown in Figure 3.7.

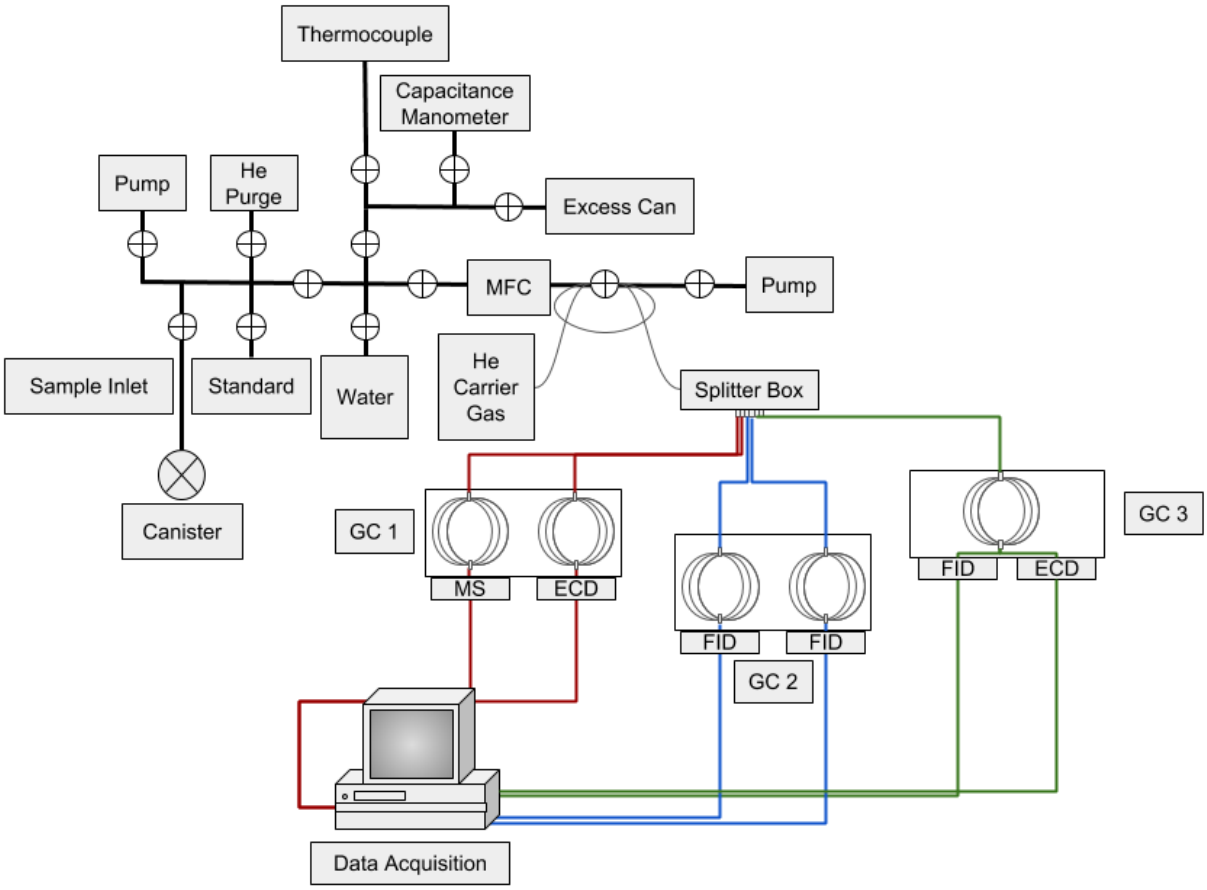


**Figure 3.7** A diagram of the three gas chromatographs used for NMHC analysis.

System 1 and 2 had identical analysis protocols. Each began with two "junk" runs and one standard run before beginning sample analysis. Up to eight samples followed the standard before the next standard was injected. When a "junk," standard, or sample was ready to be analyzed, it was first loaded onto the evacuated manifold. Pressures of the loaded samples ranged from 100.0 torr to 900.0 torr. Airborne and remote samples required higher amounts of sample to distinguish the lower analyte concentrations. Dairy and landfill samples required a lower amount; typically, between 400.0 torr and 600.0 torr was injected for analysis. Regardless of pressure, a turn of the switching valve directed the air to a 5 $cm^3$ preconcentration loop packed with glass beads. The loop was submerged in liquid nitrogen to keep it at 77 K for two minutes prior to sample introduction. This step removed highly volatile "bulk" gases like $O_2$, $N_2$, and argon, but condensed the trace gases of interest on the glass beads.

After the bulk gases were removed, the liquid nitrogen was replaced by water at near-boiling temperature, which caused the loop to heat back up and volatilize the trace gases of interest. Then, the oven temperature in the 3 GCs cooled down to their respective initial temperatures. The sample was injected from the loop to a splitter box using helium carrier gas. The splitter box consistently divided the sample and directed it to one of the three GCs for separation. The total runtime for one airborne or remote coastline sample on System 2 was 17.6 minutes, but the runtime for a landfill or dairy sample on System 1 was 19.5 minutes. The runtime on System 1 was longer to include the analysis of less volatile biogenic gases that eluted after 17.6 minutes.

Each GC contained two columns. Each column had its own detector: FID, electron capture detector (ECD), or mass spectrometer (MS). In general, the FIDs detected hydrocarbons, the ECDs detected alkyl nitrates, nitrous oxide, or halocarbons, and MS identified many different gases using their mass-to-charge ratio. Like the other analysis systems that were previously described, the raw data from the NMHC analysis were inspected and manually integrated as a chromatogram using Thermo Dionex Chromeleon software. A close-up example of a chromatogram collected from 15.34 minutes to 18.07 minutes for a typical sample using the DB-1 column and FID detector from GC 2 is shown in Figure 3.8. Each peak of every sample was manually inspected, integrated, and labelled for every chromatogram created by the response of each detector. Note that peaks are well-resolved despite their quantity.

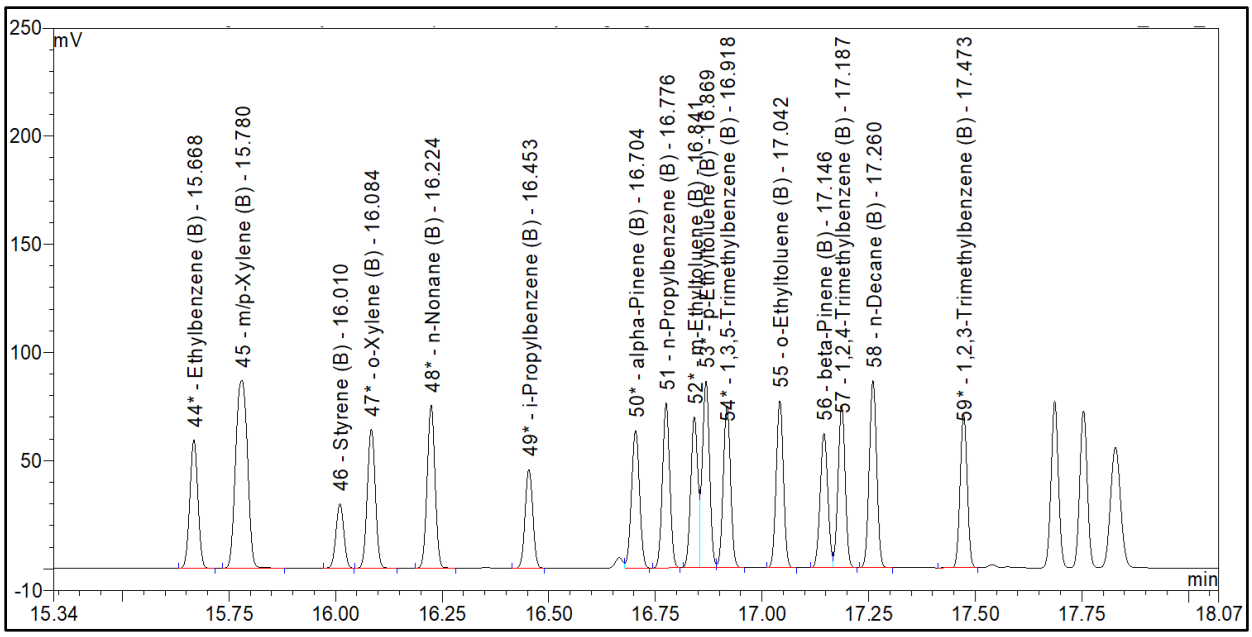


**Figure 3.8** An example of a typical chromatogram from 15.34 minutes to 18.07 minutes using the DB-1 column and FID detector during NMHC analysis of source samples.

Although the methods of injection were the same for System 1 and System 2, special focus is given here to the analysis methods for System 1, as it was used to analyze all the dairy and landfill samples. For more information on the parameters used for System 2, which was used to analyze remote coastline and airborne samples, readers are directed to Hughes (2018). The analysis methods between System 1 and 2 had a few differences: the runtime on System 1 was longer, System 1 had a special column installed to measure $N_2O$, and System 2 used both columns in GC 2. The parameters for the gas chromatographs used in System 1 are shown in Table 3.1.

**Table 3.1** Parameters for the gas chromatographs used in System 1

| Parameter | GC #1 | GC #2 | GC #3 |
|---|---|---|---|
| Temperature 1 (ºC) | -60 | -60 | -20 |
| Wait time 1 (min) | 1.5 | 1.5 | 1.5 |
| Rate 1 (ºC/min) | 15 | 10 | 30 |
| Temperature 2 (ºC) | 110 | 0 | 60 |
| Wait time 2 (min) | 0 | 0 | 0 |
| Rate 2 (ºC/min) | 29 | 17 | 14 |
| Temperature 3 (ºC) | 220 | 145 | 200 |
| Wait time 3 (min) | 2.9 | 0 | 5.8 |
| Rate 3 (ºC/min) | - | 65 | - |
| Temperature 4 (ºC) | - | 220 | - |
| Wait time 4 (min) | - | 2.3 | - |

### 3.2.4 Compounds Analyzed for All Systems

The $CH_4$, $CO/CO_2$, and NMHC systems were used to analyze all samples from the California coastline trips, SARP, landfills, and the dairy farm. Table 3.2 summarizes some of the gases that each system measured. The instruments in the Rowland-Blake lab can measure many gases with great sensitivity. The precision and accuracy for many hydrocarbons measured by the Rowland-Blake lab are presented in Colman et al. (2001).

**Table 3.2** An example of compounds measured by the three GC systems with their respective limits of detection (LODs) for System 1. All LODs are in units of ppt unless noted.

| GC # | Detector | Column | Compound (LOD) | |
|---|---|---|---|---|
| 1 | MS | DB-5-MS | OCS (50)<br>HFC-134a (1)<br>HFC-152a (1)<br>$CHCl_3$ (0.10)<br>$CH_3CH_2Cl$ (0.10)<br>$CH_2Cl_2$ (1)<br>$CH_2Br_2$ (0.10)<br>$CHBr_3$ (0.10)<br>$C_2HCl_3$ (0.10)<br>$CH_3Br$ (0.1)<br>1,2-DCE (0.1)<br>MIBK (0.1)<br>1-Pentene (10)<br>Isoprene (10) | Ethylbenzene (10)<br>m/p-Xylene (10)<br>o-Xylene (10)<br>3-Ethyltoluene (10)<br>4-Ethyltoluene (10)<br>α-Pinene (10)<br>Methanol (10)<br>Ethanol (10)<br>Limonene (10)<br>Butanal (10)<br>Butanone (10)<br>2-Butanol (10)<br>Acetone (10)<br>Acetaldehyde (10) |
| | ECD | DB-5, Rtx-1701 | $CHCl_3$ (0.10)<br>$CCl_4$ (1)<br>$C_2Cl_4$ (0.10)<br>$CH_3I$ (0.10) | $MeONO_2$ (0.1)<br>$EtONO_2$ (0.1)<br>i-$PrONO_2$ (0.1)<br>n-$PrONO_2$ (0.1) |
| 2 | FID | DB-1 | DMS (1)<br>$CH_3Cl$ (50)<br>1-Pentene (10)<br>Isoprene (10)<br>Toluene (10) | α-Pinene (10)<br>Methanol (10)<br>Ethanol (10)<br>Acetaldehyde (10) |
| 3 | ECD | PLOT, DB-1 | $N_2O$ (50 **ppb**) | |
| | FID | PLOT | Ethane (10)<br>Ethene (10)<br>Ethyne (10)<br>Propane (10)<br>Propene (10)<br>i-Butane (10)<br>n-Butane (10)<br>1-Butene (10)<br>i-Butene (10) | trans-2-butene (10)<br>cis-2-butene (10)<br>i-Pentane (10)<br>n-Pentane (10)<br>1-Pentene (10)<br>Isoprene (10)<br>n-Hexane (10)<br>n-Heptane (10)<br>Benzene (10) |
| $CH_4$ | FID | Packed Molecular Sieve | $CH_4$ (0.010 **ppm**) | |
| $CO_x$ | TCD | Packed Molecular Sieve | $CO_2$ (10 **ppm**) | |
| | FID | Packed Molecular Sieve | CO (1 **ppb**) | |

For the landfills and dairy farms analyzed in this project, one of the FID detectors on GC 2 was not used in the analysis. The ECD on GC 3 was used to measure $N_2O$, which was an addition specific to the landfill and dairy trace gas analyses. System 2 was not equipped to measure $N_2O$, so that gas was not included for remote coastline or airborne data analysis.

### 3.3 Target Compounds

As shown in Table 3.2, there was a wide range of gases to choose from for this research thanks to the highly selective and sensitive equipment in the Rowland-Blake laboratory. The

following gases were a priority for this study: methane, carbon dioxide, ethanol, acetaldehyde, methanol, dimethyl sulfide, carbonyl sulfide, and nitrous oxide. These gases are discussed in more detail below. Methane and carbon dioxide have been shown to be emitted from dairy farms and waste management industries. They are also typically targeted in GHG legislation. Therefore, it is important to narrow down their sources and enhancements at landfills and dairy farms and assess how their emissions could be reduced.

Ethanol, methanol, and acetaldehyde are short-lived oxygenates that are harmful to human health and the environment. Previous Rowland-Blake lab member Melissa Yang confirmed that these gases are found at dairy farms (Yang, 2009). Their enhancements at dairy farms, landfills, and at the regional scale is important for statewide air quality and residential well-being, particularly for disadvantaged communities that may live near their sources. Dimethyl sulfide is typically an oceanic gas, but previous SARP campaigns have shown it can be elevated at low altitudes inland, which may imply some interesting sources in the SJV.

Carbonyl sulfide is a prominent atmospheric sulfur-containing gas, but not all its sources are understood (Lennartz et al., 2017). Understanding possible carbonyl sulfide emissions from unlikely sources in California could help to narrow this knowledge gap. Lastly, nitrous oxide is a potent GHG with a long lifetime. It is typically considered negligible from landfills and some parts of dairies. This study explores whether that should be reconsidered.

### 3.3.1 Methane ($CH_4$)

Dairy farms and landfills are nontrivial sources of methane gas. It has long been known that farming, particularly of ruminant animals such as cows, is an important source of methane in the atmosphere. This methane is released through two different pathways: enteric fermentation and manure management. Enteric fermentation occurs within the digestive tract of ruminant animals, such as cattle, sheep, pigs, buffalo, and goats. Their digestive systems contain a special stomach called a *rumen*. The rumen digests carbohydrates, particularly cellulose and

hemicellulose, and then reprocesses them into useable nutrients for the animal. This enteric fermentation process produces methane as a byproduct. The animal then burps, exhales, or passes the methane as gas (CARB, 2019). The amount of methane that the animal produces can be affected by the animal's breed, age, activity level, pregnancy status, and feed.

Through another pathway at dairy farms, $CH_4$ can be emitted from animal waste, known as manure, during anaerobic decomposition (Eggleston et al., 2006). Most of the dairies in the SJV use slurries and lagoons as their manure management strategy (Meyer et al., 2011). In general, the higher the storage temperature of the slurries and manure, the higher the potential for $CH_4$ production (Chadwick et al., 2011). Recent field studies have suggested that $CH_4$ emissions specifically from manure management may be underestimated by a factor of 2 (Owen & Silver, 2015). Therefore, it is important to understand more about these emissions at dairy farms.

Landfills also emit $CH_4$ as a byproduct of waste decomposition. This occurs when waste decomposes on the surface of the landfill during active dumping, and long afterward within the ground as an LFG component (Lisk, 1991; Crawford & Smith, 2016; Farquhar & Rovers, 1973). Regardless of its source, methane is undoubtedly a very important GHG. Although its lifetime is shorter than that of $CO_2$, it is between 72 and 84 times more efficient at trapping radiation (thereby warming the earth) over a 20-year period (Eggleston et al., 2006; Myhre et al., 2013).

Not only is $CH_4$ an important GHG, but it is also reactive in the atmosphere and has a lifetime of under a decade (Blake, 1984). One of the main sinks of $CH_4$ is the hydroxyl radical. Methane reacts with the hydroxyl radical to create a methyl radical and water, as shown in Reaction 3-2.

$$CH_4 + \bullet OH \rightarrow \bullet CH_3 + H_2O \qquad \text{Reaction 3-2}$$

The methyl radical is highly unstable in the atmosphere and undergoes reactions that can eventually create ozone, which has its own associated health effects and issues (Lippmann,

1989). One methane molecule, when oxidized, can yield at least two molecules of ozone, as shown in Reaction 3-3 (Seinfeld & Pandis, 2016):

$$CH_4 + 4O_2 + 2h\nu \rightarrow HCHO + 2O_3 + H_2O \qquad \text{Reaction 3-3}$$

Previous studies have shown that methane can be used as a tracer gas for dairy identification to study other gases, such as ethanol. Both methane and ethanol appeared to correspond with each other even at high altitudes and away from the dairy (Yang, 2009).

### 3.3.2 Carbon Dioxide ($CO_2$)

Carbon dioxide is one of the most important GHGs. It can be emitted biogenically (e.g., from decomposition, ocean release, and respiration) or anthropogenically (e.g., cement production, fossil fuel combustion, and land use changes). Carbon dioxide sinks include terrestrial ecosystems, particularly plants, as well as the ocean (Finlayson-Pitts & Pitts, 1999; Seinfeld & Pandis, 2016). The lifetime of carbon dioxide is often controversial because of the time it takes to equilibrate with the ocean and plants, which can also release carbon dioxide. Overall, the reported relaxation time for carbon dioxide to reach a new steady state in the atmosphere is calculated to be between 34 and 44 years (Seinfeld & Pandis, 2016).

Carbon dioxide emissions follow a seasonal pattern. During summer in the Northern Hemisphere, atmospheric carbon dioxide decreases worldwide as plants incorporate it into their leaves, stems, roots, and eventually the soil. However, during the winter in the Northern Hemisphere, photosynthesis is limited to the tropical regions. The Southern Hemisphere contains fewer green spaces than the Northern Hemisphere, so carbon dioxide uptake decreases. Therefore, carbon dioxide typically increases globally from October to January each year. In 2020, average carbon dioxide levels exceeded 410 ppm worldwide.

Carbon dioxide was selected as a gas of interest for this work because numerous studies from all over the world have reported it at landfills and dairy farms. For example, landfills in Finland, Taiwan, Italy, and California have reported enhanced carbon dioxide coming from the

decomposing waste and landfill cover materials (Lohila et al., 2007; Hegde et al., 2003; Lombardia et al., 2011; Bogner et al., 2011). At dairy farms, carbon dioxide is known to be emitted from animal exhalation and the respiration of soil, plants, and manure microbes (Chianese et al., 2009a). The prevalence of carbon dioxide at both types of study sites made it an important gas to investigate for this work.

### 3.3.3 Ethanol

The transportation sector is one of the main sources of ethanol in the atmosphere. Over 98% of gasoline in the United States contains ethanol (typically at 10% ethanol and 90% gasoline). Ethanol is added to reduce the vehicular emissions of volatile organic compounds and carbon monoxide (United States Department of Energy, 2020). However, ethanol is also found on dairy farms. Previous research conducted by the Rowland-Blake laboratory has shown that silage is a prominent source of ethanol—as well as methanol, acetone, and acetaldehyde—on dairy farms in California (Yang, 2009). Silage is a type of fodder, or feed, typically for ruminant animals. It can be made of grass or crop waste, like corn or alfalfa, that has been fermented (Kung, 2018).

Ethanol, as well as other oxygenated species, is produced during the fermentation process. Organic matter, which is found in abundance at landfills as decomposing waste and cover material, also has been shown to emit ethanol (Chester & Martin, 2009). Ethanol's prevalence at both sample areas as well as its importance in the atmosphere make it an interesting gas to include for this study.

Meier et al. (1985) and Atkinson (1997a) showed that ethanol in the atmosphere reacts with the hydroxyl radical to first primarily make an α-hydroxyalkyl radical, as shown in Reaction 3-4 (Meier et al., 1985; Atkinson, 1997a):

$$C_2H_5OH + \bullet OH \rightarrow CH_3CHOH + H_2O \qquad \text{Reaction 3-4}$$

Following this reaction, the α-hydroxyalkyl radical reacts with oxygen to form acetaldehyde and a hydroperoxyl radical in Reaction 3-5 (Grosjean, 1997):

$$CH_3CHOH + O_2 \rightarrow CH_3CHO + HO_2\bullet \qquad \text{Reaction 3-5}$$

The average atmospheric lifetime of ethanol in the atmosphere is around 4 days, but it could be as low as 2.4 days depending on atmospheric conditions (Grosjean, 1997; Seinfeld & Pandis, 2016). The main oxidation product, acetaldehyde, has a high ozone forming potential and is discussed below.

### 3.3.4 Acetaldehyde

Acetaldehyde is the second most abundant aldehyde in the atmosphere, following formaldehyde (Finlayson-Pitts & Pitts, 1999). Vehicles are a major source of acetaldehyde, but it can also be emitted biogenically from plant leaves, grasses, clovers, oaks, and pines (Kirstine et al., 1998; Seinfeld & Pandis, 2016; Kesselmeier et al., 1997). As previously mentioned, acetaldehyde can also be made when ethanol is oxidized by the hydroxyl radical in the atmosphere.

Typical acetaldehyde mixing ratios vary by location. Urban areas contain more acetaldehyde than suburban or rural areas, which contain more than remote areas. Studies around the United States have shown that the average mixing ratios of acetaldehyde in suburban or rural areas, such as those seen within the SJV, are between 0.1 and 4 ppb (Apel et al., 1998; Riemer et al., 1998; Goldan et al., 1995; Fried et al., 1997; Grosjean et al., 1996; Lee et al., 1995). Landfills in Orange County are in mostly urban or suburban areas. Enhanced levels of acetaldehyde are expected but could be further enhanced by decomposition at the landfill. According to CARB, acetaldehyde is a toxic air contaminant and a probable carcinogen (CARB, 2020).

The average atmospheric residence time for acetaldehyde is 10 hours. It can react with hydroxyl radicals (rate constant $k = 1.6 \times 10^{-11}$ $cm^3$ $molec^{-1}$ $s^{-1}$), $NO_3$ ($k = 1.6 \times 10^{-11}$ $cm^3$ $molec^{-1}$ $s^{-}$

[1]), or the chlorine radical ($k$ = 7.2 x $10^{-11}$ $cm^3$ $molec^{-1}$ $s^{-1}$) through hydrogen abstraction shown in Reaction 3-6 (Atkinson, 1994; Atkinson et al., 1997b; Finlayson-Pitts & Pitts, 1999).

$$CH_3CHO + \bullet OH\ (NO_3\bullet, Cl\bullet) \rightarrow CH_3CO\bullet + H_2O\ (HNO_3, HCl) \qquad \text{Reaction 3-6}$$

The $CH_3CO\bullet$ radical can go on to react further with $NO_x$, eventually creating peroxyacytyl nitrate (PAN), a toxic compound and an important component of smog (Finlayson-Pitts & Pitts, 1999).

### 3.3.5 Methanol

According to CARB, methanol is a toxic air contaminant and a probable carcinogen (CARB, 2020). Like acetaldehyde, methanol can be biogenically emitted from plants, including grasses, clovers, plant leaves, oaks, and pines, among other sources (Nemecek-Marshall et al., 1995; Fall & Benson, 1996; Kesselmeier et al., 1997; Kirstine et al., 1998). Methanol can also react with the hydroxyl radical (rate constant $k$ = 9.3 x $10^{-13}$ $cm^3$ $molec^{-1}$ $s^{-1}$), $NO_3$ ($k$ = 2.4 x $10^{-16}$ $cm^3$ $molec^{-1}$ $s^{-1}$), and the chlorine radical ($k$ = 5.5 x $10^{-11}$ $cm^3$ $molec^{-1}$ $s^{-1}$) (Atkinson et al., 1997b; Atkinson, 1994; Bierbach et al., 1992). The average lifetime of methanol in the atmosphere is about two weeks (Seinfeld & Pandis, 2016).

The reaction of methanol with the hydroxyl radical proceeds through hydrogen atom abstraction followed by a reaction with oxygen to make formaldehyde (HCHO) and the hydroperoxyl radical, as shown in the overall Reaction 3-7 (Atkinson, 1989; Mellouki et al., 2003).

$$CH_3OH + \bullet OH + O_2 \rightarrow H_2O + HO_2\bullet + HCHO \qquad \text{Reaction 3-7}$$

Assuming that methanotrophic bacteria are likely present at both dairy farms and landfills, it seems likely that methanol could be emitted from the decomposing organic material and possibly from solvent dumping.

### 3.3.6 Dimethyl Sulfide (DMS)

Marine inhabitants, such as phytoplankton, are prominent emitters of dimethyl sulfide (DMS), an important form of reduced sulfur in the atmosphere (Finlayson-Pitts & Pitts, 1999). Terrestrial biogenic sources are typically assumed to be quite small in comparison. However,

recent studies have revealed the possibility of DMS emissions from ruminant animals, like dairy cows. A study in the United Kingdom showed that cows in more developed parts of the world are fed diets higher in protein, which typically have a higher amount of sulfur-containing amino acids. Cows expel this excess sulfur when they ruminate (Hobbs & Mottram, 2000). It is therefore especially important to determine whether DMS is emitted by cows in the SJV. Understanding DMS sources from volatilization and decomposition in the waste management industry is also important to identify additional inland sources. Therefore, it is important to study DMS emissions at landfills as well.

Some major sinks of DMS in the atmosphere are hydroxyl radicals in the daytime (lifetime 1/*e*, $\tau$ = 2 days) and $NO_3$ radicals in the nighttime (lifetime 1/*e*, $\tau$ = 10 hours) (Atkinson et al., 1997b). DMS can be oxidized to $SO_2$, which can lead to sulfuric acid and sulfate particle formation. Sulfate particles can take between three and sixteen days to undergo deposition, which means that they have time to travel significant distances. Wet deposition can lead to acid rain, and dry deposition can lead to inhalation by humans, which is correlated with adverse health effects (Rodhe, 1978). DMS can also be oxidized to other low-volatility products, such as methanesulfonic acid, which can lead to the formation of cloud condensation nuclei (Finlayson-Pitts & Pitts, 1999). DMS is an important climate gas that should perhaps be recognized as more than simply a “marine gas” to fully understand its sources.

### 3.3.7 Carbonyl Sulfide (OCS)

Direct sources of OCS emissions include natural sources such as oceans, wetlands, volcanoes, and anoxic soils, as well as anthropogenic sources such as burning rubber and oil and gas refineries. Indirect sources of OCS may include the oxidation of $CS_2$ and DMS. However, it is assumed that the *dominant* source of OCS is the ocean (Lennartz et al., 2017). Carbonyl sulfide is commonly found in cold water; in warm water, the OCS molecule forms but often falls apart

before outgassing into the atmosphere. Total ocean flux is estimated to be between 235 and 289 Gg S $yr^{-1}$ (Suntharalingam et al., 2008; Berry et al., 2013; Kuai et al., 2015; Glatthor et al., 2015).

Major sinks include vegetative uptake and oxic soils (Brown & Bell, 1986; Protoschill-Krebs & Kesselmeier, 1992; Campbell et al., 2008). Minor sinks include photolysis and reaction with the hydroxyl radical (Chin & Davis, 1993; Watts, 2000; Kettle et al., 2002). Because the vegetative uptake process also destroys OCS, the molecule is an important proxy for $CO_2$, which is not necessarily destroyed during the uptake process (Von Hobe et al., 1999; Lennartz et al., 2017).

OCS is the most abundant source of sulfur in the atmosphere and the main source of sulfur for the stratospheric aerosol layer, which is thought to be important in combatting climate change. It is also a GHG, and its potential heating and cooling effects are thought to currently be in balance (Lennartz et al., 2017). Carbonyl sulfide exhibits an annual cycle, but its interannual and decadal variation is low (Montzka et al., 2007). The average worldwide mixing ratio varies seasonally, but it is on average 500 ppt (Von Hobe et al., 1999; Lennartz et al., 2017).

Although OCS emissions globally are thought to be balanced, a recent re-evaluation of the contribution of vegetative uptake has revealed that OCS may have an unknown missing source between 230 Gg S $yr^{-1}$ and 800 Gg S $yr^{-1}$ (Lennartz et al., 2017). Previous studies have assumed that this missing source comes exclusively from the ocean to provide total ocean fluxes of between 465 and 1089 Gg S $yr^{-1}$ (Suntharalingam et al., 2008; Berry et al., 2013; Kuai et al., 2015; Glatthor et al., 2015). This implies that the missing source of OCS is at least the same as the known ocean flux, and in some estimates more than double the estimated ocean emissions. Although previous work has assumed that the missing source can be found simply in a different part of the ocean, it is possible that the missing source is instead composed of a variety of different sources, some of which might be located inland. This work explores whether dairy farms and landfills could contribute, even minutely, to this missing source.

### 3.3.8 Nitrous Oxide ($N_2O$)

Nitrous oxide is an important GHG, with a relatively long lifetime of 120 years and a global warming potential (GWP) of 298 at the 100-year scale, making it a much more potent GHG than $CO_2$ or even $CH_4$ (Minschwaner et al., 1993; Myhre et al., 2013). Nitrous oxide has increased by 20% since the pre-industrial 1750s, rising from 270 ppb to 331 ppb by 2018 (Prinn et al., 2018). While nitrous oxide has a variety of anthropogenic and natural sources, some of the most intriguing are the emissions from manure management at dairy farms. These emissions are produced directly and indirectly. Directly, $N_2O$ can be emitted as part of the nitrogen cycle in animal feces and urine. Indirectly, $N_2O$ is emitted during the volatilization of the nitrogen in the manure and as a byproduct during the subsequent decomposition of emitted gases. Additionally, $N_2O$ can be emitted indirectly from water leached from manure into groundwater systems (EPA, 2020c)

Total $N_2O$ emissions in 2018 from the manure management of dairy cows in the United States were estimated to be 6.1 million metric tons of $CO_2$ equivalent (MMT $CO_2e$), which is a 15% increase from 1990 levels (EPA, 2020c). At the farm level, $N_2O$ is often emitted from the nitrification and denitrification of soil. Nitrous oxide can also be emitted from the waste management sector, particularly from anaerobic parts of landfills. However, the contribution of $N_2O$ emissions to the total GHG emissions at landfills is thought to be trivial compared to the $CH_4$ and $CO_2$ emissions. Nitrous oxide emissions at landfills were not included in the latest 2020 EPA Greenhouse Gas Inventory (EPA, 2020c). However, as decomposition still occurs on the surface of landfills where rogue gases can escape, this project also analyzes $N_2O$ emissions at landfills in Orange County.

### 3.4 References


Apel, E. C., Calvert, J. G., Riemer, D., Pos, W., Zika, R., Kleindienst, T. E., ... & Starn, T. K. (1998). Measurements comparison of oxygenated volatile organic compounds at a rural site during the 1995 SOS Nashville Intensive. *Journal of Geophysical Research: Atmospheres*, *103*(D17), 22295-22316.

Atkinson, R. (1989). Kinetics and mechanisms of the gas-phase reactions of the hydroxyl radical with organic compounds. *Journal of Physical and Chemical*.

Atkinson, R. (1994). Gas-phase tropospheric chemistry of organic compounds. *J. Phys. Chem. Ref. Data, Monograph*, *2*, 1-216.

Atkinson, R. (1997a). Gas-phase tropospheric chemistry of volatile organic compounds: 1. Alkanes and alkenes. *Journal of Physical and Chemical Reference Data*, *26*(2), 215-290.

Atkinson, R., Baulch, D. L., Cox, R. A., & Hampson, R. (1997b). FJ, Kerr, J. A., Rossi, MJ, and Troe, J.: Evaluated kinetic and photochemical data for atmospheric chemistry: supplement VI. IUPAC subcommittee on gas kinetic data evaluation for atmospheric chemistry. *J. Phys. Chem. Ref. Data*, *26*, 1329-1499.

Baker, A. K. (2008). Ground-based and aircraft measurements of volatile organic compounds in United States and Mexico City urban atmospheres.

Berry, J., Wolf, A., Campbell, J. E., Baker, I., Blake, N., Blake, D., ... & Stimler, K. (2013). A coupled model of the global cycles of carbonyl sulfide and CO2: A possible new window on the carbon cycle. *Journal of Geophysical Research: Biogeosciences*, *118*(2), 842-852.

Bierbach, A., Barnes, I., & Becker, K. H. (1992). Rate coefficients for the gas-phase reactions of hydroxyl radicals with furan, 2-methylfuran, 2-ethylfuran and 2, 5-dimethylfuran at 300±2 K. *Atmospheric Environment. Part A. General Topics*, *26*(5), 813-817.

Blake, D. (1984). Increasing concentrations of atmospheric methane, 1979-1983 (Doctoral dissertation, Ph. D., thesis, University of California, Irvine).

Bogner, J. E., Spokas, K. A., & Chanton, J. P. (2011). Seasonal greenhouse gas emissions (methane, carbon dioxide, nitrous oxide) from engineered landfills: Daily, intermediate, and final California cover soils. *Journal of environmental quality*, *40*(3), 1010-1020.

Brown, K. A., & Bell, J. N. B. (1986). Vegetation—the missing sink in the global cycle of carbonyl sulphide (COS). *Atmospheric Environment (1967)*, *20*(3), 537-540.

California Agency Air Resources Board (CARB). (2019). California Greenhouse Gas Emissions for 2000 to 2017. Retrieved from https://ww3.arb.ca.gov/cc/inventory/pubs/reports/2000_2017/ghg_inventory_trends_00-17.pdf

California Agency Air Resources Board (CARB). (2020). CARB Identified Toxic Air Contaminants. Retrieved from https://ww2.arb.ca.gov/resources/documents/carb-identified-toxic-air-contaminants

Campbell, J. E., Carmichael, G. R., Chai, T., Mena-Carrasco, M., Tang, Y., Blake, D. R., ... & Berry, J. A. (2008). Photosynthetic control of atmospheric carbonyl sulfide during the growing season. *Science*, *322*(5904), 1085-1088.

Chadwick, D., Sommer, S., Thorman, R., Fangueiro, D., Cardenas, L., Amon, B., & Misselbrook, T. (2011). Manure management: Implications for greenhouse gas emissions. *Animal Feed Science and Technology*, *166*, 514-531.

Chester, M., & Martin, E. (2009). Cellulosic ethanol from municipal solid waste: a case study of the economic, energy, and greenhouse gas impacts in California.

Chianese, D. S., Rotz, C. A., & Richard, T. L. (2009a). Simulation of nitrous oxide emissions from dairy farms to assess greenhouse gas reduction strategies. *Transactions of the ASABE, 52*(4), 1325-1335.

Chin, M., & Davis, D. D. (1993). Global sources and sinks of OCS and CS2 and their distributions. *Global Biogeochemical Cycles*, *7*(2), 321-337.

Colman, J. J., Swanson, A. L., Meinardi, S., Sive, B. C., Blake, D. R., & Rowland, F. S. (2001). Description of the analysis of a wide range of volatile organic compounds in whole air samples collected during PEM-Tropics A and B. *Analytical Chemistry*, *73*(15), 3723-3731.

Crawford, J. F., & Smith, P. G. (2016). *Landfill technology*. Elsevier.

Eggleston, S., Buendia, L., Miwa, K., Ngara, T., & Tanabe, K. (Eds.). (2006). *2006 IPCC guidelines for national greenhouse gas inventories* (Vol. 5). Hayama, Japan: Institute for Global Environmental Strategies.

Environmental Protection Agency (EPA). (2020c). Inventory of U.S. Greenhouse Gas Emissions and Sinks: 1990-2018. Retrieved from https://www.epa.gov/sites/production/files/2020-04/documents/us-ghg-inventory-2020-main-text.pdf

Fall, R., & Benson, A. A. (1996). Leaf methanol—the simplest natural product from plants. *Trends in Plant Science, 1(*9), 296-301.

Farquhar, G. J., & Rovers, F. A. (1973). Gas production during refuse decomposition. *Water, Air, and Soil Pollution*, 2(4), 483-495.

Finlayson-Pitts, B. J., & Pitts, J. N. (1999). *Chemistry of the upper and lower atmosphere: theory, experiments, and applications*. Elsevier.

Fried, A., Sewell, S., Henry, B., Wert, B. P., Gilpin, T., & Drummond, J. R. (1997). Tunable diode laser absorption spectrometer for ground-based measurements of formaldehyde. *Journal of Geophysical Research: Atmospheres*, *102*(D5), 6253-6266.

Glatthor, N., Höpfner, M., Baker, I. T., Berry, J., Campbell, J. E., Kawa, S. R., ... & Stinecipher, J. (2015). Tropical sources and sinks of carbonyl sulfide observed from space. *Geophysical Research Letters*, *42*(22), 10-082.

Goldan, P. D., Kuster, W. C., Fehsenfeld, F. C., & Montzka, S. A. (1995). Hydrocarbon measurements in the southeastern United States: The rural oxidants in the southern environment (ROSE) program 1990. *Journal of Geophysical Research: Atmospheres*, *100*(D12), 25945-25963.

Grosjean, D. (1997). Atmospheric chemistry of alcohols. *Journal of the Brazilian Chemical Society*, *8*(5), 433-442.

Grosjean, E., Grosjean, D., Fraser, M. P., & Cass, G. R. (1996). Air quality model evaluation data for organics. 2. C1− C14 carbonyls in Los Angeles air. *Environmental science & technology*, *30*(9), 2687-2703.

Hegde, U., Chang, T. C., & Yang, S. S. (2003). Methane and carbon dioxide emissions from Shan-Chu-Ku landfill site in northern Taiwan. *Chemosphere*, *52*(8), 1275-1285.

Hobbs, P., & Mottram, T. (2000). New directions: Significant contributions of dimethyl sulphide from livestock to the atmosphere. *Atmospheric Environment*, *34*(21), 3649-3650.

Hughes, S. C. (2018). *Characterization of Trace Gases During the Front Range Air Pollution and Photochemistry Experiment (FRAPPÉ) Field Campaign* (Doctoral dissertation, Ph. D., thesis, University of California, Irvine).

Kesselmeier, J., Bode, K., Hofmann, U., Müller, H., Schäfer, L., Wolf, A., ... & Foster, P. (1997). Emission of short chained organic acids, aldehydes and monoterpenes from Quercus ilex L. and Pinus pinea L. in relation to physiological activities, carbon budget and emission algorithms. *Atmospheric Environment*, *31*, 119-133.

Kettle, A. J., Kuhn, U., Von Hobe, M., Kesselmeier, J., & Andreae, M. O. (2002). Global budget of atmospheric carbonyl sulfide: Temporal and spatial variations of the dominant sources and sinks. *Journal of Geophysical Research: Atmospheres*, *107*(D22), ACH-25.

Kirstine, W., Galbally, I., Ye, Y., & Hooper, M. (1998). Emissions of volatile organic compounds (primarily oxygenated species) from pasture. *Journal of Geophysical Research: Atmospheres, 103*(D9), 10605-10619.

Kuai, L., Worden, J. R., Campbell, J. E., Kulawik, S. S., Li, K. F., Lee, M., ... & Baker, I. (2015). Estimate of carbonyl sulfide tropical oceanic surface fluxes using Aura Tropospheric Emission Spectrometer observations. *Journal of Geophysical Research: Atmospheres*, *120*(20), 11-012.

Kung, L. (2018). Silage fermentation and additives. *Archivos Latinoamericanos de Producción Animal, 26*(3-4).

Lee, Y. N., Zhou, X., & Hallock, K. (1995). Atmospheric carbonyl compounds at a rural southeastern United States site. *Journal of Geophysical Research: Atmospheres, 100*(D12), 25933-25944.

Lennartz, S., Marandino, C. A., Von Hobe, M., Cortes, P., Quack, B., Simo, R., ... & Kloss, C. (2017). Direct oceanic emissions unlikely to account for the missing source of atmospheric carbonyl sulfide. *Atmospheric Chemistry and Physics*, *17*, 385-402.

Lippmann, M. (1989). Health effects of ozone a critical review. *Japca*, *39*(5), 672-695.

Lisk, D. J. (1991). Environmental effects of landfills. *Science of the total environment*, 100, 415-468.

Lohila, A., Laurila, T., Tuovinen, J. P., Aurela, M., Hatakka, J., Thum, T., ... & Vesala, T. (2007). Micrometeorological measurements of methane and carbon dioxide fluxes at a municipal landfill. *Environmental science & technology*, *41*(8), 2717-2722.

Lombardia, L., Corti, A., Carnevale, E., Baciocchi, R., & Zingaretti, D. (2011). Carbon dioxide removal and capture for landfill gas up-grading. *Energy Procedia*, *4*, 465-472.

Meier, U., Grotheer, H. H., Riekert, G., & Just, T. (1985). Temperature dependence and branching ratio of the C2H5OH+ OH reaction. *Chemical physics letters*, *115*(2), 221-225.

Mellouki, A., Le Bras, G., & Sidebottom, H. (2003). Kinetics and mechanisms of the oxidation of oxygenated organic compounds in the gas phase. *Chemical Reviews, 103*(12), 5077-5096.

Meyer, D., Price, P. L., Rossow, H. A., Silva-del-Rio, N., Karle, B. M., Robinson, P. H., ... & Fadel, J. G. (2011). Survey of dairy housing and manure management practices in California. *Journal of dairy science*, *94*(9), 4744-4750.

Minschwaner, K., Salawitch, R. J., & McElroy, M. B. (1993). Absorption of solar radiation by $O_2$: Implications for $O_3$ and lifetimes of $N_2O$, $CFCl_3$, and $CF_2Cl_2$. *Journal of Geophysical Research: Atmospheres*, *98*(D6), 10543-10561.

Montzka, S. A., Calvert, P., Hall, B. D., Elkins, J. W., Conway, T. J., Tans, P. P., & Sweeney, C. (2007). On the global distribution, seasonality, and budget of atmospheric carbonyl sulfide (COS) and some similarities to CO2. *Journal of Geophysical Research: Atmospheres*, *112*(D9).

Myhre, G., Shindell, D., Bréon, F.-M., Collins, W., Fuglestvedt, J., Huang J., … & Zhang, H. (2013). Anthropogenic and Natural Radiative Forcing. In: *Climate Change 2013: The Physical Science Basis. Contribution of Working Group I to the Fifth Assessment Report of the Intergovernmental Panel on Climate Change* [Stocker, T.F., D. Qin, G.-K. Plattner, M. Tignor, S.K. Allen, J. Boschung, A. Nauels, Y. Xia, V. Bex and P.M. Midgley (eds.)]. Cambridge University Press, Cambridge, United Kingdom and New York, NY, USA.

Nemecek-Marshall, M., MacDonald, R. C., Franzen, J. J., Wojciechowski, C. L., & Fall, R. (1995). Methanol emission from leaves (enzymatic detection of gas-phase methanol and relation of methanol fluxes to stomatal conductance and leaf development). *Plant Physiology*, *108*(4), 1359-1368.

Owen, J. J., & Silver, W. L. (2015). Greenhouse gas emissions from dairy manure management: a review of field-based studies. *Global change biology*, *21*(2), 550-565.

Prinn, R. G., Weiss, R. F., Arduini, J., Arnold, T., DeWitt, H. L., Fraser, P. J., ... & Zhou, L. (2018). History of chemically and radiatively important atmospheric gases from the Advanced Global Atmospheric Gases Experiment (AGAGE). *Earth System Science Data*, *10*(2), 985-1018.

Protoschill-Krebs, G., & Kesselmeier, J. (1992). Enzymatic pathways for the consumption of carbonyl sulphide (COS) by higher plants. *Botanica Acta*, *105*(3), 206-212.

Riemer, D., Pos, W., Milne, P., Farmer, C., Zika, R., Apel, E., ... & Shepson, P. (1998). Observations of nonmethane hydrocarbons and oxygenated volatile organic compounds at a rural site in the southeastern United States. *Journal of Geophysical Research: Atmospheres*, *103*(D21), 28111-28128.

Rodhe, H. (1978). Budgets and turn-over times of atmospheric sulfur compounds. In *Sulfur in the Atmosphere* (pp. 671-680). Pergamon.

Seinfeld, J. H., & Pandis, S. N. (2016). *Atmospheric chemistry and physics: from air pollution to climate change*. John Wiley & Sons.

Sive, B. C. (1999). Atmospheric nonmethane hydrocarbons: Analytical methods and estimated hydroxyl radical concentrations. (Doctoral dissertation, Ph. D., thesis, University of California, Irvine).

Suntharalingam, P., Kettle, A. J., Montzka, S. M., & Jacob, D. J. (2008). Global 3-D model analysis of the seasonal cycle of atmospheric carbonyl sulfide: Implications for terrestrial vegetation uptake. *Geophysical Research Letters*, *35*(19).

Thompson, B. & Wood, R. (1981). The Methanizer in the Model 3700 & Vista Series Gas Chromatograph. *Varian Instruments at Work*, *54*.

United States Department of Energy. (2020). Ethanol Fuel Basics. Retrieved from https://afdc.energy.gov/fuels/ethanol_fuel_basics.html

Von Hobe, M., Kettle, A. J., & Andreae, M. O. (1999). Carbonyl sulphide in and over seawater: summer data from the northeast Atlantic Ocean. *Atmospheric Environment*, *33*(21), 3503-3514.

Watts, S. F. (2000). The mass budgets of carbonyl sulfide, dimethyl sulfide, carbon disulfide and hydrogen sulfide. *Atmospheric Environment*, *34*(5), 761-779.

Yang, M. (2009). Characterization of VOC Emissions from Various Components of Dairy Farming and Their Effect on San Joaquin Valley Air Quality. (Doctoral dissertation, Ph. D., thesis, University of California, Irvine).

# 4. Methane and Carbon Dioxide

Methane and carbon dioxide mixing ratios were determined for all samples collected at the Visalia dairy farm and at the Orange County landfills. These mixing ratios were compared to the $CH_4$ and $CO_2$ at the California coastline (34.5 °N – 40.0 °N) to determine whether the $CH_4$ and $CO_2$ at the dairy farm and landfills exceeded the amounts assumed to be entering California. Additional analysis was performed on dairy farm samples to estimate emission factors for methane from enteric and manure sources. The potential effect of climate change on future emissions at the dairy farm was also explored. Additional analysis was performed for landfill samples to estimate the amount of carbon dioxide emitted and its contribution to the landfill's GWP.

## 4.1 Background Methane and Carbon Dioxide from Remote Coastal Sampling

For decades, members of the Rowland-Blake laboratory have participated in seasonal trips to coastal locations along the Pacific Ocean to determine trace gas concentrations in remote places. More information about these trips was presented in Chapter 2.2. Average mixing ratios and standard deviations of $CH_4$ from 1980 to 2018 for samples collected on the coast of California at the same latitudes as the SJV (between 34.5 °N and 40.0 °N) are shown in Figure 4.1.

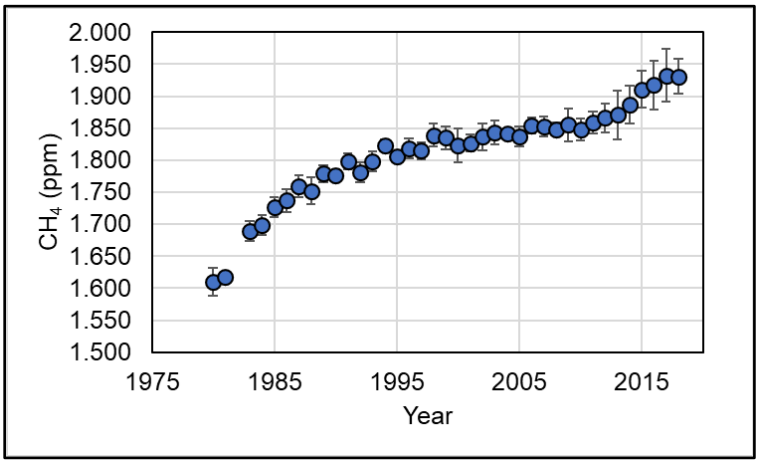


**Figure 4.1** $CH_4$ mixing ratios and standard deviations on the California coast at latitudes from 34.5 °N to 40.0 °N from 1980 to 2018

These values represent a subset of the methane values collected worldwide during this period. Each point represents an average of all samples collected over the year between 34.5 °N and 40.0 °N on the California coastline. These averages represent typical methane mixing ratios found in the clean, remote air that enters the state from the ocean to cross over the land. These data show that $CH_4$ has gradually increased over the last four decades. The average $CH_4$ mixing ratio on the California coast (34.5 °N to 40.0 °N) in the year 1980 was 1.610 ppm. The average $CH_4$ mixing ratio on the California coast (34.5 °N to 40.0 °N) increased to an average of 1.931 ppm by 2018, nearly a 20% increase in 38 years. This upwards trend agrees with other worldwide trace gas monitoring networks, such as the Advanced Global Atmospheric Gases Experiment (AGAGE) based at the Massachusetts Institute of Technology (Prinn et al., 2018). Therefore, any samples collected in this study exceeding 1.931 ppm $CH_4$ can be considered “enhanced” as they are higher than the air traveling into the state based on typical wind patterns. These enhancements are presumed to be created by inland sources.

The Rowland-Blake laboratory has collected remote air samples for the analysis of methane and a handful of other gases for over thirty-five years. The group now reports other gases, including carbon dioxide. The average carbon dioxide mixing ratio on the remote California coastline (34.5 °N to 40.0 °N) in 2018 was 410 ppm. Carbon dioxide is known to have seasonal variation, so this value does fluctuate over the course of a year. However, any carbon dioxide mixing ratios that well exceed this amount in samples collected inland can be thought of as “enhanced” as they are higher than the average mixing ratio of carbon dioxide that is presumably entering the state based on the typical wind blowing from the northwest. The seasonality of $CO_2$ is accounted for by comparing coastline averages to dairy farm averages.

### 4.2 Methane and Carbon Dioxide at the Dairy Site

Methane and carbon dioxide were measured at the dairy site in Visalia, CA for all samples collected during each seasonal campaign. The average and median $CH_4$ and $CO_2$ for each

campaign are shown in Table 4.1. These values were calculated based only on samples collected at the main dairy farm and did not include any samples collected at other dairies or at the nearby Visalia landfill. Additionally, Table 4.1 does not include any samples collected from a flux chamber that was utilized only during the January 2020 campaign.

**Table 4.1** Average and median mixing ratios for $CH_4$ (ppm) and $CO_2$ (ppm) for dairy campaigns

| Campaign | $CH_4$ (ppm) | | $CO_2$ (ppm) | |
|---|---|---|---|---|
| | Average | Median | Average | Median |
| September 2018 | 16.80 | 5.24 | 443 | 421 |
| March 2019 | 14.23 | 7.74 | 469 | 450 |
| June 2019 | 14.09 | 3.30 | 526 | 537 |
| September 2019 | 11.29 | 4.16 | 484 | 462 |
| January 2020 | 43.36 | 9.79 | 938 | 525 |

The January 2020 campaign had the highest overall values for $CH_4$ average, $CH_4$ median, and $CO_2$ average. It has been shown that seasonality does affect emissions. More specifically, studies have shown that manure slurries and lagoons at a higher temperature emit more methane than those at a lower temperature (Chadwick, 2011). Although temperature did play a role in this study, trace gas trends were also greatly influenced by the sample location and manure management style, as samples were collected at a wide selection of locations around the dairy. To determine how sample location played a role, the data were further divided into categories representing the most common locations at which samples were collected.

The average and median $CH_4$ and $CO_2$ at the Free Stalls, Lagoons, and Cows in open lots for each campaign are shown in Table 4.2. The “Free Stalls” category in Table 4.2 included all samples collected within the free stalls, where the milk cows spend most of their time eating, ruminating, and excreting waste. The “Free Stalls” category also included samples of cow breath that were collected from the cows housed in the free stalls. Emissions in this category are assumed to be mostly enteric, with some influence of manure emissions from excreted waste. The “Cows” category in Table 4.2 was very broad, but included any samples collected near cows *outside of the free stalls*. This included any heifers, calves, and dry cows near the corral areas,

and any samples collected of their breath. Methane in the samples in this category was assumed to be mostly enteric, with a small contribution from manure emissions. The “Lagoons” category included samples collected near the slurries, lagoons, and processing pit. Samples in this category were assumed to represent mostly manure emissions, with negligible contribution from enteric sources as the samples were collected almost always upwind of the cows.

**Table 4.2** Average and median mixing ratios for $CH_4$ (ppm) and $CO_2$ (ppm) for select dairy locations

| Location | Campaign | $CH_4$ (ppm) | | $CO_2$ (ppm) | |
|---|---|---|---|---|---|
| | | **Average** | **Median** | **Average** | **Median** |
| Free Stalls | Sept. 2018 | 10.05 | 10.69 | 493 | 502 |
| | March 2019 | 13.98 | 13.69 | 645 | 658 |
| | June 2019 | 4.36 | 2.550 | 541 | 544 |
| | Sept. 2019 | 8.17 | 6.010 | 551 | 528 |
| | Jan. 2020 | 16.11 | 12.34 | 517 | 502 |
| | **Average** | **10.53** | **9.06** | **549** | **547** |
| Cows | Sept. 2018 | 2.26 | 2.21 | 433 | 429 |
| | March 2019 | 5.66 | 4.99 | 517 | 495 |
| | June 2019 | 4.67 | 3.85 | 568 | 567 |
| | Sept. 2019 | 3.80 | 3.23 | 503 | 496 |
| | Jan. 2020 | 5.27 | 5.23 | 577 | 540 |
| | **Average** | **4.33** | **3.90** | **520** | **505** |
| Lagoons | Sept. 2018 | 22.37 | 5.52 | 425 | 411 |
| | March 2019 | 20.92 | 17.06 | 443 | 438 |
| | June 2019 | 33.17 | 6.45 | 533 | 537 |
| | Sept. 2019 | 21.43 | 6.91 | 464 | 454 |
| | Jan. 2020 | 147.9 | 137.9 | 550 | 537 |
| | **Average** | **49.17** | **34.77** | **483** | **475** |

For the “Free Stalls” category, June 2019 had the lowest methane mixing ratios, but the rest of the seasons were similar to each other. For the outdoor “Cows” category, no seasonal trend was apparent either. The lack of seasonal trends for the “Free Stalls” and “Cows” was similar to results reported in Arndt et al. (2018), which found no clear seasonal patterns for animal housing at two dairy farms in California. This may be explained by the cows’ feed, which indicates the maximum amount of enteric methane that can be released from a cow (Eggleston et al., 2006). While it is difficult to track down the specific makeup of the food provided to the cows at the Visalia dairy site, most of the cows are primarily fed some mixture of distiller’s grains (i.e., wheat, barley,

corn, and others). According to the owner, the cows eat about the same base diet year-round. This consists of a C-4 diet (i.e., mostly corn-based) for the milk cows and calves, and a C-3 diet (i.e., mostly wheat) for the dry cows and heifers. Although outside the scope of this study, additional isotopic methane studies could be performed between these diets that could be of interest to determine the difference between diet-related enteric methane emissions. For this study, the diets are assumed to stay the same throughout all the campaigns. This could explain the lack of obvious seasonality of the enteric emissions.

Although there was little seasonal influence within the “Free Stalls” and “Cows” categories, the methane in the “Free Stalls” category was more elevated than the “Cows” category. This was likely because the emissions that occur during rumination and waste accumulation are more easily trapped within a covered free stall than an open-air corral. Additionally, as is shown in Chapter 4.2.2, milk cows (which were housed only in the free stalls) likely release more $CH_4$ than the heifers and dry cows (which were housed in the corrals). Although the “Cows” category had lower methane mixing ratios, it was still higher than the average methane mixing ratio assumed to enter California based on averages along the coastline (i.e., 1.931 ppm).

The “Lagoons” category had the highest methane mixing ratios overall. January 2020 was particularly high and exhibited the highest methane average and median methane mixing ratios of all three categories for all campaigns. The “Lagoons” category and its possible seasonality is discussed in more detail in Chapter 4.2.1. It is important to mention that even though the “Lagoons” category exhibited the largest methane mixing ratios, that does not necessarily imply that the Lagoons category contributed the most methane emissions. The large difference between the average and median of the “Lagoons” category in Table 4.2 indicated that the emissions were likely more variable than the emissions from “Cows” or “Free Stalls.” In other words, while “Cows” and “Free Stalls” likely emit methane more constantly, the lagoons may emit methane more

sporadically through temperature-dependent decomposition. Chapters 4.2.1 and 4.2.2 further explore this, where annual emissions from enteric and manure sources were estimated.

For the “Lagoons” category, it was important to determine whether the majority of methane emissions primarily originated from the two large lagoons or from the smaller slurries. This was achieved by overlaying the samples from all campaigns on an aerial view of the dairy. Figure 4.2 shows this aerial view of the dairy farm with the $CH_4$ mixing ratios from various sources scaled by color and height. Points shown were collected during all the campaigns and are not separated by season. Typical wind direction was from the northwest. Methane was binned into eight discrete mixing ratio ranges and colored accordingly. Height was scaled on a continuum, where the lowest methane mixing ratios are shown closer to the ground and the more elevated mixing ratios are shown higher above the ground for illustration, but all samples were collected on the ground.

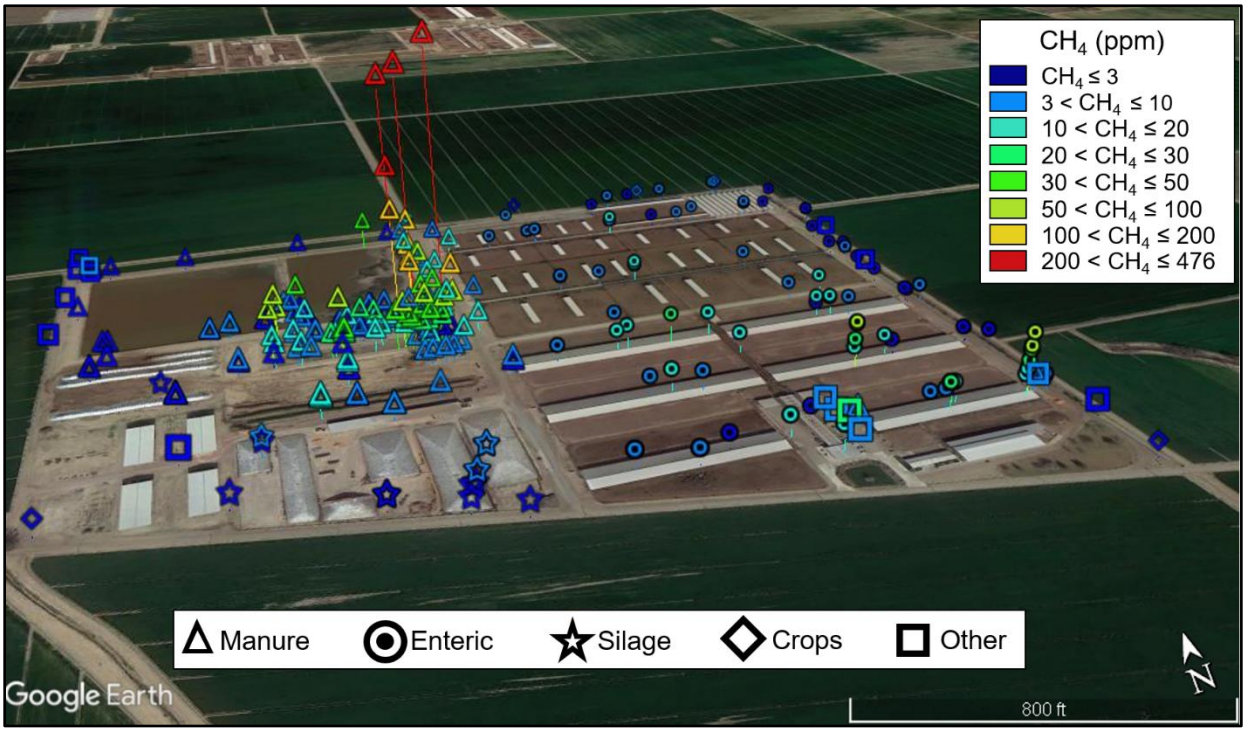


**Figure 4.2** Methane (ppm) at the dairy farm binned by mixing ratio ranges and grouped by source. Height of the points also indicates mixing ratio. Typical wind direction was from the northwest.

According to Figure 4.2, the most enhanced methane at this dairy farm was found near the wet manure management system, labelled “Manure” in Figure 4.2. For the purposes of labelling this figure, this “Manure” category included sources for which waste was the major constituent: the processing pit, bedding, flush water, the two lagoons, and the two slurries. Methane mixing ratios were lowest near the bedding, which was drying and often covered, thereby resulting in lower enhancements. Methane mixing ratios were highest downwind of the two slurries rather than the two lagoons. Initially, this was surprising given that Owen and Silver (2015), after examining 38 field dairy farm studies in the United States and Europe, determined that lagoons have a higher annual per-head emission rate and per-head GWP than slurries. However, Owen and Silver (2015) also reported that lagoons have a lower annual per-area emission rate than slurries. This means that dairy lagoons typically have a higher emission rate *per cow*, but a lower emission rate *per area* when compared to slurries. Therefore, the number of cows present at the dairy farm and the surface area of the liquid storage systems are important.

For the Visalia dairy farm, the methane mixing ratios represent a snapshot of the air at a certain time. A large mixing ratio, while it *can* be the result of a consistently high emission rate, it can also be caused by variability in the emission rate. Samples collected near the slurries exhibited quite a range of mixing ratios. For example, one location at the southeast corner of Slurry 1 had a methane mixing ratio of 476 ppm during the September 2018 campaign. At the same location during the next (March 2019) campaign, methane was only 2.5 ppm, close to background. This variability likely occurred for the slurries because they are more sensitive to temperature changes, crust and bubble formation, and the mechanical removal of solids, which are discussed below.

The two slurries are much more concentrated than the two lagoons, and the waste often floats up to the surface to form a natural crust, which helps to reduce $CH_4$ emissions by creating anaerobic and aerobic zones where $CH_4$ oxidation can occur (Sommer et al., 2000; Petersen et

al., 2005; Petersen & Sommer, 2011; Grant et al., 2015). In summertime, when temperatures increase, the crust normally dries up and becomes more porous, which allows more methane to permeate through (Leytem et al., 2017). This is typically also important for bubble formation, which is thought to increase the transfer rate of the gases from liquid to air (but not the biological production rate within the manure) during the summer (Baldé et al., 2016). At this dairy farm, the crust was present nearly year-round but was most prominent during the colder campaigns. It even sometimes covered parts of the first lagoon as well. Similar to Baldé et al. (2016), bubbles occurred throughout all seasons, but they were most prominent during the warmer September and June campaigns. This could explain why the slurries had overall higher mixing ratios than the lagoons during the summer.

However, the crust and the bubbles likely did not play as large of a role in methane emissions at this dairy farm as they have in some other studies. Previous literature like Husted (1994), Borhan et al. (2011), and Leytem et al. (2017) predicted that the lagoons would emit more methane than the slurries in the winter (i.e., when the crust on the slurries is thickest), while slurries would produce more methane than lagoons in the summer (i.e., when the crust thins, and bubble production is highest). However, the slurries predominantly had the highest methane mixing ratios across all seasons. The seasonal temperature variation and the mechanical removal of solids from the slurries were likely more important factors than the crust and the bubble formation at this dairy farm.

The solids that accumulate at the bottom of the slurry ponds were only removed in August 2018 and April 2019. By January 2020, the solids had nine months to accumulate, which likely led to higher methane mixing ratios in January—the highest of any location or season throughout the campaigns. This agrees with findings from Baldé et al. (2016), which reported that by changing the annual solids removal schedule (from late fall to early fall), annual emissions were reduced by 21%. Removal of the solids interrupts the methanogenesis process, thereby decreasing the

potential for methane production (Baldé et al., 2016). The samples collected in January 2020 contained more methane than samples collected during the other campaigns likely because of the uninterrupted methanogenesis process. As shown in Table 4.2, the next highest average methane mixing ratio for the wet manure management system, after January 2020, was for the June 2019 campaign, when temperatures were at their highest. The temperature dependence of the manure management system at this dairy is revisited in Chapter 4.2.1.

One of the other major sources of methane at this dairy farm, according to Figure 4.2, were the enteric emissions from the cows themselves. These were labelled “Enteric” in Figure 4.2, and included samples collected in the free stalls, near the cows housed outdoor, and of cow breath. In Figure 4.2, elevated mixing ratios can be seen near the free stalls, where the milk cows eat most of the day. Methane mixing ratios were also elevated near the open corrals at the north side of the farm, where the young cows (i.e., heifers) and dry cows live. Methane emissions from these areas may originate from the cows ruminating, but they are also likely combined with emissions from the manure when the cows excrete waste.

Owen and Silver (2015), which combined results from thirty-eight field studies in the United States and Europe, reported that the per-head methane emissions from enteric sources were over three times less than per-head methane emissions from manure sources, particularly anaerobic lagoons (Owen & Silver, 2015). This also agreed with results reported in Arndt et al. (2018), which measured methane emissions from wet manure management systems and free stalls during summer and winter at two dairy farms in California. Arndt et al. (2018) found that during summer, liquid manure at one dairy emitted more methane than the animal housing for both summer and winter. However, at a different dairy, even though manure emitted more methane in the summer, the animal housing emitted more methane during winter. Arndt et al. (2018) hypothesized that the difference between the behaviors of the two dairies could be explained by the amount of solids stored in the manure management system.

More solids were stored in the slurries and lagoon at the first dairy in Arndt et al. (2018), so the emissions were higher there than at the lagoons and slurries of the second dairy (Arndt et al., 2018). Similarly, for this study, methane mixing ratios recorded from enteric sources were less than those near the manure collection systems. However, although mixing ratios were higher near manure management systems, this does not necessarily imply that the contribution of manure management to the total methane emissions from the dairy farm was higher than that of the contribution of enteric emissions—this would depend on the per-head emission rate and the number of cows present at the dairy.

As shown in Table 4.1, Summer (June 2019) and Winter (January 2020) had the highest $CO_2$ average and median mixing ratios. It is important to point out that January 2020 was the only campaign that measured trace gases from cow breath, which may have led to higher $CO_2$ mixing ratios during that campaign. Seasonal trends were not apparent, but the average and median for all seasons were higher than the air entering California from the coastline (410 ppm), which indicated a source either at the dairy or nearby. Table 4.2 separated the emissions again into “Free Stalls,” “Cows,” and “Lagoons” categories. Unlike methane emissions, carbon dioxide mixing ratios were highest from enteric sources (i.e., “Free Stalls” and “Cows”) rather than manure sources (i.e., “Lagoons”). This can also be seen when the data are plotted over an aerial view of the dairy farm.

Figure 4.3 shows an aerial view of the dairy farm with the $CO_2$ mixing ratios scaled by color and height. Similar to the methane overlay in Figure 4.2, carbon dioxide mixing ratios were binned into eight discrete mixing ratio ranges. Height was scaled on a continuum, where the lowest carbon dioxide mixing ratios are shown closer to the ground and the more elevated mixing ratios are shown higher above the ground. This does not indicate the altitude at which the samples were collected.

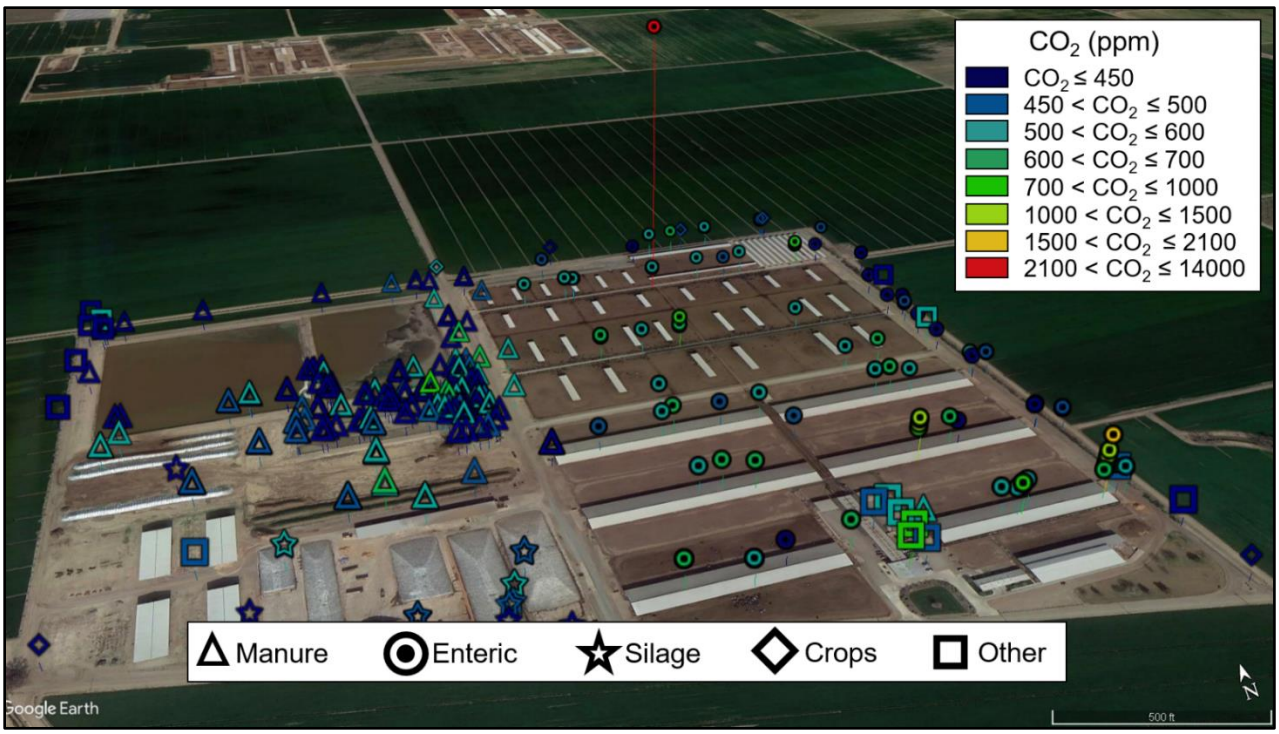


**Figure 4.3** Carbon dioxide (ppm) at the dairy farm binned by mixing ratio ranges and grouped by source. Height of the points also indicates mixing ratio. Typical wind direction was from the northwest.

Samples collected in the free stalls had the highest $CO_2$ mixing ratios. This can be explained in two ways. First, cows breathe, ruminate, and excrete waste within the free stalls. Although the free stalls are open on the sides, these emissions could be trapped for a while before exiting the free stall, leading to an increase in $CO_2$ levels. Secondly, some vehicular machinery travels into the free stalls to drop off food for the cows and maintain the area, which could also lead to a slight increase of carbon dioxide. Regardless of source, many dairy farm areas exhibited higher levels of carbon dioxide than those measured in the coastal samples (34.5 °N – 40.0 °N) of California ($CO_2$ average = 410 ppm) as well as the upwind area of the dairy (northwest corner), indicating the likelihood that there were sources present at the dairy farm itself.

The top ten highest mixing ratios of carbon dioxide across all five seasonal campaigns came from samples that were collected from cow breath during January 2020. There was one extremely elevated sample collected from cow breath (seen with a red circle high above the dairy in Figure 4.3), which reached a mixing ratio of nearly 14,000 ppm. This was much higher than

$CO_2$ mixing ratios in the other cow breath samples, with a mean and standard deviation of 814±451 ppm without including the sample of 14,000 ppm.

Previous studies have shown that $CO_2$ emissions at dairy farms primarily come from animal, plant, and soil respiration, with only a small contribution from microbial decomposition (Chianese et al., 2009a). It was estimated in Chianese et al. (2009b) that about 90% of dairy farm emissions from a dairy farm in Pennsylvania were from animal respiration followed by a smaller percentage from manure and fossil fuel combustion by the farm vehicles and equipment (Chianese et al., 2009b). A different study conducted at a dairy farm in southern Idaho found that out of three sources—open lots, a wastewater pond, and compost—80% of the annual carbon dioxide emissions came from the open lots, a highly enteric source (Leytem et al., 2011).

For this dairy in Visalia, CA, this could explain why the most elevated $CO_2$ mixing ratios were from samples collected near predominantly enteric sources, and why the manure management area had lower $CO_2$ mixing ratios than those sources. While the decomposition of the organic matter in manure has the capability of producing $CO_2$, the animals on the dairy likely emit it at a much greater rate.

### 4.2.1 Estimated Methane Emissions from Manure Management

In the International Panel for Climate Change's (IPCC) *2006 Guidelines for National Greenhouse Gas Inventories*, the IPCC recommends different methods for calculating methane emissions from manure management and enteric emissions from ruminant animals in different locations worldwide. For manure management, these methods are broken down into three different tiers. Tier 1 requires only the population data for animals in various categories (e.g., number of dairy cows, number of calves, number of heifers, etc.) and the region's average annual temperature combined with their recommended emission factors associated with those temperatures.

Tier 2 requires more detailed information about the animals' characteristics and manure management practices to develop specific emission factors for a region or country. Lastly, Tier 3 uses measurement-based approaches and models to predict highly specific emission factors for a specific region (Eggleston et al., 2006). Despite having been initially published in 2006, the methods presented in the IPCC's three tiers are still widely used in dairy farm studies to estimate methane emissions from manure management.

The EPA's most recent United States GHG inventory, published in 2020, still uses the basis of the IPCC's methods (typically Tier 1 or 2) to calculate methane emissions for various animal populations. Their approach to the Tier 2 method uses the following Equation 4-1 (EPA, 2020c):

$$\mathrm{EF} = \mathrm{VS} * 365 \frac{\mathrm{days}}{\mathrm{yr}} * \mathrm{B_0} * 0.662 * \sum_{\mathrm{jk}} \mathrm{MCF_{jk}} * \mathrm{MS_{jk}} \qquad \text{Equation 4-1}$$

where

EF = annual emission factor for defined animal population, in (kg $CH_4$/yr)

VS = daily volatile solids excreted for an animal within a defined population, in (kg/day)

$B_0$ = maximum methane-producing capacity for manure produced by animal within a defined population, in ($m^3$ $CH_4$/kg VS)

0.662 = the density of $CH_4$ at 25 °C, in (kg $CH_4$/$m^3$ $CH_4$)

$\mathrm{MCF_{jk}}$ = methane conversion factor for each manure management system *j* by climate region *k*

$\mathrm{MS_{jk}}$ = fraction of defined animal population's manure handled using manure system *j* in climate region *k*, also known as a *management and design practices factor*, or MDP

By modifying this equation to include only one animal population (e.g., milk cows) at a single dairy farm at the monthly scale, the formula can be rewritten as Equation 4-2:

$$\mathrm{EF} = \mathrm{VS} * \mathrm{B_0} * \mathrm{MCF} * \rho_{CH4} * \mathrm{MDP} \qquad \text{Equation 4-2}$$

where

EF = monthly emission factor for defined animal population, in (kg $CH_4$/month)

VS = volatile solids entering the lagoon each month, in (kg VS)

$B_0$ = maximum $CH_4$-producing capacity of manure, in ($m^3$ $CH_4$/kg VS)

MCF = methane conversion factor

$\rho_{CH4}$ = 0.662, the density of $CH_4$ at 25 °C, in (kg $CH_4$/$m^3$ $CH_4$)

MDP = management and design practices factor, the fraction of the animal population's manure handled using manure system. An MDP < 1.0 represents a system operating at a less than optimal level.

This study closely examines the methane conversion factor (MCF) for dairy farms in Visalia, Tulare County, California. The MCF is an important factor, as it is directly proportional to the amount of methane that could be emitted from a wet manure management system. In their Tier 1 methodology, the IPCC recommends various MCFs for different ambient air temperatures, but only provides values for regions whose annual air temperatures fall within a certain temperature range (10 °C to 28 °C) (Eggleston et al., 2006). The IPCC assumes that regions below 10 °C emit the same as an area at 10 °C, and that regions above 28 °C emit the same amount as a region at 28 °C. Unfortunately, these are not very good assumptions.

Although the annual average in the SJV is within the IPCC's range, the average monthly air temperatures range from 5 °C to 28 °C, which is outside of the IPCC's range during the colder months (USA.com, 2020a – h). Additionally, the SJV often reaches daily temperatures above 28 °C despite having lower monthly average temperatures. Using the IPCC's pre-determined values to estimate emissions would likely overpredict emissions in cold months and underpredict them in warm months. Owen & Silver (2015) and Baldé et al. (2016) determined that the IPCC's pre-determined values as well as the EPA's Tier 2 model systematically underestimated emissions

from manure management. Instead, this study calculated a proxy for MCF using an *f* value calculated from a modified van't Hoff-Arrhenius equation, discussed in more detail below.

In 1972, Metcalf & Eddy showed that the performance of many biological systems is heavily dependent on temperature and could be predicted by the van't Hoff-Arrhenius equation, which predicts the unknown behavior of a system at a new temperature based on its known performance at a known temperature (Metcalf & Eddy, 1972). The equation they used was the following, Equation 4-3:

$$k_2 = k_1 \exp\left[\frac{E(T_2 - T_1)}{RT_1T_2}\right] \qquad \text{Equation 4-3}$$

where

$k_2$ = reaction-rate constant at temperature $T_2$

$k_1$ = reaction-rate constant at temperature $T_1$

E = activation energy constant (cal/mol)

R = ideal gas constant (1.987 cal/mol)

$T_1$, $T_2$ = temperature (K)

In 1990, Safley and Westerman rearranged Equation 4-3 to derive Equation 4-4 (Safley & Westerman, 1990):

$$f = \exp\left[\frac{E(T_2 - T_1)}{RT_1T_2}\right] \qquad \text{Equation 4-4}$$

In this formula, all the inputs described for Equation 4-3 are identical for Equation 4-4 to calculate an *f* value. In Equation 4-4, the dependent variable *f* represents the proportion of volatile solids that are biologically available for conversion to methane based on the lagoon or slurry's temperature. Volatile solids represent organic matter in the manure, and they can be either biodegradable or nonbiodegradable based on their temperature. Only *biodegradable* volatile solids can produce methane, so the *f* value is very important in figuring out how much methane can be emitted from a particular biological system as it gives the fraction that is biodegradable.

As *f* approaches a value of one, the maximum amount of methane can be produced from that system. The *f* value can be thought of as the same as the MCF parameter from Equation 4-2, a temperature-dependent modification to the $B_0$ parameter in Equation 4-3 that indicates the efficiency of the biological system.

Mangino et al. (2002) further developed the Safley and Westerman (1990) formula and noted that this *f* value is ideally calculated based on the temperature of the system itself (i.e., the lagoon or slurry temperature), but that the air temperature can be used as a decent surrogate for the system temperature when those parameters are unavailable. Mangino et al. (2002) introduced the mathematical foundation for all future IPCC and EPA manure management emissions calculations.

Currently, the EPA calculates nationwide methane emissions from manure management by first calculating the *f* value by state. They use a weighted state air temperature value calculated using average monthly air temperatures only from the counties containing the animal populations of interest. For example, if the EPA wanted to calculate manure management emissions from buffalo farms in California, but buffalo live only in Fresno and Orange Counties, then the EPA would calculate emissions for California by including only the average monthly air temperatures of Fresno and Orange Counties. This is an improvement to the IPCC (Eggleston et al., 2006) recommendations, which recommend simply using annual average temperatures (not monthly) for an entire region (not the county level). However, Lory et al. (2010) found that the traditional IPCC and EPA methodology underestimated $CH_4$ emissions from dairies by over 130%. The enteric emissions calculations can clearly be improved.

One way to improve the calculation is to incorporate more accurate temperature data. As Mangino et al. (2002) noted, the *f* value calculation should be done, ideally, using the lagoon or slurry temperature rather than air temperature. Krider (1981) and Payne et al. (1981) demonstrated that the mean annual temperature of anaerobic lagoons in the northeastern United

States and Alabama were < 2 °C higher than the ambient air temperature, but they did not measure monthly or daily differences. It is important to note again that methane production from methanogenesis in any system is not linear (Baldé et al., 2016; Schulz, 1997; Smith & Franco, 1985). This implies that the temperature change at a higher temperature (e.g., 24 °C to 25 °C) produces a change in the emission rate of methane that is much greater than a change at a lower temperature (e.g., 4 °C to 5 °C) in the same manure management system. Therefore, it is especially important to properly estimate the temperature of a manure management system for accurate predictions of methane emissions.

As the importance of accurate temperature is clear, and Mangino et al. (2002) recommended using the system temperature rather than the air temperature whenever possible, the slurry temperatures at the dairy farm in this study were calculated using a formula developed by Smith and Franco (1985). They developed a computer model using data obtained by Fischer (1977) during a 3-year campaign at a dairy farm in the Midwest United States, which tracked air temperature and lagoon temperature during that time. Smith and Franco (1985) developed the computer model to predict lagoon temperature based on air temperature using the following Equation 4-5:

$$TL_i = \frac{TA_i\alpha_i + TA_{i-1}\alpha_{i-1} + \cdots + TA_{i-n}\alpha_{i-n}}{\alpha_i + \alpha_{i-1} + \cdots + \alpha_{i-n}} \qquad \text{Equation 4-5}$$

where

$TL_i$ = lagoon temperature (°C) for day *i*

$TA_i$ = mean air temperature (°C) for day *i*

$\alpha = e^{-bt}$, a weight factor that simulates the response of the lagoon to air temperature

b = constant

t = number of days (0, 1, 2, …, 365)

Equation 4-5 relates the lagoon temperature of one day to the air temperature of that day and the air temperature of prior days, up to a full year. The current day, day $i = 0$, is weighted 1, and other days are weighted by α, with weights decreasing as $i$ increases. The choice of $b$ determines how rapidly the weighting factor shrinks to a value that is small enough to be considered negligible. Smith and Franco (1985) recommended a value of $b = 0.2$ to produce the lowest deviation when predicting a lagoon temperature based on the air temperature. Smith and Franco (1985) found good agreement between their modelled and measured data when predicting lagoon temperatures for Fischer (1977) at a Midwest dairy lagoon.

Similar to Smith and Franco (1985), the temperature was predicted for the slurries at the studied dairy site in Visalia, California using daily average temperatures for the city for each month from February 2019 through January 2020, a full year. This range was selected because average slurry temperatures were obtained at the dairy farm for March 2019, June 2019, September 2019, and January 2020 and could be compared to the modelled output temperatures. Modelled temperatures for the manure management at the Visalia dairy farm during the months of these dairy campaigns are shown in Figure 4.4. The focus here was primarily on the slurry methane emissions, as the methane mixing ratios were much higher near the slurries and slurries are considered a larger contributor to methane emissions than lagoons when comparing surface area (Owen & Silver, 2015).

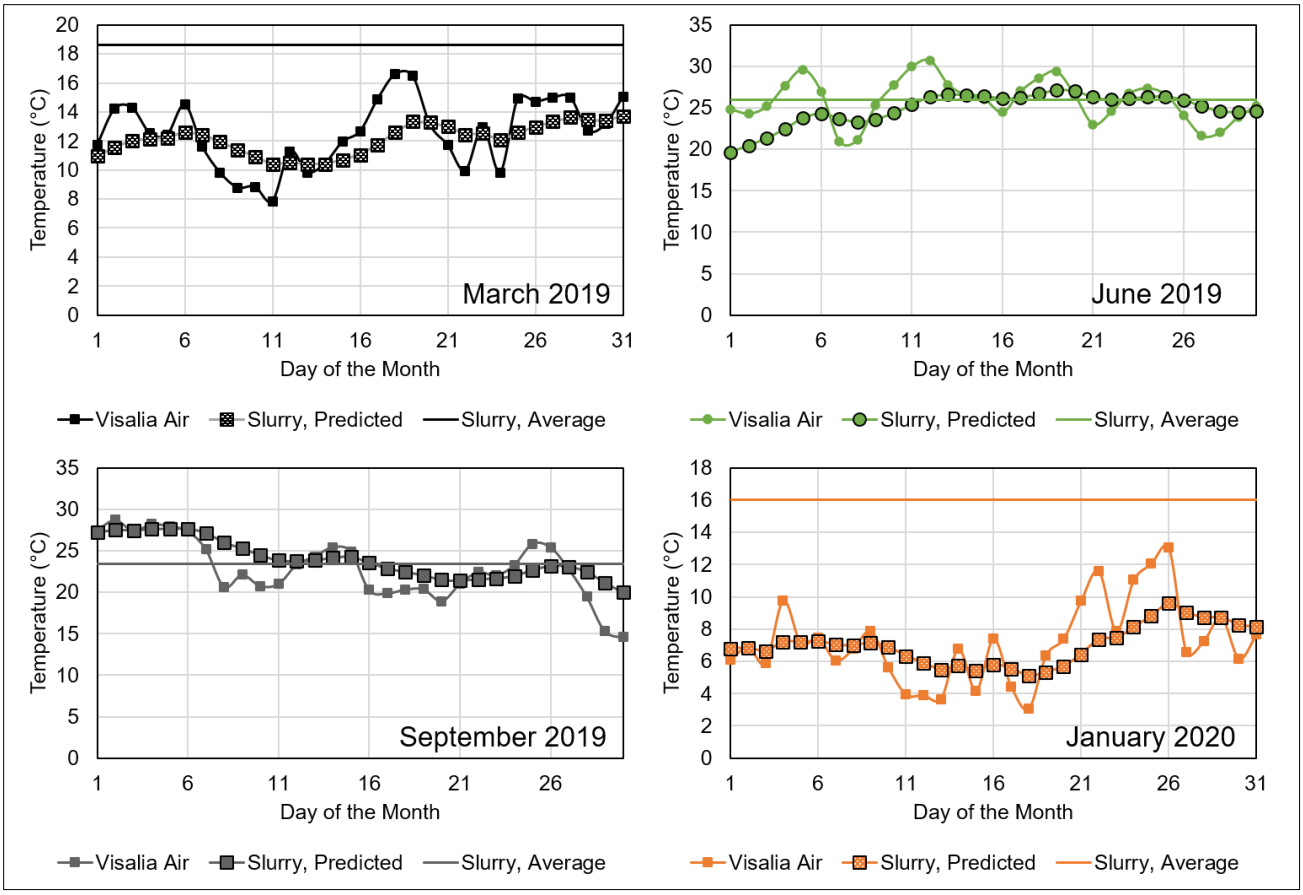


**Figure 4.4** Average daily air temperature (°C) at the dairy site in Visalia, CA, the predicted slurry temperature (°C), and the measured average slurry temperature (°C) for the March 2019, June 2019, September 2019, and January 2020 campaigns. Slurry temperatures were not measured for September 2018. Slurry temperatures were calculated with the equation introduced in Smith and Franco (1985), Equation 4-5, using daily average air temperatures for Visalia, California, where the dairy farm is located.

As shown in Figure 4.4, the predicted slurry temperature followed air temperature, with a slight time lag and dampening effect. Although the air temperature follows a diurnal pattern as the sun sets and rises, the temperature of the lagoons and slurries follows the average air temperature per day rather than per hour. The lagoons and slurries are primarily composed of water and waste solids, which take longer to respond to the sun's radiation than the ambient air.

The average modelled slurry temperatures for June (24.9 °C) and September 2019 (24.0 °C) were only 4% and 2% different, respectively, than the measured slurry temperatures during those campaigns, implying that the model was successful in predicting temperatures for those

months. This could have been because the measured slurry temperature was close to the ambient air temperature in Visalia, CA. However, the modelled slurry temperatures for March 2019 and January 2020 were much different than the measured values. The average measured slurry temperature for March 2019 was 53% higher than the modelled emissions, while the average measured slurry temperature for January 2020 was 128% higher than the modelled emissions. Although Smith and Franco (1985) had shown good agreement between their model and measured emissions, they had based their model on lagoon data only.

Lagoons traditionally hold a much larger volume than slurries and are less sensitive to ambient air changes (Leytem et al., 2017). Additionally, the slurries and lagoons at the studied dairy farm were relatively deep, up to four meters. Smith and Franco (1985) showed that the temperature profiles in lagoons < 2 meters deep followed the average air temperature very closely, as they could quickly adapt to changes (Smith & Franco, 1985). However, Hamilton & Cumba (2000) showed that uncovered lagoons > 2 meters deep formed thermal layers. They found that the upper layer closely followed that ambient air temperature, while the bottom layer exhibited fewer extreme changes and lagged behind the upper layer's monthly cycles (Hamilton & Cumba, 2000). This could help explain why the predicted slurry temperatures for the March and January campaigns—which occurred following colder times of the year—were so different from the measured temperatures. Additionally, the sludge that accumulated at the bottom of the slurry was emptied in August 2018 and again in April 2019. March 2019 temperature samples were collected about seven months after the slurries had been cleaned, and January 2020 temperature samples were collected about nine months after. In contrast, the June 2019 and September 2019 temperature samples had been collected only two and five months, respectively, after the slurries had been dredged. The extra solids in the lagoons during March 2019 and January 2020 may have contributed to the higher temperatures by decreasing the responsiveness of the slurries to

temperature change, which could also cause elevated methane emissions because of the higher temperature.

Modelled temperatures for the slurries at this dairy farm were calculated for all twelve months using average daily air temperatures for Visalia, CA, from February 2019 through January 2020. These numbers were obtained from the weather station at Visalia Municipal Airport, which is located about six miles from the dairy farm by air. After the calculation was completed, the *f* values for this dairy were calculated using Equation 4-3 using the model temperature outputs. These were compared to the *f* values that would be obtained using the EPA's Tier 2 methodology (i.e., using monthly air temperatures for the entire county rather than by city), which is how the methane contribution from manure management is calculated for the nationwide GHG inventory (EPA, 2020c). The *f* values for the modelled outputs compared to the *f* values calculated using EPA methodology for Spring, Summer, Fall, and Winter are shown in Figure 4.5A through Figure 4.5D.

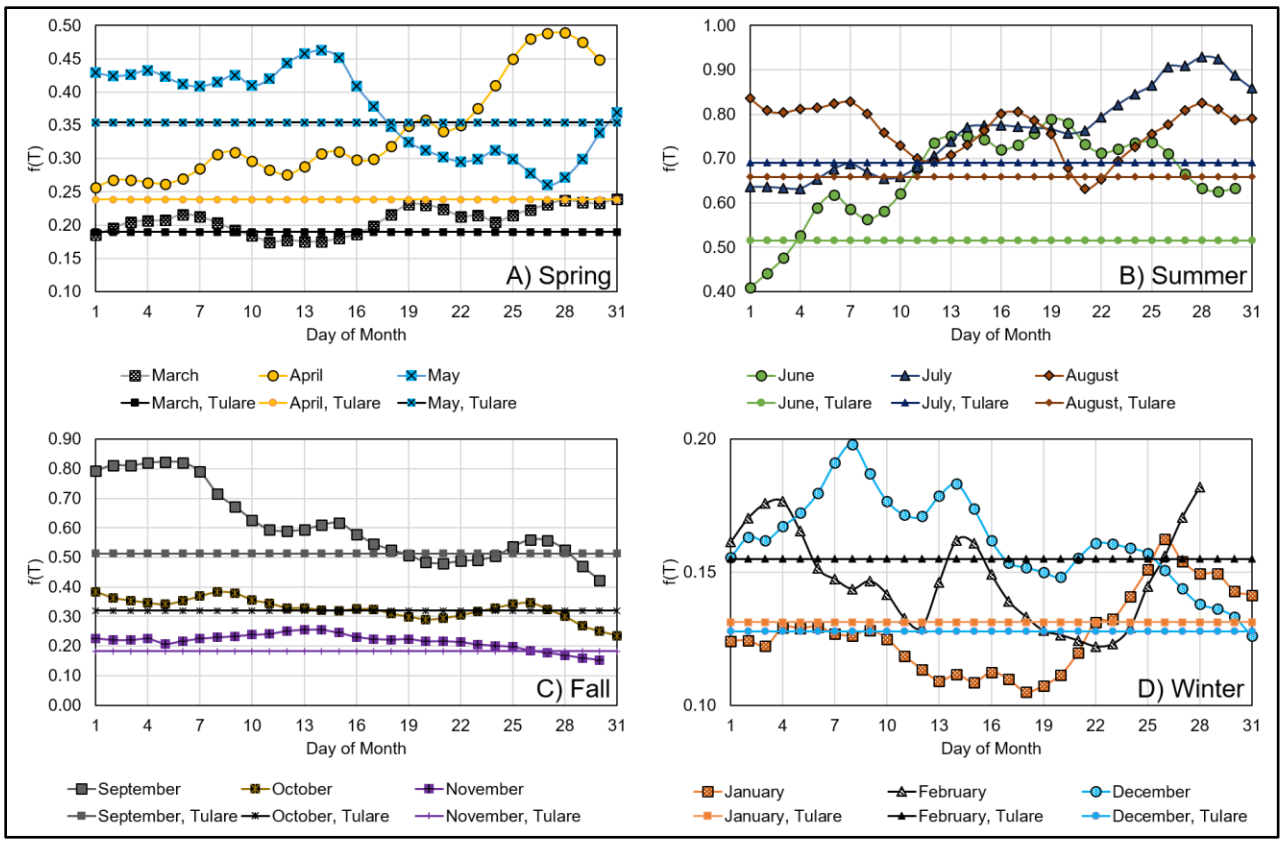


**Figure 4.5** Calculated *f* values using the modelled lagoon and slurry outputs compared to *f* values calculated using traditional EPA methodology (i.e., using the county average monthly air temperature) for A) Spring (March, April, and May), B) Summer (June, July, August), C) Fall (September, October, November), and D) Winter (December, January, February).

The *f* values shown in Figure 4.5 are directly proportional to the amount of methane that could be emitted by the slurries—the higher the *f* value, the more methane could be emitted. Based on the lower predicted lagoon temperatures for March 2019 and January 2020, the *f* values likely underestimate the amount of methane that could be produced during those months. The *f* values using the modelled lagoon emissions were much higher in April, all of Summer, part of September, and in December than the *f* values that were calculated using the EPA methodology from the 2020 GHG inventory (labelled "month, Tulare" in Figure 4.5). The percent difference between these values by month was calculated using Equation 4-6:

$$\text{Percent Difference } (\%) = \frac{\text{modelled } f \text{ value} - \text{EPA } f \text{ value}}{\text{EPA } f \text{ value}} * 100\% \qquad \text{Equation 4-6}$$

The EPA currently recommends using monthly ambient air temperatures of the entire county to calculate *f* values, while this study recommends modelling the temperature of the manure management system using the *daily* ambient air temperatures of the immediate area, rather than the county. A positive percent difference from Equation 4-6 means that the modelled *f* value using the modelled slurry and lagoon temperatures (this study, Equation 4-5) predicted that a higher amount of methane would be formed than the *f* value calculated from the monthly ambient air temperature of Tulare County (EPA inventory methodology) predicted. A negative percent difference indicated when the *f* value calculated from the County's ambient air temperature (EPA inventory methodology) predicted that a higher amount of methane would be released than the *f* values calculated from lagoon and slurry temperatures (this study, Equation 4-5) predicted. A graph representing these percent differences across all months is shown in Figure 4.6.

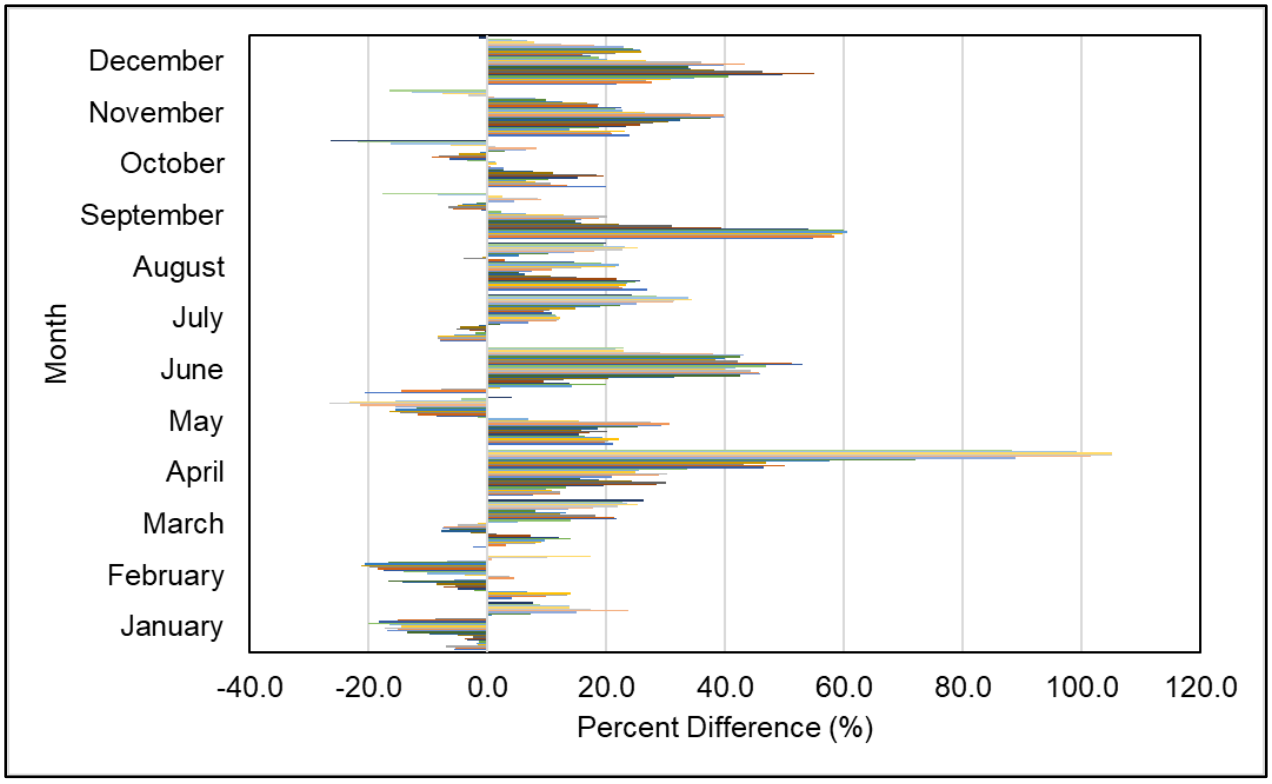


**Figure 4.6** Percent difference (%) between the *f* values calculated using modelled lagoon temperature at the dairy site and the *f* values calculated using Tulare County's ambient air temperature. Each individually colored bar represents one day in a specific month.

As the calculated *f* values are likely underestimated for March and January, the percent differences for those months, and possibly additional cold months, are expected to be much higher. However, the calculated *f* values for the warmer months are expected to predict more accurate emissions because the slurry temperature in June 2019 and September 2019 were in good agreement with the calculations. Overall, using the modelled slurry temperatures predicted much higher emissions than those using the traditional EPA (EPA, 2020c) methodology. Table 4.3 shows the average *f* value percent difference calculated using Equation 4-6 along with the standard deviations for each month.

**Table 4.3** Average, standard deviation, and maximum percent differences between the newly calculated *f* values based on slurry temperatures and the EPA (2020c) methodology based on average monthly ambient air temperatures in Tulare County

| Month | Average ± Standard Deviation (%) | Maximum (%) |
|---|---|---|
| January | -3±12 | 24 |
| February | -5±12 | 17 |
| March | 9±11 | 26 |
| April | 42±32 | 105 |
| May | 5±18 | 31 |
| June | 28±20 | 53 |
| July | 10±14 | 34 |
| August | 16±9 | 27 |
| September | 19±25 | 61 |
| October | 2±11 | 20 |
| November | 18±15 | 40 |
| December | 27±14 | 55 |

Based on Table 4.3, the EPA's GHG inventory, released in 2020, is underestimating methane emissions from manure management in Visalia by up to 105% depending on the month. It is likely that this underestimation expands to the entire Tulare County and possibly the entire SJV. These data suggest that, whenever possible, the manure management system's temperature should be used to calculate methane emissions rather than ambient air temperature, as there can be quite a large difference in predicted *f* values, and therefore a large difference in calculated methane emissions. Additionally, this study also suggests that using a daily (rather than monthly) average temperature might provide more accurate estimates for methane emissions.

To calculate the methane emissions from manure management at the dairy site, Equation 4-2 was used to calculate a methane emission factor. The *f* values calculated from the predicted slurry temperatures (Equation 4-4) were used in place of the MCF parameter. The $B_0$ values for dairy cows and heifers were selected to match the values chosen in the EPA 2020 GHG inventory methodology (EPA, 2020c). For mature dairy cows, 0.24 $m^3$ $CH_4$/kg VS was selected as $B_0$, as reported by Morris (1976). Additionally, 0.17 $m^3$ $CH_4$/kg VS was chosen as the $B_0$ for heifers, as reported by Bryant et al. (1976). For these values, "kg VS" indicates the weight of volatile solids produced. Overall, the $B_0$ represents the maximum amount of methane that can be produced by 1 kg VS under ideal conditions in a manure treatment system. The EPA inventory still uses these $B_0$ values to calculate methane emissions from dairy manure, despite that both values were first reported in 1976.

Although the $B_0$ represents a maximum and is not temperature dependent, it does depend on the feed ration and animal type as well as the manure age, quantity, and type of additional equipment (Godbout et al., 2010). More recent work suggests that the $B_0$ values might need to be revisited. Godbout et al. (2010) determined that the $B_0$ for Canadian dairy cows was 0.30 – 0.35 (± 2%) $m^3$ $CH_4$/kg VS, higher than Morris (1976). As shown in Equation 4-2, the emission factor (EF) is directly proportional to the $B_0$; the larger the $B_0$, the larger the EF. If the $B_0$ were closer to the higher-end Canadian estimate in Godbout et al. (2010), 0.35 $m^3$ $CH_4$/kg VS, then the EF would be nearly 150% higher than if the EPA's suggested value from Morris (1976) was used. Although recalculating the $B_0$ is outside the scope of this work, future studies should be done for California dairy cows to determine whether the estimates in Morris (1976) and Bryant et al. (1976) still hold true. The MDP value in Equation 4-2 was chosen as 0.8 overall as recommended by the EPA 2020 GHG inventory methodology, based on comparisons of models to empirical methane measurements from anaerobic manure management systems in the United States (EPA, 2020c).

The VS parameter in Equation 4-2 was estimated for each cow type (i.e., milk cows, dry cows, and heifers) at the dairy during March 2019, June 2019, September 2019, and January 2020. The values were very similar to the values recommended for dairy animals in Table A-187 in the EPA 2020 methodology (EPA, 2020c). The methane emissions from manure management were calculated in kilograms per hour, with the months of January, March, May, July, August, October, and December = 744 hours, February = 672 hours, and April, June, September, November = 720 hours as in a typical non-leap year (during which these dairy campaigns occurred). The methane emissions from the slurries per hour are shown in Figure 4.7 calculated using the estimated manure management temperatures to calculate the *f* value and overall $CH_4$ EF. Also included in Figure 4.7 are the calculated methane emissions using the EPA Tier 2 method, which only considers average *monthly air temperatures* in Visalia, and the IPCC Tier 1 estimate, which uses the average *annual air temperature* of the region, in this case the SJV (16.28 °C), to suggest an $EF_{dairy\ cow}$ = 65 kg $CH_4$ $hd^{-1}$ $yr^{-1}$ and $EF_{other\ cattle}$ = 2 kg $CH_4$ $hd^{-1}$ $yr^{-1}$ from their Table 10.14 (Eggleston et al., 2006). For the IPCC calculation, dairy cows and dry cows were considered “dairy cows,” while “heifers” were considered “other cattle.”

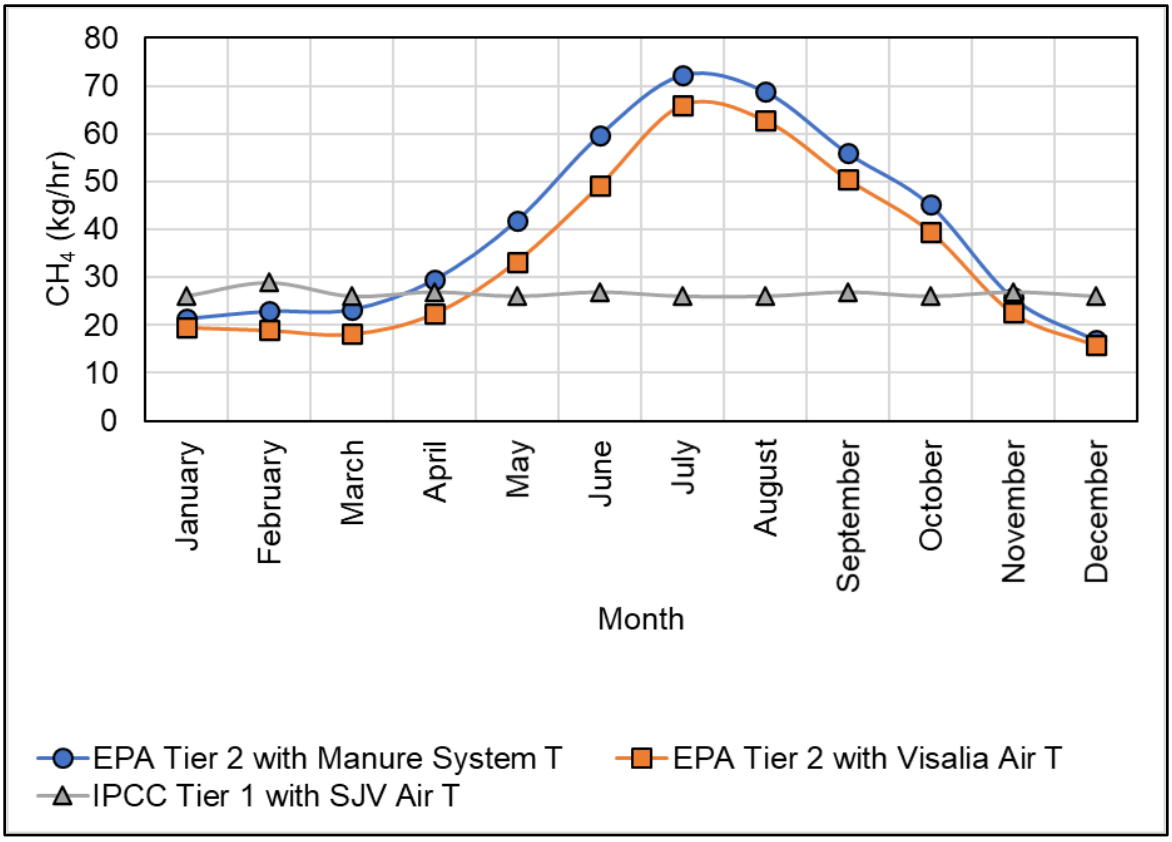


**Figure 4.7** Hourly emissions of methane from slurries at the dairy farm each month calculated using three methods: the EPA Tier 2 with manure management system temperature estimates to calculate *f* values (blue circles), the EPA Tier 2 with monthly Visalia air temperatures to calculate *f* values (orange squares), and the IPCC Tier 1 method with emission factors given based on annual air temperature for the entire SJV region (gray triangles).

Overall, the monthly contribution to methane emissions was calculated. Annually, this dairy farm releases at least 350 metric tonnes $CH_4$ from manure management of its slurries. Because the slurry temperatures were much warmer than the air temperature during the March 2019 and January 2020 campaigns, this calculation likely underestimates the methane emissions during the colder months. Overall, the EF estimates were higher using the manure management temperature estimates than they were when calculated using EPA Tier 2 or the IPCC Tier 1, which grossly underestimates the $CH_4$ emissions during warmer months. The annual value of 350 metric tonnes of $CH_4$ $yr^{-1}$ was compared to expected values from other slurry systems in previous studies.

Owen and Silver (2015) reviewed thirty-eight field studies of methane emissions at dairy farms and found that the average slurry system emitted 101±47 kg $CH_4$ $hd^{-1}$ $yr^{-1}$ (Owen & Silver, 2015). This expected value was scaled to determine the expected emissions from the dairy farm studied for this project using a weighted count of cows that contribute to manure management. Volatile solids were inputted to the manure management system, on average, at a rate of 21.2 Mg/day. Of this, milk cows contributed about 84%, dry cows contributed about 5%, and heifers contributed about 11%, on average throughout all the campaigns. These percentages were used to scale the contributions of the cow groups to effectively determine a new count for the number of animals that could be used to compare to the estimated emissions from Owen and Silver (2015). The equation created for this purpose is shown in Equation 4-7.

$$\mathrm{Head_{eff}} = \sum \mathrm{F_i N_i} \qquad \text{Equation 4-7}$$

where

$Head_{eff}$ = effective number of cows at the selected dairy site, in (hd)

i = cow category (i.e., milk cows, dry cows, heifers)

$F_i$ = scaling factor based on how much a cow category *i* contributed to the manure entering the slurries, averaged over the campaigns

$N_i$ = number of cows of category *i*, averaged over the campaigns, in (hd)

A table of the parameters used in Equation 4-7 is shown in Table 4.4.

**Table 4.4** List of inputs used for Equation 4-7

| **Inputs** | **Cow Category, *i*** | | |
|---|---|---|---|
| | **Milk Cows** | **Dry Cows** | **Heifers** |
| $F_i$ | 0.84 | 0.05 | 0.11 |
| $N_i$ | 3106 | 386 | 2985 |

Using Equation 4-7, the weighted effective number of cows that contribute to the manure management methane emissions was $Head_{eff}$ = 2954 hd. Using $Head_{eff}$ = 2954 hd and the expected emission rate for slurries from Owen and Silver (2015), 101±47 kg $CH_4$ $hd^{-1}$ $yr^{-1}$, an

average slurry system at the studied dairy site would be expected to emit a range of 34±16 kg $CH_4$ $hr^{-1}$. The calculation for average amount of methane emissions from manure management at the dairy farm revealed that the studied dairy farm emits, on average, 40±20 kg $CH_4$ $hr^{-1}$ from its slurries, very similar to the expected amount using the adjusted average slurry emission rate in Owen and Silver (2015).

In conclusion, future studies are encouraged to use the temperature of the manure management systems whenever possible (daily temperatures would be ideal) and to measure these temperatures during their campaigns rather than depending on a monthly or annual air temperature average for an entire county or region. It is also important to note that these emissions will change as temperatures are expected to increase. This is explored more in Chapter 4.2.1a below.

**4.2.1a Climate Change Analysis**

Methane emissions from dairy farms, particularly manure management emissions, are temperature dependent. Future temperature changes will greatly affect their potential emissions. Projected temperate changes are predicted depending on strategies that the world will take, and is taking, to try to prevent climate change. The IPCC released modelled projections of future radiative forcing that depend on these strategies in their 5$^{th}$ Assessment Report (AR5) (Pachauri et al., 2014). When radiative forcing is positive, Earth receives more incoming energy from the Sun than it radiates into space, which results in net warming. This is exacerbated by GHG emissions, which trap the heat close to the earth. Negative radiative forcing is the opposite: Earth radiates more energy into space than it receives from the Sun, which results in net cooling.

In all scenarios, known as Representative Concentration Pathways (RCPs), positive radiative forcing will likely lead to rising sea level and global temperatures over at least the next few decades, up to a century from now or more. For this study, an RCP known as “RCP4.5” was used to examine future climate change effects on the dairy site in Visalia, CA. In this scenario,

radiative forcing is expected to increase to, and stabilize at, 4.5 W/m$^2$ by 2100. Specific details about this pathway are given in Moss et al. (2008, 2010). For this exploration, it is important to know that RCP4.5 is a stabilization scenario which assumes that climate policies are put in place to limit emissions and radiative forcing. RCP4.5 also looks at the introduction of a set of GHG emission prices to limit emissions globally (Thomson et al., 2011). In RCP4.5, an increase of temperature with a mean and likely range of 1.4 °C (0.9 to 2.0 °C) is predicted by the mid-21$^{st}$ century, between the years 2046 and 2065. An increase of temperature with a mean and likely range of 1.8 °C (1.1 to 2.6 °C) is predicted by the end of the 21$^{st}$ century, between the years 2081 and 2100.

As shown in Chapter 4.2.2, a temperature increases will increase the *f* values and therefore the potential methane emissions from manure management in the SJV. The average *f* values by month for the studied dairy site in Visalia were calculated for 2020, 2046 to 2065, and 2081 to 2100 according to the RCP4.5 average temperature increases. These were calculated by first determining the corresponding slurry temperatures that would result from the air temperature increase using Equation 4-5, and then using those slurry temperatures to recalculate the *f* values according to Equation 4-4. A plot showing these predicted *f* values for 2020 and the two additional date ranges is shown in Figure 4.8.

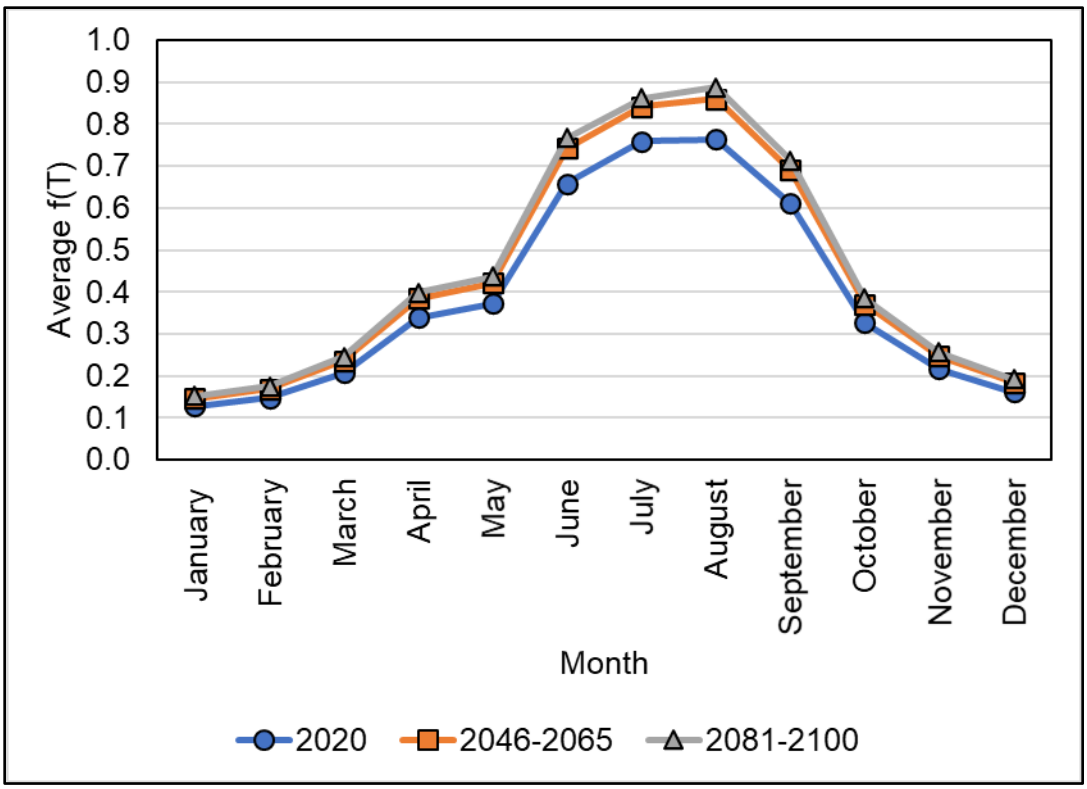


**Figure 4.8** Average monthly *f* values for 2020 compared to calculated *f* values according to the RCP4.5 projected temperature increase of 1.4 °C between 2046 to 2065 and 1.8 °C between 2081 to 2100.

The increase in temperature from 1.4 to 1.8 °C only slightly changed the *f* value. However, the *f* value from 2020 to the *f* value calculated using the two RCP4.5 temperature increases varied. The percent increase from the *f* value of 2020 to the *f* values predicted for the other two date ranges was calculated using Equation 4-8.

$$\text{Percent difference } (\%) = \frac{f_{RCP} - f_{2020}}{f_{2020}} \qquad \text{Equation 4-8}$$

where

$f_{RCP}$ = the average *f* value for each month, calculated using the 2020 Visalia air temperature (added to either 1.4 °C or 1.8 °C, depending on the date range for the RCP4.5 scenario) to calculate new slurry temperatures for each day of the month (following Equation 4-5)

$f_{2020}$ = the average *f* value for each month, using the 2020 Visalia air temperature to calculate slurry temperatures for each day of the month (following Equation 4-5)

Equation 4-8 calculated a percent difference, which can be also be considered an indicator of how much methane emissions could increase from manure management based solely on the temperature increase, which will increase the efficiency of the conversion of organic matter to methane by bacteria during decomposition. It is important to note that Mangino et al. (2002) recommended that any *f* values that exceed *f* = 0.95 be set to *f* = 0.95 to better mimic likely field conditions. In this calculation, the *f* value for some days of July (7 days for the 2046 – 2065 range; 9 days for the 2081 – 2100 range) and August (3 days for the 2081 – 2100 range) approached f = 1.0, which would indicate maximum conversion of organic matter to methane (Mangino et al., 2002). This is unlikely under field conditions, so all *f* values exceeding f = 0.95 in these months were set to *f* = 0.95. The average percent differences from the 2020 *f* values, with their standard deviations, across a whole year for the two different RCP4.5 time ranges (2046 – 2065 and 2081 – 2100) is shown in Table 4.5.

**Table 4.5** The percent difference between the average monthly *f* values for RCP4.5 in date ranges from 2046 – 2065 and 2081 – 2100 from the *f* values calculated for 2020, with values given as the mean and standard deviation

| **Month** | **Percent Difference (%)** | |
|---|---|---|
| | **2046 – 2065** | **2081 – 2100** |
| January | 14.5±0.1 | 19.0±0.2 |
| February | 14.4±0.1 | 18.8±0.2 |
| March | 14.0±0.1 | 18.3±0.2 |
| April | 13.5±0.2 | 17.6±0.3 |
| May | 13.3±0.2 | 17.4±0.3 |
| June | 12.7±0.2 | 16.6±0.2 |
| July | 11.1±3.2 | 14.0±4.5 |
| August | 12.6±0.1 | 16.2±0.6 |
| September | 12.8±0.2 | 16.7±0.3 |
| October | 13.5±0.1 | 17.6±0.2 |
| November | 13.9±0.2 | 18.2±0.2 |
| December | 14.2±0.1 | 18.7±0.2 |

The standard deviation was higher in July and August (for 2081 – 2100) as some of the values exceeding 0.95 were capped at 0.95 to mimic likely field conditions. The *f* values calculated for the later date period (years 2081 – 2100) in the RCP4.5 scenario had a greater percent increase from the 2020 values than the earlier date range because the temperature is expected

to increase with time. Based on Table 4.5, in terms of percentage, the temperature increase predicted by RCP4.5 would affect the colder winter months the most and hot summer months the least. However, it is clear from Figure 4.8 that the summer months will experience the greatest magnitude of *f* value change, and therefore an even greater increase for potential methane generation.

On average, based on the *f* value increase, the methane emissions from manure management at the selected dairy farm, and at Visalia in general could increase by up to 14.5±0.1% by 2046 and 19.0±0.2% by 2081. Although calculating emissions for all dairy farms in the SJV is outside the scope of this work, it is expected that counties with colder temperatures, such as Madera and Tulare, would be affected disproportionately more by the expected temperature increase based on the exponential nature of the *f* value calculation. As Tulare County has the highest number of cows in the SJV, this percent increase with temperature will likely become very important in the future as the winter months get warmer over time. Additionally, this does not account for how the extra GHG emissions produced because of the temperature increase could further increase the temperature, resulting in a positive feedback loop.

These projections are important because they can help dairy farmers plan for the future as well as inform legislators about which geographical regions to target for methane mitigation strategies. For example, knowing that colder counties with lots of cows (e.g., Tulare) will experience a disproportionately high shift in methane emissions from manure management will encourage interested parties to invest in new infrastructure (e.g., anaerobic digesters) for those locations. These options are discussed more in Chapter 8.5.2.

### 4.2.2 Estimated Methane Emissions from Enteric Sources

Manure management practices are clearly responsible for methane emissions within the SJV, and they will become even more important as global temperatures increase. Enteric emissions from the cows themselves represent another major source, although they are not

expected to change with rising temperatures. Enteric emissions of methane from the Visalia dairy farm were estimated using multiple approaches using IPCC and EPA methodologies.

As mentioned at the beginning of Chapter 4.2.1, the IPCC *2006 Guidelines for National Greenhouse Gas Inventories* also described methods (Tier 1 and Tier 2 approaches) for estimating enteric emissions from dairy cows in addition to their methodology for calculating manure management emissions (Eggleston et al., 2006). For their Tier 1 method, the IPCC simply recommends an already-calculated emission factor from a list of emissions factors. To select one of these emissions factors only requires knowing the animal populations present at the dairy farm.

The complexity increases with the Tier. For their Tier 1 method, the IPCC recommends using a standard enteric emission factor of EF = 128 kg $CH_4$ $hd^{-1}$ $yr^{-1}$ for fully grown milk cows and a value of EF = 53 kg $CH_4$ $hd^{-1}$ $yr^{-1}$ for all other cattle, including calves, heifers, and dry cows in North America (Eggleston et al., 2006). This Tier 1 method makes the calculation simpler if data for $Y_m$ and GE are unavailable. These Tier 1 EF estimates presented by IPCC were updated since 2006 by the EPA (2020c). Using the IPCC's methodology updated with more recent data, the EPA (2020c) now recommends a value of EF = 146 kg $CH_4$ $hd^{-1}$ $yr^{-1}$ for dairy cows, EF = 12 kg $CH_4$ $hd^{-1}$ $yr^{-1}$ for calves, EF = 46 kg $CH_4$ $hd^{-1}$ $yr^{-1}$ for replacement heifers between seven and eleven months old, and an EF = 69 kg $CH_4$ $hd^{-1}$ $yr^{-1}$ for replacement heifers between twelve and twenty-three months old. These will be known in this project as the EPA Tier 1 emission factors. The EPA (2020c) did not distinguish between dry cows and milk cows; all were grouped as "dairy cows" and there was no option for other cattle beyond these "dairy cows," "calves," and "heifers."

If additional information is known, Eggleston et al. (2006) recommends using a Tier 2 approach. The ideology behind the IPCC's Tier 2 approach is still commonly used in current literature, despite being published in 2006. All the enteric emissions factors presented in the IPCC (for Tier 1 and 2) do not depend on temperature, and instead depend on other parameters. For the Tier 2 approach, these include the gross energy (GE) intake (which, in turn, depends on

additional factors), a methane conversion factor, and the energy content of methane. The IPCC (Eggleston et al., 2006) proposed the following equation, Equation 4-9, for estimating an enteric emission factor (EF) using their Tier 2 method:

$$\mathrm{EF} = \frac{\mathrm{GE} * \left(\frac{\mathrm{Ym}}{100}\right) * 365}{55.65} \qquad \text{Equation 4-9}$$

where

EF = emission factor, in (kg $CH_4$ $hd^{-1}$ $yr^{-1}$)

GE = gross energy intake, in (MJ $hd^{-1}$ $day^{-1}$), which depends on the digestibility of the feed (i.e., how much is excreted versus absorbed); see Equation 4-10

$Y_m$ = methane conversion factor (i.e., the percentage of gross energy in the feed that is converted to methane)

55.65 = energy content of methane, in (MJ/kg $CH_4$)

365 = days in a year, in (day/yr)

The calculation for *GE* requires additional information, including the net energies of the animals' daily lives, activities, and duties. This information is not always easily accessible to dairy farmers or researchers, which is why Tier 1 is still often used. The formula to calculate *GE* from Eggleston et al. (2006) for the Tier 2 calculation in Equation 4-9 is shown in Equation 4-10:

$$\mathrm{GE} = \left[\frac{\left(\frac{\mathrm{NE_m}+\mathrm{NE_a}+\mathrm{NE_l}+\mathrm{NE_{work}}+\mathrm{NE_p}}{\mathrm{REM}}\right)+\left(\frac{\mathrm{NE_g}}{\mathrm{REG}}\right)}{\frac{\mathrm{DE\%}}{100}}\right] \qquad \text{Equation 4-10}$$

where

GE = gross energy, in (MJ/day)

$NE_m$ = net energy required by the animal for maintenance, in (MJ/day)

$NE_a$ = net energy for animal activity, in (MJ/day)

$NE_l$ = net energy for lactation, in (MJ/day)

$NE_{work}$ = net energy for work, in (MJ/day)

$NE_p$ = net energy required for pregnancy, in (MJ/day)

REM = ratio of net energy available in a diet for maintenance to digestible energy consumed

$NE_g$ = net energy needed for growth, in (MJ/day)

REG = ratio of net energy available for growth in a diet to digestible energy consumed

DE = Digestible energy expressed as a percent of gross energy, in (%)

Each of the net energy factors as well as *REM* and *REG* have a respective equation (Equations 4-11 to 4-18) that is used to calculate them. Table 4.6 summarizes these equations, their equation numbers, and their necessary parameters. These formulas are also presented in Eggleston et al. (2006).

**Table 4.6** Equations and parameters for the calculation of *GE* in Equation 4-10

| Factor | Eqn. # | Equation | Parameters |
|---|---|---|---|
| $NE_m$ | 4-11 | $\mathrm{NE_m} = \mathrm{Cfi} * (\mathrm{BW})^{0.75}$ | **$NE_m$** = net energy required by the animal for maintenance, in (MJ/day)<br>**$CF_i$** = coefficient for animal category, *i*<br>**BW** = live body weight, in (kg) |
| $NE_a$ | 4-12 | $\mathrm{NE_a} = \mathrm{C_a} * \mathrm{NE_m}$ | **$NE_a$** = net energy for animal activity, in (MJ/day)<br>**$C_a$** = coefficient for feeding situation<br>**$NE_m$** = net energy required by the animal for maintenance, in (MJ/day) |
| $NE_l$ | 4-13 | $\mathrm{NE_l} = \mathrm{milk}(1.47 + 0.40 * \mathrm{fat})$ | **$NE_l$** = net energy for lactation, in (MJ/day)<br>**milk** = amount of milk produced (kg milk/day)<br>**fat** = fat content of milk, in (% by weight) |
| $NE_{work}$ | 4-14 | $\mathrm{NE_{work}} = 10 * \mathrm{NE_m} * \mathrm{t}$ | **$NE_{work}$** = net energy for work, in (MJ/day)<br>**$NE_m$** = net energy required by the animal for maintenance, in (MJ/day)<br>**t** = number of hours per workday |
| $NE_p$ | 4-15 | $\mathrm{NE_p} = \mathrm{S}_{pregnancy} * \mathrm{C_{pregnancy}} * \mathrm{NE_m}$ | **$NE_p$** = net energy required for pregnancy, in (MJ/day)<br>**$C_{pregnancy}$** = pregnancy coefficient<br>**$S_{pregnancy}$** = portion of mature females that go through gestation each year<br>**$NE_m$** = net energy required by the animal for maintenance, in (MJ/day) |
| REM | 4-16 | $\mathrm{REM} = \left[1.123 - (4.092 * 10^{-3} * \mathrm{DE\%}) + [1.126 * 10^{-5} * (\mathrm{DE\%})^2] - \left(\frac{25.4}{\mathrm{DE\%}}\right)\right]$ | **REM** = ratio of net energy available in a diet for maintenance to digestible energy consumed<br>**DE** = Digestible energy expressed as a percent of gross energy, in (%) |
| $NE_g$ | 4-17 | $\mathrm{NE_g} = 22.02\left(\frac{\mathrm{BW}}{\mathrm{C}_g * \mathrm{MW}}\right)^{0.75} * \mathrm{WG}^{1.097}$ | **$NE_g$** = net energy needed for growth, in (MJ/day)<br>**BW** = live body weight, in (kg)<br>**$C_g$** = growth coefficient<br>**MW** = mature live body weight adult animal in moderate condition, in (kg)<br>**WG** = average daily weight gain of animals, in (kg/day) |
| REG | 4-18 | $\mathrm{REG} = \left[1.164 - (5.160 * 10^{-3} * \mathrm{DE\%}) + [1.308 * 10^{-5} * (\mathrm{DE\%})^2] - \left(\frac{37.4}{\mathrm{DE\%}}\right)\right]$ | **REG** = ratio of net energy available for growth in a diet to digestible energy consumed<br>**DE** = Digestible energy expressed as a percent of gross energy, in (%) |

Solving each of the Equations 4-11 through 4-18 generates the necessary information to solve for *GE* in Equation 4-10 and eventually for the enteric emission factor, EF, for which the calculation was shown in Equation 4-9.

For the Visalia dairy site, a Tier 2 approach, as outlined by Eggleston et al. (2006) was used to estimate enteric EFs for the milk cows, dry cows, and heifers present at the dairy. A list of the parameters used, their sources, and their values for these three categories are shown in Table 4.7.

**Table 4.7** Values for the parameters used to calculate the enteric EF for milk cows, dry cows, and heifers at the dairy site

| Parameter (Units) | Milk Cow | Dry Cow | Heifer |
|---|---|---|---|
| $Cf_i$ | 0.386 [a,b,c] | 0.322 [a,b,c] | 0.322 [a,b,c] |
| BW (kg) | 680 [d] | 680 [d] | 364 [e] |
| $C_a$ | 0.00 [c] | 0.00 [c] | 0.00 [c] |
| milk (kg milk/day) | 23.7 [f] | 0 | 0 |
| fat (% by weight) | 3.5 [f] | 0 | 0 |
| t | 0 | 0 | 0 |
| $S_{pregnancy}$ | 0.1 | 1 | 0 |
| $C_{pregnancy}$ | 0.1 [a,c] | 0.1 [a,c] | 0 |
| DE | 66.7 [g] | 66.7 [g] | 63.7 [g] |
| $C_g$ | 0.8 [a] | 0.8 [a] | 0.8 [a] |
| MW | 680 [d] | 680 [d] | 680 [d] |
| WG | 0 | 0 | 0.683 [e] |
| $Y_m$ | 5.9 | 5.9 | 6.0 |

[a] NRC (1996)
[b] AFRC (1993)
[c] Eggleston et al. (2006)
[d] Holstein Association (2021)
[e] Heinrichs and Losinger (1998)
[f] Mylostyvyi and Chernenko (2019)
[g] EPA (2020c)

The parameter $Cf_i$ was developed by Eggleston et al. (2006) using data reported in NRC (1996) and AFRC (1993). Cattle and buffalo categories that include non-lactating cows, steers, and juveniles have $Cf_i$ = 0.322. It is estimated that a cow's maintenance requirement during lactation is 20% more than a non-lactating cow, so milk cows' $Cf_i$ values were increased by 20%. For average *BW*, the Holstein Association (2021) reported that the average weight of a Holstein cow (i.e., the only breed of cow at the dairy site) was 1,500 lbs, or 680 kg.

Much less information is collected on the *BW* of heifers, as they are not slaughtered for meat, so there are little industry data, and their body weight is not typically recorded for scientific studies. However, Heinrichs and Losinger (1998) evaluated data from the National Dairy Heifer Evaluation Project in 1991 to 1992, which included data from nearly nine thousand Holstein cows from 659 dairy farms nationwide. Heinrichs and Losinger (1998) was used to determine the *BW* for heifers and the *WG* for heifers for this study. Heinrichs and Losinger (1998) pooled the weights of heifers in different national regions for different ages within a linear growth range. Age categories included 90 days, 180 days, 208 days, 365 days, and 545 days. It was assumed for this study that the heifers on site were less than two years old, as most heifers first calve after two years old (EPA, 2020c). The age for all heifers on site for this study was assumed to be 15 months to calculate their *BW*. Pooled data from Heinrichs and Losinger (1998) revealed a linear trend until 545 days, as shown in Figure 4.9.

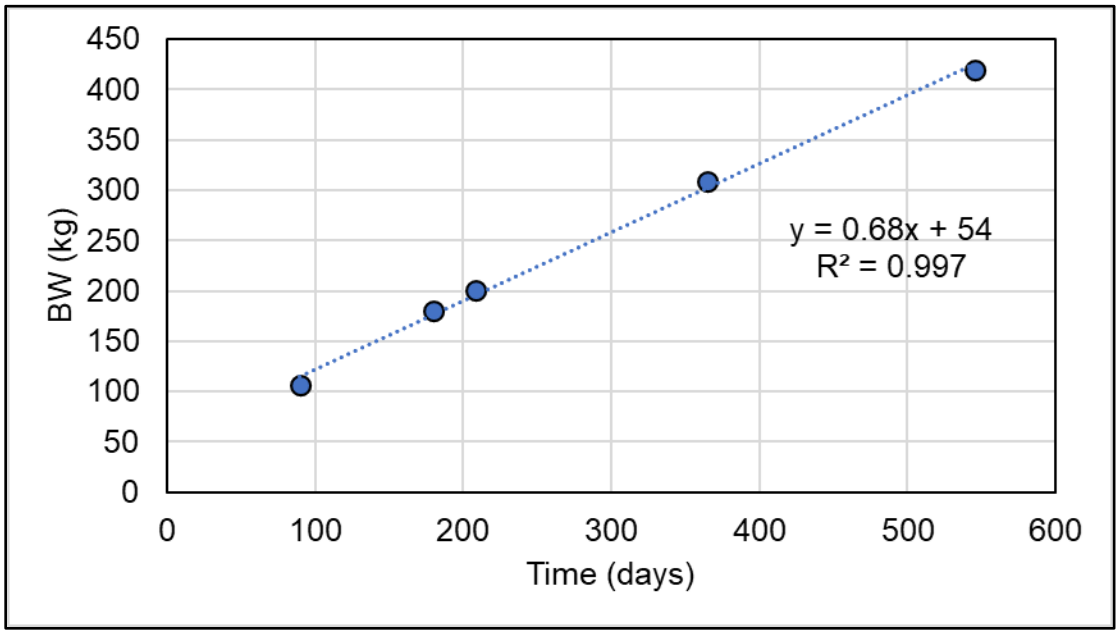


**Figure 4.9** Data adapted from Heinrichs and Losinger (1998) showing average weights for Holstein heifers. The slope (0.68 kg/day) represents the average weight gain (*WG*) of a heifer at the dairy farm during the linear growing period. The body weight (*BW*) for 15-month-old heifers at the dairy farm was calculated using the formula given in the figure, y = 0.68x + 54.

The formula in Figure 4.9, y = 0.68x + 54, was used to calculate the *BW* of the heifers at 15 months (i.e., 456 days, within the linear growth range). Eventually, the growth of heifers levels off, but data were extrapolated only within the linear range. The slope shown in Figure 4.9, 0.68 kg/day, was used as the *WG* value in Table 4.7. Dairy cows and dry cows are mature animals that are finished growing, and they were assumed to have a negligible weight change over course of the campaign. Therefore, they were given a value of *WG* = 0 kg/day in Table 4.7.

The coefficient that corresponds to the animals' feeding situation, $C_a$, is defined by how much effort the cows exert trying to get food. For cattle and buffalo that are confined to a small area, Eggleston et al. (2006) recommends $C_a$ = 0.00 because the cows expend a negligible amount of energy to reach their food. Cows in pastures or in large grazing areas have larger $C_a$ values, $C_a$ = 0.17 or $C_a$ = 0.36, respectively (Eggleston et al., 2006).

The specific values for the milk production (i.e., *milk* in Table 4.7) and milk fat percentages (i.e., *fat* in Table 4.7) were unknown for the Visalia dairy farm but were estimated using Holstein cow data collected by Mylostyvyi and Chernenko (2019), which collected statistics from 700 milk cows and recorded the daily milk production and milk fat weight over a fourth month period. Using this data, an average daily milk production from Holstein cows was calculated as milk = 23.7 kg/day, and the average milk fat weight was 0.83 kg (Mylostyvyi & Chernenko, 2019). Milk fat percentage was obtained by dividing the average milk fat weight by the average daily milk production to calculate fat = 3.5%. Dry cows and heifers do not produce milk, and therefore have the values of *milk* = 0 kg/day and *fat* = 0% in Table 4.7.

The *t* parameter only applies to draft animals that draw heavy loads. None of the animals work at the dairy, so *t* = 0 for all three categories. For the $S_{pregnancy}$ parameter, a scaling factor was selected based the fraction of cows at the dairy that go through gestation each year. This value was unknown for this dairy but was estimated to be the full value of $S_{pregnancy}$ = 1 for dry cows, which were separated from the milk cows because they were currently pregnant and unable to

produce milk. Cows cannot produce milk when they are well along in their pregnancy, so it was assumed that only a small fraction of milk cows were in an early enough stage of their current pregnancy to still produce milk from their previous pregnancy. Therefore, a value of $S_{pregnancy}$ = 0.1 was assumed for the milk cows. The scaling factor $S_{pregnancy}$ was only applied to the milk cows and the dry cows, as heifers are unable to become pregnant at the assumed age of 15 months old. Similarly, a $C_{pregnancy}$ value of $C_{pregnancy}$ = 0.1 was selected for the milk cows and dry cows only. This $C_{pregnancy}$ value was developed by NRC (1996) for the cattle and buffalo category and recommended by Eggleston et al. (2006).

The *DE* parameter, which indicates the portion of the *GE* that is not excreted as waste, had outdated ranges presented by Eggleston et al. (2006). Generally, Eggleston et al. (2006) recommended that cows that are fed crop byproducts have a *DE* = 45 – 55%, cows that graze good pastures have a *DE* = 75 – 85%, and cows fed grain-based diets in feedlots have a *DE* > 90%. However, the EPA (2020c) reported after analyzing literature values of *DE* that, while there was little regional variability, there was greater variability over time as diets have changed nationwide. They created specific date ranges for *DE* values: 1990 – 1993, 1994 – 1998, 1999 – 2003, 2004 – 2006, 2007, and 2008+ (EPA, 2020c). The EPA (2020c) recommends slightly different *DE* values for California, the West, Northern Great Plains, Southcentral, Northeast, Midwest, and Southeast. Therefore, their *DE* values updated for 2017 for California were used in Table 4.7 for milk cows and dry cows. There are fewer studies about heifers than full grown cows, so the EPA (2020c) recommends subtracting 3% from the *DE* of dairy cows based on the relationship of the data collected in the literature regarding the nuances of heifer and dairy cows' diets.

The $C_g$ value, which scales how much energy a cow expends into growing, was dictated by gender. The NRC (1996) recommended $C_g$ = 0.8 for females, $C_g$ = 1.0 for castrates, and $C_g$ = 1.2 for bulls. As all the cows on the dairy are females, a value of $C_g$ = 0.8 was used for all cows.

The $Y_m$ parameter changes as the cow ages. For example, Soliva et al. (2006) found that $Y_m$ = 7.8% for calves at four months, $Y_m$ = 8.03% for calves at five months, and $Y_m$ = 8.27% at six months old. However, the parameter decreases again as the cow ages. For the $Y_m$ parameter for fully grown cows, the EPA (2020c) recommends $Y_m$ = 5.9% for milk cows. As there are not enough data available for heifers, the EPA (2020c) estimated based on current literature that the $Y_m$ for heifers is slightly larger, as the heifers are younger. They suggest $Y_m$ = 6.0% for heifers.

The EF values for milk cows, dry cows, and heifers at the dairy farm were calculated using the inputs in Table 4.7 using the IPCC Tier 2 methodology presented in Equation 4-9. The $EF_{milk\ cow}$ = 134 kg $CH_4$ $hd^{-1}$ $yr^{-1}$, $EF_{dry\ cow}$ = 53 kg $CH_4$ $hd^{-1}$ $yr^{-1}$, and the $EF_{heifer}$ = 55 kg $CH_4$ $hd^{-1}$ $yr^{-1}$. These calculated EFs for the dairy farm were compared to the Tier 1 estimates given by the 2006 IPCC report (Eggleston et al., 2006) and the EPA Greenhouse Gas Inventory (EPA, 2020c). The comparison is shown in Table 4.8.

**Table 4.8** Enteric Emission Factors estimated using three different methods: IPCC Tier 1, EPA Tier 1, and IPCC Tier 2

| Category | Enteric Emission Factor (kg $CH_4$ $hd^{-1}$ $yr^{-1}$) | | |
|---|---|---|---|
| | IPCC Tier 1[a] | EPA Tier 1[b] | IPCC Tier 2[a] (this study) |
| **Milk Cow** | 128 | 146 | 134 |
| **Dry Cow** | 53 | 146 | 53 |
| **Heifer (15 months)** | 53 | 69 | 55 |

[a] Eggleston et al. (2006)
[b] EPA (2020c)

Using the IPCC Tier 2 methodology for this dairy farm estimated a slightly higher EF for milk cows than the IPCC Tier 1 methodology. However, it was lower than the suggested Tier 1 estimate for California presented by the EPA Tier 1 methodology. For dry cows, the estimated EF using the IPCC Tier 2 methodology was identical to the suggested EF from the IPCC Tier 1 methodology. However, it was an order of magnitude lower than the suggested value from the EPA Tier 1 methodology. This is likely because the EPA Tier 1 calculation does not distinguish between dry cows and milk cows, which ends up overestimating the amount of methane they produce. Additionally, the difference between milk cows and dry cows might also have to do with

the dominant terms used in Equation 4-10 for each cow type. The largest term for dry cows was $NE_p$ (Equation 4-15), but this was much smaller than the dominant term for milk cows, $NE_l$ (Equation 4-13). It was also smaller than the heifers' most dominant term, $NE_g$ (Equation 4-17). As $NE_p < NE_g < NE_l$, it should not be surprising that $EF_{dry\ cow} < EF_{heifer} < EF_{milk\ cow}$.

For heifers (aged fifteen months), the IPCC Tier 2 methodology predicted a similar EF value to the IPCC Tier 1 and EPA Tier 1 methodologies, but it was closer to the IPCC Tier 1 estimate at the lower end. Total annual enteric methane emissions using the average population numbers of cows in each category at the dairy farm were estimated using all three methodologies. These results are shown in Table 4.9.

**Table 4.9** Average annual animal numbers and the total annual enteric emissions (metric tonnes $CH_4$) calculated using IPCC Tier 1, EPA Tier 1, and IPCC Tier 2 methodologies

| Category | Average (hd) | Total Annual Emissions (metric tonnes $CH_4$) | | |
|---|---|---|---|---|
| | | IPCC Tier 1[a] | EPA Tier 1[b] | IPCC Tier 2[a] (this study) |
| Milk Cows | 3106 | 398 | 453 | 417 |
| Dry Cows | 386 | 20 | 56 | 20 |
| Heifers | 2985 | 158 | 206 | 163 |
| **Total** | **6477** | **576** | **715** | **600** |

[a] Eggleston et al. (2006)
[b] EPA (2020c)

Based on Table 4.9, the IPCC Tier 1 method would have underestimated enteric emissions from milk cows by only 5%, but the EPA Tier 1 method would have overestimated them by 9%. For dry cows, the IPCC Tier 2 and IPCC Tier 1 methodologies predicted identical annual enteric emissions, 20 metric tonnes $CH_4$. Surprisingly, the newer EPA Tier 1 methodology overestimated dry cow enteric emissions by 180%. Lastly, for the heifers, the IPCC Tier 1 estimates were only 3% lower than the IPCC Tier 2 estimates, while the EPA Tier 1 estimates overestimated emissions from heifers by 26%.

Therefore, for this dairy farm, the IPCC Tier 1 methodology (i.e., simply selecting an appropriate pre-determined EF) was surprisingly close to the estimated values at the dairy farm for using the IPCC Tier 2 methodology (calculated using Equations 4-9 through 4-18). The updated EPA Tier 1 methodology (i.e., selecting updated pre-determined EFs for various cow

categories) did a poor job of predicting emissions, particularly for the dry cow and heifer categories. Overall, using the more involved IPCC Tier 2 calculation, this dairy farm was estimated to release 600 metric tonnes per year of enteric methane total summed over all three types of cows (i.e., milk cows, dry cows, and heifers), where $EF_{milk\ cow}$ = 134 kg $CH_4$ $hd^{-1}$ $yr^{-1}$, $EF_{dry\ cow}$ = 53 kg $CH_4$ $hd^{-1}$ $yr^{-1}$, and $EF_{heifer}$ = 55 kg $CH_4$ $hd^{-1}$ $yr^{-1}$.

### 4.3 Methane at Orange County Landfills

California, in particular Orange County, has some of the strictest landfill requirements in the country. Therefore, it was expected that Orange County landfills likely do not release as much methane into the atmosphere as other landfills nationwide. It was also expected that Orange County landfills would not emit as much methane as the SJV dairy farms because of their installed LFG capture and energy conversion infrastructure, effective cover materials, and interior liners. Landfills accounted for over 17% of total anthropogenic $CH_4$ emissions in 2018 in the United States, the third largest contribution of methane (behind enteric fermentation and natural gas systems) (EPA, 2020c).

Raw, undiluted, and unflared landfill gas samples collected by representatives of Cal Poly SLO at Chiquita Canyon and Santa Maria Regional landfills revealed that high amounts of methane and carbon dioxide are indeed released by the decomposing waste, but that the gases are effectively trapped under the surface. Raw LFG samples collected at the Chiquita Canyon landfill in July 2018 had excessively high $CH_4$ and $CO_2$, with each contributing about 30%. However, the $CH_4$ and $CO_2$ at the landfill's surface were nowhere near these values. On the surface, the mixing ratios were highest near the new waste, with maximum values of 20.80 ppm $CH_4$ and 1140 ppm $CO_2$ at the beginning (time = 0 minutes) of Cal Poly's flux chamber measurement.

Although underground LFG samples were unable to be collected at the landfills in Orange County, it is assumed that the mixing ratios of $CH_4$ and $CO_2$ were likely much lower on the surface

than in the ground because of the implementation of modern landfill engineering techniques which prevent the escape of rogue LFG emissions. Orange County also follows very stringent landfill guidelines and has installed perimeter monitors to track fugitive emissions.

The maximum, minimum, average, and median $CH_4$ mixing ratios for Orange County landfills across all four seasons are presented in Figure 4.10. In general, the active landfills (Frank R. Bowerman, Olinda Alpha, and Prima Deshecha) had higher methane mixing ratios than the closed landfills (Coyote Canyon and Santiago Canyon)

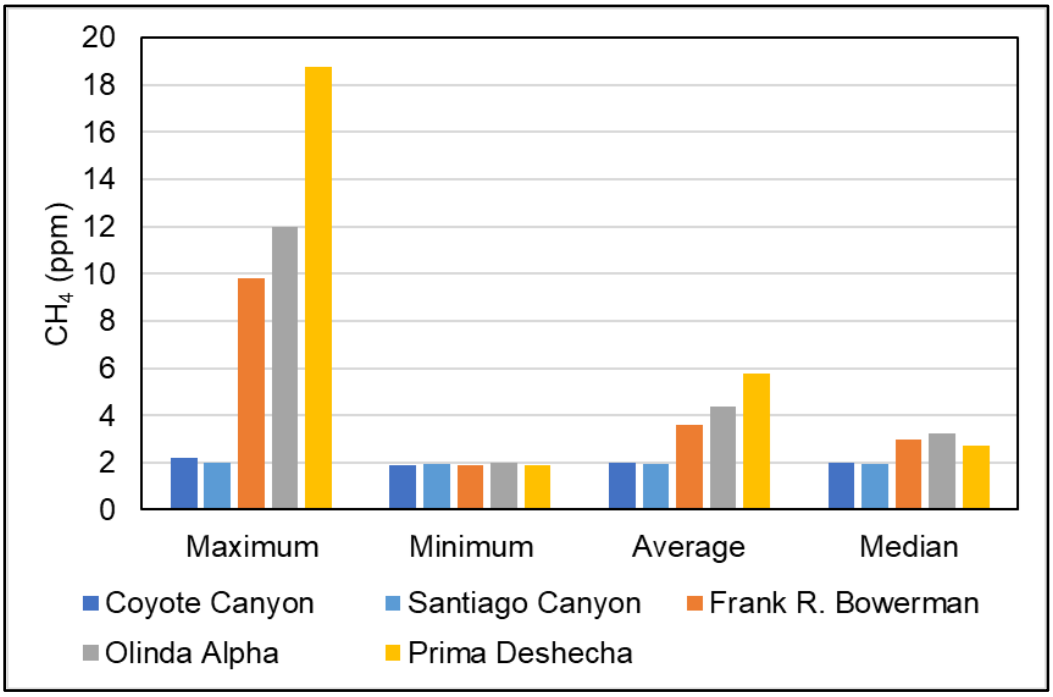


**Figure 4.10** Methane (ppm) maximum, minimum, average, and median mixing ratios across all campaigns at Orange County landfills. Coastal background was 1.931 ppm.

Prima Deshecha had the highest maximum and average $CH_4$, at 18.8 ppm and 5.78 ppm. The closed landfills, Coyote Canyon and Santiago Canyon, had the lowest maximum and average values of $CH_4$. Coyote Canyon had maximum and average $CH_4$ mixing ratios of 2.20 ppm and 1.99 ppm. Santiago Canyon was even lower, with a maximum $CH_4$ mixing ratio of 2.01 ppm and an average of 1.96 ppm. Olinda Alpha and Frank R. Bowerman had maximum $CH_4$ values of

12.00 and 9.80 ppm, respectively. Their average $CH_4$ values across all four seasons were 4.36 ppm and 3.58 ppm, higher than the closed landfills but lower than the $CH_4$ at Prima Deshecha.

The average $CH_4$ at Prima Deshecha was higher than at the other Orange County landfills likely because of one sample collected near a potentially leaky LFG pump. Landfill gas has extremely high amounts of methane and carbon dioxide (Farquhar & Rovers, 1973). If Prima Deshecha's infrastructure was leaky during that sample, $CH_4$ would be excessively emitted. Examining the median mixing ratios for $CH_4$ at each Orange County landfill confirmed this reasoning. The median $CH_4$ values at Coyote Canyon, Santiago Canyon, Frank R. Bowerman, Olinda Alpha and Prima Deshecha landfills were 1.966 ppm, 1.956 ppm, 2.993 ppm, 3.258 ppm, and 2.736 ppm, respectively. Prima Deshecha's median $CH_4$ value, 2.736 ppm, was the lowest median out of the three active landfills; this supports that its high methane average was indeed caused by leaky infrastructure from one sample collected at one campaign.

Interestingly, the median $CH_4$ did not seem to vary seasonally at the active landfills. For active landfill samples collected during Spring 2018, Summer 2018, Fall 2018, and Winter 2019, the median $CH_4$ mixing ratios were 2.564 ppm, 3.295 ppm, 3.250 ppm, and 2.993 ppm, respectively. This shows little seasonal dependence. However, the average $CH_4$ mixing ratio was slightly higher in Summer and Fall than it was in Spring and Winter. According to a personal interview with landfill engineers at Frank R. Bowerman and Olinda Alpha, the landfills had reached their maximum daily waste disposal limit multiple times throughout Summer 2018. For some summer days, Orange County active landfills received more waste than was allowed, causing them to turn away the dump trucks. Whenever one landfill was full for the day, waste disposal rose at the other local landfills that could still accept waste. This unexpectedly excessive waste disposal throughout Summer 2018 could account for the elevated methane during the Summer and Fall 2018 samples. Although $CH_4$ was elevated more at the active landfills than the closed landfills, it was not nearly as elevated as the methane found at some locations at the dairy site in

Visalia. Surprisingly, the methane at the active landfills was closer to the average "background" of 1.931 ppm $CH_4$ along on the California coast in 2018 than it was to most of the average mixing ratios for various locations around the dairy farm.

The difference between the lower mixing ratios of methane at the landfills and the higher mixing ratios of methane at the dairy farm can be partially explained by how methane enters the atmosphere at both locations. At landfills, waste must begin to decompose before $CH_4$ and $CO_2$ can begin to form. By this time, the waste is typically buried in the ground under layers of cover material, with pumps to suck out the LFG before it can get to the surface. This leads to a lower amount of methane on the surface of the landfill. Dairy farms do not have such mitigation measures in place, which explains why their $CH_4$ levels were much higher. Although methane mixing ratios were only slightly elevated on the surface of the landfill compared to the dairy farm, these emissions can add up over the course of the year. The annual amount of methane emitted at Orange County landfills is explored in the next section, Chapter 4.3.1.

### 4.3.1 Estimated Methane Emissions at Orange County Landfills

Landfills in California calculate and report their methane emissions yearly to the EPA Greenhouse Gas Reporting Program (GHGRP) as required by the federal Code of Regulations, Title 40, Part 98, "Mandatory Greenhouse Gas Emissions" (Calculating GHG Emissions, 2013). Landfills that have gas collection systems (all Orange County sites in this study), are required to calculate emissions using two different methods and report the results from each. In the first method, the amount of $CH_4$ recovered from the LFG destruction system is subtracted from the modeled annual $CH_4$ generation ($G_{CH4}$) and adjusted to include soil oxidation and the efficiency of the LFG destruction system. In the second method, a gas collection efficiency value is applied to the amount of $CH_4$ recovered to account for $CH_4$ that is emitted through the landfill surface, also adjusted for the soil oxidation. More information about the two methods and their associated parameters is presented in Bronstein et al. (2011).

As part of the GHGRP, landfills model their methane emissions using the following Equation 4-19, which is described in the federal Code of Regulations, Title 40, Part 98, "Mandatory Greenhouse Gas Emissions" as Equation HH-1 (Calculating GHG Emissions, 2013). This $G_{CH4}$ value represents the maximum amount of methane generated by the landfill.

$$G_{CH4} = \left[\sum_{X=S}^{T-1}\left\{W_x * DOC_x * MCF_x * DOF_F * F * \left(\frac{16}{12}\right) * \left(e^{-k(T-x-1)} - e^{-k(T-x)}\right)\right\}\right] \quad \text{Equation 4-19}$$

where

$G_{CH4}$ = amount of $CH_4$ generated (metric tonnes $yr^{-1}$)

X = year in which waste was disposed

S = start year of the calculation

T = reporting year for which emissions were calculated

$W_x$ = quantity of waste disposed in landfills in year X, in (metric tonnes, as received)

$DOC_x$ = degradable organic carbon for waste disposal in year X, in (metric tonnes C/metric tonnes waste)

$DOC_F$ = fraction of DOC dissimilated

MCF = methane correction factor

F = fraction by volume of $CH_4$ in generated LFG

k = decay rate constant ($yr^{-1}$)

This $G_{CH4}$ value is then used to calculate actual methane emissions using the first method, titled Equation HH-6 in the federal Code of Regulations, and Equation 4-20 here (Calculating Greenhouse Gas Emissions, 2013). Equation 4-20 should be applied to each recovery system (e.g., flare) and summed to determine total methane emissions after subtracting out the methane that was destroyed.

$$CH_4 = \left[(G_{CH4} - R) * (1 - OX) + R * \left(1 - (DE * f_{Dest})\right)\right] \quad \text{Equation 4-20}$$

where

$CH_4$ = $CH_4$ emissions from the landfill in the reporting year, in (metric tonnes $CH_4$)

$G_{CH4}$ = amount of $CH_4$ generated, in (metric tonnes $yr^{-1}$)

R = quantity of $CH_4$ recovered from Equation HH-4 of the GHGRP, in (metric tonnes)

OX = oxidation factor, in (%)

DE = destruction efficiency, in (%)

$f_{Dest}$ = fraction of hours the destruction device was operating during active gas flow

As previously mentioned, landfills with LFG collection systems are required to also report their methane emissions using a second method, titled Equation HH-8 in the federal Code of Regulations, Title 40, Part 98, and Equation 4-21 here. Equation 4-21 should be applied to each recovery system (e.g., flare) and summed to determine total methane emissions after subtracting out the methane that was destroyed (Calculating Greenhouse Gas Emissions, 2013). Equation HH-8 is written here as Equation 4-21.

$$\mathrm{CH_4} = \left[\left(\frac{\mathrm{R}}{\mathrm{CE}*\mathrm{f_{Rec}}} - \mathrm{R}\right) * (1 - \mathrm{OX}) + \mathrm{R} * (1 - \mathrm{DE} * \mathrm{f_{Dest}})\right] \qquad \text{Equation 4-21}$$

where

$CH_4$ = $CH_4$ emissions from the landfill in the reporting year, in (metric tonnes $CH_4$)

R = quantity of $CH_4$ recovered from Equation HH-4 of the GHGRP, in (metric tonnes)

CE = collection efficiency estimated at landfill

$f_{Rec}$ = fraction of hours the recovery system associated with a measurement location was operating

OX = oxidation factor, in (%)

DE = destruction efficiency, in (%)

$f_{Dest}$ = fraction of hours the destruction device was operating during active gas flow

Although landfills must report both emissions estimations to the GHGRP, the larger value between the two emissions calculations (using Equations 4-20 and 4-21) is typically used to formally express methane emissions from the landfill on the GHGRP database (EPA, 2021). Values of

methane generation from the $GE_{CH4}$ equation (Equation 4-19), the formally reported methane emissions (the larger value between Equations 4-20 and 4-21), the fraction of methane in the LFG, the amount of waste disposed, and the amount of methane recovered (and flared or used for energy) for 2019 and 2018 for the landfills in Orange County are shown in Table 4.10. These data are publicly available from the EPA Facility Level Information on GreenHouse gases Tool (FLIGHT) (EPA, 2021). Emissions, generation, and recovered amounts of methane are given in metric tonnes of methane. The amount recovered does not include the amount of methane lost through oxidation in the soil or by other pathways.

**Table 4.10** The generated methane, actual emissions, fraction of $CH_4$ in LFG, waste disposed, and recovered $CH_4$ at Orange County landfills during 2019 and 2018. Data were obtained from the GHGRP database (EPA, 2021).

| **2019** | | | | | |
|---|---|---|---|---|---|
| **Landfill** | **$G_{CH4}$ (metric tonnes $CH_4$)** | **Emissions (metric tonnes $CH_4$)** | **Fraction $CH_4$** | **Waste Disposed (metric tonnes)** | **Recovered (metric tonnes $CH_4$)** |
| Frank R. Bowerman | 51,803 | 11,818 | 0.501 | 2,497,112 | 45,943 |
| Olinda Alpha | 69,632 | 16,753 | 0.513 | 2,114,767 | 47,567 |
| Prima Deshecha | 18,425 | 5,147 | 0.492 | 550,126 | 14,297 |
| Santiago Canyon | 5,918 | 1,654 | 0.363 | 0 | 3,763 |
| Coyote Canyon | 16,065 | 1,743 | 0.393 | 0 | 13,593 |
| **2018** | | | | | |
| **Landfill** | **$G_{CH4}$ (metric tonnes $CH_4$)** | **Emissions (metric tonnes $CH_4$)** | **Fraction $CH_4$** | **Waste Disposed (metric tonnes)** | **Recovered (metric tonnes $CH_4$)** |
| Frank R. Bowerman | 49,571 | 10,907 | 0.500 | 2,370,291 | 42,448 |
| Olinda Alpha | 67,410 | 15,637 | 0.508 | 2,157,813 | 46,827 |
| Prima Deshecha | 18,764 | 4,596 | 0.510 | 522,486 | 12,984 |
| Santiago Canyon | 6,097 | 1,759 | 0.367 | 0 | 3,803 |
| Coyote Canyon | 15,264 | 1,866 | 0.366 | 0 | 12,587 |

For both 2018 and 2019, the methane fractions at the active landfills (0.492 – 0.513) were within the percentage ranges reported by Lisk (1991), Crawford and Smith (2016), and Farquhar and Rovers (1973) shown in Table 1.3. At the closed landfills, methane fractions were lower (0.363 – 0.393), and outside of the typical methane fraction range expected in LFG. This may indicate a loss of nutrient productivity in the closed landfills, which have not received waste in nearly thirty years. It is interesting to point out that although Prima Deshecha had the highest maximum and average mixing ratio in Figure 4.10, it had the lowest median out of the active landfills. This might have been because it had the lowest amount of waste disposed, less than a quarter of the waste disposed at the other two active landfills, as shown in Table 4.10. Prima Deshecha also had the fewest total emissions out of the active landfills.

### 4.3.2 Comparison of Dairy Farm and Landfill Methane Emissions

The reported values of methane emissions from the Orange County landfills (given in the "Emissions" column in Table 4.10) were compared to the enteric and manure methane produced at the dairy farm by normalizing by surface area. The dairy farm was estimated to annually produce 600 metric tonnes of methane from enteric emissions, and 354 metric tonnes of methane from its manure emissions (which were mostly defined by emissions from its slurry systems). Therefore, the dairy farm is expected to produce 954 metric tonnes of methane annually. The size of the dairy farm was measured as a polygon with a surface area of 651,419 $m^2$. An average of the surface areas of the waste-containing areas at each landfill were obtained from the GHGRP for 2018 and 2019 (EPA, 2021). Average annual emissions of methane with regards to surface area were then calculated (in kg $CH_4/m^2$) and are shown in Table 4.11.

**Table 4.11** Location, average expected $CH_4$ emissions annually, surface area, and $CH_4$ emissions by area for the dairy farm and Orange County landfills

| Location | Average Emissions (metric tonnes $CH_4$ $yr^{-1}$) | Surface Area ($m^2$) | Average Emissions (kg $CH_4$ $m^{-2}$) |
|---|---|---|---|
| Visalia Dairy Farm | 954 | 651,419 | 1.46 |
| Frank R. Bowerman | 11,363 | 1,1514,31 | 9.87 |
| Olinda Alpha | 16,195 | 1,700,297 | 9.52 |
| Prima Deshecha | 4,872 | 1,034,727 | 4.71 |
| Santiago Canyon | 1,707 | 455,682 | 3.74 |
| Coyote Canyon | 1,805 | 1,315,234 | 1.37 |

Surprisingly, although the dairy farm was much smaller in size than most of the landfills, its emissions were within the same order of magnitude as the Orange County landfills when normalized by area. This becomes important when the number of dairies are considered. The SJV contained a little over one thousand dairy farms in 2017, while the last active landfill count in the United States revealed 1,540 operational MSW landfills in 2013 *nationwide* (EREF, 2016), only five hundred more. The dairy farm's average emissions by area were calculated as 1.46 kg $CH_4/m^2$, while emissions at the three active landfills ranged from 4.71 to 9.87 kg $CH_4/m^2$, with Prima Deshecha having the lowest methane emissions of the three active landfills. Closed Orange County landfills ranged from 1.37 to 3.74 kg $CH_4/m^2$ and were closer to the dairy farm's methane emissions. The similarity between the normalized emissions from the Visalia dairy farm and the landfills is likely as a result of the lack of regulations for dairy farms in California. Landfills have infrastructure in place to flare or reuse the methane they emit, while most dairy farms allow the methane to outgas into the atmosphere with no collection or recovery system. Landfills are large point sources with the potential to emit a huge quantity of methane, but these emissions are largely prevented by modern infrastructure. Dairy farms, on the other hand, are moderately-sized point sources with the potential to emit a moderate quantity of methane, and unfortunately this is exactly what gets emitted.

### 4.4 Carbon Dioxide at Orange County Landfills

Although methane emissions receive the most attention and monitoring efforts at landfills, carbon dioxide is emitted nearly equally during the waste decomposition process (Farquhar & Rovers, 1973; Lisk, 1991). The $CO_2$ mixing ratios at the five Orange County landfills are shown in Figure 4.11. The active landfills (Frank R. Bowerman, Olinda Alpha, and Prima Deshecha) had similar minimum, average, and median $CO_2$ mixing ratios to the closed landfills (Coyote Canyon and Santiago Canyon), and they differed mostly in their maximum $CO_2$ mixing ratios.

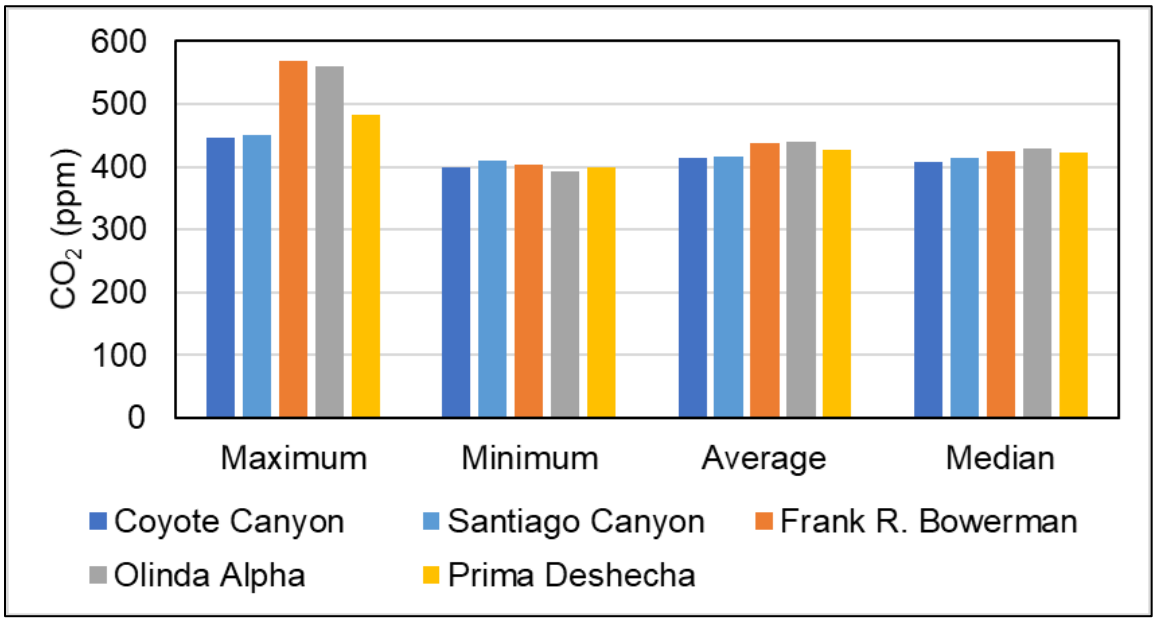


**Figure 4.11** Carbon dioxide (ppm) maximum, minimum, average, and median mixing ratios across all campaigns at Orange County landfills. Coastal background was 410 ppm.

Frank R. Bowerman and Olinda Alpha had the highest maximum, average, and median $CO_2$. Frank R. Bowerman had maximum, average, and median $CO_2$ mixing ratios of 568 ppm, 438 ppm, and 425 ppm, respectively, while Olinda Alpha had maximum, average, and median $CO_2$ mixing ratios of 651 ppm, 440 ppm, and 430 ppm, respectively. Prima Deshecha had maximum, average, and median $CO_2$ mixing ratios of 483 ppm, 427 ppm, and 423 ppm, respectively, lower than the other two active landfills. Generally, active landfills had higher $CO_2$ mixing ratios than the closed landfills. The maximum $CO_2$ at each active landfill (Frank R. Bowerman, Olinda Alpha, and

Prima Deshecha) was always found near the active dumping area, where emissions from waste decomposition commonly mix with exhaust from dump trucks and landfill machinery. This may explain the elevated $CO_2$ in this area.

The closed Orange County landfills (Coyote Canyon and Santiago Canyon) had lower maximum, average, and median $CO_2$ mixing ratios than active Orange County landfills. Coyote Canyon had maximum, average, and median $CO_2$ mixing ratios of 447 ppm, 415 ppm, and 408 ppm, respectively. Santiago Canyon had maximum, average, and median $CO_2$ mixing ratios of 450 ppm, 417 ppm and 414 ppm, respectively. Minimum $CO_2$ at all the landfills, closed and active, was around 400 ppm. As shown previously, data from the Rowland-Blake group determined that the average $CO_2$ at the remote California coastline was 410 ppm in 2018. The mixing ratios of $CO_2$ at the closed Orange County landfills were close to this, if not below it. Mixing ratios of $CO_2$ at active landfills were more commonly above 410 ppm, indicating that landfills are a likely source of $CO_2$.

### 4.4.1 Estimated Carbon Dioxide Emissions at Orange County Landfills

Interestingly, although $CO_2$ is an important GHG that accounts for a large percentage of the LFG generated at a landfill, the landfills do not need to monitor or report the amount of $CO_2$ they produce. While methane and its emission calculation methodology are well defined within the Waste category for the IPCC (Eggleston et al., 2006) and the most recent EPA GHG inventory (2020c), $CO_2$ was removed from that section. Carbon dioxide emissions from landfills are now only considered in the Land Use, Land-Use Change and Forestry (LULUCF) section in the EPA GHG inventory (2020c). Within LULUCF, the carbon stocks from the disposal of food scraps and yard trimmings in a landfill are estimated, but overall $CO_2$ estimates are not given, and no methodology is defined (EPA, 2020c).

Although the mixing ratios of ambient $CO_2$ at the landfills were generally low, waste decomposition at landfills does generate $CO_2$ at similar rates to $CH_4$, making the contribution of

$CO_2$ from landfills important (Lisk, 1991; Crawford & Smith, 2016; Farquhar & Rovers, 1973). Carbon dioxide at landfills can be a primary or secondary emission. As a primary emission, $CO_2$ can be emitted by the landfill vehicles and dump trucks or biogenically during waste decomposition. As a secondary emission, $CO_2$ is emitted during the recovery process of LFG. During this recovery process, methane is converted to $CO_2$ during flaring or during the gas-to-energy process. This section deals primarily with *direct* biogenic $CO_2$ emissions. The smaller $CO_2$ emissions specifically from vehicles on the surface is difficult to account for, but the larger biogenic $CO_2$ emissions produced during waste decomposition underground are important and can be estimated.

While landfills do convert their emissions of flared and generated $CH_4$ into $CO_2e$ equivalents using the less recent IPCC AR4 report (i.e., $CH_4$ has a 100-year GWP of 25 times that of $CO_2$), biogenic $CO_2$ emissions from the decomposition of waste are not quantified. For this study, $CO_2$ from biogenic emissions within the LFG of Orange County landfills was estimated using the expected ratio of $CH_4$ to $CO_2$ in LFG. Lisk (1991), Crawford and Smith (2016), and Farquhar and Rovers (1973) indicated a range of percentages of $CH_4$, $CO_2$, and trace gases at landfills, which were shown in Table 1.3. To repeat here, $CO_2$ can range from 30 to 60% by volume, $CH_4$ can range from 45 to 70% by volume, and trace gases can range from 0 to 9% by volume. If methane by volume is much less than 50%, it is likely that its production is hindered by something, such as a loss of nutrients to continue the Anaerobic Methanogenic Steady Stage presented in Table 1.3 (Farquhar & Rovers, 1973). Farquhar and Rovers (1973) noted that the ratio of $CH_4$ to $CO_2$ should not drastically change, or else something has gone wrong in the anaerobic digestion process. This implies that closed landfills should maintain the same ratio even as nutrients are lost.

Previous lab studies have shown that Stages I – III in Table 1.3 occur as quickly as 180 – 500 days before Stage IV (i.e., Anaerobic Methanogenic Steady Stage) begins (Ramaswamy,

1970; Rovers & Farquhar, 1973; Beluche, 1968). As the landfills in Orange County have been operational for decades, it was assumed that all of them were mostly in Stage IV with a constant ratio of $CH_4$ to $CO_2$ in the LFG. First, a "typical" expected ratio for the Orange County landfills was calculated based on the possible ranges of $CH_4$ and $CO_2$ in LFG. Although researchers have previously reported ranges for the percentages of $CO_2$ and $CH_4$ in LFG, they are usually equally represented on a per volume basis, with $CO_2$ only slightly smaller. For example, if $CH_4$ is 47.5% by volume, $CO_2$ might be 47%, or 98.9% of the $CH_4$ fraction (Gautam & Kumar, 2019). For this study, it was assumed that the $CO_2$ fraction was 95% of the $CH_4$ fraction, so that the $CH_4$:$CO_2$ ratio was 1.00:0.95. This ratio was applied to each of the fractions of $CH_4$ in LFG of the various landfills from Table 4.10. The fraction of $CO_2$ was assumed to be 95% of the fraction of $CH_4$ in the LFG for each landfill.

The ratio was first used to determine the amount of biogenic $CO_2$ that is likely emitted into the atmosphere from the LFG recovery systems, which either flare or filter the LFG to create energy. More specifically, flaring the gas is a method of converting $CH_4$, which has a high GWP, to $CO_2$, which has a lower GWP. Successful flaring follows Reaction 4-1 but can also produce $H_2$ and CO in small quantities if the combustion is inefficient (Gautam & Kumar, 2019).

$$CH_4 + 2O_2 \rightarrow CO_2 + 2H_2O \qquad \text{Reaction 4-1}$$

Although the conversion of $CH_4$ to $CO_2$ is preferable for the environment, the $CO_2$ already in the LFG is simply outgassed to the environment during this flaring process, which can be damaging to the environment because it is still a GHG. To determine the amount of biogenic $CO_2$ in the recovery gas, $Rec_{CO2}$, (not including the $CH_4$ that is converted to $CO_2$), the known fraction of $CH_4$ by volume in the LFG (as shown in Table 4.10 from the EPA GHGRP database (EPA, 2021)) was used along with the calculated ratio of $CH_4$:$CO_2$ = 1.00:0.95. The following equation, Equation 4-22, was developed to determine the amount of biogenic $CO_2$ emitted from the landfills during the recovery process.

$$\mathrm{Rec_{CO2}} = \frac{\mathrm{Rec_{CH4}}}{\mathrm{Ratio}} * \frac{\rho_{CO2}}{\rho_{CH4}} \qquad \text{Equation 4-22}$$

where

$Rec_{CO2}$ = amount of biogenic $CO_2$ emitted from landfill during recovery process, in (metric tonnes $CO_2$ $yr^{-1}$)

$Rec_{CH4}$ = amount of $CH_4$ emitted from landfill during recovery process, from Table 4.10, in (metric tonnes $CH_4$ $yr^{-1}$)

Ratio = selected $CH_4$:$CO_2$ ratio, in ($m^3$ $CH_4$/$m^3$ $CO_2$)

$\rho_{CO2}$ = density of $CO_2$ at 25 °C and 1 atm, in (metric tonnes/$m^3$ $CO_2$)

$\rho_{CH4}$ = density of $CH_4$ at 25 °C and 1 atm, in (metric tonnes/$m^3$ $CH_4$)

The $Rec_{CO2}$ parameter determines the quantity of $CO_2$ that escapes during the recovery process. This only considers biogenic $CO_2$ and does not include the methane converted to $CO_2$ during the recovery process. For example, for Frank R. Bowerman, solving Equation 4-22 yields:

$$\mathrm{Rec_{CO2}} = \frac{45{,}943 \text{ metric tonnes } \mathrm{CH_4}}{\frac{1.5 \text{ m}^3 \mathrm{CH_4}}{\mathrm{m^3\ CO_2}}} * \frac{\rho_{CO2}}{\rho_{CH4}} = 130{,}207 \text{ metric tonnes } CO_2$$

A similar calculation was performed to determine how much $CO_2$ was in emissions that occur directly ($Dir_{CO2}$) from the landfill using the values of the "Emissions" column in Table 4.10 in place of the $Rec_{CH4}$ parameter in Equation 4-22. The $Dir_{CO2}$ parameter represent the estimated emissions of $CO_2$ that escape through the landfill directly by using the known emissions of $CH_4$ that escape. For example, for Frank R. Bowerman, Equation 4-22 to determine direct $CO_2$ emissions becomes:

$$\mathrm{Dir_{CO2}} = \frac{11{,}818 \text{ metric tonnes } \mathrm{CH_4}}{\frac{1.5 \text{ m}^3 \mathrm{CH_4}}{\mathrm{m^3\ CO_2}}} * \frac{\rho_{CO2}}{\rho_{CH4}} = 37{,}113 \text{ metric tonnes } CO_2$$

The biogenic $CO_2$ emitted from the recovery systems ($Rec_{CO2}$) and the landfill directly ($Dir_{CO2}$) for each Orange County landfill during 2019 and 2018, and their summation ($Total\ CO_2$) is shown in

Table 4.12. Additionally, the total emissions in $CO_2e$ were calculated by first calculating the amount of methane emissions from all sources (including methane recovery, destruction, and other factors) and converting it to metric tonnes $CO_2e$ and then adding it to the sum of the $CO_2$ emitted directly and during recovery.

For the conversion of $CH_4$ to $CO_2e$, the landfills recommend using the 100-year GWP for methane outlined in the IPCC AR4 (rather than the AR5), so the total methane emissions, "*Emissions*" in Table 4.10 was multiplied by twenty-five to determined $CO_2e$. This was added to the "$Rec_{CO2}$" and "$Dir_{CO2}$" to determine the total amount of emissions from the landfills, given as "*Total* $CO_2$" in Table 4.12. Finally, the ratio of the contribution of $CO_2$ emissions from the landfill ($Dir_{CO2}$) and during recovery ($Rec_{CO2}$) to the total metric tonnes of $CO_2e$ from the landfill was determined ("*%* $CO_2e$" column). This contribution only accounts for the biogenic carbon dioxide released directly from rogue emissions or during the recovery process (Reaction 4-1).

**Table 4.12** Emissions of $CO_2$ from recovery systems ($Rec_{CO2}$), direct emissions ($Dir_{CO2}$), total emissions (metric tonnes $CO_2e$) and the contribution of biogenic $CO_2$ to the total emissions (%) for Orange County landfills during 2018 and 2019

| **2019** | | | | |
|---|---|---|---|---|
| **Landfill** | **$Rec_{CO2}$ (metric tonnes $CO_2$)** | **$Dir_{CO2}$ (metric tonnes $CO_2$)** | **Total $CO_2$ (metric tonnes $CO_2e$.)** | **% $CO_2e$ (%)** |
| Frank R. Bowerman | 130207 | 37113 | 462778 | 34 |
| Olinda Alpha | 134811 | 52608 | 606232 | 29 |
| Prima Deshecha | 40518 | 16163 | 185357 | 29 |
| Santiago Canyon | 10665 | 5193 | 57199 | 26 |
| Coyote Canyon | 38522 | 5475 | 87581 | 48 |
| **2018** | | | | |
| **Landfill** | **$Rec_{CO2}$ (metric tonnes $CO_2$)** | **$Dir_{CO2}$ (metric tonnes $CO_2$)** | **Total $CO_2$ (metric tonnes $CO_2e$)** | **% $CO_2e$ (%)** |
| Frank R. Bowerman | 120302 | 30910 | 423877 | 34 |
| Olinda Alpha | 132713 | 44318 | 567965 | 29 |
| Prima Deshecha | 36797 | 13026 | 164731 | 29 |
| Santiago Canyon | 10777 | 4985 | 59737 | 25 |
| Coyote Canyon | 35673 | 5288 | 87604 | 45 |

A sample calculation showing the method used to calculate the final column in Table 4.12, "*% $CO_2$e (%)*" is shown below in Equation 4-23. The contributions of methane and carbon dioxide to the total GWP for the landfills are added together, and the individual contribution of the *Total $CO_2$* (*$Rec_{CO2}$* and *$Dir_{CO2}$*) to the overall GWP is determined.

$$\%\ \mathrm{CO_2\ Eq.}\ (\%) = \frac{\mathrm{Total\ CO_2}}{\mathrm{Total\ CO_2} + (\mathrm{Emitted\ CH_4}) * \mathrm{GWP_{CH4}}} * 100 \qquad \text{Equation 4-23}$$

where

Total $CO_2$ = *$Rec_{CO2}$* + *$Dir_{CO2}$*, given in Table 4.12, in (metric tonnes $CO_2$e)

Emitted $CH_4$ = $CH_4$ emitted, given in Table 4.10, in (metric tonnes $CH_4$)

$GWP_{CH4}$ = 25, the GWP of $CH_4$ for a 100-year period, as developed for IPCC AR4

During 2019, the biogenic $CO_2$ emissions associated with recovery of LFG and general emissions from the landfill accounted for 29 to 34% of the total emissions in metric tonnes $CO_2$e at the active landfills (Frank R. Bowerman, Prima Deshecha, and Olinda Alpha). The closed landfills exhibited a wider range because of their different abilities to recover LFG: biogenic $CO_2$ emissions accounted for 26% of the total metric tonnes of $CO_2$e. at Santiago Canyon, and 48% at Coyote Canyon landfills. Santiago Canyon recovered four times less LFG than Coyote Canyon, which led to a lower amount of $CO_2$ emitted during the recovery process.

During 2018, biogenic $CO_2$ emissions accounted for 29 to 34% of the total emissions in metric tonnes of $CO_2$e at the active landfills. At Santiago Canyon, biogenic $CO_2$ emissions accounted for 25% of the total $CO_2$e, while biogenic $CO_2$ accounted for 45% at Coyote Canyon. This difference is again caused by the difference in recovery capabilities.

These $CO_2$ emissions associated with LFG recovery were likely not noticed when collecting canisters during the campaigns because much of the recovery process occurs at a different facility at the landfill. For example, at Coyote Canyon, which had the highest contribution of $CO_2$ towards their GWP, the recovery systems were located across the street at a different

facility. This is shown in Figure 4.12, which marks the samples collected at all campaigns, the landfill itself, and the location of the recovery facility. No samples were collected at the recovery facility, which would have likely had higher mixing ratios of $CO_2$. This was the case for every landfill.


**Figure 4.12** Coyote Canyon landfill (outlined in orange), the locations of samples collected during all campaigns (red points), and the LFG recovery facility (outlined in blue).

These percentages are certainly non-trivial and likely have a big impact on the environment. Biogenic $CO_2$ at landfills is not currently required to be reported or considered part of the $CO_2e$ reported in the "Waste" category in the EPA GHG inventory (2020c). However, the calculated contribution of $CO_2$ to the GWP of landfill implies that the gas should be considered in future estimates. The United States contained 1,540 operational MSW landfills in 2013 (EREF, 2016) and there have been 3,200 MSW landfills closed since 1980 (EPA, 2020b; EPA, 2020c). If

these landfills emit similar amounts of $CO_2$ as the landfills in Orange County, there is a large source of $CO_2$ unaccounted for and currently unreported. Future studies are encouraged to 1) collect samples of the LFG to determine more accurate $CH_4$:$CO_2$ ratios tailored to each landfill, 2) conduct flights over the landfills and their recovery systems to better estimate $CO_2$ mixing ratios, and 3) collect ambient samples near the recovery facilities to confirm whether $CO_2$ is more enhanced at those locations.

### 4.5 Summary and Conclusion

Methane and carbon dioxide mixing ratios were determined for the remote California coastline. In 2018, average methane and carbon dioxide for the coast (34.5 °N – 40.0 °N) was 1.931 ppm and 410 ppm, respectively. For the purposes of this study, enhancements of these gases at the dairy farm or landfills in excess of these mixing ratios are assumed to be enhanced by inland sources.

The dairy farm showed that lagoons and slurries had higher overall $CH_4$ mixing ratios than the free stalls or outdoor cows (i.e., heifers and dry cows). January 2020 had the highest average $CH_4$ mixing ratio, nearly 150 ppm near lagoons and slurries. Although the temperature dependence of methane production during decomposition was important for this study, this elevated winter methane also shows the importance of the regular removal of solids from the manure management system. Unlike methane, carbon dioxide was most enhanced in the free stalls, with an average of 549 ppm, likely because of a mixture of trapped air from vehicles and cow breath.

Emissions were estimated from manure management using the EPA's Tier 2 calculation but with modelled liquid temperatures rather than average air temperature of the area. It was shown the methods used to create the EPA 2020 GHG inventory would have underestimated the potential methane formation from manure management by up to 105% depending on the season. Slurries at the dairy farm emit 40±20 kg $CH_4$ $hr^{-1}$, which amounts to 354 metric tonnes annually.

These emissions are temperature dependent and will be affected by climate change. As temperatures heat up over the next few decades, lagoons and slurries are expected to emit more methane. Using RCP4.5, manure management $CH_4$ could increase up to a mean and standard deviation of 14.5±0.1% by 2046 and 19±0.2% by 2081. Colder counties, like Madera and Tulare, will be disproportionately affected by this temperature increase. This is important particularly for Tulare County, which has historically had the highest cow populations. It is suggested that Tulare County consider and invest in methane reduction strategies before the temperatures start to rise.

Methane associated with enteric emissions was also calculated for cows at the dairy using IPCC Tier 2 methodology. The emission factors were calculated: $EF_{milk\ cow}$ = 134 kg $CH_4$ $hd^{-1}$ $yr^{-1}$, $EF_{dry\ cow}$ = 53 kg $CH_4$ $hd^{-1}$ $yr^{-1}$, and $EF_{heifer}$ = 55 kg $CH_4$ $hd^{-1}$ $yr^{-1}$. Annually, this means that 417 metric tonnes $CH_4$ are emitted from milk cows, 20 metric tonnes $CH_4$ are emitted from dry cows, and 163 metric tonnes $CH_4$ are emitted from heifers. Overall, the dairy farm emits 600 metric tonnes of enteric $CH_4$ annually. This brings the total of manure and enteric emissions to 954 metric tonnes annually from just the Visalia dairy farm.

Methane was measured at the Orange County landfills. Prima Deshecha had the most enhanced $CH_4$ overall, likely because of leaky infrastructure and not because of their low disposal rate. The median $CH_4$ did not show seasonal dependence. Average $CH_4$ at the landfills was closer to the coastal “background” of 1.931 ppm than to the high averages found at the dairy farm. Low enhancements of $CH_4$ at landfills can be explained by the slow decomposition process; landfills do not start generating high quantities of methane until the waste is well buried, where it can maintain steady anaerobic conditions. By then, the modern landfill infrastructure prevents a large percentage of emissions from escaping freely into the atmosphere.

Landfills report their methane to the GHGRP. Based on the GHGRP reports, methane at Olinda Alpha > Frank R. Bowerman > Prima Deshecha and Santiago Canyon ≈ Coyote Canyon. Although the dairy farm has a much smaller surface area than the landfills, it has a comparable

amount of methane emissions, where Frank R. Bowerman ≈ Olinda Alpha > Prima Deshecha > Santiago Canyon > Coyote Canyon ≈ Visalia dairy farm. Landfills are large point sources, but they are constantly monitored and well controlled. On the contrary, dairy farms are moderate point sources but are typically unmonitored and relatively uncontrolled. This becomes important when one considers nationwide numbers. There are nearly as many dairy farms in the SJV alone as there are active landfills *nationwide*, making dairy farms an important source of GHG emissions.

Much of the GHG prevention at landfills has focused on methane mitigation, and carbon dioxide is not reported. All carbon dioxide mixing ratios at the Orange County landfills were below 600 ppm, but still often above the coastal background of 410 ppm. This study calculated the amount of biogenic carbon dioxide (i.e., created during decomposition, not from conversion during the methane recovery process) released from the Orange County landfills through rogue emissions and during recovery. The total $CO_2$ from direct and recovery emissions ranged from 29 to 34% of the total $CO_2e$ at the active landfills, and 25 to 48% of the total $CO_2e$ at the closed landfills. Therefore, it is recommended to include $CO_2$ in future monitoring and to include it for future GHG estimates from landfills.

## 4.6 References


Agricultural and Food Research Council (AFRC) (1993). Energy and Protein Requirements of Ruminants. Technical Committee on Responses to Nutrients 24-159.

Arndt, C., Leytem, A. B., Hristov, A. N., Zavala-Araiza, D., Cativiela, J. P., Conley, S., ... & Herndon, S. C. (2018). Short-term methane emissions from 2 dairy farms in California estimated by different measurement techniques and US Environmental Protection Agency inventory methodology: A case study. *Journal of dairy science*, *101*(12), 11461-11479.

Baldé, H., VanderZaag, A. C., Burtt, S., Evans, L., Wagner-Riddle, C., Desjardins, R. L., & MacDonald, J. D. (2016). Measured versus modeled methane emissions from separated liquid dairy manure show large model underestimates. *Agriculture, Ecosystems & Environment*, *230*, 261-270.

Beluche, R. (1968). Degradation of Solid Substrate in a Sanitary Landfill. (Doctoral dissertation, Ph.D. thesis, University of Southern California at Los Angeles, California).

Borhan, M. S., Capareda, S., Mukhtar, S., Faulkner, W. B., McGee, R., & Parnell Jr, C. B. (2011). Determining seasonal greenhouse gas emissions from ground-level area sources in a dairy operation in central Texas. *Journal of the Air & Waste Management Association*, *61*(7), 786-795.

Bronstein, K., Coburn, J., & Schmeltz, R. (2011). Understanding the Inventory of US Greenhouse Gas Emissions and Sinks and the Greenhouse Gas Reporting Program for Landfills: Methodologies, Uncertainties, Improvements and Deferrals.

Bryant, M. P., Varel, V. H., Frobish, R. A., & Isaacson, H. R. (1976). Seminar on Microbial Energy Conversion. *E. Goltz KG, Gottingen, Germany*.

Calculating GHG emissions, 40 C.F.R. § 98.343 (2013).

Chadwick, D., Sommer, S., Thorman, R., Fangueiro, D., Cardenas, L., Amon, B., & Misselbrook, T. (2011). Manure management: Implications for greenhouse gas emissions. *Animal Feed Science and Technology*, *166*, 514-531.

Chianese, D. S., Rotz, C. A., & Richard, T. L. (2009a). Simulation of carbon dioxide emissions from dairy farms to assess greenhouse gas reduction strategies. *Transactions of the ASABE*, *52*(4), 1301-1312.

Chianese, D. S., Rotz, C. A., & Richard, T. L. (2009b). Whole-farm greenhouse gas emissions: A review with application to a Pennsylvania dairy farm. *Applied Engineering in Agriculture*, *25*(3), 431-442.

Crawford, J. F., & Smith, P. G. (2016). *Landfill technology*. Elsevier.

The Environmental Research & Education Foundation (EREF). (2016). Municipal Solid Waste Management in the United States: 2010 & 2013.

Eggleston, S., Buendia, L., Miwa, K., Ngara, T., & Tanabe, K. (Eds.). (2006). *2006 IPCC guidelines for national greenhouse gas inventories* (Vol. 5). Hayama, Japan: Institute for Global Environmental Strategies.

Environmental Protection Agency (EPA). (2020b). Landfill Methane Outreach Program (LMOP). Retrieved from https://www.epa.gov/lmop

Environmental Protection Agency (EPA). (2020c). Inventory of U.S. Greenhouse Gas Emissions and Sinks: 1990-2018. Retrieved from https://www.epa.gov/sites/production/files/2020-04/documents/us-ghg-inventory-2020-main-text.pdf

Environmental Protection Agency (EPA). (2021). Greenhouse Gas Reporting Program (GHGRP). Retrieved from https://ghgdata.epa.gov/ghgp/main.do

Farquhar, G. J., & Rovers, F. A. (1973). Gas production during refuse decomposition. *Water, Air, and Soil Pollution, 2(*4), 483-495.

Fischer, J. R. 1977. Three years of evaluating a midwest anaerobic dairy lagoon. ASAE Paper No. 77-4571, *ASAE*.

Gautam, P., & Kumar, S. (2019). Landfill Gas as an Energy Source. *In Current Developments in Biotechnology and Bioengineering* (pp. 93-117). Elsevier.

Godbout, S., Verma, M., Larouche, J. P., Potvin, L., Chapman, A. M., Lemay, S. P., ... & Brar, S. K. (2010). Methane production potential (B0) of swine and cattle manures–a Canadian perspective. *Environmental technology*, *31*(12), 1371-1379.

Grant, R. H., Boehm, M. T., & Bogan, B. W. (2015). Methane and carbon dioxide emissions from manure storage facilities at two free-stall dairies. *Agricultural and Forest Meteorology*, *213*, 102-113.

Hamilton, D. W., & Cumba, H. J. (2000). Thermal phenomena in animal waste treatment lagoons. *Proc. Animal, Agricultural and Food Processing Wastes*, 672-678.

Heinrichs, A. J., & Losinger, W. C. (1998). Growth of Holstein dairy heifers in the United States. *Journal of animal science*, *76*(5), 1254-1260.

Holstein Association. (2021*). History of the Holstein Breed*. Retrieved from http://www.holsteinusa.com/holstein_breed/breedhistory.html

Husted, S. (1994). Seasonal variation in methane emission from stored slurry and solid manures. *Journal of environmental quality*, *23*(3), 585-592.

Krider, J. N. (1981). Milk center waste treatment lagoons in the northeastern United States. Livestock Waste: A Renewable Resource, *ASAE*.

Leytem, A. B., Dungan, R. S., Bjorneberg, D. L., & Koehn, A. C. (2011). Emissions of ammonia, methane, carbon dioxide, and nitrous oxide from dairy cattle housing and manure management systems. *Journal of Environmental Quality*, *40*(5), 1383-1394.

Leytem, A. B., Bjorneberg, D. L., Koehn, A. C., Moraes, L. E., Kebreab, E., & Dungan, R. S. (2017). Methane emissions from dairy lagoons in the western United States. *Journal of dairy science*, *100*(8), 6785-6803.

Lisk, D. J. (1991). Environmental effects of landfills. *Science of the total environment, 100*, 415-468.

Lory, J. A., Massey, R. E., & Zulovich, J. M. (2010). An evaluation of the USEPA calculations of greenhouse gas emissions from anaerobic lagoons. *Journal of environmental quality*, *39*(3), 776-783.

Mangino, J., Bartram, D., & Brazy, A. (2002). Development of a methane conversion factor to estimate emissions from animal waste lagoons. *US Environmental Protection Agency, Methane Sequestration Branch. Washington, DC*.

Metcalf & Eddy. (1972). *Wastewater engineering: collection, treatment, disposal*. McGraw-Hill.

Morris, G. R. (1976). Anaerobic fermentation of animal wastes: A kinetic and empirical design Evaluation (Doctoral dissertation, Ph. D., thesis, Cornell University).

Moss, R., Babiker, W., Brinkman, S., Calvo, E., Carter, T., Edmonds, J., ... & Jones, R. (2008). *Towards new scenarios for the analysis of emissions: Climate change, impacts and response strategies*. Intergovernmental Panel on Climate Change Secretariat (IPCC).

Moss, R. H., Edmonds, J. A., Hibbard, K. A., Manning, M. R., Rose, S. K., Van Vuuren, D. P., ... & Meehl, G. A. (2010). The next generation of scenarios for climate change research and assessment. *Nature*, *463*(7282), 747-756.

Mylostyvyi, R., & Chernenko, O. (2019). Correlations between environmental factors and milk production of Holstein cows. *Data*, *4*(3), 103.

National Research Council (NRC) (1996). Nutrient Requirement of Beef Cattle. *Nat. Acad. Sci., Washington, DC*.

Owen, J. J., & Silver, W. L. (2015). Greenhouse gas emissions from dairy manure management: a review of field-based studies. *Global change biology*, *21*(2), 550-565.

Pachauri, R. K., Allen, M. R., Barros, V. R., Broome, J., Cramer, W., Christ, R., ... & Dubash, N. K. (2014). *Climate change 2014: synthesis report. Contribution of Working Groups I, II and III to the fifth assessment report of the Intergovernmental Panel on Climate Change* (p. 151). IPCC.

Payne, V. W. E., Shipp Jr., J. W., and Miller III, F.A. (1981). Supernatant characteristics of three animal waste lagoons in North Alabama. Livestock Waste: A Renewal Resource, *ASAE*.

Petersen, S. R. O., Amon, B., & Gattinger, A. (2005). Methane oxidation in slurry storage surface crusts. *Journal of Environmental Quality*, *34*(2), 455-461.

Petersen, S. O., & Sommer, S. G. (2011). Ammonia and nitrous oxide interactions: roles of manure organic matter management. *Animal Feed Science and Technology*, *166*, 503-513.

Prinn, R.G., Weiss, R. F., Arduini, J., Arnold, T., DeWitt, H.L., Fraser, P.J., … Zhou, L. (2018). History of chemically and radiatively important atmospheric gases from the Advanced Global Atmospheric Gases Experiment (AGAGE), *Earth Syst. Sci. Data*, 10, 985-1018.

Ramaswamy, J. N. (1970). Effects on acid and gas production in sanitary landfills (Doctoral dissertation, Ph. D., thesis, University of West Virginia, Morgantown).

Safley Jr, L. M., & Westerman, P. W. (1990). Psychrophilic anaerobic digestion of animal manure: proposed design methodology. *Biological wastes*, *34*(2), 133-148.

Schulz, S., Matsuyama, H., & Conrad, R. (1997). Temperature dependence of methane production from different precursors in a profundal sediment (Lake Constance). *FEMS Microbiology Ecology*, *22*(3), 207-213.

Smith, R. E., & Franco, T. L. (1985). Predicting anaerobic lagoon temperatures from weather data. *Transactions of the ASAE*, *28*(2), 551-0554.

Soliva, C. R. (2006). Report to the attention of IPCC about the data set and calculation method used to estimate methane formation from enteric fermentation of agricultural livestock population and manure management in Swiss agriculture. FOEN, Berne, Switzerland. *On behalf of the Federal Office for the Environment (FOEN), Bern, Switzerland*.

Sommer, S. G., Petersen, S. O., & Søgaard, H. T. (2000). Greenhouse gas emission from stored livestock slurry. *Journal of Environmental quality*, *29*(3), 744-751.

Thomson, A. M., Calvin, K. V., Smith, S. J., Kyle, G. P., Volke, A., Patel, P., ... & Edmonds, J. A. (2011). RCP4. 5: a pathway for stabilization of radiative forcing by 2100. *Climatic change*, *109*(1-2), 77.

USA.com. (2020a). Fresno County Weather. Retrieved from http://www.usa.com/fresno-county-ca-weather.htm

USA.com. (2020b). Kern County Weather. Retrieved from http://www.usa.com/kern-county-ca-weather.htm

USA.com. (2020c). Kings County Weather. Retrieved from http://www.usa.com/kings-county-ny-weather.htm

USA.com. (2020d). Madera County Weather. Retrieved from http://www.usa.com/madera-county-ca-weather.htm

USA.com. (2020e). Merced County Weather. Retrieved from http://www.usa.com/merced-county-ca-weather.htm

USA.com. (2020f). San Joaquin County Weather. Retrieved from http://www.usa.com/san-joaquin-county-ca-weather.htm

USA.com. (2020g). Stanislaus County Weather. Retrieved from http://www.usa.com/stanislaus-county-ca-weather.htm

USA.com. (2020h). Tulare County Weather. Retrieved from http://www.usa.com/tulare-county-ca-weather.htm

# 5. Methanol, Ethanol, and Acetaldehyde

This chapter examines the mixing ratios of methanol, ethanol, and acetaldehyde at the Visalia dairy farm, Orange County landfills, and over the SJV. The goal of the chapter was to determine contributing sources of these oxygenates so they can be further explored as potential contributors to odor and ozone formation in California, a visibility and health concern for disadvantaged communities living in the state. The contribution of methanol, ethanol, and acetaldehyde to ozone formation is examined more in Chapter 8.2.1, while Chapter 8.4.1 examines their contribution (particularly ethanol) to odor.

## 5.1 Methanol, Ethanol, and Acetaldehyde at the Dairy Site

Three hundred and fifty-nine whole air samples containing methanol, ethanol, and acetaldehyde from Visalia, CA were quantified using gas chromatography for all five dairy campaigns (September 2018, March 2019, June 2019, September 2019, and January 2020). To determine common sources responsible for their production, their mixing ratios were spatially overlaid on aerial photographs of the dairy farm. Following that, the top ten percent of samples were examined to determine large potential contributors of each gas across all campaigns.

Figure 5.1 shows an aerial view of the dairy farm with the methanol mixing ratios from various sources scaled by color and height. The points shown represent samples that were collected during all the campaigns; they are not separated by season. Typical wind direction was from the northwest. Methanol was binned into seven discrete mixing ratio ranges and colored accordingly. The height of the points was scaled on a continuum, where the lowest methanol mixing ratios are shown closer to the ground and the more enhanced mixing ratios are shown higher above the dairy. This is for illustrative purposes only, as all the samples were collected on foot or from the mobile lab at ground level.

For the aerial figures presented in this chapter (Figures 5.1 – 5.3), points are grouped by likely source in the following way: “Manure” includes samples collected near the manure

management system (lagoons, slurries, processing pit), flush water and bedding; “Enteric” includes samples collected near milk cows in the free stalls, outdoor heifers and dry cows in corral areas, and cow breath; “Silage” includes samples collected near the silage piles; “Crops” includes samples collected near the crops; and “Other” includes samples collected near the milk parlor, office area, upwind, and downwind of the dairy.

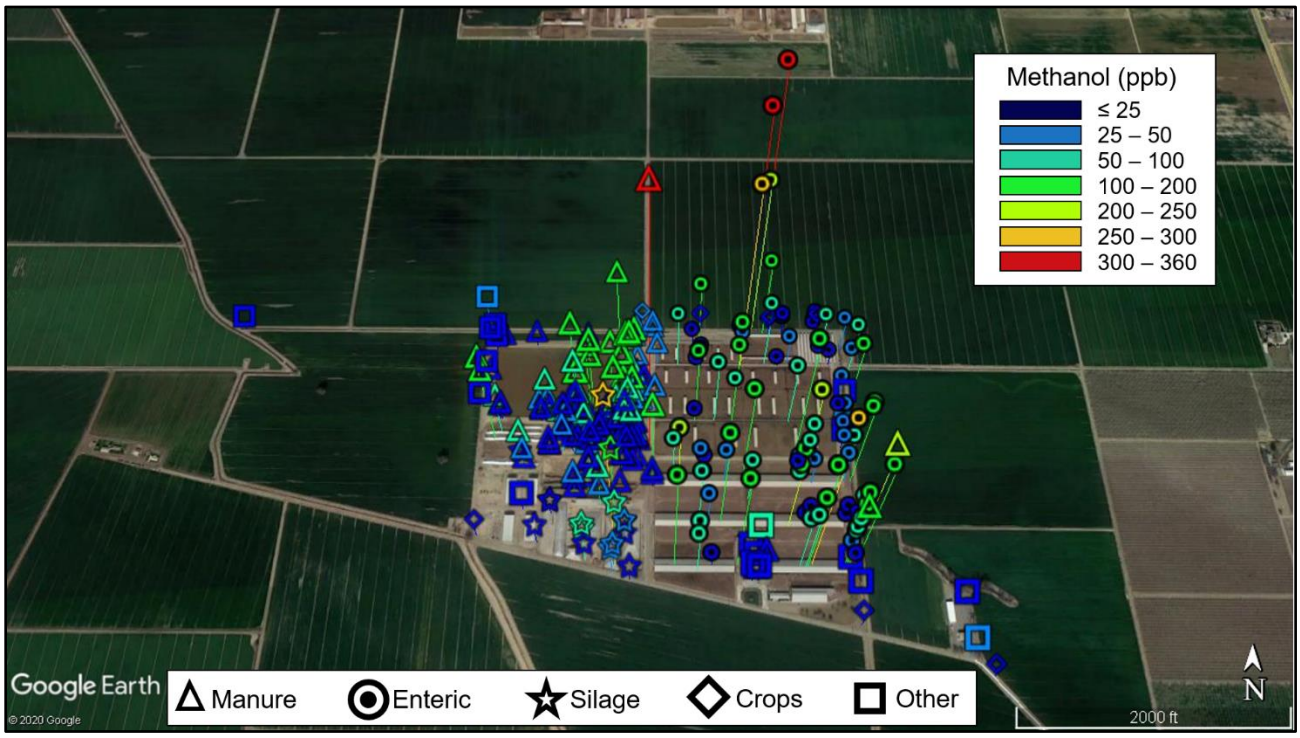


**Figure 5.1** Methanol (ppb) at the dairy farm binned by mixing ratio ranges and grouped by source. Height of the points also indicates the mixing ratios of methanol. Typical wind direction was from the northwest.

Methanol mixing ratios at the dairy varied and ranged from below 25 ppb to nearly 360 ppb. Based on Figure 5.1, methanol mixing ratios were highest near manure, enteric, and silage sources. This was initially surprising, as silage was expected to be the only major source. Although silage appeared to contribute to methanol emissions at the dairy farm, other sources were likely present as well. This is explored later in this chapter by examining which sources may have contributed to the top 10% methanol across all campaigns.

Figure 5.2 shows an aerial view of the dairy farm with ethanol mixing ratios from various sources scaled by color and height, binned into seven discrete mixing ratio ranges and colored accordingly. Height was scaled on a continuum above the dairy and is proportional to the mixing ratios of ethanol.

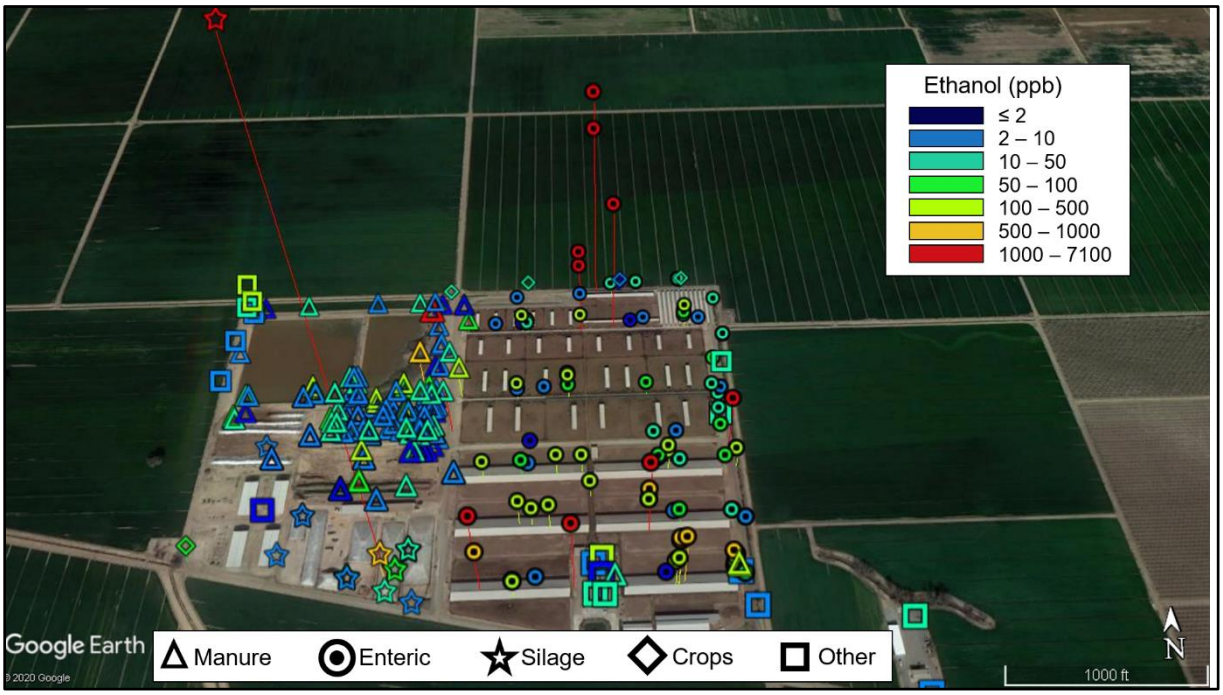


**Figure 5.2** Ethanol (ppb) at the dairy farm binned by mixing ratio ranges and grouped by source. Height of the points also indicates the mixing ratios of ethanol. Typical wind direction was from the northwest.

Binned ethanol mixing ratios varied from below 2 ppb to nearly 7100 ppb, and they were consistently highest near enteric sources, such as the cows in the corrals and free stalls. Ethanol was also elevated near the silage and in some samples collected near the manure management system. The sources that may have contributed to the top 10% ethanol are determined later in this chapter.

Figure 5.3 shows an aerial view of the dairy farm with the acetaldehyde mixing ratios from various sources scaled by color and height, binned into seven discrete mixing ratio ranges, and colored accordingly. Height was scaled on a continuum above the dairy to indicate the acetaldehyde mixing ratios.

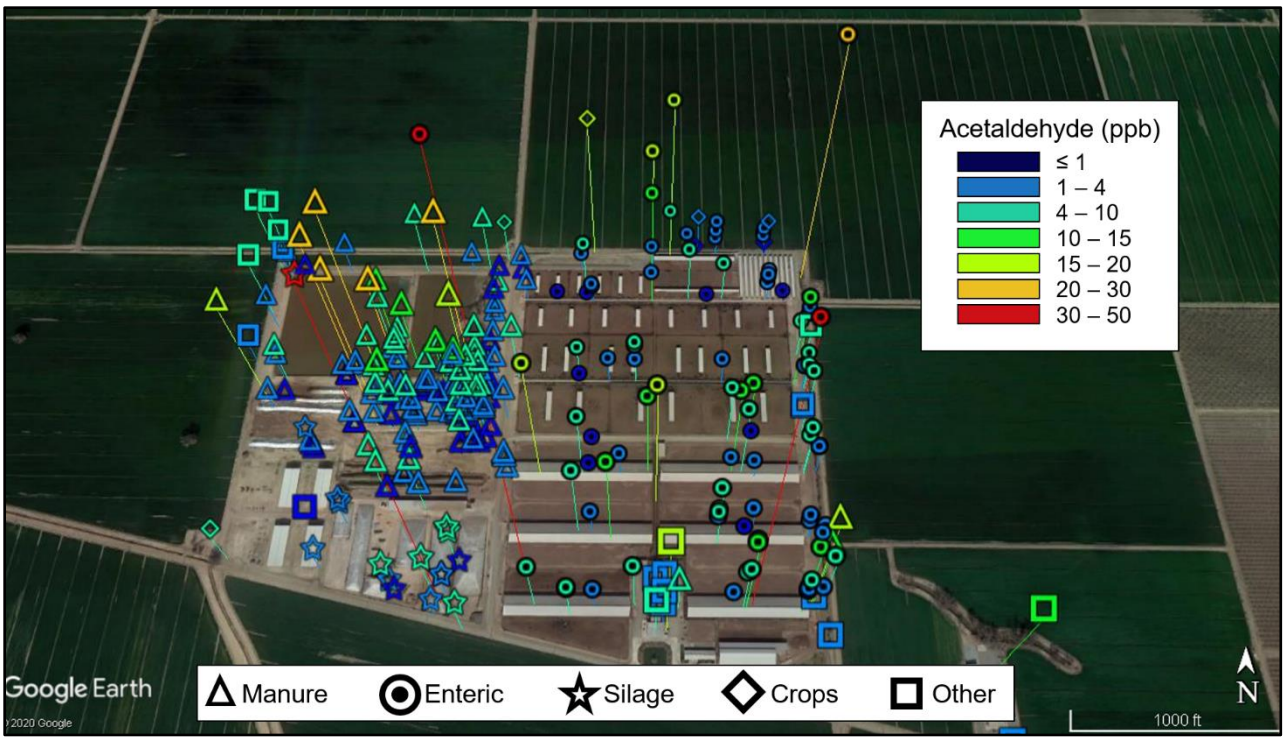


**Figure 5.3** Acetaldehyde (ppb) at the dairy farm binned by mixing ratio ranges and grouped by source. Height of the points also indicates the mixing ratios of acetaldehyde. Typical wind direction was from the northwest.

Acetaldehyde mixing ratios ranged from below 1 ppb to nearly 50 ppb. Acetaldehyde background mixing ratios for the SJV, a suburban and rural area, were expected to be between 0.1 – 4 ppb because it is a common compound in the atmosphere (Apel et al., 1998; Riemer et al., 1998; Goldan et al., 1995; Fried et al., 1997; Grosjean et al., 1996; Lee et al., 1995), but samples at the dairy farm often exceeded this range. Acetaldehyde was consistently enhanced near the manure management system and near enteric sources like the free stalls and the corrals. Acetaldehyde was also elevated near the silage piles as well.

All three oxygenates (methanol, ethanol, and acetaldehyde) were enhanced near the silage, which was used as feed for the cows and was stored on-site. Previous studies have shown that oxygenates are normally found in silage, so it was expected to have variable quantities of ethanol, propanol, 2-butanol, and their associated esters (Morgan & Pereira, 1962; Yang, 2009). These compounds, particularly ethanol, are absorbed by the rumen in ruminant animals up to a

certain maximum quantity (Jean-Blain et al., 1992). The cows at the dairy farm in this study are primarily on a diet incorporating corn silage, so it was expected that alcohols would be elevated around them, their feed, and their waste. Although these gases do not likely harm the animals (Jean-Blain et al., 1992), the high mixing ratios of oxygenates at this dairy farm have a strong odor and a very large ozone creation potential, as presented in Derwent et al. (2007). The consequences of this are examined more in Chapter 8.2.1.

In this current chapter, the sources likely contributing to the highest methanol, ethanol, and acetaldehyde mixing ratios were determined. These sources are considered potential ozone generators and possible odor contributors at the dairy farm. First, the three hundred fifteen samples (out of three hundred and fifty-nine collected in Visalia total) that were collected on-site at the dairy farm from the mobile lab and on foot were sorted by the highest methanol, ethanol, or acetaldehyde mixing ratios. To determine the locations likely responsible for the largest enhancements, the samples were ordered from least to greatest mixing ratio of each respective gas. The top thirty-one samples, or 10%, were determined. Table 5.1 shows the maximum, minimum, average, and median for all samples as well as for the top 10%.

**Table 5.1** Maximum, minimum, average, and median mixing ratios (ppb) for methanol, ethanol, and acetaldehyde at the dairy

| | **All Samples** | | |
|---|---|---|---|
| | **Methanol (ppb)** | **Ethanol (ppb)** | **Acetaldehyde (ppb)** |
| Minimum | 1 | 1.2 | 0.1 |
| Median | 25 | 8.9 | 3.0 |
| Average | 52 | 134 | 4.8 |
| Maximum | 360 | 7060 | 52 |
| | **Top 10%** | | |
| | **Methanol (ppb)** | **Ethanol (ppb)** | **Acetaldehyde (ppb)** |
| Minimum | 136 | 262 | 11 |
| Median | 187 | 636 | 16 |
| Average | 197 | 1089 | 19 |
| Maximum | 360 | 7060 | 52 |

Ethanol had the highest mixing ratios overall, with a maximum of over 7 ppm next to a pile of silage. This elevated ethanol correlates well with a previous Rowland-Blake study of silage

emissions, which showed that silage is responsible for the release of many oxygenates on dairy farms in California (Yang, 2009). Yang (2009), which examined six different dairies in California, reported average ethanol mixing ratios as high as 17 ppm near silage piles, 380 ppb near manure handling systems, and 530 ppb from cows in open lots. These ethanol averages from Yang (2009) were much higher than the ethanol average of all samples collected at the Visalia dairy (i.e., 134 ppb), but this study shows that some of the contributing sources across different dairy farms may be similar. However, differences can still be found, as discussed further below.

After ethanol, methanol had the second highest overall mixing ratios of the selected oxygenates at the Visalia dairy, with the maximum value of 360 ppb near a lagoon. This location was surprising, given that Yang (2009) reported that the highest methanol mixing ratios came from silage, with an average of 4000 ppb, while the average methanol mixing ratios near the manure for Yang (2009) were about 130 ppb, an order of magnitude smaller. The Visalia dairy's manure management system had more enhanced methanol than expected and even had higher methanol mixing ratios than the silage.

The difference between the results in Yang (2009) and in this study may come down to a difference in the manure management systems. Yang (2009) measured mixing ratios from six California dairies with different manure handling methods, but none of them perfectly matched the Visalia dairy's approach of using a separator, slurries, and lagoons. The Visalia dairy's highly concentrated slurries and the high number of cows (which create a large quantity of manure solids daily) likely contributed to the enhanced methanol mixing ratios near the manure management system rather than near the silage piles.

Lastly, acetaldehyde had a maximum mixing ratio of 50 ppb in free stall area. This was much higher than the average near cows (i.e., 4.0 ppb), but was much lower than the average reported near silage (i.e., 100 ppb) in Yang (2009). This study shows that silage is likely not the only source of these oxygenates at a dairy farm. Instead, methanol, ethanol, and acetaldehyde

come from a variety of sources. The locations that contributed to the highest thirty-one samples for these select oxygenates are shown in Figure 5.4. These locations differ for different gases. For example, the highest thirty-one samples for methanol were not necessarily collected in the same locations as the highest thirty-one samples for ethanol, but there was often some overlap.

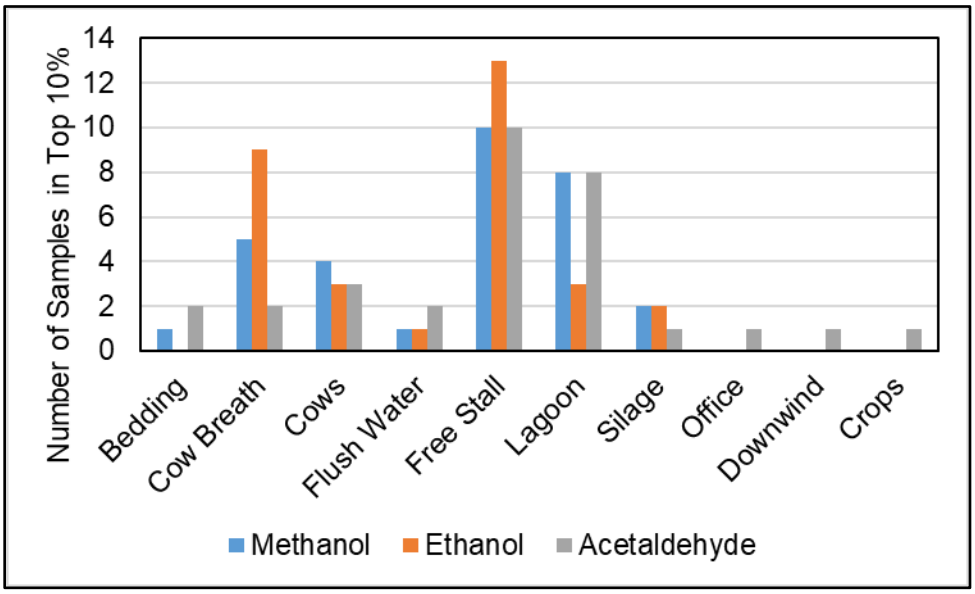


**Figure 5.4** Locations likely producing the highest 10% of methanol, ethanol, acetaldehyde mixing ratios at the Visalia dairy

Free stalls, lagoons, and cow breath were big contributors to the list of the top thirty-one samples. Other locations, such as “Cows” (which represents heifers and dry cows in corral areas), flush water, and silage also had samples in the top 10%. It is important to not only determine the locations that may have contributed the most, but also how much they contributed compared to the total for all campaigns. For methanol, the highest 10% samples contributed 37% of the total methanol across all dairy farm campaigns. This means that the free stalls, lagoons, cow breath, cows, and a little bit of bedding, silage, and flush water contributed over a third of the methanol across the campaigns. For ethanol, the highest 10% of samples contributed even more to the total—about 80% of the ethanol across all campaigns. This means that most of the ethanol for the campaigns likely came from free stalls, cow breath, cows, and lagoons, with a little bit from silage and flush water. Finally, for acetaldehyde, the highest 10% of samples contributed 39% of

the acetaldehyde across all campaigns. Acetaldehyde had the largest variety of sources. The largest contributors were free stalls, lagoons, and cows, but there was some contribution from bedding, cow breath, flush water, and silage, with some large acetaldehyde mixing ratios also found near the office, downwind, and near the crops. Acetaldehyde appeared to be more widespread throughout the dairy than methanol and ethanol.

Although it was true that methanol, ethanol, and acetaldehyde were enhanced near silage, there were likely other sources around the dairy. These are likely still influenced by the silage in its different forms. For example, the silage is piled in the free stalls for the cows to eat. If the cows eat the silage and expel air containing gases from the silage—this would create elevated oxygenate mixing ratios in the free stalls. At the Visalia dairy, the milk cows' diet incorporates more corn than the dry cows' and heifers' diets (which contains more wheat). This also explains why the oxygenate mixing ratios in the free stalls (i.e., where the milk cows are fed) were higher than near the cows in corrals (i.e., where the other cows are fed). The free stall structures themselves also likely trapped air more easily than the corrals, allowing gases to accumulate.

Figure 5.5 can be further expanded upon by examining the percentages that each of these locations contribute within the top 10% of oxygenate mixing ratios. This implies which locations may contribute the most methanol, ethanol, and acetaldehyde, which is important to determine which locations can most easily contribute to ozone formation. Figure 5.5 shows the percentage that each location contributes to the top 10% of the dairy farm mixing ratios.

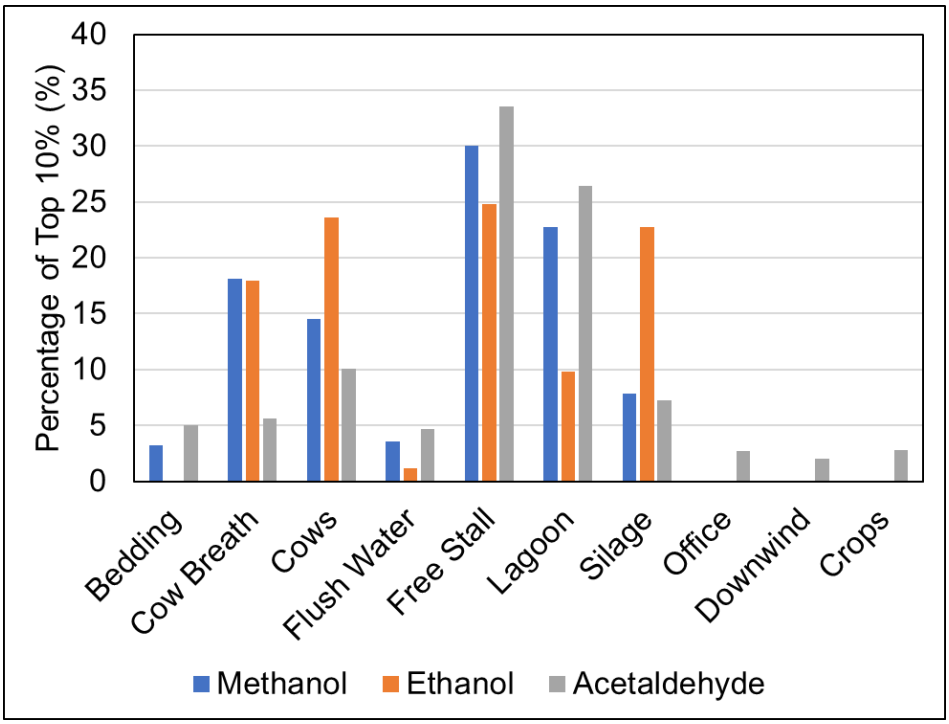


**Figure 5.5** Percentage of oxygenate mixing ratios in the top 10% of samples, categorized by dairy location

As shown in Figure 5.5, nearly 30% of the top 10% of methanol emissions came from the free stalls. These enhancements are likely a combination of piled silage and enteric emissions under the long, covered feed hutches. Surprisingly, lagoons contributed much more methanol and acetaldehyde than ethanol. Lagoons were responsible for about 23% of methanol in the top 10%, likely as a product of decomposition. Samples collected near the outdoor cows and cow breath were responsible for 14% and 18% of the top 10% of methanol at the dairy, respectively. This could partially be because the cows eat the silage and expel methanol. Silage was only responsible for about 8% of the top 10% of methanol at the dairy.

The dairy keeps their silage piles covered for most seasons, so this may have blocked some of the ethanol emissions from the silage itself. Even still, 23% of the top 10% of ethanol at the dairy likely came from the silage. This is a high amount considering that only two samples made it into the top 10% ethanol, but they contributed nearly a quarter of that 10%. Figure 5.5 also highlights other likely ethanol sources, like the free stalls, cows, and cow breath. Just like

with methanol, cows eat the silage and likely expel ethanol as they ruminate. About 25% of the top 10% of ethanol at the dairy came from the free stalls, where air gets trapped under the feed hutches. Feed, including silage, is typically piled on the ground in the free stalls, which could also contribute to elevated ethanol from non-enteric sources at that location. About 18% of the top 10% of ethanol came from cow breath, likely from the cows eating the silage. Outside cows (not in the free stalls) were responsible for 24% of the top 10% of the ethanol, again likely because of the silage that they eat. Less than 10% of the top 10% ethanol mixing ratios came from the lagoons, presumably as a byproduct of decomposition.

Although the acetaldehyde was enhanced near a variety of potential sources, it was most elevated near the free stalls and lagoons. Free stalls were responsible for nearly 34% of the top 10%, the highest location contribution out of all locations across all three oxygenates. Acetaldehyde also likely came from the lagoons, which were responsible for over 26% of the top 10%. Acetaldehyde is a byproduct of decomposition as well as ethanol oxidation reactions. Ethanol is oxidized by the hydroxyl radical to form acetaldehyde in the reactions presented below (Carter et al., 1979). In Reaction 5-1, ethanol is oxidized by a hydroxyl radical to form water and a hydroxyethyl radical. In Reaction 5-2, the hydroxyethyl radical reacts with oxygen to form acetaldehyde and a hydroperoxyl radical.

$$CH_3CH_2OH + OH \rightarrow H_2O + CH_3CHOH \qquad \text{Reaction 5-1}$$

$$CH_3CHOH + O_2 \rightarrow CH_3CHO + HO_2 \qquad \text{Reaction 5-2}$$

Carter et al. (1979) noted that these reactions form 80±15% acetaldehyde under atmospheric conditions. Wallington and Kurlyo (1987) showed that the reaction rate constant for Reaction 5-1 is temperature dependent with $k = (7.4 \pm 3.2)\text{x}10^{-12} * \exp\left(\frac{-240 \pm 110}{\text{T}}\right)$ cm$^3$ molec$^{-1}$ s$^{-1}$. For this study, one can assume that the production of ethanol from the manure management system and the concentration of the hydroxyl radical are constant during the daytime hours. The average acetaldehyde mixing ratio near the manure management system was 4.2 ppb. Assuming a warm

Visalia day of 80 °C, this is a concentration of $8.6x10^{10}$ molec acetaldehyde $cm^{-3}$. Using the stoichiometric mole ratio of 1:1 (moles ethanol reacted to moles acetaldehyde produced), and assuming that 80% of the ethanol reacted would form acetaldehyde, one would need $1.1x10^{11}$ molec ethanol $cm^{-3}$, or 5.2 ppb ethanol to make the 4.2 ppb average acetaldehyde near the manure management system. The average ethanol found near the lagoons was about 40 ppb, plenty to contribute to acetaldehyde formation. This possible contribution from ethanol oxidation means that acetaldehyde at the dairy farm may be formed from a combination of primary and secondary emissions.

A much smaller percentage of acetaldehyde, only 10% of the top 10%, likely came from the outdoor cows, perhaps as a byproduct of ethanol oxidation or a primary enteric emission from the cows themselves. As cow breath contributed about 5% of the top 10%, it is possible that cows emit acetaldehyde directly, which would also explain the elevated acetaldehyde in the free stalls. Samples collected near silage contributed only about 7% of the top 10% of acetaldehyde at the dairy, the lowest contribution of all three oxygenates.

Future studies could consider trapping and collecting gas exclusively from the lagoons and slurries and then comparing it to air that is trapped and collected from the silage. This would help determine whether the oxygenates were already present when they reached the manure management system and whether they were enhanced during the decomposition of manure. Overall, out of methanol, ethanol, and acetaldehyde, ethanol had the highest mixing ratios across all campaigns. Methanol had the second highest, and acetaldehyde had the lowest. Ethanol was highest near free stalls, cow breath, silage, and outdoor cows. Methanol was highest near free stalls, lagoons, outdoor cows, and cow breath. Finally, acetaldehyde was highest near free stalls and lagoons. Knowing that these locations are likely sources of these three gases helps determine where ozone generation could occur at the dairy, as well as possible sources of odor. This is examined in finer detail in Chapter 8.

### 5.2 Methanol, Ethanol, and Acetaldehyde at Orange County Landfills

Methanol, ethanol, and acetaldehyde mixing ratios at Orange County landfills were quantified for the Spring and Summer 2018 landfill campaigns (60 samples total). All active landfills (Prima Deshecha, Frank R. Bowerman, and Olinda Alpha) and closed (Vista Grande Park, Santiago Canyon, and Coyote Canyon) were included for this analysis. The top 10% of samples (6 samples) were selected based on the highest mixing ratios for each oxygenate to determine the landfills responsible. These locations sometimes differed for different gases. Table 5.2 shows the maximum, minimum, median, and average mixing ratios of methanol, ethanol, and acetaldehyde at Orange County landfills as well as for the top 10%.

**Table 5.2** Maximum, minimum, average, and median mixing ratios (ppb) for methanol, ethanol, and acetaldehyde at the Orange County landfills

| | **All samples** | | |
|---|---|---|---|
| | **Methanol (ppb)** | **Ethanol (ppb)** | **Acetaldehyde (ppb)** |
| Minimum | 1.28 | 0.42 | 0.6 |
| Median | 4.52 | 2.81 | 2.4 |
| Average | 68.2 | 86.4 | 4.1 |
| Maximum | 1580 | 2530 | 59 |
| | **Top 10%** | | |
| | **Methanol (ppb)** | **Ethanol (ppb)** | **Acetaldehyde (ppb)** |
| Minimum | 107 | 147 | 9.1 |
| Median | 390 | 417 | 11 |
| Average | 604 | 762 | 19 |
| Maximum | 1580 | 2530 | 59 |

At the landfills, similar to the dairy farm, ethanol had the highest overall mixing ratios out of the select oxygenates in Table 5.2. However, ethanol mixing ratios at the landfills were lower overall than at the dairy farm. Contrarily, acetaldehyde and methanol maximum mixing ratios were higher at the landfills than at the dairy farm. The sample with the maximum value of acetaldehyde was collected, surprisingly, at the closed Santiago Canyon landfill, and was 7 ppb higher than the maximum acetaldehyde at the dairy farm. Maximum methanol was nearly 350% higher at the landfills than at the dairy farm. The difference between the oxygenate mixing ratios at the dairy farm and at the landfill could be explained by their method of entering the atmosphere.

Landfill gases are emitted through two main pathways: decomposition, which can occur on the surface but occurs primarily underground, and evaporation, which occurs on the surface (Giess et al., 1999). Methane and carbon dioxide were much lower at the surface of the landfill than at the dairy farm because the landfills have methods in place (e.g., liners, collection tanks, cover material, pumps) to trap many gases emitted during methanogenic decomposition, which does not typically start to occur until the waste is well buried. However, evaporation from active dumping areas at landfills is not well controlled. As waste is dumped on the surface, it can release gases into the air. This, combined with any above-surface decomposition, may explain why methanol and acetaldehyde were higher at the landfills than at the dairy farm, while methane and carbon dioxide mixing ratios were lower at the landfills than at the dairy farm.

Previous studies have also found similar results at active waste areas. For example, Young and Parker (1983) examined LFG at six different landfills in the United Kingdom. Each site accepted different waste. They reported high concentrations of alcohols (i.e., [$CH_3CH_2OH$] = 650 mg/$m^3$; [$CH_3OH$] = 210 mg/$m^3$) at a site that contained 3-week-old uncovered domestic waste. This LFG at the landfill was only 0.05% $CH_4$, meaning that it was only in the beginning stages of methanogenesis. However, for their sites with older waste (i.e., 7 months old with 65% $CH_4$ or 6 years old with 37.5% $CH_4$), alcohol concentrations were negligible. This means that alcohol emissions likely decrease as methanogenesis begins. According to Table 1.3 from Chapter 1.4.1, the alcohol emissions associated with decomposition occur mostly during Stage II. Once a landfill reaches Stage IV, its long-haul stage of LFG production, alcohol emissions from decomposition are expected to be quite low. This means that the elevated oxygenates found at Orange County landfills are likely from a combination of the early stages of decomposition (i.e., Stage II) and some contribution from evaporation.

Allen et al. (1997) went on to note that alcohol emissions at landfills also depend heavily on the type of waste (e.g., industrial or municipal), and the geography of the landfill (e.g., quarry

infill or extraction site). Allen et al. (1997) noted that at seven landfills in the United Kingdom, alcohol and ketone emissions ranged from 2 to 2069 mg/m$^3$. This large range was caused by differences in waste management practices and in the layout of the landfills themselves. Similarly, for the Orange County landfills, the oxygenate mixing ratios varied widely between locations.

Overall, for the Orange County landfills, it seems that alcohols and acetaldehyde are only emitted during the first stages of decomposition or during evaporation from the surface. Various landfills were represented in the top 10% of methanol, ethanol, and acetaldehyde. Figure 5.6 shows the percentage of landfills responsible for the top 10% of mixing ratios of methanol, ethanol, and acetaldehyde regardless of season.

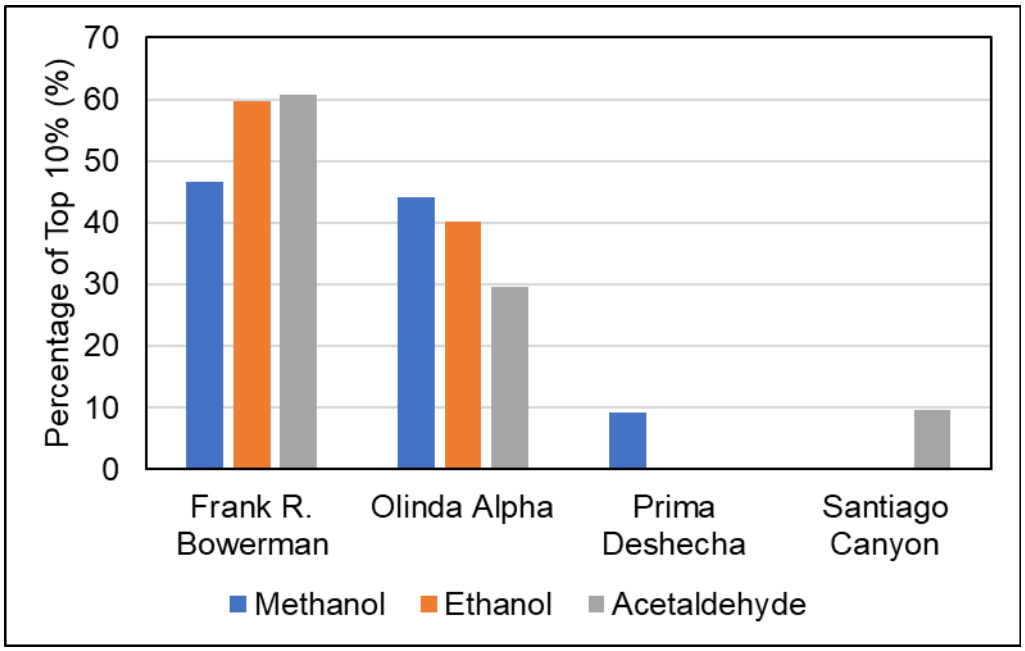


**Figure 5.6** Orange County landfills responsible for top 10% of mixing ratios of methanol, acetaldehyde, and ethanol during Spring and Summer 2018 campaigns

Frank R. Bowerman and Olinda Alpha were responsible for most of the top 10% of methanol, ethanol, and acetaldehyde. Both are active Orange County landfills. Nearly 50% of the top 10% methanol came from Frank R. Bowerman, and 44% came from Olinda Alpha. None of the closed landfills contributed to the top 10% for methanol. Nearly all the samples in the top 10% for methanol were collected on top of—or downwind of—active dumping at the landfill. This could

be a result of the emissions from the waste itself combined with the daily cover material, which was often organic material like mulch.

Two samples included in the top 10% of methanol that were not collected at active dumping were collected at extremely stinky and leaky compost piles of decomposing trash. These were piles that the landfills created for their on-site pilot composting programs to prepare for the start of AB-1594. Figure 5.7 shows a compost pile that was part of the on-site composting pilot program at Frank R. Bowerman landfill. The temperature probe indicated that the temperature of the compost pile was over 150 °F.

**Figure 5.7** On-site composting program at Frank R. Bowerman landfill in Irvine, California. The temperature of the compost's interior was over 150 °F. Photo by Brenna Biggs in 2018.

The compost piles take several months to mature and require frequent maintenance. All the active landfills engaged in some type of composting process. A photo of the author collecting a sample near a compost windrow at Prima Deshecha is shown in Figure 5.8.

**Figure 5.8** The author collecting an air sample from a compost windrow at Prima Deshecha landfill in Orange County. Photo by Alicia Hoffman in April 2018.

Compost from MSW is low quality because of plastic and glass contamination (Farrell & Jones, 2009). If MSW composting programs continue, they will likely exist to create a product that can be used as an approved daily cover material for the landfill. Whether or not MSW decomposes as compost or within the landfill itself, it still will release contaminated water (i.e., leachate) into the ground and potentially harmful emissions freely into the atmosphere. It would require additional infrastructure to be built to better prevent these rogue emissions and possible water contamination from occurring (Hurst et al., 2005). Properly composting MSW takes at least six months; if this process is stopped prematurely, no GHG reduction is achieved. Additionally, composted MSW also requires an aftercare period like that of a landfill and should be considered a long-term investment of time and resources.

Literature has shown that composting MSW completely can reduce biogas (i.e., mostly $CH_4$ and $CO_2$) emissions by over 80% versus leaving the MSW to decay in a landfill (Farrell & Jones, 2009; Adani et al., 2004). This was noted in the composting area at Prima Deshecha in Figure 5.8. Municipal solid waste that had finished composting had a $CH_4$ mixing ratio of 2.13 ppm while the background was 1.95 ppm, but the MSW that was actively composting had a $CH_4$ mixing ratio of 7.8 ppm and a background of 1.88 ppm $CH_4$. Although methane emissions are

reduced by composting, this does not account for other emissions (i.e., alcohols) that will not be easily controlled and can still damage the environment or cause unpleasant odors (Nagata & Takeuchi, 2003). Landfill engineers will need to weigh the benefits and drawbacks of letting compost outgas on the surface of the landfill or within the landfill itself, where modern infrastructure can better prevent rogue emissions and leachate accumulation.

The top 10% ethanol mixing ratios came from only two landfills: Frank R. Bowerman and Olinda Alpha. Frank R. Bowerman contributed nearly 60% to the top 10%, and Olinda Alpha contributed about 40%. All the samples in the top 10% for ethanol were collected on top of—or downwind of—active dumping at the landfill. The proximity to active dumping areas seemed to greatly influence enhancements of ethanol and methanol mixing ratios in the top 10%, indicating that these gases likely come from the evaporation of waste, the daily cover material, or the very beginning stages of decomposition. No samples collected over intermediate or final cover were in the top 10%, meaning that the engineering methods in place at the landfills are efficient at trapping oxygenate emissions from underground decomposition.

The top 10% acetaldehyde mixing ratios came from three landfills: Frank R. Bowerman, Olinda Alpha, and Santiago Canyon. All the samples collected at Frank R. Bowerman and Olinda Alpha were collected near active dumping areas. The active dumping area at Frank R. Bowerman is pictured in Figure 5.9. Samples were collected very close to the waste. This active dumping area would be covered with daily cover material before the end of the disposal for the day.

**Figure 5.9** Active dumping area at Frank R. Bowerman landfill during 2018. Photo by Brenna Biggs.

Frank R. Bowerman was responsible for nearly 60% of the top 10% of acetaldehyde mixing ratios, all of which came from samples collected near the active dumping site in Figure 5.9. Olinda Alpha was responsible for nearly 30% of the top 10% of acetaldehyde mixing ratios; again, these were in samples collected near active dumping. Surprisingly, the closed Santiago Canyon landfill also had elevated acetaldehyde and was responsible for nearly 10% of the top 10%. The mixing ratio for acetaldehyde in the Santiago Canyon sample was about one order of magnitude higher than the acetaldehyde in other samples collected at the same landfill during the same day. This sample also contained elevated levels of other gases, including butanal and acetone, also elevated by about an order of magnitude. The sample was collected close to the entrance to Santiago Canyon, so it was possible that there was a source of these gases hidden

nearby. As $CH_4$ and $CO_2$ were not elevated much over the background in that sample, the source is likely not leaky LFG infrastructure.

Overall, methanol, ethanol, and acetaldehyde were more enhanced at active landfills than the closed landfills. On-site contributors included the green material (e.g., mulch as daily cover or the MSW compost), early stages of decomposition, and likely some evaporation. Knowing these locations and sources is important for Chapter 8, which examines odor and ozone creation at landfills.

### 5.3 Regional Ethanol, Methanol, and Acetaldehyde in the San Joaquin Valley

Samples collected above the SJV for SARP 2011, 2013, 2014, 2015, and 2017 below a pressure altitude of 3,000 feet were examined to determine general mixing ratios of methanol, ethanol, and acetaldehyde above the Valley. More information about the logistics of these flights was given in Chapter 2.1. Although all samples used for the majority of this oxygenate analysis were collected below 3,000 feet, a range of altitudes from 455 – 2,898 feet (average = 1,625 feet) was used. Table 5.3 shows the maximum, minimum, average, and median mixing ratios for methanol, ethanol, and acetaldehyde in the samples collected during these flights. The minimum for the oxygenates was determined by taking an average of samples collected between pressure altitudes of 3,000 and 5,000 feet.

**Table 5.3** Maximum, average, and median mixing ratios (ppb) of select oxygenates above SJV from low altitude (< 3,000 feet) SARP data. Typical minimum values were determined using an average of samples (n = 43) collected between pressure altitudes of 3,000 and 5,000 feet.

| | **Methanol (ppb)** | **Ethanol (ppb)** | **Acetaldehyde (ppb)** |
|---|---|---|---|
| Minimum | 1.53 | 0.46 | 0.34 |
| Median | 3.20 | 1.15 | 0.56 |
| Average | 3.21 | 1.32 | 0.71 |
| Maximum | 13.6 | 7.61 | 4.1 |

Methanol exhibited the highest mixing ratios of these three gases over the SJV. Average and median values of methanol over the SJV were about an order of magnitude smaller than methanol at the dairy farm. The median methanol mixing ratio was the same order of magnitude

as the median methanol mixing ratio at the landfills. However, the maximum methanol mixing ratio over the SJV was two orders of magnitude smaller than the maximum at the Orange County landfills, and about one order of magnitude smaller than the maximum methanol at the dairy farm. This implies that methanol is likely emitted by ground-level sources, like the dairy farms, landfills, and more (e.g., wineries). By the time that the air reached higher altitudes in the boundary layer, it would have dispersed and reacted, resulting in smaller methanol mixing ratios than those found at the surface.

An overlay of the methanol mixing ratios in the SJV is shown in Figure 5.10. Methanol mixing ratios were colored and binned by range, and they varied from < 1 ppb to about 14 ppb over various parts of the SJV. The height of the points also indicates methanol mixing ratio. Additional points (e.g., black rings) were included showing bovine-containing areas, which had been manually identified by the author using aerial imagery and described in Chapter 2.4.1. These areas are most often dairies but can include some cattle feedlots as well.

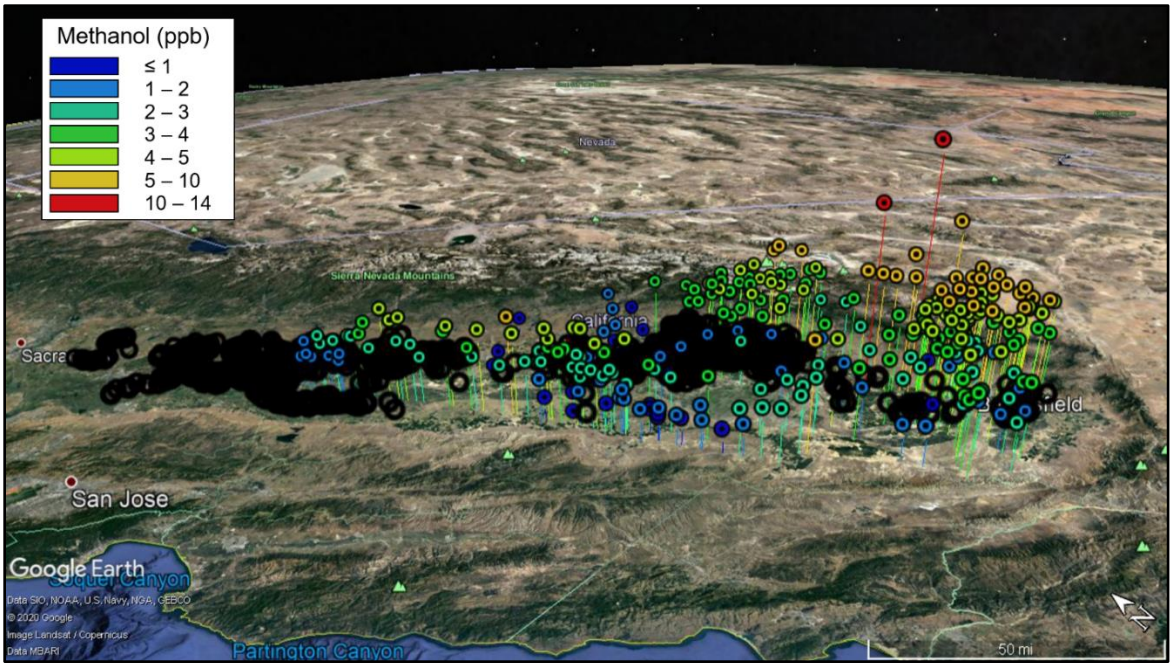


**Figure 5.10** Methanol mixing ratios during SARP flights from 2011, 2013, 2014, 2015, and 2017 below 3,000 feet pressure altitude. Mixing ratios are binned by range, which is indicated by color. The height of the points also indicates methanol mixing ratio. Black rings are bovine-containing areas, typically dairies, in the SJV.

The most elevated samples were collected above Kern County, followed by Tulare County. Methanol was more elevated, in general, on the eastern side of the SJV than on the western side of the SJV. This is likely because of the typical wind direction, which usually blows from the northwest, bringing pollutants from the ground sources up to a higher altitude on the eastern side. Based on Figure 5.10 alone, it is difficult to determine whether methanol is elevated because of the dairy farms in the SJV or because of other reasons. For example, while Tulare County contains the most cows in the SJV, Kern County contains a very active airport and the aptly named city of Oildale.

To better determine the source of the methanol, methane was used as a dairy tracer. In Chapter 4.2, large quantities of methane were shown to originate from enteric and manure sources at the dairy farm, which contributed to much higher mixing ratios than the samples that were collected at landfills. For airborne data collected at higher altitude, Yang (2009) also showed that methane was correlated with oxygenates and that it can be used to trace air back to dairy farms. Methane was assumed to still be present in air that had been emitted at dairy farms as the air traveled to higher altitudes. This means that if a sample had a high mixing ratio of an alcohol *and* a high mixing ratio of methane, that air likely originated from a dairy farm somewhere in the SJV. Figure 5.11 shows the same aerial photograph as Figure 5.10, but with the height of the points determined by the *methane* mixing ratio of each sample rather than methanol. The higher the point above the SJV, the higher the methane in the sample.

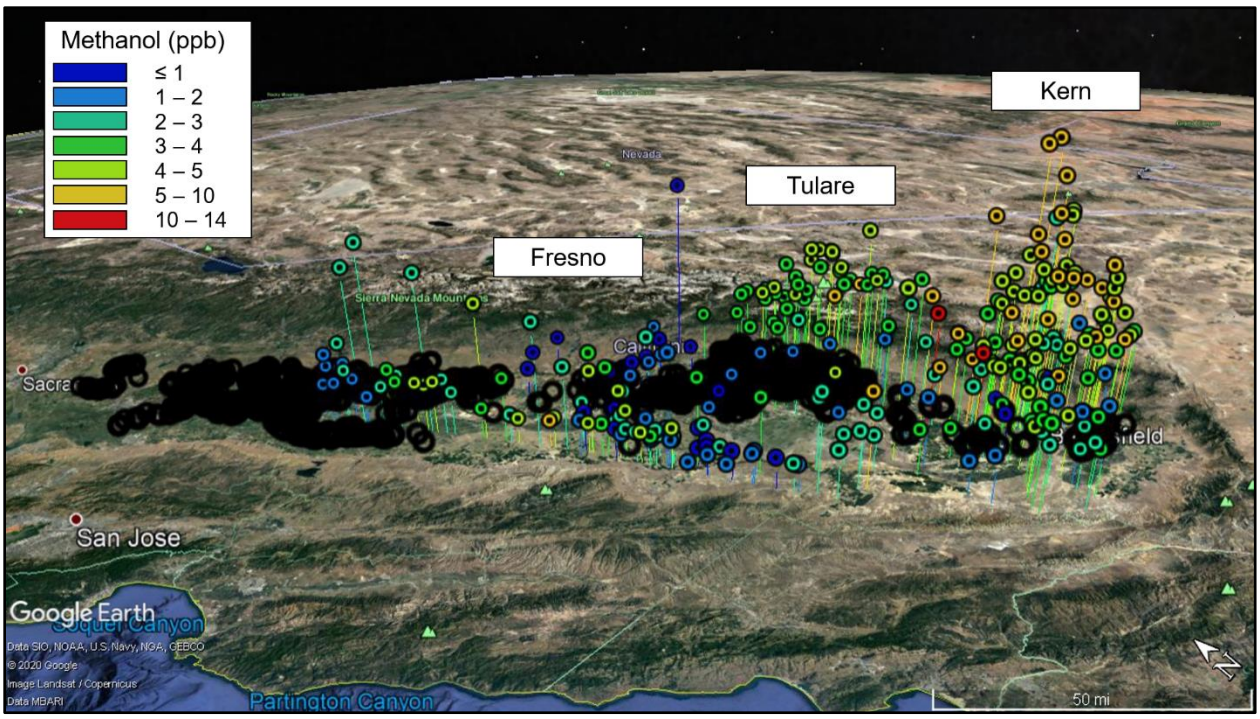


**Figure 5.11** Methanol mixing ratios during SARP flights from 2011, 2013, 2014, 2015, and 2017 below 3,000 feet pressure altitude. Mixing ratios are binned by range, which is indicated by color. The height of the points indicates methane mixing ratios. Black rings are bovine-containing areas, typically dairies, in the SJV. Three of the SJV counties are labelled for reference.

Based on the lower height of the red points in the highest range (10 – 14 ppb), Figure 5.11 shows that dairy farms are likely less responsible for the very elevated methanol mixing ratios (i.e., range 10 – 14 ppb), but likely contribute many of the mid-range methanol mixing ratios (i.e., ranges 3 – 10 ppb). The air that was collected at the southern end of the SJV had likely passed through much of the Valley, accumulating methane and methanol as it traveled based on the typical northwest wind direction. Figure 5.12 shows the correlation between methane and methanol over the SJV for the same SARP samples.

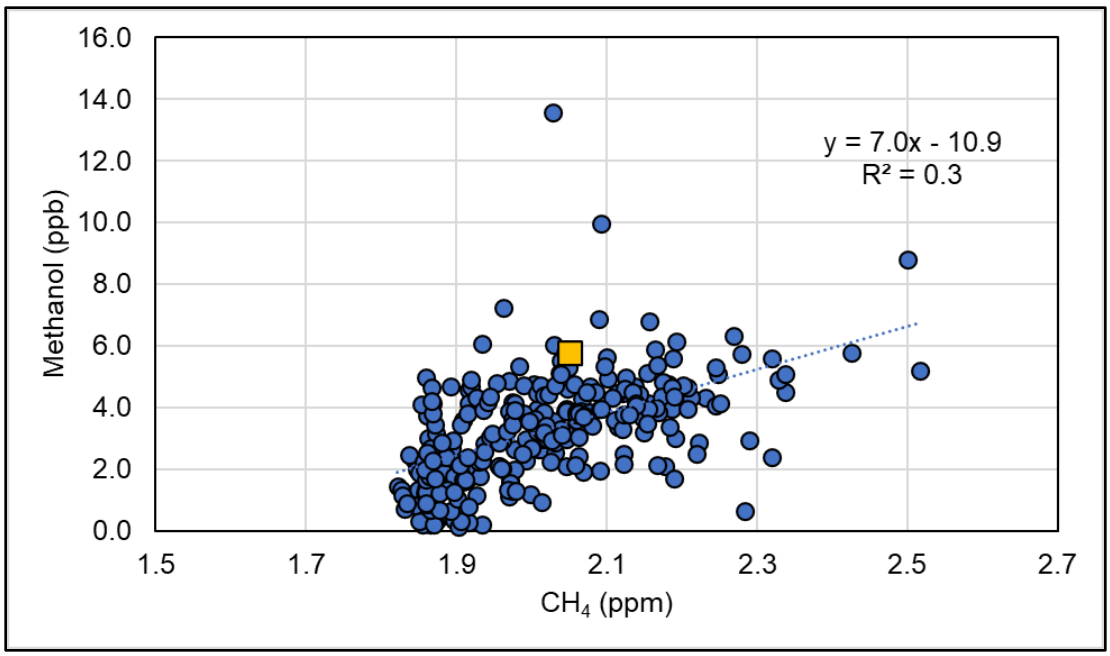


**Figure 5.12** Correlation of methane (ppm) and methanol (ppb) from SARP flights from 2011, 2013, 2014, 2015, and 2017 below 3,000 feet pressure altitude over the SJV. The yellow square corresponds to the average $CH_4$ and methanol at the dairy farm scaled down nine times.

Figure 5.12 also includes the ratio of average $CH_4$ to average methanol at the dairy farm, given as a yellow square. The ratio was scaled down nine times and shows that similar ratios were found in the SJV airborne data. Based on the correlation of $R^2$ = 0.3, Figure 5.12 shows that methanol and methane over the SJV are likely related. A significant amount of methanol in the SJV likely came from dairy farm practices. This finding agrees with previous studies done in the Rowland-Blake lab (Yang, 2009). It seems likely that some of the methanol in the SJV, even at altitudes up to 3,000 feet, come from dairy farms. The contribution of methanol from dairy farms to the SJV is important. As methanol moves throughout the Valley, it can react and contribute to pollution, visibility issues, and potential health concerns for the disadvantaged communities living throughout the area. Methanol can also contribute to ozone formation, which is discussed later in Chapter 8.2.1.

After methanol, ethanol had the second highest mixing ratios of the three gases over the SJV based on Table 5.3. An overlay of the ethanol mixing ratios in the SJV is shown in Figure 5.13. Ethanol mixing ratios were colored and binned by range, and they varied from < 0.5 ppb to

about 8 ppb over various parts of the SJV. The height of the points also indicates ethanol mixing ratios. Additional points (e.g., black rings) were included again to show manually identified bovine-containing areas.

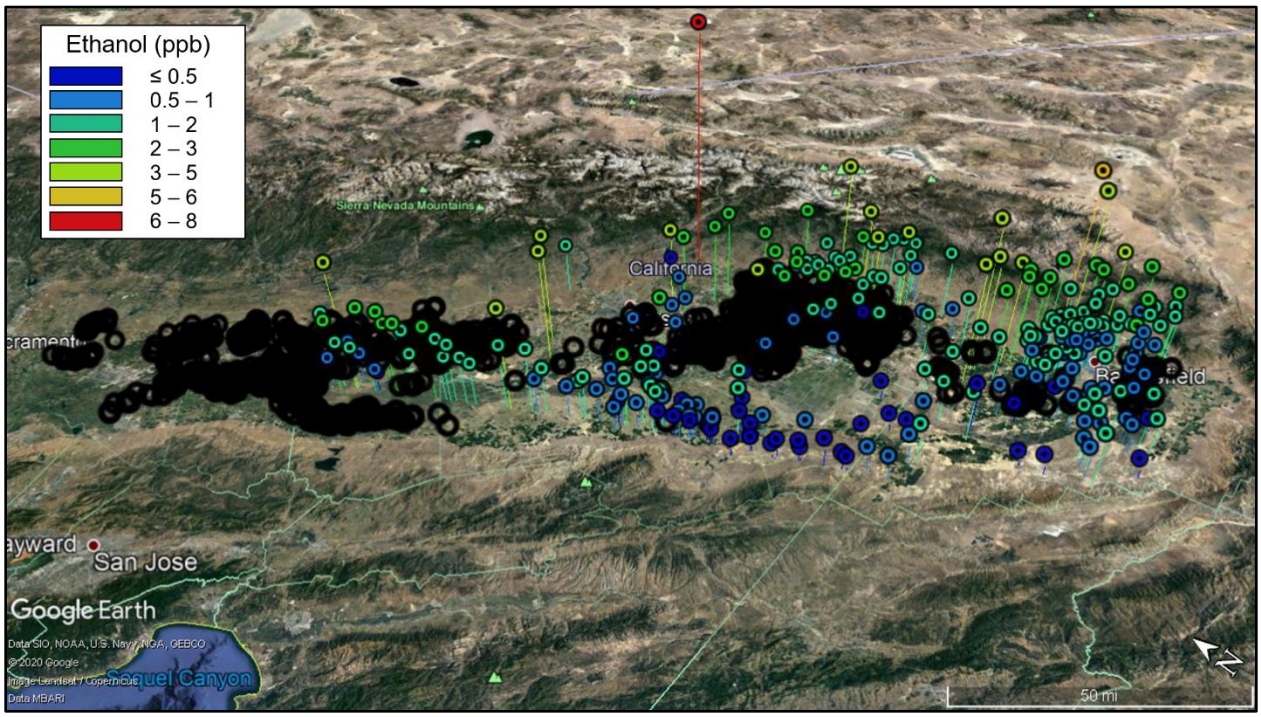


**Figure 5.13** Ethanol mixing ratios during SARP flights from 2011, 2013, 2014, 2015, and 2017 below 3,000 feet pressure altitude. Mixing ratios are binned by range, which is indicated by color. The height of the points also indicates ethanol mixing ratios. Black rings are bovine-containing areas, typically dairies, in the SJV.

The most elevated samples were collected over Fresno and Kern counties. The median ethanol mixing ratios over the SJV were the same order of magnitude as the median mixing ratios at the dairy and at the Orange County landfills. The maximum ethanol mixing ratio over the SJV was about three orders of magnitude smaller than the maximum ethanol at the dairy farm and landfills. Interestingly, while ethanol was greater than methanol in dairy and landfill samples, the reverse was true for the SARP data. This is likely a result of their different atmospheric lifetimes: methanol has a lifetime of about two weeks, while ethanol has a lifetime of 4 days, respectively (Seinfeld & Pandis, 2016).

To better determine the source of the ethanol, methane was again used as a dairy tracer. Figure 5.14 shows the same aerial photograph as Figure 5.13, but with the height of the points determined by the *methane* mixing ratio of each sample rather than ethanol.

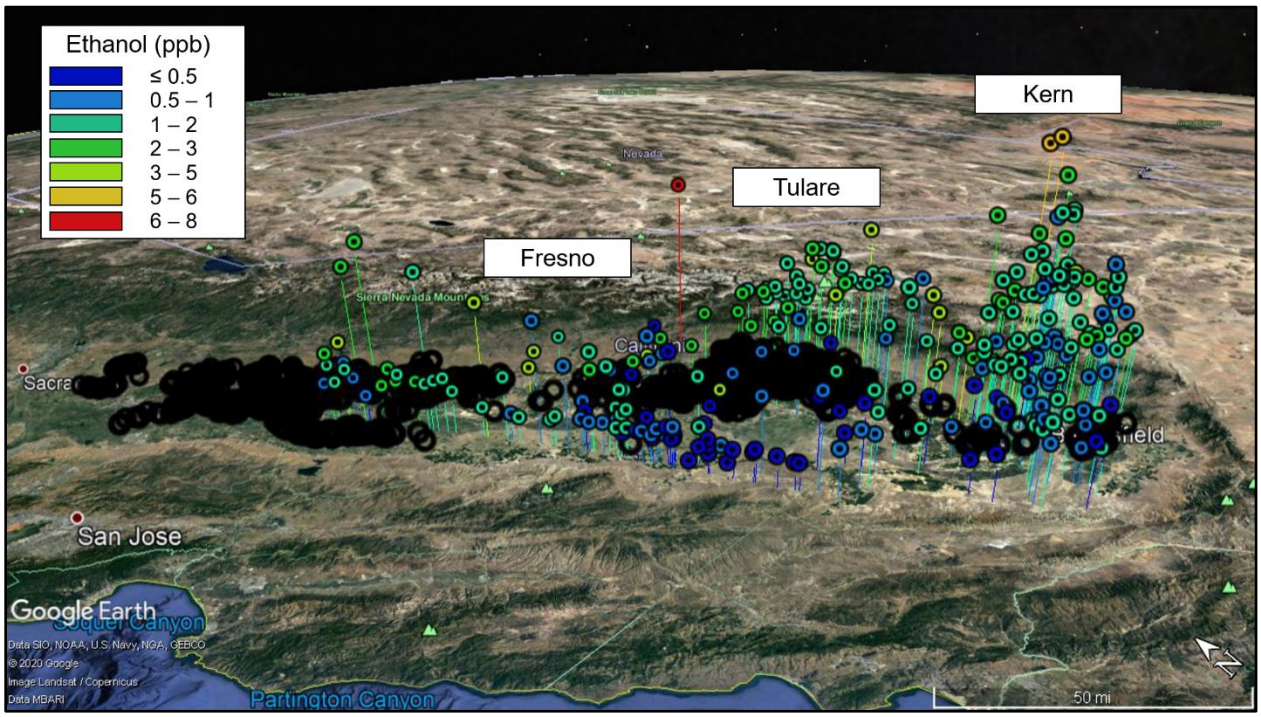


**Figure 5.14** Ethanol mixing ratios during SARP flights from 2011, 2013, 2014, 2015, and 2017 below 3,000 feet pressure altitude. Mixing ratios are binned by range, which is indicated by color. The height of the points indicates methane mixing ratios. Black rings are bovine-containing areas, typically dairies, in the SJV. Three of the SJV counties are labelled for reference.

Most of the ethanol points in the lowest range (dark blue, ≤ 0.5 ppb) also contained low mixing ratios of methane, as shown by the low height of the points plotted above the Valley. The points at the southeastern end of the SJV contained the most methane and ethanol overall, while there was a handful of points with high ethanol and high methane within the middle of the Valley. Therefore, it again seems likely that dairy farms are responsible for a large amount of the ethanol within the SJV, at least during the mid-summertime when the samples were collected. To further determine whether there was a general relationship between the two gases, Figure 5.15 shows the correlation between methane and ethanol over the SJV from the same SARP samples.

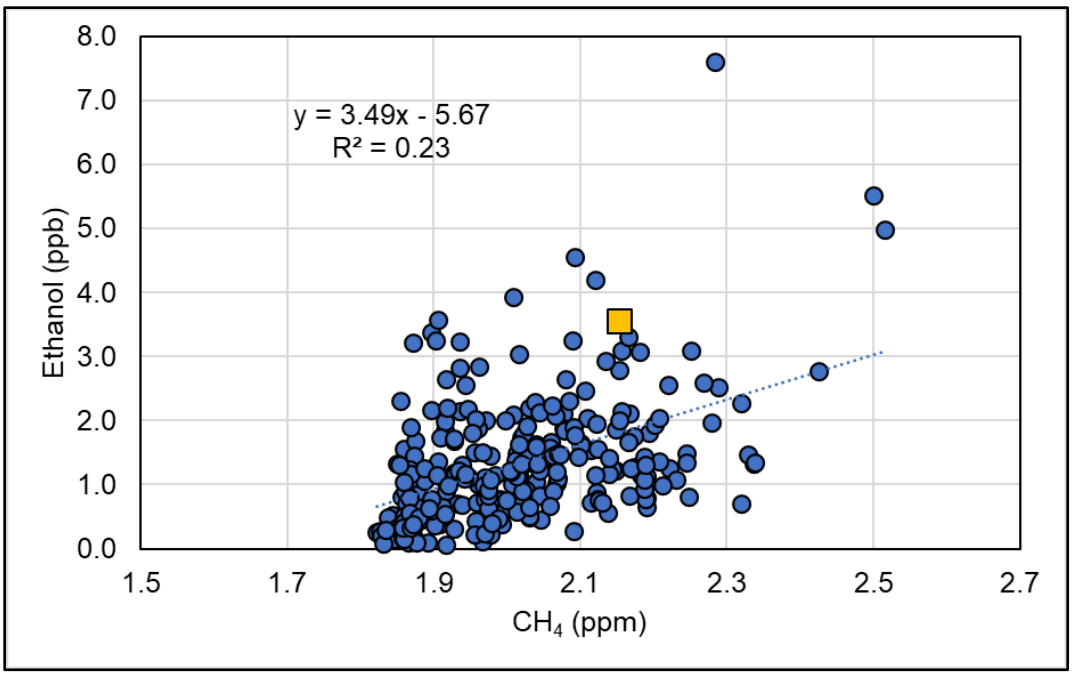


**Figure 5.15** Correlation of methane (ppm) and ethanol (ppb) from SARP flights from 2011, 2013, 2014, 2015, and 2017 below 3,000 feet pressure altitude over the SJV. The yellow square corresponds to the median $CH_4$ and ethanol at the dairy farm scaled down 2.5 times.

Figure 5.15 also includes the ratio of median ethanol and median $CH_4$ at the dairy farm scaled down 2.5 times, given as a yellow square. Based on the correlation of $R^2 = 0.23$, Figure 5.15 shows that ethanol and methane over the SJV could be related and that dairy practices are likely responsible for a large amount of ethanol in the SJV. This relationship agrees with previous studies done in the SJV. Yang (2009) determined that methane and ethanol are both emitted by dairy farms, and they have a correlation of $R^2 = 0.15$ at high altitude (> 20,000 feet) over the SJV. At lower altitudes, this correlation is greater possibly because ethanol has had less time to react. The lifetime of ethanol is only 2.4 – 4 days depending on atmospheric conditions (Grosjean, 1997; Seinfeld & Pandis, 2016), while the lifetime of methane is a little under a decade (Blake, 1984). Therefore, the farther away from the source an air parcel travels, the lower the ethanol will be while methane would stay rather constant (assuming no dilution). Ethanol from dairy farms in the SJV is an important contributor to ozone formation and odor, discussed later in Chapter 8.

According to Table 5.3, acetaldehyde mixing ratios were the smallest of the three examined oxygenates. Acetaldehyde above the SJV was within background, which has been shown to be between 0.1 and 4 ppb for rural or suburban areas (Apel et al., 1998; Riemer et al., 1998; Goldan et al., 1995; Fried et al., 1997; Grosjean et al., 1996; Lee et al., 1995). All the acetaldehyde mixing ratios above the SJV, including the maximum, were within this expected range. Additionally, the maximum acetaldehyde above the SJV was an order of magnitude smaller than the maximum acetaldehyde at the landfills or the dairy farm. The lack of acetaldehyde mixing ratios above background might be attributed to the vertical distance from its sources. Point sources were located, on average, at least 1,500 feet below the airborne sampling locations. Because of acetaldehyde's short atmospheric lifetime (i.e., about 10 hours), much of its emissions from dairy farms and other point sources were likely unable to travel up to the sampling altitude while maintaining similar mixing ratios to the samples collected at ground level. Some of the acetaldehyde in airborne data was likely formed at higher altitudes rather than being emitted directly from ground sources, as it is a common reaction product in the atmosphere.

An overlay of the acetaldehyde mixing ratios in the SJV is shown in Figure 5.16. Acetaldehyde mixing ratios were colored and binned by range, and they varied from < 0.25 ppb to about 4 ppb over various parts of the SJV. The height of the points also indicates acetaldehyde mixing ratio on a continuum. Additional points (e.g., black rings) were included showing bovine-containing areas.

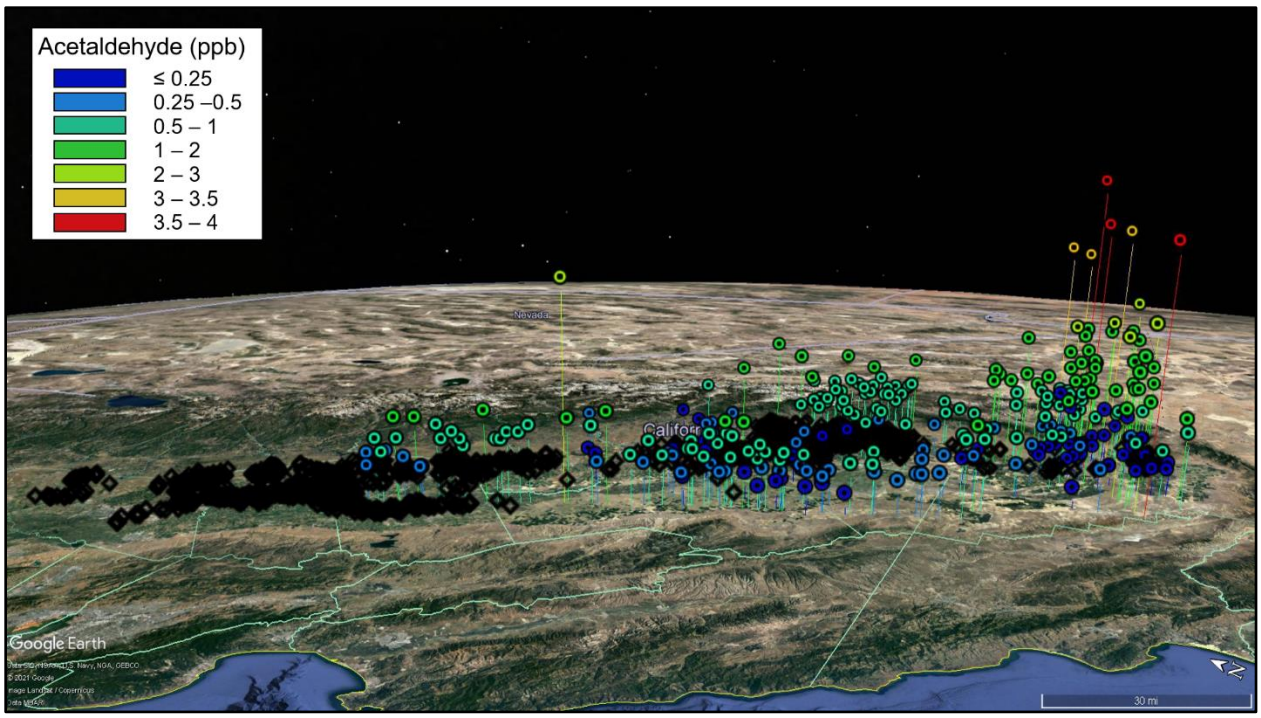


**Figure 5.16** Acetaldehyde mixing ratios during SARP flights from 2011, 2013, 2014, 2015, and 2017 below 3,000 feet pressure altitude. Mixing ratios are binned by range, which is indicated by color. The height of the points also indicates acetaldehyde mixing ratios. Black rings are bovine-containing areas, typically dairies, in the SJV.

Although all acetaldehyde mixing ratios were within the expected range of typical values for the SJV, there were some clear latitudinal and longitudinal trends. The most elevated samples were collected above Kern County, followed by Tulare County. Acetaldehyde was more elevated, in general, on the southeastern side of the SJV than on the western side of the SJV, likely because of the wind direction. It was expected that acetaldehyde's very short lifetime would make it more difficult to trace back to dairy farms. To try to determine the source of the acetaldehyde, methane was again used as a dairy tracer. Figure 5.17 shows the same aerial photograph as Figure 5.16, but with the height of the points given by the *methane* mixing ratio of each sample rather than acetaldehyde.

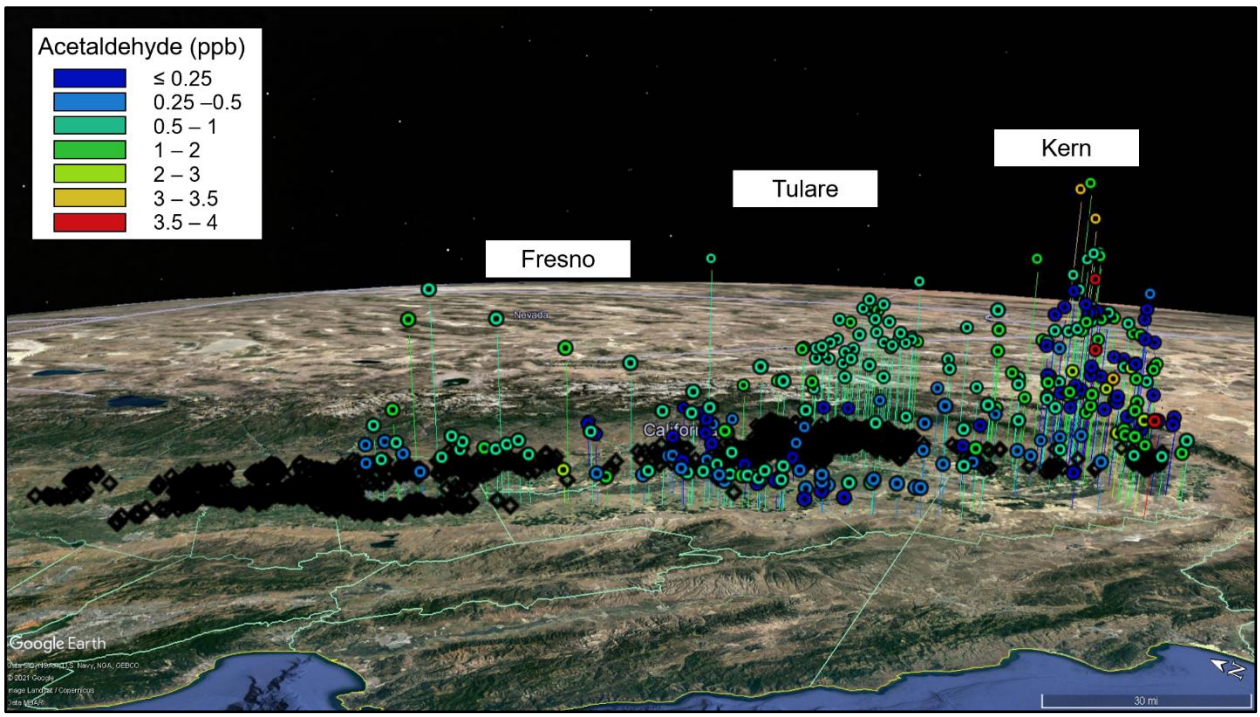


**Figure 5.17** Acetaldehyde mixing ratios during SARP flights from 2011, 2013, 2014, 2015, and 2017 below 3,000 feet pressure altitude. Mixing ratios are binned by range, which is indicated by color. The height of the points indicates methane mixing ratio. Black rings are bovine-containing areas, typically dairies, in the SJV. Three of the SJV counties are labelled for reference.

Some of the acetaldehyde points in the lower range (dark blue, ≤ 0.25 ppb) had elevated methane on the southeastern end of the SJV in Kern County, as marked by the increased height of the points. In Tulare County, slightly north of Kern County, methane and acetaldehyde seemed slightly more correlated (i.e., mid-range acetaldehyde from 0.5 – 2 ppb and mid-range methane point heights). Tulare County is a very productive dairy zone, and the closer proximity to Tulare as a large source of both acetaldehyde and methane resulted in this slightly better agreement in Figure 5.17. To further determine the relationship between methane and acetaldehyde, Figure 5.18 shows the correlation of the two gases over the SJV from the same SARP samples.

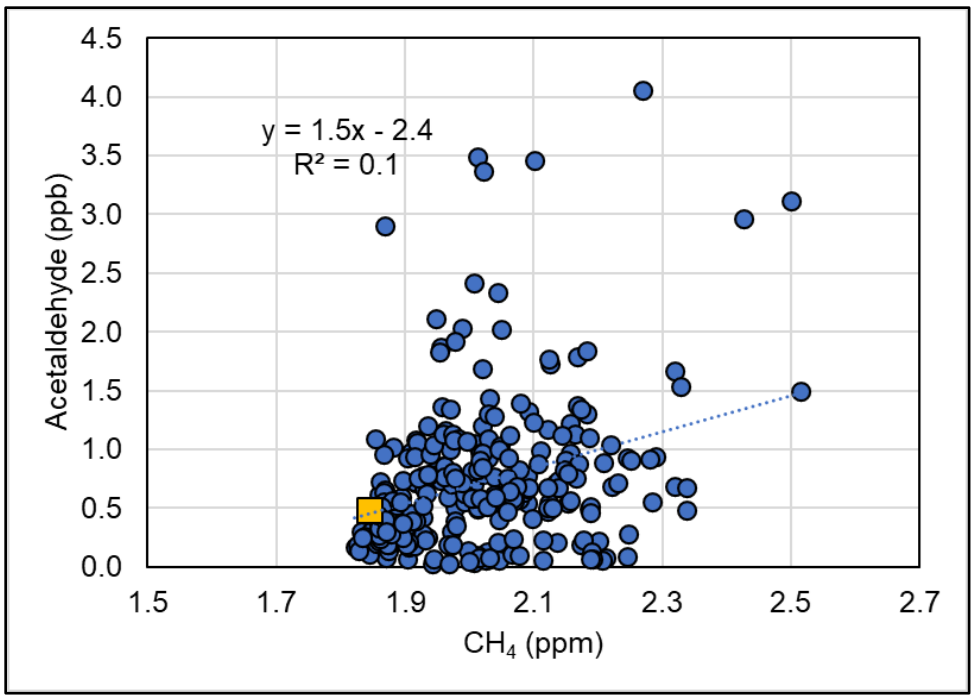


**Figure 5.18** Correlation of methane (ppm) and acetaldehyde (ppb) from SARP flights from 2011, 2013, 2014, 2015, and 2017 below 3,000 feet pressure altitude over the SJV. The yellow square corresponds to the average $CH_4$ and acetaldehyde at the dairy farm scaled down ten times.

Figure 5.18 also shows the ratio of the average $CH_4$ and acetaldehyde at the dairy farm scaled down by ten, given as a yellow square. Out of three oxygenates presented in this chapter, acetaldehyde had the weakest correlation with methane ($R^2$ = 0.1) over the SJV. It was already shown in this chapter that acetaldehyde was commonly found near the free stalls and manure management systems at the dairy farm. However, likely because of its short lifetime and variety of primary and secondary sources, it was not well correlated with methane over the entire SJV. The mixing ratios of acetaldehyde in the SARP samples above the SJV were within typical expected values (i.e., 0.1 – 4 ppb), however, this study still identified dairy farms as a source of acetaldehyde. Although it is not well-correlated with methane, acetaldehyde is still an important gas in the SJV because of its ozone formation potential and possible odor contribution, examined in more detail in Chapter 8.

## 5.4 Summary and Conclusion

The goal of this chapter was to determine sources of select oxygenates (ethanol, methanol, and acetaldehyde) and their respective mixing ratios so that their ozone generation potential and odor contribution could be determined in Chapter 8. Yang (2009) showed that silage produces a considerable amount of oxygenates at dairy farms. Although mixing ratios of oxygenates near silage were not as enhanced at the Visalia dairy farm in this study, silage and its different forms (e.g., as feed in free stalls, in cow breath, and during decomposition of organic matter as manure) still likely contributed. At the Orange County landfills, the oxygenates were likely a product of Stage II decomposition or surface-level evaporation. Oxygenates were not enhanced above the final cover material or even the intermediate cover, indicating that production is likely low underground and that the landfill engineering infrastructure successfully prevents rogue emissions.

During the dairy campaigns, methanol was highest near free stalls, lagoons, outdoor cows, and cow breath and had a mean and standard deviation of 52±61 ppb across all campaigns. At the Orange County landfills, methanol was lower at the closed sites, 4±1.8 ppb, but higher at the active sites, 86±270 ppb. Ethanol at the dairy farm had the largest mixing ratios overall, with a mean and standard deviation of 134±520 ppb. Ethanol was most prominent near the free stalls, cow breath, silage, and outdoor cows and had the highest mixing ratios of all three oxygenates. Ethanol mixing ratios were lower at the Orange County landfills. Ethanol had a mean and standard deviation of 3±7 ppb at closed landfills and 110±400 ppb at the active landfills. Lastly, acetaldehyde at the dairy farm was most prominent near the free stalls and lagoons, and acetaldehyde mixing ratios varied with a mean and standard deviation of 4.8±6.1 ppb. At the Orange County landfills, acetaldehyde was lower at the closed sites, 2.8±3.3 ppb. Acetaldehyde at active Orange County landfills had similar mixing ratios to the dairy farm with a mean and standard deviation of 4.5±8.8 ppb.

For the samples collected over the SJV (< 3,000 feet), methanol mixing ratios were the largest, with a mean and standard deviation of 3.2±1.7 ppb, followed by ethanol with a mean and standard deviation of 1.3±1.0 ppb, followed by acetaldehyde with a mean and standard deviation of 0.71±0.62 ppb. Methanol and ethanol were better correlated with methane over the SJV, while acetaldehyde was not well correlated. This is probably a result of their lifetimes— $\tau_{methane} >> \tau_{methanol} > \tau_{ethanol} > \tau_{acetaldehyde}$. The farther away the air travels from the source, the more that the short-lifetime gases would be depleted relative to methane or even longer-lifetime oxygenates. Methanol and ethanol at low altitudes (< 3,000 ft) above the SJV were roughly an order of magnitude smaller than at the dairy farm. This may imply that ground-level sources, including dairy farms, are responsible for methanol and ethanol emissions. Acetaldehyde was lower in the airborne data than at ground level. Some of the acetaldehyde in the airborne samples may have originated at dairy farms (or as secondary products of reactive dairy farm gases, like ethanol), but acetaldehyde is also generated from biomass burning and as a photochemical product of other atmospheric VOC reactions; therefore, it is unlikely that acetaldehyde above the SJV comes exclusively from dairy farms.

Methanol, ethanol, and acetaldehyde react relatively quickly in the atmosphere and can lead to secondary reactions, eventually creating ozone and smog, which can worsen the air pollution in the SJV, an area already famous for non-attainment, as well as for communities living near landfills. They also can contribute to odor at landfills and dairy farms. These consequences are discussed further in Chapter 8.

## 5.5 References


Adani, F., Tambone, F., & Gotti, A. (2004). Biostabilization of municipal solid waste. *Waste Management*, *24*(8), 775-783.

Allen, M. R., Braithwaite, A., & Hills, C. C. (1997). Trace organic compounds in landfill gas at seven UK waste disposal sites. *Environmental Science & Technology*, *31*(4), 1054-1061.

Apel, E. C., Calvert, J. G., Riemer, D., Pos, W., Zika, R., Kleindienst, T. E., ... & Starn, T. K. (1998). Measurements comparison of oxygenated volatile organic compounds at a rural site during the 1995 SOS Nashville Intensive. *Journal of Geophysical Research: Atmospheres*, *103*(D17), 22295-22316.

Blake, D. (1984). Increasing concentrations of atmospheric methane, 1979-1983 (Doctoral dissertation, Ph. D., thesis, University of California, Irvine).

Carter, W. P., Darnall, K. R., Graham, R. A., Winer, A. M., & Pitts, J. N. (1979). Reactions of C2 and C4. alpha-hydroxy radicals with oxygen. *Journal of Physical Chemistry*, *83*(18), 2305-2311.

Derwent, R. G., Jenkin, M. E., Passant, N. R., & Pilling, M. J. (2007). Reactivity-based strategies for photochemical ozone control in Europe. *Environmental science & policy*, *10*(5), 445-453.

Farrell, M., & Jones, D. L. (2009). Critical evaluation of municipal solid waste composting and potential compost markets. *Bioresource technology*, *100*(19), 4301-4310.

Fried, A., Sewell, S., Henry, B., Wert, B. P., Gilpin, T., & Drummond, J. R. (1997). Tunable diode laser absorption spectrometer for ground-based measurements of formaldehyde. *Journal of Geophysical Research: Atmospheres*, *102*(D5), 6253-6266.

Giess, P., A. Bush, and M. Dye. "Trace gas measurements in landfill gas from closed landfill sites." *International Journal of Environmental Studies 57.1 (1999)*: 65-77.

Goldan, P. D., Kuster, W. C., Fehsenfeld, F. C., & Montzka, S. A. (1995). Hydrocarbon measurements in the southeastern United States: The rural oxidants in the southern environment (ROSE) program 1990. *Journal of Geophysical Research: Atmospheres*, *100*(D12), 25945-25963.

Grosjean, D. (1997). Atmospheric chemistry of alcohols. *Journal of the Brazilian Chemical Society*, *8*(5), 433-442.

Grosjean, E., Grosjean, D., Fraser, M. P., & Cass, G. R. (1996). Air quality model evaluation data for organics. 2. C1− C14 carbonyls in Los Angeles air. *Environmental science & technology*, *30*(9), 2687-2703.

Hurst, C., Longhurst, P., Pollard, S., Smith, R., Jefferson, B., & Gronow, J. (2005). Assessment of municipal waste compost as a daily cover material for odour control at landfill sites. *Environmental pollution*, *135*(1), 171-177.

Jean-Blain, C., Durix, A., & Tranchant, B. (1992). Kinetics of ethanol metabolism in sheep.

Lee, Y. N., Zhou, X., & Hallock, K. (1995). Atmospheric carbonyl compounds at a rural southeastern United States site. *Journal of Geophysical Research: Atmospheres, 100*(D12), 25933-25944.

Morgan, M. E., & Pereira, R. L. (1962). Volatile constituents of grass and corn silage. II. Gas-entrained aroma. *Journal of Dairy Science, 45*(4), 467-471.

Nagata, Y., & Takeuchi, N. (2003). Measurement of odor threshold by triangle odor bag method. *Odor measurement review*, *118*, 118-127.

Riemer, D., Pos, W., Milne, P., Farmer, C., Zika, R., Apel, E., ... & Shepson, P. (1998). Observations of nonmethane hydrocarbons and oxygenated volatile organic compounds at a rural site in the southeastern United States. *Journal of Geophysical Research: Atmospheres*, *103*(D21), 28111-28128.

Seinfeld, J. H., & Pandis, S. N. (2016). *Atmospheric chemistry and physics: from air pollution to climate change*. John Wiley & Sons.

Wallington, T. J., & Kurylo, M. J. (1987). The gas phase reactions of hydroxyl radicals with a series of aliphatic alcohols over the temperature range 240–440 K. *International journal of chemical kinetics*, *19*(11), 1015-1023.

Yang, M. (2009). Characterization of VOC Emissions from Various Components of Dairy Farming and Their Effect on San Joaquin Valley Air Quality. (Doctoral dissertation, Ph. D., thesis, University of California, Irvine).

Young, P. J., & Parker, A. (1983). The identification and possible environmental impact of trace gases and vapours in landfill gas. *Waste Management & Research*, *1*(3), 213-226.

# 6. Dimethyl Sulfide and Carbonyl Sulfide

## 6.1 Background Mixing Ratios of Dimethyl Sulfide and Carbonyl Sulfide

As discussed in Chapter 2.2, the Rowland-Blake laboratory has measured DMS and OCS in remote coastal regions of California (34.5 °N – 40.0 °N) for years to determine “background” mixing ratios unpolluted by inland anthropogenic sources. Data containing OCS and DMS measurements from 2015 through 2018 on the California coastline were used in this study. As discussed in Chapter 3.3.7, OCS is typically found in ocean water and is abundant in the Pacific Ocean, so these coastal samples were ideal for measuring typical concentrations in air entering the state and eventually the SJV and Orange County. Like OCS, DMS is also created in the ocean. Although mixing ratios near the coast represent a “background” of the air entering the state, DMS was expected to be slightly enhanced at the coast. The number of samples used for the analysis in Chapter 6.1 are summarized in Table 6.1.

**Table 6.1** Number of samples used for OCS and DMS air analysis at the California coast (34.5 °N – 40.0 °N) at ground level from 2015 – 2018

| Compound | 2015 | 2016 | 2017 | 2018 | Total |
|---|---|---|---|---|---|
| OCS | 13 | 16 | 19 | 16 | **64** |
| DMS | 13 | 16 | 13 | 16 | **58** |

The OCS mixing ratios from sixty-four samples collected by the Rowland-Blake lab between 2015 and 2018 were used to determine background mixing ratios of OCS at the California coast (34.5 °N – 40.0 °N). To determine DMS background mixing ratios in the same geographical area, the DMS mixing ratios from fifty-eight samples were used. The DMS background determination used slightly fewer samples than the OCS background determination because some samples contained DMS < LOD. These were not used to determine DMS background.

An annual average of the median mixing ratios was calculated for each gas, with respective standard deviations. First, a median mixing ratio was determined for each seasonal campaign. Then, those medians were averaged to calculate a yearly mean. The median mixing ratios and standard deviations of OCS and DMS entering the California coast (34.5 °N – 40.0 °N)

and heading inland over time are shown in Figure 6.1. As dimethyl sulfide is expected to be higher near the coastline, Figure 6.1 represents an upper limit to the DMS background in the SJV.

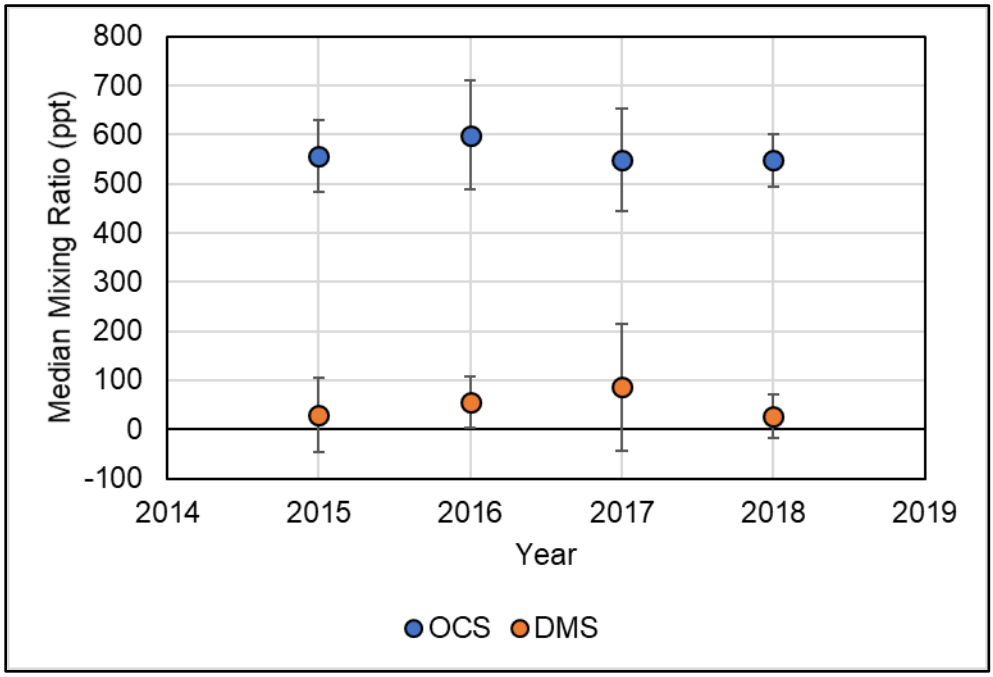


**Figure 6.1** OCS and DMS average median mixing ratios and standard deviations from samples collected on the remote California coast near the Pacific Ocean (34.5 °N – 40.0 °N) from 2015 to 2018.

The median mixing ratios for OCS did not fluctuate much over the years, and overall had an average median value of 560±24 ppt, which was only slightly higher than the global average (500 ppt) presented in Lennartz et al. (2017). This slightly elevated California average was likely a result of the additional sources in the Northern Hemisphere coupled with the heavy influence of the nearby Pacific Ocean on the samples used in this analysis. The average median mixing ratios for DMS in Figure 6.1 fluctuated a little bit more over the years: DMS mixing ratios in 2017 were nearly triple those in 2015. Dimethyl sulfide is more sensitive to fluctuating ocean conditions, particularly algal blooms. This could explain the higher mixing ratios in 2017, although the average median in all cases remained below 100 ppt. Overall, the average of the median mixing ratios for DMS for this time frame was 50±30 ppt. These “typical” values of OCS and DMS found at the California coastline were compared to OCS and DMS at the dairy site and at the Orange County

landfills to determine whether these inland sources may also contribute to the formation of these trace gases.

### 6.2 Carbonyl Sulfide and Dimethyl Sulfide at the Visalia Dairy Site

Carbonyl sulfide and dimethyl sulfide are traditionally considered “marine” gases that are prevalent near the ocean. Surprisingly, these gases were also found at the dairy site. There is not a lot of existing literature examining OCS emissions from dairy farms, and its sources are not fully understood. Most of the literature focuses on the oceans, wetlands, anoxic soils, and volcanoes as its main sources (Lennartz et al., 2017). Assuming the amount of OCS in the atmosphere is currently balanced, there remains an unaccounted source, as discussed in Chapter 3.3.7.

Median mixing ratios for OCS and DMS at the Visalia dairy site across all five campaigns (September 2018, March 2019, June 2019, September 2019, and January 2020) were determined. Figure 6.2 shows binned OCS mixing ratios for samples collected at the dairy farm across all campaigns. Carbonyl sulfide mixing ratios were binned into 8 different ranges. The height of the points above the dairy farm also indicates OCS mixing ratio. For the aerial figures of the dairy farm in this chapter (Figure 6.2 and Figure 6.3), the “Manure” category includes samples collected near the manure management system (lagoons, slurries, processing pit), flush water, and bedding; “Enteric” includes samples collected near the outdoor cows, in the free stalls, and from cow breath. “Silage” represents samples collected near the silage piles, while “Crops” represents samples collected downwind of the crops and upwind of the dairy. “Other” includes samples collected by the office, upwind, and downwind of the dairy.

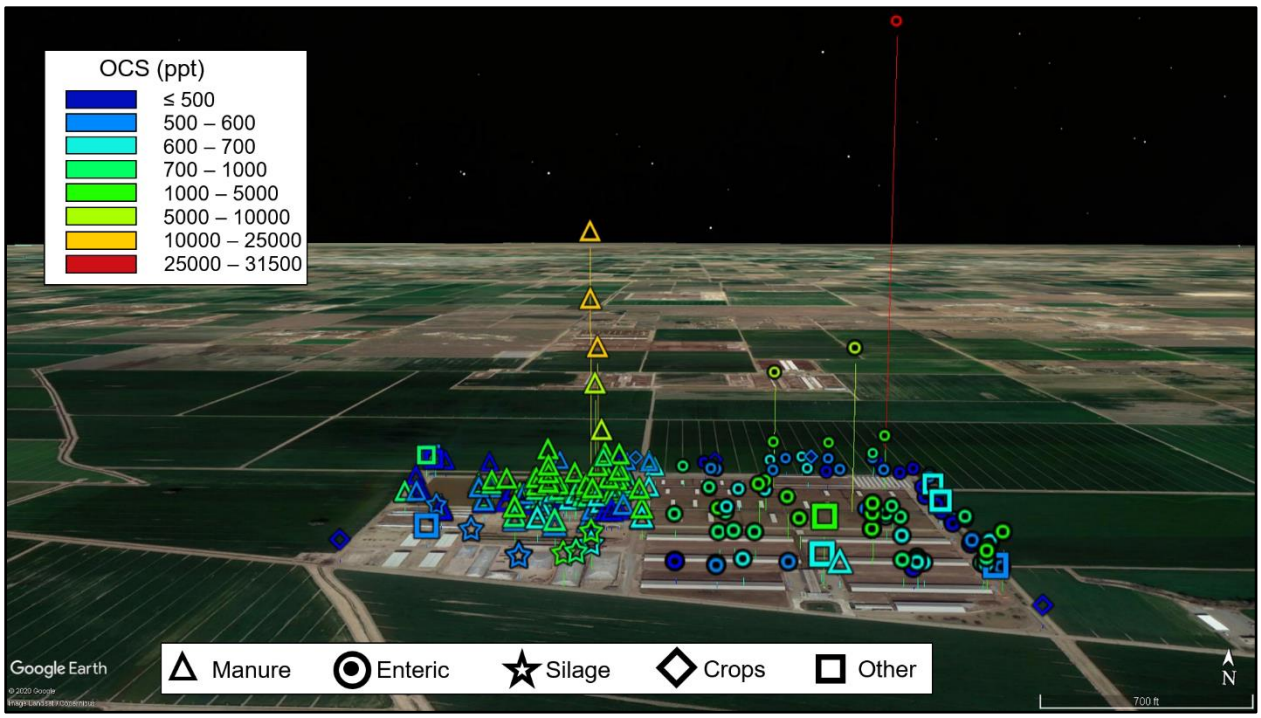


**Figure 6.2** Carbonyl sulfide (ppt) at the dairy farm binned by mixing ratio ranges and grouped by source. Height of the points also indicates mixing ratio of OCS. Typical wind direction was from the northwest.

Figure 6.2 shows that OCS was primarily elevated near the manure management systems and near the cows. Similarly, Figure 6.3 shows binned DMS mixing ratios for samples collected at the dairy farm across all campaigns. Dimethyl sulfide mixing ratios were binned into 8 different ranges, and the height of the points above the dairy farm also indicates the respective DMS mixing ratios.

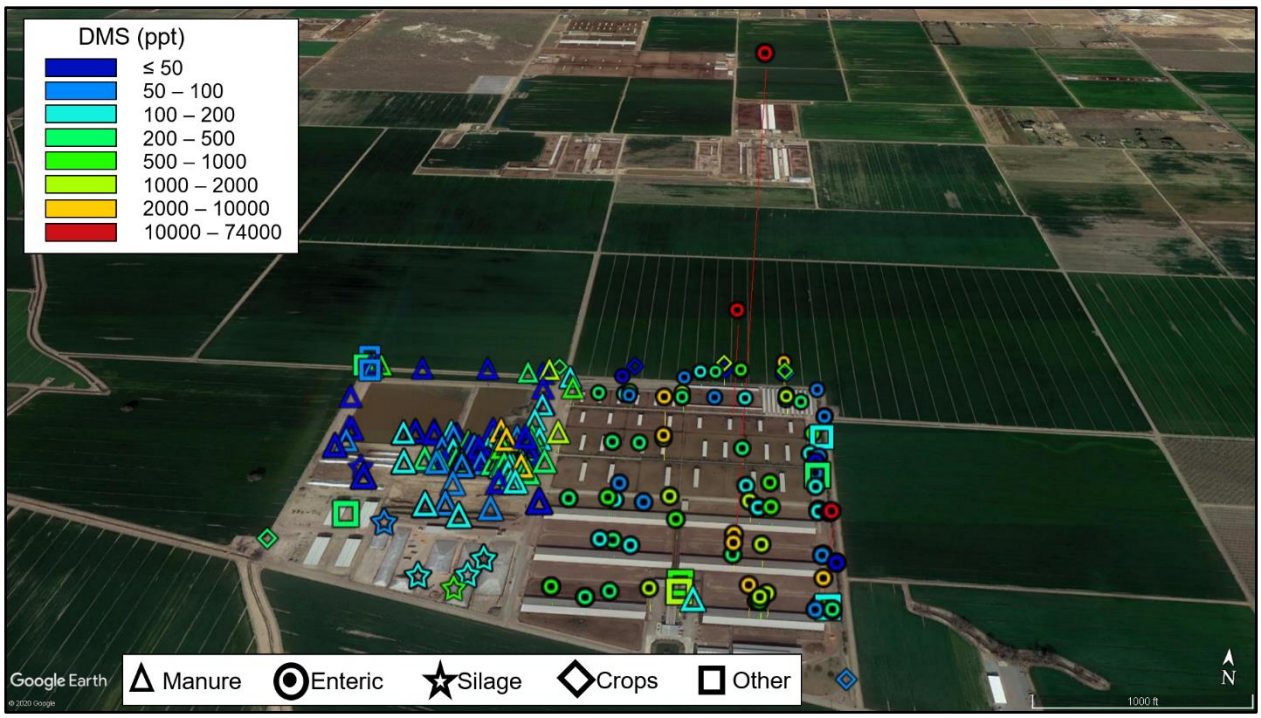


**Figure 6.3** Dimethyl sulfide (ppt) at the dairy farm binned by mixing ratio ranges and grouped by source. Height of the points also indicates mixing ratio of DMS. Typical wind direction was from the northwest.

Like OCS, DMS was also prevalent in various locations around the dairy. Dimethyl sulfide mixing ratios were highest near the cows outdoors and in the free stalls, with a handful of elevated samples near the slurries. Figure 6.4 shows the mixing ratios of OCS and DMS separated by location: crops, cows, bedding, silage, free stall, lagoon, and cow breath. Figure 6.4 also includes the average of the coastal median mixing ratios for OCS and DMS from Chapter 6.1. These were overlaid for comparison using blue and orange transparent bars marking 560±24 ppt and 50±30 ppt. The solid line in the middle of the transparent bars marks the middle of each of these ranges. The category of “Enteric” from Figure 6.3 was separated into the outdoor “Cows” (i.e., near dry cows and heifers), “Free Stall” (i.e., near milk cows), and “Cow Breath.” The “Lagoon” category in Figure 6.4 includes samples collected near the processing pit, lagoons, and slurry systems.

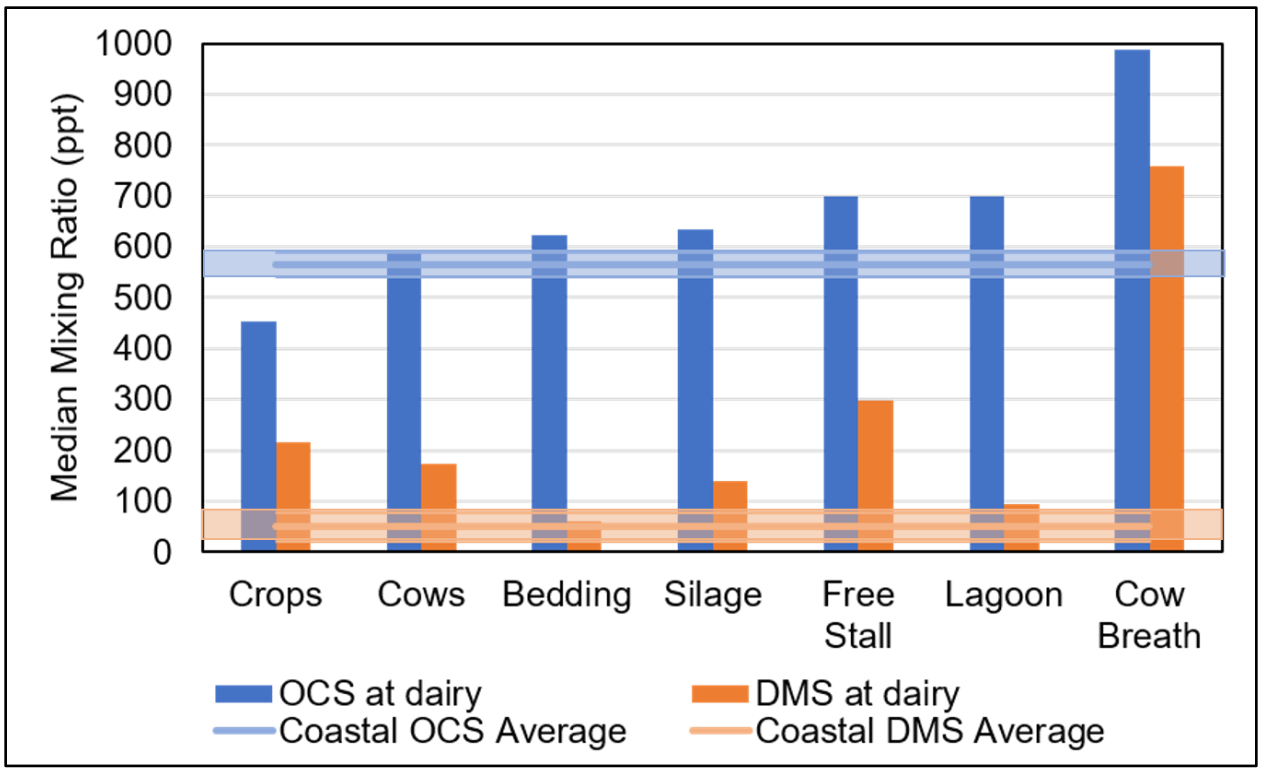


**Figure 6.4** OCS and DMS median mixing ratios at the dairy site across all five campaigns. The transparent bars indicate the average of the median mixing ratios for OCS and DMS along the California coastline from 2015 to 2018 (34.5 – 40.0 °N) as a range, 560±24 ppt OCS and 50±30 ppt DMS for comparison to the dairy samples.

As shown in Figure 6.4, the median mixing ratio for OCS near crops was much lower than the OCS mixing ratios near the coastline. This was the only location at the dairy at which median OCS was below the coastal range (560±24 ppt). This may reinforce the idea that OCS is destroyed via vegetative uptake (Montzka et al., 2007; Campbell et al. 2008; Campbell et al., 2017). The median mixing ratios of OCS near the outdoor cows, bedding, and silage areas were not elevated too much over the coastal range. However, OCS near the free stalls and lagoons was about 25% higher than OCS near the coastline. Median mixing ratios of OCS in dairy cow breath were even more elevated, about 75% higher than those found at the coastline. Surprisingly, it seemed likely that the cows themselves emit OCS through enteric fermentation, which would explain the high mixing ratios found in cow breath. Because cows are placed in free stalls to eat, their enteric emissions are often trapped within those areas. This could explain the

elevated OCS in the free stalls, while the cows outside of the free stalls had OCS mixing ratios closer to the coastline values. This could be a result of the different diets between the outdoor cows (i.e., dry cows and heifers) and the free stall cows (i.e., milk cows), or in the way the air becomes trapped and accumulates in the free stalls, not the outdoors. As the OCS from silage was much closer to background levels, it does not seem like that OCS is directly emitted in large quantities from the feed. Instead, the OCS seemed to be coming from the cows themselves. Lastly, lagoons are often highly anaerobic environments. Like the release of OCS from anoxic soil, it is possible that the wet, anaerobic lagoons can also produce OCS, which resulted in median OCS around 700 ppt near the manure management system, similar to the free stalls. The implications of OCS emissions from cow breath as well as manure management systems are examined later in Chapter 6.2.1.

Although DMS does not have as much mystery surrounding its global emissions as OCS does, it was similarly elevated in the cow breath and other areas around the dairy farm. As shown in Figure 6.4, the DMS mixing ratios for most areas at the dairy were above the coastal average of 50±30 ppt. The median DMS mixing ratio near bedding storage areas was within the range of the coastal average, while the median DMS mixing ratio near the lagoons was only slightly elevated above the DMS measured at the California coastline. All other areas were about double the coastal mixing ratio—or more. Samples collected near cow breath had the most enhanced DMS, with mixing ratios 1400% higher than those at the coastline, approaching 800 ppt. The second highest DMS mixing ratios were found in the free stalls, over 500% higher than DMS at the coastline, approaching 300 ppt. This means that DMS is likely enterically emitted in cow breath. Mixing ratios of DMS near crops, cows, silage, and lagoons were also elevated over the coastline DMS, but were not nearly as excessive as those found in cow breath and free stalls. Knowing that DMS is likely emitted from cow breath and free stalls, but not so much from the silage, could help to further explain the emissions found at other parts of the dairy.

For example, elevated DMS near the cows in outdoor corrals (i.e., dry cows and heifers) can be attributed to their breath as well, rather than to their feed. If the feed were one of the main DMS emitters, mixing ratios of DMS near the silage piles would likely be more elevated. However, as only the mixing ratios in the free stalls and cow breath were elevated, it is more likely coming from the cows themselves. The bedding and lagoon areas also did not show enhanced DMS, meaning that DMS is likely not produced much during bovine waste decomposition. While other sources at the dairy may exist, the enteric sources are perhaps the most important. Not much has been written about DMS at dairy farms, but emissions of DMS in cow breath is completely feasible because of the high protein diets fed to North American cows. Hobbs and Mottram (2000) showed that cows that consume high protein diets expel excess sulfur, often in the form of DMS in their breath. Hobbs et al. (1998) found that mixing ratios varied between 0 and 25 ppm DMS in undiluted cow breath, with the concentration depending on various factors. The diet of the cows at the dairy site for this study likely plays an important role in the emission of both DMS and OCS. The contribution of cow breath to emissions of DMS in the SJV is explored more in Chapter 6.2.2, while the contribution of cow breath to the OCS in the SJV is explored more below in Chapter 6.2.1.

### 6.2.1 Estimated Bovine Activity Contribution to the Missing OCS Source

It was quite interesting that OCS mixing ratios were elevated in cow breath and near the manure management system, as enteric and manure emissions from ruminant animals are not included in the global budget for OCS emissions. After the OCS global budget was recalculated to consider the effects of vegetative uptake more accurately, a missing source that is thought to contribute between 230 and 800 Gg S $yr^{-1}$ was revealed (Suntharalingam et al., 2008; Berry et al., 2013; Kuai et al., 2015; Glatthor et al., 2015; Lennartz et al., 2017). This missing source is currently assumed to entirely come out of the ocean. However, this study shows that dairy practices (i.e., cow breath and manure management) may provide additional sources that

previous estimates did not consider. In this study, the contribution of milk cow breath at the Visalia dairy and worldwide was considered, as well as possible contributions from wet manure management systems and other bovine industries.

To determine whether milk cow enteric emissions contributed to the missing OCS source, a ratio of $CH_4$ to OCS in the dairy cows' breath was first calculated for the samples collected from the dairy cows. Samples were collected less than six inches away from the mouth of the cows. Therefore, while the mixing ratios of $CH_4$ and OCS were expected to be diluted by the ambient air outside of the cow, the ratio of $CH_4$ to OCS was expected to stay the same. Minimum, median, and maximum ratios of $CH_4$ to OCS were determined for the milk cows' breath at the dairy farm by dividing the mixing ratio of $CH_4$ (ppm) by the mixing ratio of OCS (ppm). Table 6.2 shows temporal information, the mixing ratios of $CO_2$, $CH_4$, and OCS, the $CH_4$:OCS ratio, and relevant ratio labels for the samples (n = 7) representing milk cow (no dry cows or heifers) breath.

**Table 6.2** Date, time, mixing ratios of $CO_2$, $CH_4$, OCS, and the $CH_4$:OCS ratio and relevant labels for samples of milk cow breath (n = 7 samples) collected at the dairy farm

| Date | Time | $CO_2$ (ppm) | $CH_4$ (ppm) | OCS (ppt) | $CH_4$:OCS (ppm/ppm) | Label |
|---|---|---|---|---|---|---|
| 1/15/2020 | 11:23 | 2080 | 47.3 | 1482 | 31911 | |
| 1/15/2020 | 11:24 | 1333 | 76.1 | 1334 | 57044 | |
| 1/15/2020 | 11:25 | 504 | 53.5 | 614 | 87184 | High |
| 1/15/2020 | 11:26 | 1079 | 15.5 | 988 | 15681 | |
| 1/15/2020 | 11:27 | 731 | 29.0 | 834 | 34785 | Median |
| 1/15/2020 | 11:34 | 855 | 26.3 | 2646 | 9936 | |
| 1/15/2020 | 11:35 | 1408 | 12.6 | 2090 | 6011 | Low |

Table 6.2 shows that there was a variety of $CH_4$:OCS ratios, so a ratio representing the minimum, maximum, and median were selected. Then, combining these ratios with the milk cow enteric emissions factor developed for the dairy in Chapter 4.2.2 using the EPA's Tier 2 methodology, 134 kg $CH_4$ $head^{-1}$ $yr^{-1}$, possible OCS emissions were calculated for the Visalia dairy farm and for dairy farms in the SJV. This estimate included only milk cows and not additional cattle (e.g., beef cows, bulls, calves, growing steers/heifers, or feedlot cattle).

There was quite a variety of $CH_4$ to OCS ratios, likely a result of the variability of emissions during rumination. Hobbs et al. (1998) showed that for DMS, mixing ratios in cow breath varied from 0 – 25 ppm. The same likelihood for variation is assumed to be true for OCS as well. Emission factors (EF) of OCS was calculated using the low, median, and high $CH_4$ to OCS ratios from Table 6.2 and the enteric methane EF derived in Chapter 4.2.2 (134 kg $CH_4$ $head^{-1}$ $yr^{-1}$). These EFs were used with the various $CH_4$:OCS ratios to determine the amount of OCS that would be emitted annually, which was then converted into an amount of sulfur emitted per year, which could then be directly compared to the missing sulfur source, 230 – 800 Gg S $yr^{-1}$. Table 6.3 shows these OCS EFs organized by the ratio of $CH_4$ to OCS. These OCS EFs were then used to calculate the total sulfur emitted by the dairy, the SJV and the country. These are also shown in Table 6.3.

**Table 6.3** Carbonyl sulfide emission factors and sulfur released from milk cows at the dairy farm, SJV, and nation using the methane emission factor of 134 kg $CH_4$ $head^{-1}$ $yr^{-1}$ derived from EPA Tier 2 methodology for milk cows in North America calculated for low, median, and high ratios of $CH_4$ to OCS

| Ratio | $CH_4$:OCS | Emission Factor (kg OCS $hd^{-1}$ $yr^{-1}$) | Total S (kg/yr) | | |
|---|---|---|---|---|---|
| | | | Visalia Dairy | All SJV | U.S.A. |
| Low | 6011 | 0.0835 | 500 | 236,000 | 1,473,000 |
| Median | 34785 | 0.0144 | 80 | 41,000 | 255,000 |
| High | 87184 | 0.00575 | 30 | 16,000 | 102,000 |

Quite a range of sulfur could be emitted at the dairy site in Visalia, from 30 to 500 kg S per year. When this was extrapolated to the entire SJV, between 16,000 and 236,000 kg S per year could be emitted by *just milk cows* in the SJV. When this was extrapolated to the entire country, between 102,000 and 1,473,000 kg S could be emitted annually from milk cows breathing out OCS. These calculations do not include the millions of additional non-milk cattle (e.g., beef cows, bulls, calves, growing steers/heifers, or feedlot cattle).

Additional calculations were performed to determine the OCS contribution from dairy cows at dairy farms around the world using a range of other emission factors representative of different regions. The IPCC (Eggleston et al., 2006) recommends different Tier 1 estimates for dairy cows

in parts of the world other than North America based on the typical dairy practices of those regions, cattle productivity, typical feed, and average body weight. These additional regions included in the IPCC report were Western Europe, Eastern Europe, Oceania, Latin America, Asia, Africa and the Middle East, and the Indian Subcontinent. The IPCC enteric emission factors for dairy and beef cattle in these regions are given in Table 6.4.

**Table 6.4** IPCC Tier 1 enteric emission factors (kg $CH_4$ $head^{-1}$ $yr^{-1}$) for dairy cows and other cattle in regions around the world. Adapted from Eggleston et al. (2006)

| Region | Emission Factor (kg $CH_4$ $head^{-1}$ $yr^{-1}$) | |
|---|---|---|
| | Dairy Cow | Other Cattle |
| North America | 128 | 53 |
| Western Europe | 117 | 57 |
| Eastern Europe | 99 | 58 |
| Oceania | 100 | 60 |
| Latin America | 72 | 56 |
| Asia | 68 | 47 |
| Africa & Middle East | 46 | 31 |
| Indian Subcontinent | 58 | 27 |

The lowest IPCC Tier 1 emission factor for enteric methane from dairy cows globally in Table 6.4 is 46 kg $CH_4$ $head^{-1}$ $yr^{-1}$ for African and Middle Eastern dairy cows, while North America has the highest EF, 128 kg $CH_4$ $head^{-1}$ $yr^{-1}$. In all regions, other cattle emit less methane than dairy cows likely because of their size and different feed. It is outside the scope of this project to count the cows in different categories for all countries around the world. However, a range of possible OCS emissions was estimated using the various $CH_4$ to OCS ratios and either the lowest methane emission factor (46 kg $CH_4$ $head^{-1}$ $yr^{-1}$) or the highest methane emission factor (128 kg $CH_4$ $head^{-1}$ $yr^{-1}$) presented in Table 6.4. Actual OCS emissions from dairy cows are assumed to be within this range. For all calculations, it was assumed that cows in other areas of the world would emit a similar range of ratios of $CH_4$ to OCS as the cows at the Visalia dairy farm. This estimate only includes the OCS sulfur contributions from dairy cows, not other types of cattle or ruminant animals. These were added to the calculations done for the United States of America (shown in Table 6.3), which used the calculated enteric EF of 134 kg $CH_4$ $head^{-1}$ $yr^{-1}$ derived from this study.

The same low, median, and high $CH_4$:OCS ratios presented in Table 6.3 were combined with the lowest and highest methane EFs in Table 6.4. This calculation yield gigagrams of sulfur emitted annually for cows worldwide. These results are shown in Table 6.5.

**Table 6.5** Sulfur emissions from dairy cows worldwide using the low $CH_4$ emission factor (EF) of 46 kg $CH_4$ $head^{-1}$ $yr^{-1}$ and high emission factor of 128 kg $CH_4$ $head^{-1}$ $yr^{-1}$ for non-U.S. dairy cows. All calculations assumed an emission factor of 134 kg $CH_4$ $head^{-1}$ $yr^{-1}$ for U.S. dairy cows as determined by this study

| Ratio | $CH_4$:OCS | Worldwide EF = 46 kg $CH_4$ $head^{-1}$ $yr^{-1}$ | | Worldwide EF = 128 kg $CH_4$ $head^{-1}$ $yr^{-1}$ | |
|---|---|---|---|---|---|
| | | Emissions (no U.S.A.) (Gg S/yr) | Emissions (with U.S.A.) (Gg S/yr) | Emissions (no U.S.A.) (Gg S/yr) | Emissions (with U.S.A.) (Gg S/yr) |
| Low | 6011 | 13.7 | 15.1 | 38.1 | 39.5 |
| Median | 34785 | 2.4 | 2.6 | 6.6 | 6.8 |
| High | 87184 | 0.9 | 1.0 | 2.6 | 2.7 |

Just the cows at a single dairy farm alone do not emit a large amount of sulfur in their breath. However, on the worldwide scale, which includes at least 264 million milk cows, the OCS contribution from dairy cow breath becomes quite important. Even if one assumes that all the dairy farms in the world operate similar to Africa and the Middle East (therefore making the 46 kg $CH_4$ $head^{-1}$ $yr^{-1}$ emission factor appropriate), which would be quite an underestimate, then worldwide dairy farms would emit between 2 – 6% of the missing OCS source (230 to 800 Gg S/yr) at the low $CH_4$:OCS ratio.

If, on the other hand, one assumes that all the dairy farms in the world operate similar to North America (meaning that using a methane EF of 128 kg $CH_4$ $head^{-1}$ $yr^{-1}$ is appropriate), enteric emissions from milk cows could account for 5 – 17% of the missing OCS source at the low $CH_4$:OCS ratio. Because all dairy farms worldwide have EFs between 46 and 128 kg $CH_4$ $head^{-1}$ $yr^{-1}$, dairy farms worldwide would account for 2 – 17% of the missing OCS source at the low $CH_4$:OCS ratio overall. This contribution would become even greater if emissions from other types of cattle were included, even at the lower “Other Cattle” methane EFs presented in Table 6.4. This is explored more below.

If one assumes that all other cattle emit methane at the median EF of Table 6.4, or 55 kg $CH_4$ $hd^{-1}$ $yr^{-1}$ and that the $CH_4$ to OCS ratios for these cattle are similar to the ratios for dairy cows, one can do a similar calculation at the low, median, and high $CH_4$:OCS ratios to determine the possible contribution of cattle to the total emissions of OCS worldwide. The California Department of Food and Agriculture (CDFA) Agricultural Statistics review gives the total number of other cattle in California as 5.2 million head (CDFA, 2019b), and United States Department of Agriculture Foreign Agricultural Service estimates that the world contains 987.51 million head of cattle in 2020 (USDA, 2021). Using these cattle counts, the ruminant enteric contribution of non-milk cattle to the global sulfur budget was calculated at the low, median, and high $CH_4$:OCS ratios for cattle in the SJV and worldwide. Table 6.6 shows the result of this calculation.

**Table 6.6** The estimated emissions of sulfur from other cattle in California and around the world, given in Gg S/yr at low, median, and high $CH_4$:OCS ratios found in cow breath using an EF = 55 kg $CH_4$/yr, the median value for worldwide emission factors for Other Cattle

| Ratio | $CH_4$:OCS | Gg S/yr in CA | Gg S/yr worldwide |
|---|---|---|---|
| Low | 6011 | 0.095 | 28.2 |
| Median | 34785 | 0.016 | 4.9 |
| High | 87184 | 0.007 | 1.9 |

Additionally, the amount of OCS that could come from wet manure management systems was also estimated for the state and worldwide. It is important to point out that not every part of the world uses wet manure management systems to store their manure; this calculation is merely an exploration. After reviewing 38 field studies at dairies in North America and Europe, Owen and Silver (2015) determined that lagoons and slurries emit 368±193 kg $CH_4$ $hd^{-1}$ $yr^{-1}$ and 101±47 kg $CH_4$ $hd^{-1}$ $yr^{-1}$ on average. Calculating the average of these emission factors indicates that a wet manure management system, in general, emits 235±199 kg $CH_4$ $hd^{-1}$ $yr^{-1}$. Using the lagoon and slurry data (n = 112 samples) from this study (as shown in Table 6.7), the median $CH_4$:OCS ratio using $CH_4$ = 4.15 ppm and OCS = 378 ppb was $CH_4$:OCS = 10989.

**Table 6.7** The date, time, mixing ratios of $CH_4$ and OCS, and the $CH_4$:OCS ratio from one hundred twelve samples collected near the wet manure management system (i.e., lagoons and slurries)

| Date | Time | $CH_4$ | OCS | $CH_4$:OCS |
|---|---|---|---|---|
| 9/19/2018 | 12:52 | 38.3 | 1139 | 33662 |
| 9/19/2018 | 12:57 | 29.6 | 1225 | 24196 |
| 9/19/2018 | 13:21 | 17.6 | 1036 | 17020 |
| 9/19/2018 | 13:35 | 2.35 | 524 | 4489 |
| 9/19/2018 | 13:47 | 3.49 | 310 | 11242 |
| 9/19/2018 | 13:59 | 5.54 | 451 | 12290 |
| 9/19/2018 | 14:12 | 6.43 | 383 | 16789 |
| 9/19/2018 | 14:26 | 5.24 | 692 | 7569 |
| 9/19/2018 | 14:35 | 2.47 | 314 | 7857 |
| 9/19/2018 | 14:38 | 2.69 | 268 | 10030 |
| 9/19/2018 | 14:47 | 2.64 | 308 | 8581 |
| 9/19/2018 | 14:51 | 2.29 | 415 | 5523 |
| 9/19/2018 | 15:00 | 2.16 | 357 | 6036 |
| 9/19/2018 | 15:09 | 2.22 | 270 | 8226 |
| 9/19/2018 | 15:14 | 2.12 | 354 | 5983 |
| 9/19/2018 | 15:17 | 2.15 | 586 | 3674 |
| 9/19/2018 | 15:21 | 2.15 | 797 | 2700 |
| 9/19/2018 | 15:28 | 2.15 | 342 | 6295 |
| 9/19/2018 | 15:30 | 2.06 | 518 | 3981 |
| 9/19/2018 | 15:32 | 2.09 | 339 | 6165 |
| 9/19/2018 | 15:34 | 4.15 | 378 | 10989 |
| 9/19/2018 | 15:36 | 4.93 | 776 | 6348 |
| 9/19/2018 | 15:38 | 3.24 | 447 | 7257 |
| 9/19/2018 | 15:41 | 2.16 | 752 | 2874 |
| 9/19/2018 | 15:42 | 8.13 | 458 | 17758 |
| 9/19/2018 | 15:43 | 19.6 | 1933 | 10163 |
| 9/19/2018 | 15:45 | 9.49 | 523 | 18153 |
| 9/19/2018 | 15:50 | 23.9 | 3506 | 6817 |
| 9/19/2018 | 15:52 | 41.5 | 3638 | 11399 |
| 9/19/2018 | 15:56 | 7.65 | 1024 | 7470 |
| 9/19/2018 | 15:59 | 3.20 | 591 | 5420 |
| 9/19/2018 | 16:00 | 3.43 | 611 | 5614 |
| 9/19/2018 | 16:01 | 5.28 | 1520 | 3475 |
| 9/19/2018 | 16:03 | 18.3 | 377 | 48469 |
| 9/19/2018 | 16:17 | 6.69 | 308 | 21714 |
| 9/19/2018 | 17:15 | 5.61 | 327 | 17162 |
| 3/25/2019 | 12:19 | 2.30 | 443 | 5185 |
| 3/25/2019 | 12:35 | 2.34 | 483 | 4849 |
| 3/25/2019 | 12:49 | 16.8 | 692 | 24319 |
| 3/25/2019 | 12:57 | 21.8 | 703 | 31027 |
| 3/25/2019 | 13:09 | 18.3 | 617 | 29666 |
| 3/25/2019 | 13:19 | 18.4 | 610 | 30157 |
| 3/25/2019 | 13:30 | 19.2 | 660 | 29152 |

| | | | | |
|---|---|---|---|---|
| 3/25/2019 | 13:37 | 56.9 | 810 | 70233 |
| 3/25/2019 | 13:41 | 38.0 | 758 | 50181 |
| 3/25/2019 | 13:51 | 53.3 | 952 | 56020 |
| 3/25/2019 | 14:21 | 12.6 | 619 | 20313 |
| 3/25/2019 | 14:34 | 7.74 | 553 | 13995 |
| 3/25/2019 | 14:44 | 4.25 | 539 | 7892 |
| 3/25/2019 | 14:54 | 14.5 | 605 | 23950 |
| 3/25/2019 | 15:04 | 5.11 | 604 | 8452 |
| 3/25/2019 | 15:16 | 2.42 | 505 | 4790 |
| 3/25/2019 | 15:28 | 10.6 | 552 | 19120 |
| 3/25/2019 | 15:40 | 48.1 | 894 | 53833 |
| 3/25/2019 | 17:53 | 29.9 | 651 | 45888 |
| 3/25/2019 | 18:05 | 35.7 | 661 | 54047 |
| 3/25/2019 | 18:16 | 53.0 | 806 | 65805 |
| 3/25/2019 | 18:26 | 23.8 | 629 | 37843 |
| 3/25/2019 | 18:37 | 17.1 | 546 | 31251 |
| 3/25/2019 | 18:48 | 6.36 | 545 | 11662 |
| 3/25/2019 | 19:08 | 33.5 | 771 | 43486 |
| 6/26/2019 | 12:48 | 2.11 | 510 | 4137 |
| 6/26/2019 | 13:30 | 13.2 | 1238 | 10670 |
| 6/26/2019 | 14:58 | 34.1 | 1427 | 23868 |
| 6/26/2019 | 15:02 | 27.9 | 1240 | 22500 |
| 6/26/2019 | 15:07 | 2.25 | 1111 | 2025 |
| 6/26/2019 | 15:11 | 14.0 | 741 | 18920 |
| 6/26/2019 | 15:13 | 2.63 | 676 | 3891 |
| 6/26/2019 | 15:17 | 6.45 | 530 | 12170 |
| 6/26/2019 | 15:19 | 4.74 | 504 | 9405 |
| 6/27/2019 | 9:49 | 2.59 | 721 | 3592 |
| 6/27/2019 | 9:56 | 4.26 | 749 | 5688 |
| 6/27/2019 | 10:04 | 12.1 | 777 | 15560 |
| 6/27/2019 | 10:11 | 8.09 | 695 | 11640 |
| 6/27/2019 | 10:16 | 39.5 | 929 | 42476 |
| 9/10/2019 | 12:50 | 5.69 | 621 | 9155 |
| 9/10/2019 | 14:22 | 2.70 | 502 | 5378 |
| 9/10/2019 | 14:32 | 3.45 | 695 | 4968 |
| 9/10/2019 | 14:52 | 3.29 | 572 | 5745 |
| 9/10/2019 | 14:57 | 2.33 | 807 | 2892 |
| 9/10/2019 | 15:03 | 2.06 | 579 | 3549 |
| 9/10/2019 | 15:10 | 11.3 | 1237 | 9141 |
| 9/10/2019 | 15:15 | 10.6 | 1096 | 9693 |
| 9/10/2019 | 15:20 | 5.16 | 887 | 5813 |
| 9/10/2019 | 15:27 | 5.38 | 825 | 6526 |
| 9/10/2019 | 15:32 | 6.91 | 818 | 8443 |

| | | | | |
|---|---|---|---|---|
| 9/10/2019 | 15:37 | 71.6 | 5113 | 14002 |
| 9/10/2019 | 15:44 | 25.8 | 2389 | 10792 |
| 9/10/2019 | 15:49 | 28.8 | 1951 | 14754 |
| 9/10/2019 | 15:54 | 34.4 | 2881 | 11933 |
| 9/11/2019 | 16:35 | 3.15 | 1026 | 3072 |
| 9/11/2019 | 16:38 | 3.55 | 865 | 4103 |
| 9/11/2019 | 16:42 | 4.16 | 580 | 7172 |
| 9/11/2019 | 16:55 | 5.59 | 1185 | 4714 |
| 9/11/2019 | 17:00 | 8.43 | 1684 | 5005 |
| 9/11/2019 | 17:05 | 3.28 | 901 | 3637 |
| 9/11/2019 | 17:40 | 18.3 | 1762 | 10376 |
| 9/11/2019 | 17:45 | 8.72 | 1034 | 8428 |
| 9/11/2019 | 17:57 | 72.5 | 2611 | 27760 |
| 9/11/2019 | 18:02 | 120 | 3635 | 33109 |
| 9/11/2019 | 18:12 | 82.9 | 3852 | 21531 |
| 9/11/2019 | 18:17 | 28.3 | 1726 | 16379 |
| 1/14/2020 | 16:41 | 135 | 7999 | 16850 |
| 1/14/2020 | 16:47 | 23.3 | 1984 | 11758 |
| 1/14/2020 | 16:54 | 3.16 | 1235 | 2561 |
| 1/14/2020 | 17:00 | 13.4 | 923 | 14477 |
| 1/15/2020 | 16:15 | 408 | 649 | 628391 |
| 1/15/2020 | 16:19 | 266 | 17321 | 15365 |
| 1/15/2020 | 16:23 | 194 | 13121 | 14795 |
| 1/15/2020 | 16:31 | 112 | 2598 | 43197 |
| 1/15/2020 | 16:35 | 183 | 650 | 282217 |
| 1/15/2020 | 16:37 | 141 | 10149 | 13897 |

Combining the median ratio ($CH_4$:OCS = 10989) with the average EF adapted from Owen and Silver (2015), wet manure management systems would be expected to emit 0.080±0.034 kg OCS $hd^{-1}$ $yr^{-1}$. Assuming that the worldwide dairy industry behaves similarly to North America, the total Gg S contributed by OCS from lagoon and slurry emissions was calculated for the SJV and worldwide. This estimation only included milk cow head counts, as other cattle are not as often managed by wet manure management practices. With 1,505,000 milk cows in the SJV and an EF of 0.080±0.034 kg OCS $hd^{-1}$ $yr^{-1}$, the SJV would emit 0.064±0.027 Gg S/yr from wet manure management practices. With 264 million milk cows worldwide and an EF of 0.080 kg OCS $hd^{-1}$ $yr^{-1}$, worldwide OCS emissions contribute 11.3±4.8 Gg S/yr from wet manure management systems.

Overall, the sulfur contribution from milk cows, other cattle, and wet manure management systems may account for some of the missing OCS source. Table 6.8 shows the total Gg S/yr from all cattle and dairy cows worldwide, lagoons and slurries, and the percentage toward the low and high estimates of the missing source. This calculation assumes that the median for the $CH_4$:OCS ratio in samples collected near lagoons and slurries remains constant and uses the average contribution of 11.3 Gg S/yr from those systems.

**Table 6.8** Total sulfur contribution of cattle, dairy cows, and manure management systems worldwide to the missing OCS source (230 – 800 Gg S/yr)

| Ratio | Total Cattle and Milk Cows Worldwide (Gg S/yr) | Lagoons and Slurries (Gg S/yr) | Total (Gg S/yr) | % Low Missing Source (% of 230 Gg S/yr) | % High Missing Source (% of 800 Gg S/yr) |
|---|---|---|---|---|---|
| Low | 67.8 | 11.3 | 79 | 34 | 10 |
| Median | 11.7 | 11.3 | 23 | 10 | 3 |
| High | 4.6 | 11.3 | 16 | 7 | 2 |

Overall, even without the contribution from wet manure management systems, cattle and dairy cows worldwide could contribute between 8 and 29% of the total missing OCS source (between 230 and 800 Gg S/yr) at the low $CH_4$:OCS. When the contribution from wet manure management is factored in, this increases to 10 to 34% of the total missing source that could possibly be coming from bovine-related activities (i.e., raising cattle and cows, managing manure). This is a non-trivial amount that should be looked at in further detail in the future.

Aydin et al. (2014) noted that Antarctic ice core samples dating back to the last 8,000 years of the Holocene show an overall increase in OCS as early as 5,000 years ago. Campbell et al. (2015) suggests that the most recent OCS increase may be the result in changes of vegetative uptake efficiencies, especially as $CO_2$ continues to increase. Campbell et al. (2015) also credits changes in industrial practices, particularly rayon and coal. Previous literature expects the missing OCS source to come from the ocean (Suntharalingam et al., 2008; Berry et al., 2013; Kuai et al., 2015; Glatthor et al., 2015). However, it may be possible that the dairy and cattle industries could be at least a little bit responsible for this missing source. Even if these bovine-

related emissions do not account for the entirety of the missing OCS source, they should be included in future OCS inventories and more work should be done to measure OCS fluxes at dairy farms and other bovine-containing areas.

### 6.2.2 Dimethyl Sulfide from Milk Cows and Implications for Aerosol Formation

Dimethyl sulfide is an important climate gas because of its implications for particle and cloud chemistry. It has been shown that DMS can create cloud condensation nuclei, which can potentially increase the planetary albedo, which may decrease temperature (Charlson et al., 1987). The photooxidation pathway is complicated, but it has been shown that the major products include sulfuric acid and methanesulfonic acid (Bardouki et al., 2003; Barone et al., 1995; Gaston et al., 2010; Lukács et al., 2009). Because of its implications as a climate gas, it is important to understand all sources of DMS, not just the known oceanic ones.

For this study, Figure 6.4 in Chapter 6.2 showed that DMS mixing ratios were enhanced in samples collected near the cow breath. To determine the amount of DMS that could be created by milk cows in the SJV, similar calculations to those in Chapter 6.2.1 were performed. Similar to Chapter 6.2.1, a low, median, and high $CH_4$:DMS ratio was first determined for milk cow breath samples and then combined with the enteric methane EF calculated for the dairy in Chapter 4.2.2, 134 kg $CH_4$ $head^{-1}$ $yr^{-1}$. Then, total DMS emissions at the dairy and across the SJV were calculated. This has implications for aerosol formation, which is discussed more in Chapter 8.3.1. Table 6.9 shows the temporal information and the mixing ratios of $CH_4$ and DMS. Table 6.9 also labels the low, median, and high $CH_4$:DMS ratios that were used for the calculation. Methane to DMS ratios were calculated by dividing the mixing ratio of $CH_4$ (ppm) by the mixing ratio of DMS (ppm).

**Table 6.9** Logistical information, $CH_4$ and DMS mixing ratios, $CH_4$:DMS ratio, and ratio label for milk cow breath samples at the Visalia dairy farm

| Date | Time | $CH_4$ (ppm) | DMS (ppt) | $CH_4$:DMS (ppm/ppm) | Label |
|---|---|---|---|---|---|
| 1/15/2020 | 11:23 | 47.3 | 627 | 75426 | |
| 1/15/2020 | 11:24 | 76.1 | 17080 | 4455 | |
| 1/15/2020 | 11:25 | 53.5 | 626 | 85513 | |
| 1/15/2020 | 11:26 | 15.5 | 347 | 44648 | |
| 1/15/2020 | 11:27 | 29.0 | 5410 | 5360 | |
| 1/15/2020 | 11:34 | 26.3 | 2548 | 10319 | |
| 1/15/2020 | 11:35 | 12.6 | 73890 | 170 | Low |
| 1/15/2020 | 11:36 | 56.3 | 4150 | 13576 | Median |
| 1/15/2020 | 11:39 | 52.9 | 293 | 180594 | High |

A wide range of mixing ratios of both $CH_4$ and DMS were found at the dairy site. The low $CH_4$:DMS ratio, 170, used $CH_4$ = 12.6 ppm and DMS = 73890 ppt; the median $CH_4$:DMS ratio, 13756, used $CH_4$ = 56.3 ppm and DMS = 4150 ppt; the high $CH_4$:DMS ratio, 180594, used $CH_4$ = 52.9 ppm and DMS = 293 ppt. After these ratios were calculated and selected, they were compared to the enteric EF for methane emissions from milk cows, 134 kg $CH_4$ $hd^{-1}$ $yr^{-1}$, to determine EFs for the enteric release of DMS. Then, using the DMS EFs, the amount of DMS released from milk cows at the Visalia dairy site and across the entire SJV was determined for each $CH_4$:DMS ratio. The dairy contained, on average, 3106 milk cows, while the SJV contains 1,505,000 milk cows. Table 6.10 shows the milk cow EF for DMS and the production of DMS from the dairy and SJV at the low, median, and high $CH_4$:DMS ratios.

**Table 6.10** Milk cow EFs and DMS production at the dairy and SJV at low, median, and high $CH_4$:DMS ratios

| Ratio | Milk Cow EF (kg $CH_4$ $hd^{-1}$ $yr^{-1}$) | Milk Cow EF (kg DMS $hd^{-1}$ $yr^{-1}$) | Visalia Dairy (kg DMS $yr^{-1}$) | SJV (kg DMS $yr^{-1}$) |
|---|---|---|---|---|
| Low | 134 | 3.1 | 9700 | 4592700 |
| Median | 134 | 0.038 | 120 | 57500 |
| High | 134 | 0.0091 | 30 | 13700 |

According to Table 6.10, the milk cows at the Visalia dairy enterically emit 30 – 9,700 kg DMS per year. The SJV emits 13,700 – 4,592,700 kg DMS $yr^{-1}$ from milk cows. Previous studies have reported a range of annual DMS fluxes from 15.4 – 28.0 Tg S/yr globally (Aumont et al., 2002;

Bopp et al., 2003; Kloster et al., 2006), meaning that the milk cows in the SJV could be responsible for 0.025% – 15.4% of the total global DMS flux at the low ratio. This matches up with previous studies, which showed that enteric DMS emissions from ruminant animals may account for up to 10% of sulfur emissions in the global atmosphere, with dairy cows being the largest contributors (Hobbs et al., 1998). Although a large range is possible, it shows that DMS is likely more than just a marine gas and has sources at dairy farms as well.

As a large amount of DMS is converted to aerosols, dairy farms' contribution is important. Chen and Jang (2012) showed that 61.1% of DMS is converted to secondary organic aerosols in the absence of isoprene. Although Chen and Jang (2012) also noted that $NO_x$ and relative humidity play a role in aerosol production from DMS, isoprene mixing ratios were often below the LOD (10 ppt) at the dairy farm, specifically near the cows. Therefore, as the isoprene was low, the conversion ratio of DMS to aerosols is assumed to also be 61.1% for the purposes of this study. Table 6.11 shows the potential aerosol formation from the Visalia dairy and the SJV, assuming a 61.1% by mass conversion of DMS.

**Table 6.11** Potential aerosol production from DMS at the Visalia dairy and SJV at the low, median, and high $CH_4$:DMS ratios assuming a 61.1% conversion of DMS to secondary organic aerosols

| Ratio | Milk Cow EF (kg aerosols $hd^{-1}$ $yr^{-1}$) | Visalia Dairy (kg aerosols $yr^{-1}$) | SJV (kg aerosols $yr^{-1}$) |
|---|---|---|---|
| Low | 1.9 | 5,800 | 2,806,200 |
| Median | 0.024 | 72 | 35,100 |
| High | 0.0061 | 17 | 8,400 |

Overall, Table 6.11 shows possible secondary aerosol formation based on enteric DMS emissions. This calculation shows that DMS from milk cows in the SJV may contribute between 17 and 5,800 kg aerosols $yr^{-1}$ at the farm level, while they could contribute between 8,400 and 2,806,200 kg aerosols $yr^{-1}$ on the SJV-scale. The consequences of this are discussed further in Chapter 8.3, which discusses secondary aerosol contributions from the dairy farm and landfills.

The contribution of SOA to potential particle formation in the SJV was also calculated. First, the SJV was assumed to be a box with a surface area of 30,000 $km^2$ and a PBL of about 1

km for a total SJV volume of 30,000 $km^3$. The ventilation rate in the SJV was assumed to be 1 day. The maximum SOA production given in Table 6.11, $2.8x10^6$ kg aerosols $yr^{-1}$, was converted to the production per day in the SJV box of 30,000 $km^3$. Overall, it was calculated that 0.26 µg aerosols $m^{-3}$ $d^{-1}$ are generated from DMS from enteric emissions of cows in the SJV. To figure out the contribution to particle formation in the SJV, it is assumed, as Turpin and Huntzicker (1995) suggested, that organic particulate matter in the atmosphere is up to 80% SOA. Assuming that 80% of the SOA from DMS are particles, the maximum SOA creation in the SJV would contribute 0.21 µg particles $m^{-3}$ daily. As previous SARP data have suggested, the particle counts in the SJV are 4 $µg/m^3$ (Lebel et al., 2014). Therefore, DMS from enteric emissions of milk cows would contribute 5% of the total particles in the SJV. As Yang (2009) showed that ventilation in the SJV might be as long as six or seven days, the contribution of particles from DMS to SOA might be even greater than 5% because some accumulation would occur. This is discussed more in Chapter 8.3.1.

### 6.3 Dimethyl Sulfide and Carbonyl Sulfide at Orange County Landfills

Dimethyl sulfide and carbonyl sulfide mixing ratios were determined at the active and inactive Orange County landfills across four seasons. Minimum, median, average, and maximum values of DMS and OCS were determined at active landfills (Prima Deshecha, Frank R. Bowerman, and Olinda Alpha) during Spring 2018, Summer 2018, Fall 2018, and Winter 2019. These results are shown in Table 6.12.

**Table 6.12** DMS and OCS minimum, median, average, and maximum mixing ratios at active Orange County landfills by season

| Season | OCS (ppt) | | | | DMS (ppt) | | | |
|---|---|---|---|---|---|---|---|---|
| | Min. | Med. | Avg. | Max. | Min. | Med. | Avg. | Max. |
| Spring 2018 | 266 | 600 | 652 | 1706 | 1 | 7 | 114 | 1159 |
| Summer 2018 | 466 | 568 | 585 | 787 | 0 | 6 | 29 | 344 |
| Fall 2018 | 416 | 416 | 457 | 584 | 14 | 14 | 367 | 2046 |
| Winter 2019 | 382 | 427 | 454 | 565 | 47 | 372 | 1019 | 6223 |

Rather than follow a strong seasonal trend, enhancements of DMS and OCS depended more heavily on sampling location. The minimum, median, average, and maximum OCS mixing ratios at active Orange County landfills are plotted in Figure 6.5, where they are also compared to the average (560±24 ppt) at the coast of California (34.5 °N – 40.0 °N) from 2015 to 2018, which is given as the transparent blue horizontal bar.

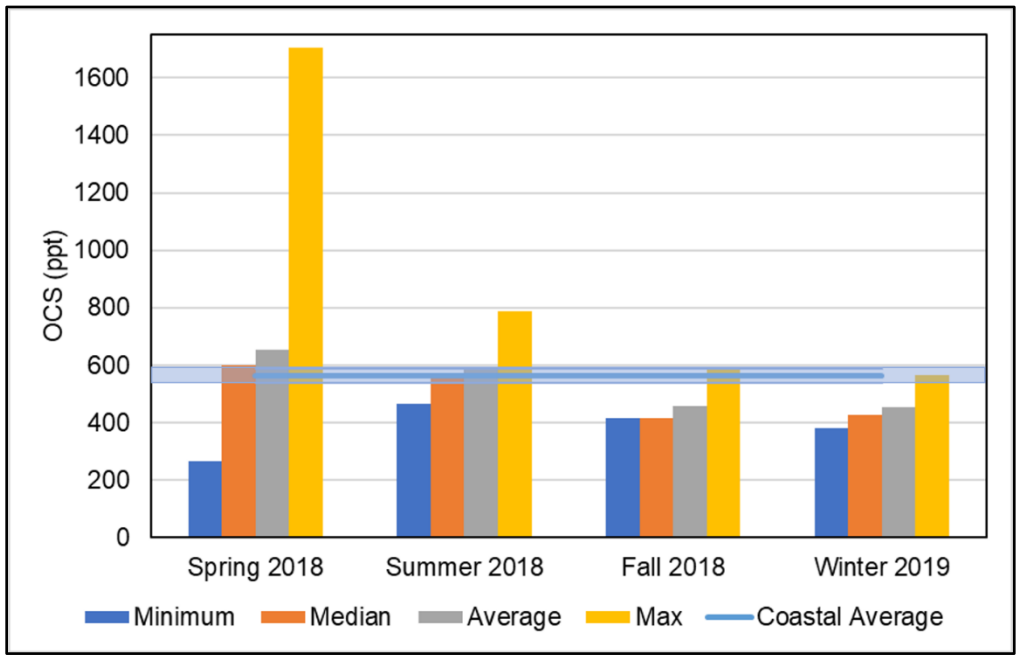


**Figure 6.5** Carbonyl sulfide minimum, median, average, and maximum mixing ratios for active Orange County landfills by season. The average range of the median OCS mixing ratios (564±24 ppt) on the California coastline (34.5 – 40.0 °N) is included as a blue horizontal bar for reference.

Nearly all the median mixing ratios of OCS at active Orange County landfills fell below the coastal average of 560±24 ppt. However, maximum values of OCS during Spring 2018, Summer 2018, and Fall 2018 campaigns exceeded the coastal average. The maximum mixing ratio of OCS for Spring 2018, 1700 ppt, was in a sample collected near a daily cover mulch pile near active dumping at Olinda Alpha. The maximum value of OCS during Summer 2018 was 787 ppt and was from a sample also collected near the active dumping area at Olinda Alpha. Olinda Alpha uses mulch as ADC, so it was initially unclear based on these two samples whether the enhanced OCS came from active dumping or from the organic cover material. For Fall 2018, the maximum

value of OCS at the active landfills was 584 ppt and was again collected near Olinda Alpha's active dumping area. Although the three highest OCS values were collected near Olinda Alpha's active dumping area during Spring, Summer, and Fall 2018, other landfills had elevated OCS near their active dumping areas as well: in Spring 2018, Prima Deshecha had OCS as high as 851 ppt near the active dumping area; in Summer 2018, Frank R. Bowerman had OCS as high as 747 ppt near the active dumping area. These landfills also use mulch as ADC and had mulch nearby. To determine whether the mulch ADC or the active dumping was the true culprit behind this elevated OCS at the active landfills, air samples were collected at an additional facility.

Four air samples were collected at a composting facility in Orange, CA. Out of the four samples collected at the facility, three were collected inside a mulch-filled room where mulch and compost at various stages were held, and one sample was collected outside the building on their loading dock. The mulch-filled room was assumed to trap the air rather efficiently. If mulch did indeed release OCS, it should be apparent from samples collected inside the room. However, the three samples collected in the mulch-filled room had an average OCS mixing ratio of 604 ppt, much lower than the elevated OCS at the landfill. The OCS outside the building on the loading dock was a bit higher at 638 ppt. Therefore, it seems more likely that the decomposition and evaporation occurring during active dumping may be emitting OCS rather than the mulch used as daily cover at the landfills. This is interesting as many California landfills are exploring using less soil and more ADC.

The minimum, median, average, and maximum DMS mixing ratios at active Orange County landfills (Frank R. Bowerman, Olinda Alpha, and Prima Deshecha) are shown in Figure 6.6, where they are also compared to the coastal average off the coast of California (34.5 – 40.0 °N) from 2015 to 2018.

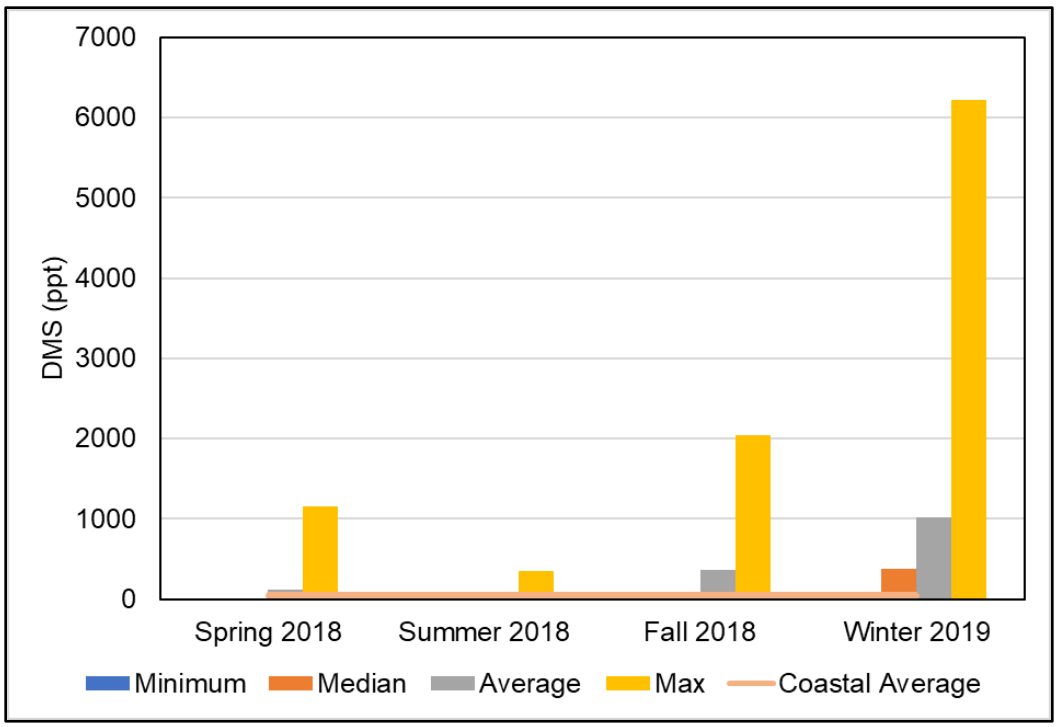


**Figure 6.6** Dimethyl sulfide minimum, median, average, and maximum mixing ratios for active Orange County landfills by season. The average of the median DMS mixing ratios (50±30 ppt) on the California coastline (34.5 – 40.0 °N) is included as a light orange horizontal bar for reference.

The maximum mixing ratios of DMS at active Orange County landfills were elevated high above the coastal average (50±30 ppt) and skewed the graph in Figure 6.6. To be able to better interpret the information presented in Figure 6.6, Figure 6.7 includes only the median levels of DMS compared to the coastal average of 50±30 ppt.

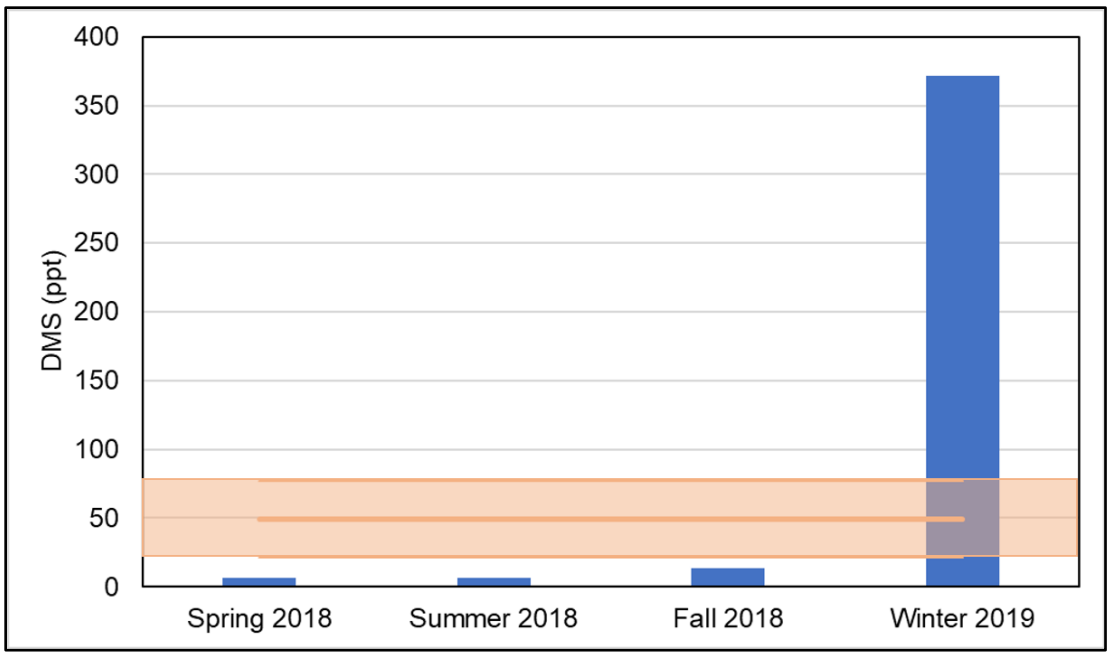


**Figure 6.7** Median DMS mixing ratios at active landfills across seasons. The average range of the median OCS mixing ratios (50±30 ppt) on the California coastline (34.5 – 40.0 °N) from 2015 – 2018 is included as an orange horizontal bar for reference.

Spring 2018 reached a maximum of 1160 ppt DMS near a foul-smelling compost pile at Olinda Alpha that had leachate leaking out of it. The second highest DMS maximum that season was 1030 ppt near a mulch pile at Olinda Alpha. Summer 2018 reached maximum DMS of 340 ppt near active dumping at Frank R. Bowerman landfill. Fall 2018 reached a maximum DMS mixing ratio of 2050 ppt near the active dumping area of Olinda Alpha landfill. It is clear from Figure 6.6 and Figure 6.7 that Winter 2019 had the highest median, average, and maximum mixing ratios of DMS. Winter 2019 had maximum DMS of 6220 ppt at the active dumping area of Prima Deshecha landfill. Elevated DMS (3260 ppt) was also found during Winter 2019 near the mulch pile and active dumping at Olinda Alpha. Similar to the OCS samples, it was initially unclear for many of these samples whether the DMS was emitted from active dumping areas or from the compost and mulch piles.

After reviewing the same four samples collected at the composting facility, the mixing ratios of DMS from the green material were determined for that facility. Inside the mulch and compost-filled room, the samples had an average of 460 ppt DMS, while the loading dock outside

the building had only 29 ppt DMS, even less than the average value at the California coastline. Because the inside of the composting facility had much higher DMS than the outside, it seems likely that mulch and compost emits DMS. Interestingly, this means that the DMS at the active landfill was likely coming from the mulch and compost storage areas *as well as* active dumping. This is different than OCS emissions, which seem to be emitted only during active dumping. It is important and intriguing that OCS and DMS mixing ratios were higher at the active landfills in many cases than they were by the ocean, as the ocean is a major source of both gases. For these trace gases to be elevated at landfills, especially at very stringent Orange County landfills, means there are other inland anthropogenic sources to think about when considering the budget of DMS and OCS globally.

Minimum, median, average, and maximum mixing ratios of OCS and DMS were also determined at inactive landfills (Coyote Canyon and Santiago Canyon) during Spring 2018, Summer 2018, Fall 2018, and Winter 2019. These are shown in Table 6.13.

**Table 6.13** DMS and OCS minimum, median, average, and maximum mixing ratios at inactive Orange County landfills by season

| Season | OCS (ppt) | | | | DMS (ppt) | | | |
|---|---|---|---|---|---|---|---|---|
| | **Min.** | **Med.** | **Avg.** | **Max.** | **Min.** | **Med.** | **Avg.** | **Max.** |
| Spring 2018 | 465 | 489 | 509 | 563 | 2 | 3 | 3 | 5 |
| Summer 2018 | 506 | 537 | 534 | 555 | 3 | 5 | 5 | 7 |
| Fall 2018 | 347 | 425 | 480 | 829 | 21 | 37 | 37 | 53 |
| Winter 2019 | 404 | 432 | 437 | 489 | < 1 | < 1 | < 1 | < 1 |

For Winter 2019, DMS mixing ratios were lower than the limit of detection (LOD = 1 ppt) at the inactive landfills. Sampling days were colder during Winter than during the other campaigns, so these decreased mixing ratios might be related to the temperature rather than source location, as most of the samples were collected in the generally same locations at the inactive landfills during all four seasons. The minimum, median, average, and maximum mixing ratios of OCS at closed Orange County landfills (Santiago Canyon and Coyote Canyon) are plotted in Figure 6.8,

where they are also compared to the OCS coastal (34.5 – 40.0 °N) average (564±24 ppt) from 2015 to 2018.

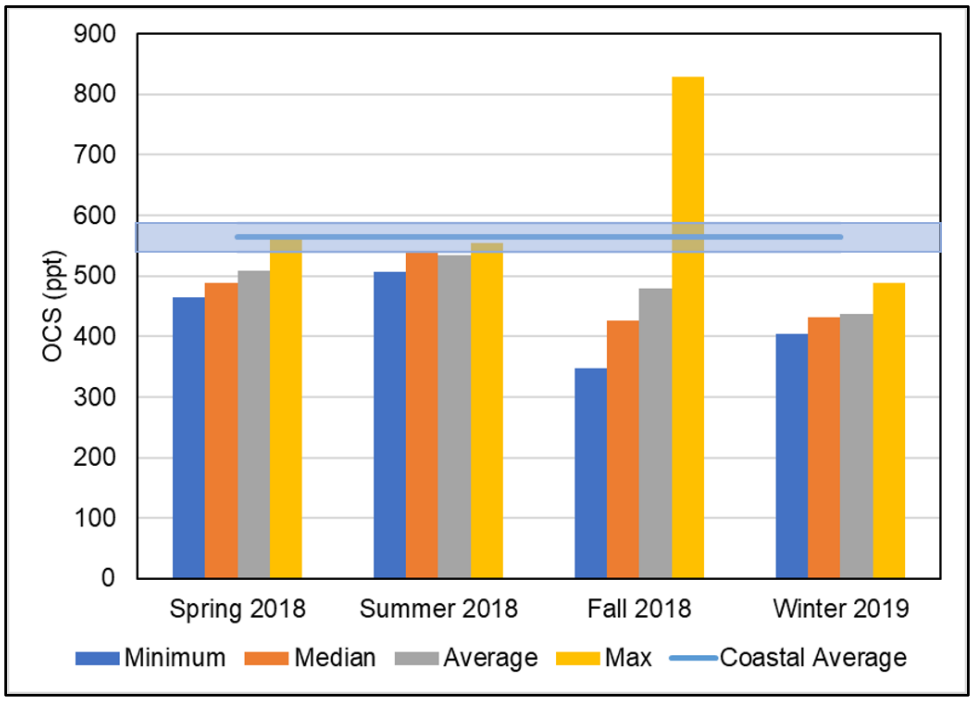


**Figure 6.8** Carbonyl sulfide minimum, median, average, and maximum mixing ratios for inactive Orange County landfills by season. The average range of the median OCS mixing ratios (564±24 ppt) on the California coastline (34.5 – 40.0 °N) is included as a blue horizontal bar for reference.

All the minimum, median, and average OCS mixing ratios at the closed landfills were below the coastal average during all four seasons. However, maximum OCS during Fall 2018 was higher than the coastal average. In Fall 2018, the maximum OCS value of 830 ppt was found near an open basin that was filled with runoff water at the Coyote Canyon landfill. It is possible that this contaminated water was emitting OCS.

The minimum, median, average, and maximum mixing ratios of DMS were also plotted for the closed Orange County landfills (Santiago Canyon and Coyote Canyon) seasonally. This plot is shown in Figure 6.9. The average range of the median DMS mixing ratios (50±30 ppt) on the California coastline (34.5 – 40.0 °N) is also plotted as an orange horizontal bar.

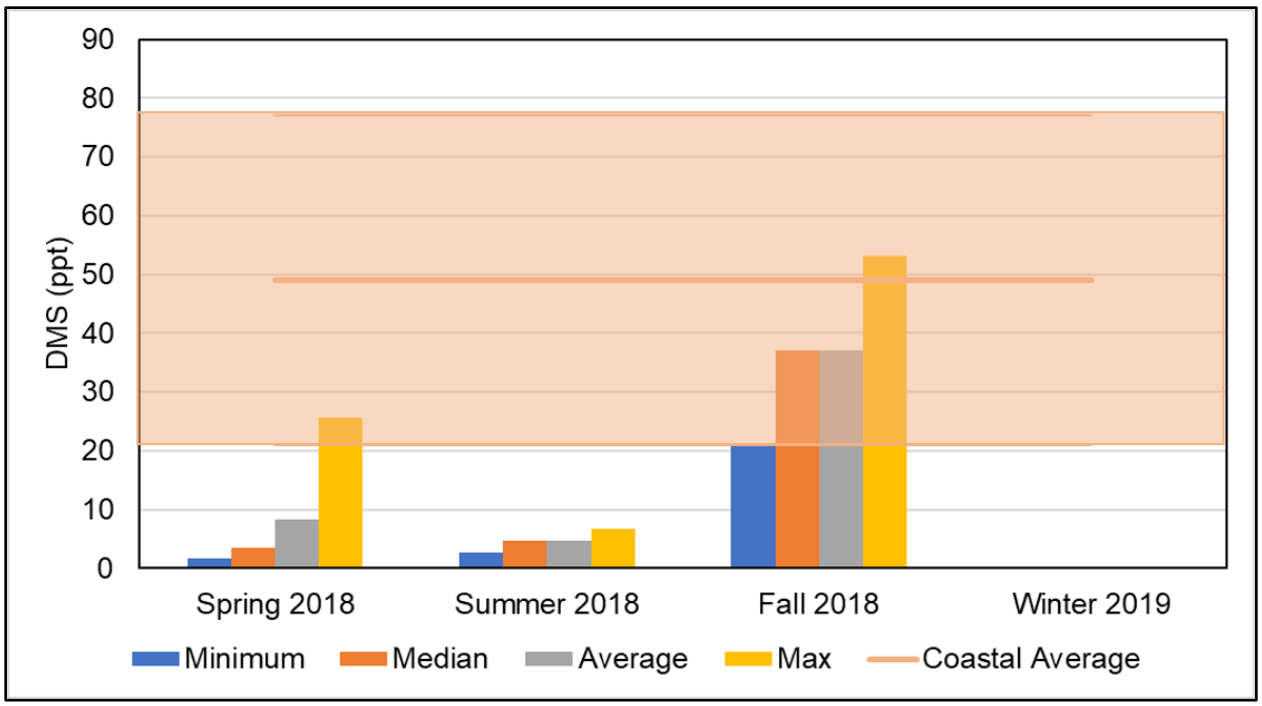


**Figure 6.9** Dimethyl sulfide minimum, median, average, and maximum mixing ratios for closed Orange County landfills by season. The average range of the median DMS mixing ratios (50±30 ppt) on the California coastline (34.5 – 40.0 °N) is included as an orange horizontal bar for reference.

The DMS mixing ratios for the closed landfills in Figure 6.9 fell below the coastal average of 50±30 ppt for Summer 2018 and Winter 2019. However, the maximum DMS mixing ratios during Spring 2018 fell within the range of average mixing ratios expected near the coastline. During Fall 2018, all mixing ratios fell within the coastal average range (50±30 ppt). The maximum DMS mixing ratio during Fall 2018 was 53 ppt and was found in a sample collected upwind of Coyote Canyon landfill. It was unclear what source during the Fall 2018 campaign led to higher DMS mixing ratios than the other seasons, but it could have been the Pacific Ocean itself. Coyote Canyon is located less than three miles from the coastline (by air), so the elevated DMS upwind of the landfills was likely from an ocean source. It seems unlikely that the inactive landfills emit much DMS, and it seems more likely the active landfills emit DMS because of their daily cover and active dumping.

## 6.4 Summary and Conclusion

Median DMS and OCS mixing ratios, for which oceanic emissions are a known source, on the coast of California from 2015 to 2018 were 50±30 ppt and 560±24 ppt, respectively. Mixing ratios of DMS and OCS were much higher at the dairy farms than at the landfills. Median mixing ratios of OCS at the dairy site near cows in corrals, bedding areas, silage, free stalls, lagoons, and cow breath exceeded the coastal values. Median DMS in many sample areas (crops, cows in corrals, bedding, silage, free stalls, lagoons, and cow breath) exceeded the coastal levels. The highest median mixing ratios of both gases were in cow breath, indicating that cows may emit OCS and DMS.

If the cows at all dairy farms worldwide emit similar ratios of $CH_4$ to OCS, the OCS from enteric emissions of milk cows alone may account for 2–17% of the missing OCS source (230–800 Gg S $yr^{-1}$). Cow breath should be considered in future estimates of global OCS emissions, and flux studies should be performed at dairy farms around the world to determine the contribution by region. Additionally, the contribution of cattle enteric emissions and manure management emissions worldwide to the OCS budget were also estimated. Total emissions from bovine activity were estimated to be between 16 to 79 Gg S/yr, which would account for 7 to 34% of the low-end estimate of the missing OCS source (230 Gg S/yr) or 2 to 10% of the high-end estimate of the missing OCS source (800 Gg S/yr). This is a non-trivial amount that should be considered a topic of future study.

Previous studies have also corroborated that cows emit sulfur, stating that higher protein diets may lead to higher DMS emissions (Hobbs et al., 2000). Additionally, studies done on cow breath reveal that the emission of DMS from ruminant animals' breath may account for up to 10% of sulfur emissions in the global atmosphere, with dairy cows being the largest contributors (Hobbs et al., 1998). Previous studies in the United Kingdom have seen a range of 0 to 25 ppm of DMS in cow breath at various stages of the cows' life cycles. Cow breath appeared to be a

contributor to DMS emissions at the Visalia dairy farm. Milk cows in the SJV may be responsible for DMS emissions between 13,700 – 4,592,700 kg DMS $yr^{-1}$, or 0.025% – 15.4% of the global DMS flux. Dimethyl sulfide can oxidize to sulfuric acid and begin cloud formation through particle nucleation, which is an important part of the global climate (Hobbs et al., 1998). This study assumed that 61.1% of the DMS is converted to aerosols, which implies a large contribution from dairy farms to secondary aerosol formation and about 5% of the submicron particle contribution in the SJV. Lagoons may also emit OCS and DMS, but with much lower enhancements than the cow breath.

When reporting sulfur compounds at landfills, researchers often focus on $H_2S$ and methyl mercaptan because of their health effects, but OCS and DMS can be emitted as well and are important for global climate. Active landfills had median OCS mixing ratios close to the background mixing ratios near the coastline. For DMS, the median for all samples collected in Spring, Summer, and Fall 2018 at active landfills was below the coastal average. Only in Winter 2019 did the median DMS exceed the coastal level, likely because of a combination of emissions from compost and mulch as well as active dumping. Studies have shown that the higher the protein content of decomposing waste, the higher the DMS emissions (Jin et al., 2020). Although DMS levels may be low, studies at a landfill in Daegu, Korea, show that DMS is one of the most important reduced sulfur compounds for contributing to the formation of sulfur dioxide, an important pollutant, at landfills (Shon et al., 2005). Sulfur dioxide is on the EPA's list of criteria pollutants and can contribute to human health problems, acid rain, and low visibility (Seinfeld & Pandis, 2016). This problem of the formation of sulfur dioxide likely persists for the dairy farms as well, which exhibited much higher DMS mixing ratios than the landfills.

For inactive Orange County landfills, all OCS mixing ratios were below those at the California coastline, except for the maximum mixing ratio during Fall 2018, which was 830 ppt. This elevated OCS was found near an open tank filled with landfill water outflow. The literature

reports finding OCS at landfills containing construction and demolition materials (Lee et al., 2006). All landfills, active and inactive, contain or accept construction and demolition materials, which could be part of the cause of OCS present at the landfills. Dimethyl sulfide at inactive landfills was well below the coastal average, except for a maximum during Fall 2018, which was 53 ppt and surprisingly collected upwind of the landfill. Therefore, it seems unlikely that inactive landfills are responsible for large DMS emissions.

## 6.5 References


Aumont, O., Belviso, S., & Monfray, P. (2002). Dimethylsulfoniopropionate (DMSP) and dimethylsulfide (DMS) sea surface distributions simulated from a global three-dimensional ocean carbon cycle model. *Journal of Geophysical Research: Oceans*, *107*(C4), 4-1.

Aydin, M., Fudge, T. J., Verhulst, K. R., Nicewonger, M. R., Waddington, E. D., & Saltzman, E. S. (2014). Carbonyl sulfide hydrolysis in Antarctic ice cores and an atmospheric history for the last 8000 years. *Journal of Geophysical Research: Atmospheres*, *119*(13), 8500-8514.

Bardouki, H., Berresheim, H., Vrekoussis, M., Sciare, J., Kouvarakis, G., Oikonomou, K., ... & Mihalopoulos, N. (2003). Gaseous (DMS, MSA, SO 2, H 2 SO 4 and DMSO) and particulate (sulfate and methanesulfonate) sulfur species over the northeastern coast of Crete. *Atmospheric Chemistry and physics*, *3*(5), 1871-1886.

Barone, S. B., Turnipseed, A. A., & Ravishankara, A. R. (1995). Role of adducts in the atmospheric oxidation of dimethyl sulfide. *Faraday discussions*, *100*, 39-54.

Berry, J., Wolf, A., Campbell, J. E., Baker, I., Blake, N., Blake, D., ... & Stimler, K. (2013). A coupled model of the global cycles of carbonyl sulfide and CO2: A possible new window on the carbon cycle. *Journal of Geophysical Research: Biogeosciences*, *118*(2), 842-852.

Bopp, L., Aumont, O., Belviso, S., & Monfray, P. (2003). Potential impact of climate change on marine dimethyl sulfide emissions. *Tellus B: Chemical and Physical Meteorology*, *55*(1), 11-22.

California Department of Food and Agriculture (CDFA). (2019b). California Agricultural Statistics Review 2018-2019. Retrieved from https://www.cdfa.ca.gov/Statistics/PDFs/AgExports2018-2019.pdf

Campbell, J. E., Carmichael, G. R., Chai, T., Mena-Carrasco, M., Tang, Y., Blake, D. R., ... & Stanier, C. O. (2008). Photosynthetic control of atmospheric carbonyl sulfide during the growing season. *Science*, *322*(5904), 1085-1088.

Campbell, J. E., Kesselmeier, J., Yakir, D., Berry, J. A., Peylin, P., Belviso, S., ... & Sitch, S. (2017). Assessing a new clue to how much carbon plants take up. *Eos*, *98*.

Campbell, J. E., Whelan, M. E., Seibt, U., Smith, S. J., Berry, J. A., & Hilton, T. W. (2015). Atmospheric carbonyl sulfide sources from anthropogenic activity: Implications for carbon cycle constraints. *Geophysical research letters*, *42*(8), 3004-3010.

Charlson, R. J., Lovelock, J. E., Andreae, M. O., & Warren, S. G. (1987). Oceanic phytoplankton, atmospheric sulphur, cloud albedo and climate. *Nature*, *326*(6114), 655-661.

Chen, T., & Jang, M. (2012). Secondary organic aerosol formation from photooxidation of a mixture of dimethyl sulfide and isoprene. *Atmospheric environment*, *46*, 271-278.

Eggleston, S., Buendia, L., Miwa, K., Ngara, T., & Tanabe, K. (Eds.). (2006). *2006 IPCC guidelines for national greenhouse gas inventories* (Vol. 5). Hayama, Japan: Institute for Global Environmental Strategies.

Gaston, C. J., Pratt, K. A., Qin, X., & Prather, K. A. (2010). Real-time detection and mixing state of methanesulfonate in single particles at an inland urban location during a phytoplankton bloom. *Environmental science & technology*, *44*(5), 1566-1572.

Glatthor, N., Höpfner, M., Baker, I. T., Berry, J., Campbell, J. E., Kawa, S. R., ... & Stinecipher, J. (2015). Tropical sources and sinks of carbonyl sulfide observed from space. *Geophysical Research Letters*, *42*(22), 10-082.

Hobbs, P., Misselbrook, T., Cumby, T., & Mottram, T. (1998). The scope and contribution of volatile organic compounds to pollution from livestock. In *2001 ASAE Annual Meeting* (p. 1). American Society of Agricultural and Biological Engineers.

Hobbs, P., & Mottram, T. (2000). New directions: Significant contributions of dimethyl sulphide from livestock to the atmosphere. *Atmospheric Environment*, *34*(21), 3649-3650.

Jin, Z., Zhang, S., Hu, L., Fang, C., Shen, D., & Long, Y. (2020). Effect of substrate sulfur state on MM and DMS emissions in landfill. *Waste Management*, *116*, 112-119.

Kloster, S., Feichter, J., Maier-Reimer, E., Six, K. D., Stier, P., & Wetzel, P. (2006). DMS cycle in the marine ocean-atmosphere system–a global model study. *Biogeosciences*, *3*(1), 29-51.

Kuai, L., Worden, J. R., Campbell, J. E., Kulawik, S. S., Li, K. F., Lee, M., ... & Baker, I. (2015). Estimate of carbonyl sulfide tropical oceanic surface fluxes using Aura Tropospheric Emission Spectrometer observations. *Journal of Geophysical Research: Atmospheres*, *120*(20), 11-012.

Lebel, E. D., Marrero, J. E., Bertram, T. H., & Blake, D. R. (2014, December). Dimethyl Sulfide Emissions from Dairies and Agriculture as a Potential Contributor to Sulfate Aerosols in the California Central Valley. In *AGU Fall Meeting Abstracts* (Vol. 2014, pp. A43H-3378).

Lee, S., Xu, Q., Booth, M., Townsend, T. G., Chadik, P., & Bitton, G. (2006). Reduced sulfur compounds in gas from construction and demolition debris landfills. *Waste Management, 26*(5), 526-533.

Lennartz, S., Marandino, C. A., Von Hobe, M., Cortes, P., Quack, B., Simo, R., ... & Kloss, C. (2017). Direct oceanic emissions unlikely to account for the missing source of atmospheric carbonyl sulfide. *Atmospheric Chemistry and Physics*, *17*, 385-402.

Lukács, H., Gelencsér, A., Hoffer, A., Kiss, G., Horváth, K., & Hartyáni, Z. (2009). Quantitative assessment of organosulfates in size-segregated rural fine aerosol. *Atmospheric Chemistry and Physics*, *9*(1), 231-238.

Montzka, S. A., Calvert, P., Hall, B. D., Elkins, J. W., Conway, T. J., Tans, P. P., & Sweeney, C. (2007). On the global distribution, seasonality, and budget of atmospheric carbonyl sulfide (COS) and some similarities to CO2. *Journal of Geophysical Research: Atmospheres*, *112*(D9).

Owen, J. J., & Silver, W. L. (2015). Greenhouse gas emissions from dairy manure management: a review of field-based studies. *Global change biology, 21*(2), 550-565.

Seinfeld, J. H., & Pandis, S. N. (2016). *Atmospheric chemistry and physics: from air pollution to climate change*. John Wiley & Sons.

Shon, Z. H., Kim, K. H., Jeon, E. C., Kim, M. Y., Kim, Y. K., & Song, S. K. (2005). Photochemistry of reduced sulfur compounds in a landfill environment. *Atmospheric Environment, 39*(26), 4803-4814.

Suntharalingam, P., Kettle, A. J., Montzka, S. M., & Jacob, D. J. (2008). Global 3-D model analysis of the seasonal cycle of atmospheric carbonyl sulfide: Implications for terrestrial vegetation uptake. *Geophysical Research Letters*, *35*(19).

Turpin, B. J., & Huntzicker, J. J. (1995). Identification of secondary organic aerosol episodes and quantitation of primary and secondary organic aerosol concentrations during SCAQS. *Atmospheric Environment*, *29*(23), 3527-3544.

United States Department of Agriculture (USDA): Foreign Agricultural Service. (2021). Livestock and Poultry: World Markets and Trade. Retrieved from https://apps.fas.usda.gov/psdonline/circulars/livestock_poultry.pdf

Yang, M. (2009). Characterization of VOC Emissions from Various Components of Dairy Farming and Their Effect on San Joaquin Valley Air Quality. (Doctoral dissertation, Ph. D., thesis, University of California, Irvine).

# 7. Nitrous Oxide

Nitrous oxide is about 298 times more potent a greenhouse gas than $CO_2$ over a 100-year period. Data from AGAGE show that $N_2O$ has been increasing in the atmosphere over the last few decades. Figure 7.1 plots data from AGAGE showing global average $N_2O$ mixing ratios from 1978 to 2018. Nitrous oxide currently increases by about 1 ppb, or 7,300 Gg $N_2O$, each year (Prinn et al., 2018). While pockets of heterogeneity might exist, the long lifetime of $N_2O$ means that its globally averaged mixing ratio is likely quite uniform around the world.

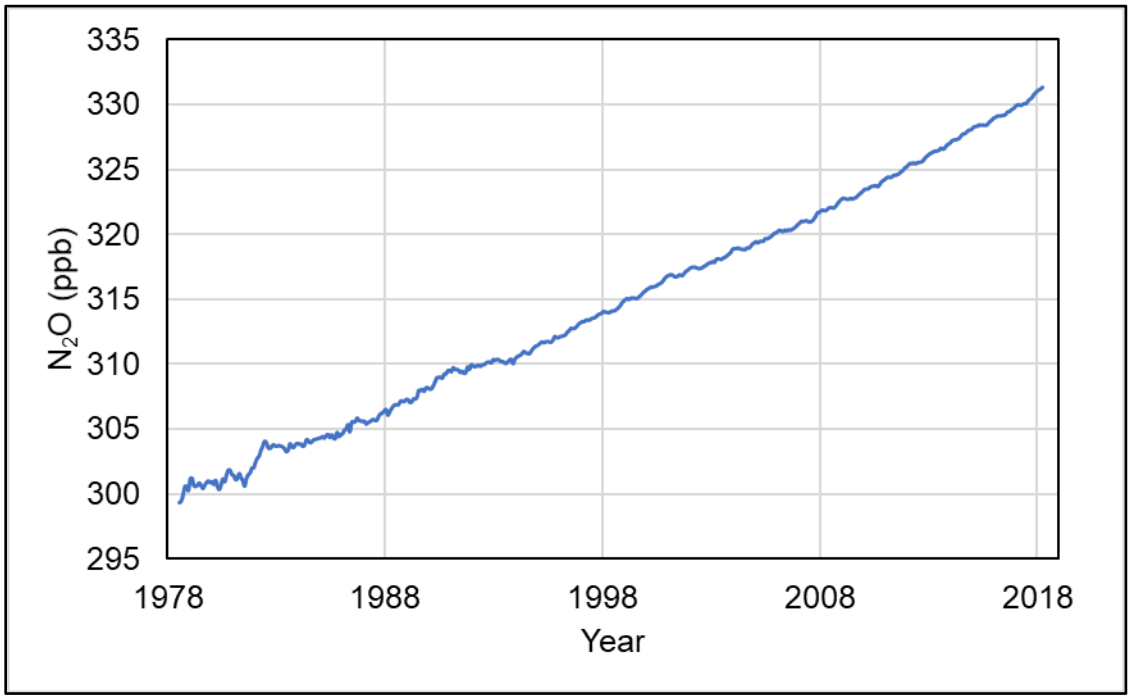


**Figure 7.1** Nitrous oxide (ppb) global mixing ratios from 1978 to 2018. Data retrieved from AGAGE (Prinn et al., 2018).

As shown in Figure 7.1, there appears to be slight variations in $N_2O$ mixing ratios over time. This can be explained by its small seasonal cycle. Minschwaner et al. (1993) showed that stratospheric photolysis is the main sink of $N_2O$ and is responsible for its long lifetime of over 120 years. This means that $N_2O$ would be depleted high up in the stratosphere, but more enhanced closer to the surface. Levin et al. (2002) showed that the seasonal cycle of tropospheric $N_2O$ is caused in part by the mixing of $N_2O$-depleted air from the stratosphere with $N_2O$-rich air in the troposphere. Jiang

et al. (2007) also noted this trend in global atmospheric data. After analyzing seven global air monitoring stations from NOAA Global Air Monitoring Division and from AGAGE, Jiang et al. (2007) found that, in the Northern Hemisphere, minimum $N_2O$ mixing ratios occur at the beginning of fall. Although $N_2O$ does exhibit very slight seasonal cycles, the amplitude between a yearly maximum and minimum is only about 1.2 ppb by mole fraction. Among possible sources such as the dairy farm and landfills, it was not expected to see this seasonal dependence. Instead, all enhancements are assumed to come from ground sources rather than seasonal changes.

### 7.1 Nitrous Oxide at the Visalia Dairy Farm

Nitrous oxide was measured at the Visalia dairy site during the September 2018, March 2019, June 2019, and September 2019 campaigns. Figure 7.2 shows an aerial view of the dairy farm with the $N_2O$ mixing ratios from various sources scaled by color and height. Points shown were collected during the campaigns through September 2019 and are not separated by season. Typical wind direction was from the northwest. Nitrous oxide was binned into five discrete mixing ratio ranges and colored accordingly. Height was scaled on a continuum, where the lowest nitrous oxide mixing ratios are shown closer to the ground and the more elevated mixing ratios are shown higher above the ground for illustration. For the purposes of labelling Figure 7.2, the “Manure” category included sources for which waste was the major constituent: the processing pit, bedding, flush water, the two lagoons, and the two slurries. The “Enteric” category included cows in outdoor spaces (i.e., dry cows and heifers) and the free stalls (i.e., milk cows). The “Other” category included samples collected upwind, downwind, and near the office and milking parlor.

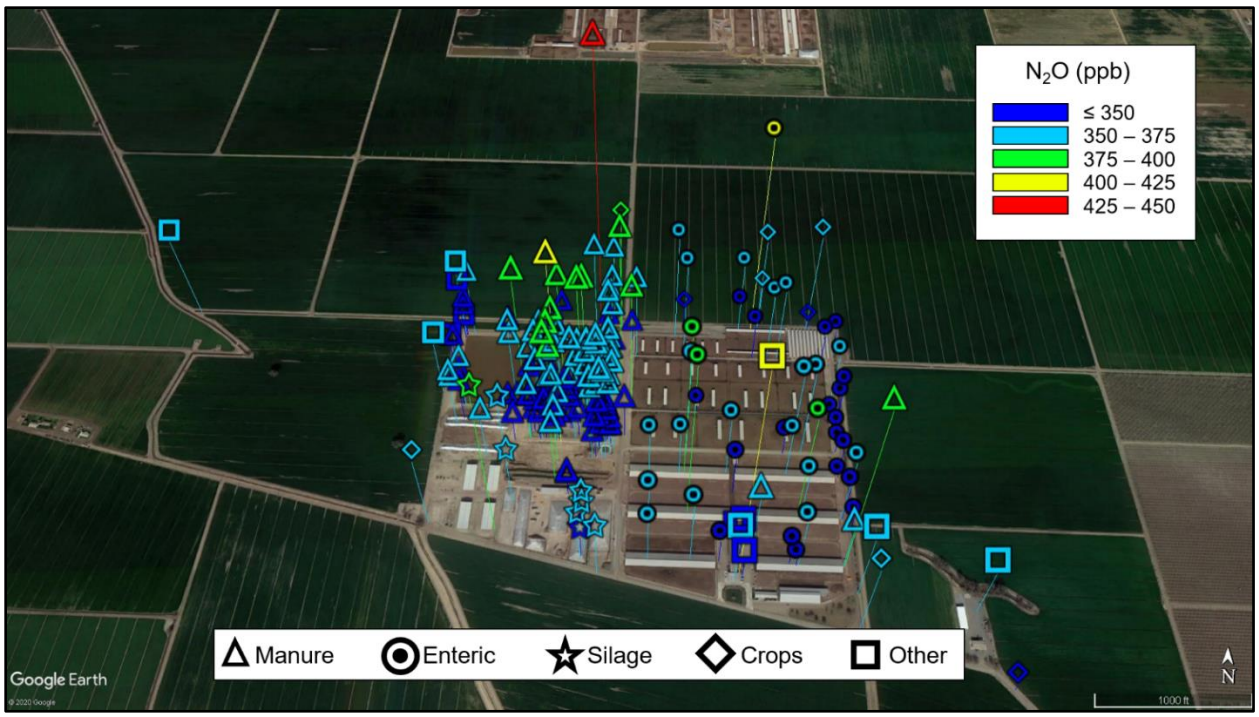


**Figure 7.2** Nitrous oxide (ppb) at the dairy farm binned by mixing ratio ranges and grouped by source. Height of the points also indicates $N_2O$ mixing ratio. Typical wind direction was from the northwest.

Although Figure 7.2 shows that there are likely a handful of distinct sources of $N_2O$ at the dairy farm, the variation between samples was rather low. Overall, across all campaigns, the average $N_2O$ mixing ratio and standard deviation was 356±16 ppb. This was a little higher than the global average, 331 ppb according to AGAGE (Prinn et al., 2018). According to Figure 7.2, one of the largest contributors of $N_2O$ at this dairy farm was likely the wet manure management system, categorized under “Manure.”

To better identify on-site locations from which $N_2O$ could originate, the samples were further separated by location for analysis. The minimum, median, average, and maximum $N_2O$ mixing ratios by location at the dairy site across all the selected campaigns are shown in Table 7.1.

**Table 7.1** Minimum, median, average, and maximum $N_2O$ mixing ratios (ppb) at the dairy site by location

| Location | $N_2O$ (ppb) | | | |
|---|---|---|---|---|
| | Minimum | Median | Average | Maximum |
| Bedding | 342 | 353 | 359 | 389 |
| Cows | 336 | 348 | 354 | 402 |
| Crops | 337 | 356 | 354 | 376 |
| Flush Water | 351 | 364 | 370 | 397 |
| Free Stall | 335 | 351 | 355 | 392 |
| Lagoon | 334 | 352 | 355 | 448 |
| Silage | 343 | 352 | 358 | 389 |

These values have also been represented by a graph of minimum, median, and maximum $N_2O$ mixing ratios shown in Figure 7.3. As shown in Table 7.1, the averages and medians were almost identical for $N_2O$, so only the medians were included in Figure 7.3. In Figure 7.3, the "Lagoon" category includes samples collected near the two lagoons and two slurries, and "Cows" includes cows outside of the free stalls (i.e., dry cows and heifers).

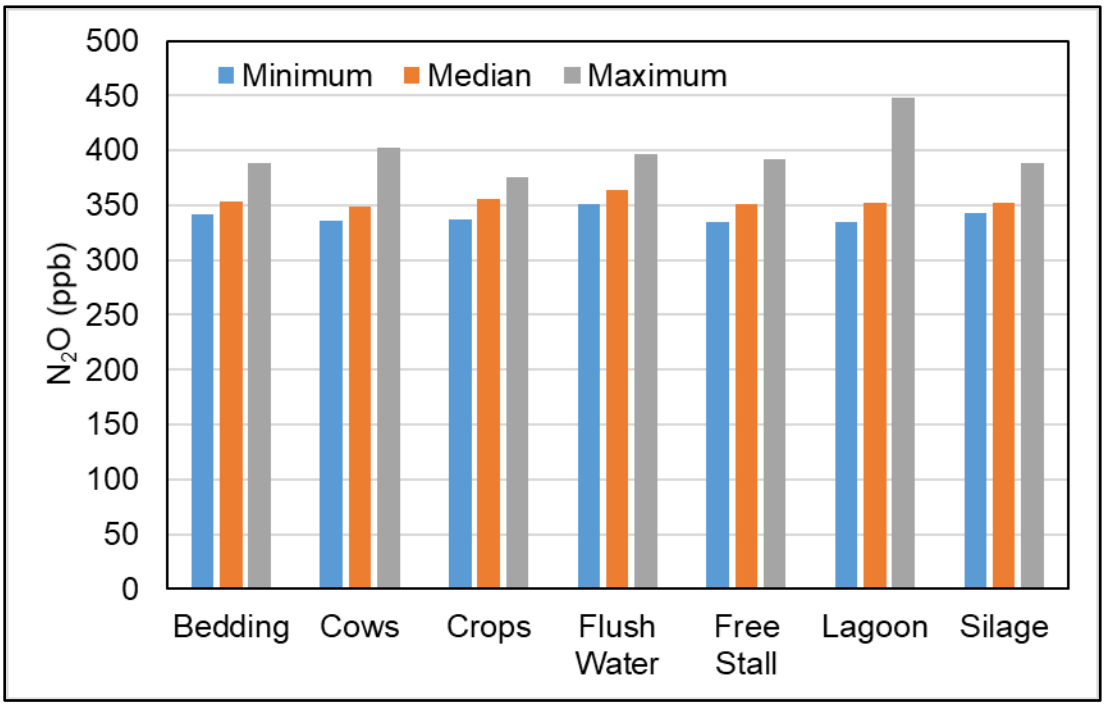


**Figure 7.3**. Minimum, median, and maximum mixing ratios of $N_2O$ (ppb) at the dairy site.

As shown in Figure 7.3, all locations listed had nearly identical minimum $N_2O$ mixing ratios. Similarly, the median mixing ratio was only slightly higher than the minimum in all cases and was

similar across all locations. Overall, the lagoons, slurries, and flush water had the highest $N_2O$ mixing ratios at the dairy site. The “Lagoons” category had a higher maximum mixing ratio (448 ppb) than other areas around the dairy, while the flush water had the highest median (364 ppb) and average (370 ppb) in Table 7.1. The outdoor cows (i.e., “Cows” in Table 7.1 and Figure 7.3) had the second highest maximum $N_2O$ mixing ratio. It seems likely that the $N_2O$ is emitted from the cow waste, which explains the elevated $N_2O$ near the manure management system and in the flush water. Although the $N_2O$ was also elevated slightly near the cows, the contribution is likely not enteric. Instead, it is likely from the cows’ waste that becomes piled up in the corrals before it is scraped.

The difference between the maximum and median $N_2O$ mixing ratios in samples collected near the manure management system show that $N_2O$ is likely emitted more during the waste collection and decomposition processes than from the cows or their feed because of the relatively lower $N_2O$ mixing ratios found near silage and free stalls. However, although there were likely some on-site $N_2O$ emissions, the mixing ratios were not as high as one would expect for a typical dairy farm based on previous studies.

For example, Owen and Silver (2015) compiled data from studies in North America and Europe with a variety of manure management systems and found that whole barns had the largest $N_2O$ emissions, 10±6 kg $N_2O$ $hd^{-1}$ $yr^{-1}$. This may imply that barns have the necessary combination of anaerobic and aerobic environments to generate $N_2O$. The dairy farm in Visalia did not have a whole barn, but it did have lagoons and slurries. In the same study, Owen and Silver (2015) found that the anaerobic lagoons emitted 0.9±0.5 kg $N_2O$ $hd^{-1}$ $yr^{-1}$ with a range of 0.004 – 3.9 kg $N_2O$ $hd^{-1}$ $yr^{-1}$, while slurries emitted 0.3±0.3 kg $N_2O$ $hd^{-1}$ $yr^{-1}$ with a range of 0 – 4.5 kg $N_2O$ $hd^{-1}$ $yr^{-1}$. This implies that dry manure management systems (i.e., in a whole barn setting) likely release more $N_2O$ because of increased favorable formation conditions, whereas lagoons and slurries tend to be more exclusively anaerobic.

Decomposition of animal waste can release $N_2O$ through direct and indirect pathways once certain environmental conditions are met. To emit $N_2O$ directly, the manure must first be handled aerobically so that the organic nitrogen is mineralized or decomposed to $NH_4$, which then becomes nitrified to nitrate ($NO_3^-$), producing a little $N_2O$ in the process. Following the aerobic handling, the manure must then be handled anaerobically, so that the nitrate is reduced and denitrified to $N_2O$ and eventually $N_2$ (EPA, 2020c). This multi-step process is more likely to occur in dry manure management strategies rather than wet manure management strategies. In a dry manure management strategy, manure is handled under mostly aerobic conditions with pockets of anaerobic conditions, making the two steps more easily accessible.

Dairy farms in the SJV, including the Visalia dairy site, use mostly a wet manure management strategy, where manure is stored mostly as liquid piles, either as lagoons or slurries. The lagoons hold the liquid fraction after the solids are mechanically separated and are homogenously anaerobic. The slurries, however, are not very diluted and are often quite heterogenous. They contain a large quantity of solids that can float up to the surface to create a crust. Peterson and Sommer (2011) showed that this crust can act as a bridge between anaerobic and aerobic environments, which can allow $N_2O$ production to occur.

Nationwide entities, such as the EPA, calculate the emission rates from these manure management systems using Equation 7-1, which is added up for all animals and waste management systems at a dairy (EPA, 2020c).

$$\text{Direct } N_2O = \sum N_{excreted} * EF * \frac{44}{28} \qquad \text{Equation 7-1}$$

where

$Direct_{N2O}$ = the amount of $N_2O$ emitted directly, in (kg $N_2O$ $yr^{-1}$)

$N_{excreted}$ = the amount of N excreted in manure, in (kg N $yr^{-1}$)

EF = direct $N_2O$ emission factor, in (kg $N_2O$-N/kg N excreted)

44/28 = conversation factor of $N_2O$-N to $N_2O$, in (kg $N_2O$/kg N)

Equation 7-1 calculates emissions of $N_2O$ from direct sources only. Indirect emissions of $N_2O$ can also occur, but through much more complicated pathways. To determine indirect emissions, such parameters as the amount of nitrogen lost through volatilization of ammonia in the manure management system and the nitrogen lost through runoff and leaching for the manure management system need to be known. Although it is outside the scope of this project to use these formulas to calculate the amount of $N_2O$ from direct and indirect sources, this study considers the parameters that the EPA 2020 Inventory used to calculate $N_2O$ emissions nationwide and suggests how they could be improved.

Specifically, the EF in Equation 7-1 is selected based on suggested values from the IPCC 2006 *Guidelines for National Greenhouse Gas Inventories* (Eggleston et al., 2006) for various manure management systems (e.g., slurries, anaerobic lagoons, deep bed, compost, digester, etc.). The IPCC recognizes slurries as $N_2O$ emitters, with an $EF_{slurry}$ = 0.005 kg $N_2O$-N/kg N excreted. However, the IPCC and EPA do not recognize anaerobic lagoons as an $N_2O$ contributor, so the $EF_{lagoon}$ = 0 kg $N_2O$-N/kg N excreted. Unfortunately, the current EPA Inventory (EPA, 2020c) is likely underestimating $N_2O$ emissions from anaerobic lagoons in the SJV.

Owen and Silver (2015) determined that anaerobic lagoons contribute 1.79 ± 0.90 Tg $CO_2e$ $yr^{-1}$ in the United States alone. The potential contribution from lagoons is small relative to the total increase of $N_2O$ (about 7,300 Gg $N_2O$) each year (Prinn et al., 2018). Using the emission factor found in Owen and Silver (2015) for lagoons (0.9±0.5 kg $N_2O$ $hd^{-1}$ $yr^{-1}$), the entire SJV (i.e., 1,505,000 milk cows) would emit 1.4±0.8 Gg $N_2O$ $yr^{-1}$, only 0.019±0.01% of the total $N_2O$ increase each year. However, that does not rule out lagoons as a small source of $N_2O$.

Figure 7.2 shows that both the lagoons and slurries likely contribute to $N_2O$ at the Visalia dairy; in fact, the sample with the highest mixing ratio of $N_2O$ (448 ppb) was collected downwind of the lagoons (not the slurries) during the September 2018 campaign. In the IPCC 2006 guidelines—and even in their updated response in Buendia et al. (2019)—it is still recommended

to use $EF_{lagoon}$ = 0 kg $N_2O$-N/kg N excreted (Eggleston et al., 2006). This is likely because the IPCC assumes that lagoons cannot form the crust necessary to create optimal conditions for $N_2O$ generation. However, the lagoons still seemed to contribute some $N_2O$, albeit a small amount, at the Visalia dairy.

As $N_2O$ is 298 times a more potent GHG than $CO_2$ at the 100-year scale, it is important that even small sources be included and well understood in the nationwide inventory. It is therefore recommended for future EPA inventories that the lagoons are considered in addition to slurries when calculating $N_2O$ emissions from dairy farms, because this amount would scale up across the SJV, and the United States, if the manure at other dairy farms is managed similarly.

### 7.2 Nitrous Oxide at Orange County Landfills

Currently, the EPA does not include the contribution of $N_2O$ to the total GWP of a landfill, and $N_2O$ emissions were not estimated for landfills in the 2020 EPA Greenhouse Gas Inventory (EPA, 2020c). However, other literature suggests that $N_2O$ is emitted from landfills. Rinne et al. (2005) conducted the first landfill $N_2O$ eddy covariance measurements at a landfill in the early 2000s. They calculated $N_2O$ emissions at Ämmässuo landfill near Helsinki, Finland and found that the landfill surface emitted 2.7 mg N $m^{-2}$ $h^{-1}$, about an order of magnitude higher than Northern European agricultural soils. Although the $N_2O$ emissions at Ämmässuo landfill were elevated, Rinne et al. (2005), like the EPA, suggested that these emissions are trivial because of the landfill's small size compared to other land uses. Although landfills in California are operated differently than those in Finland, this study examines whether Orange County landfills also generate $N_2O$ and whether the amount of also trivial. It is important to understand the sources of $N_2O$ and determine whether there is a difference in mixing ratios between the active and closed landfills in Orange County because of its high GWP.

Samples collected at active and closed Orange County landfills were analyzed for $N_2O$ during Spring 2018, Summer 2018, Fall 2018, and Winter 2019. Figure 7.4 shows the $N_2O$ mixing

ratios at active and closed Orange County landfills over Julian time. The corresponding campaigns are labelled next to each cluster of points to indicate relative seasons. Note that $N_2O$ mixing ratios were not lower than 320 ppb (which makes sense as global mixing ratios are 331 ppb), so Figure 7.4 need not include the lower part of the y-axis.

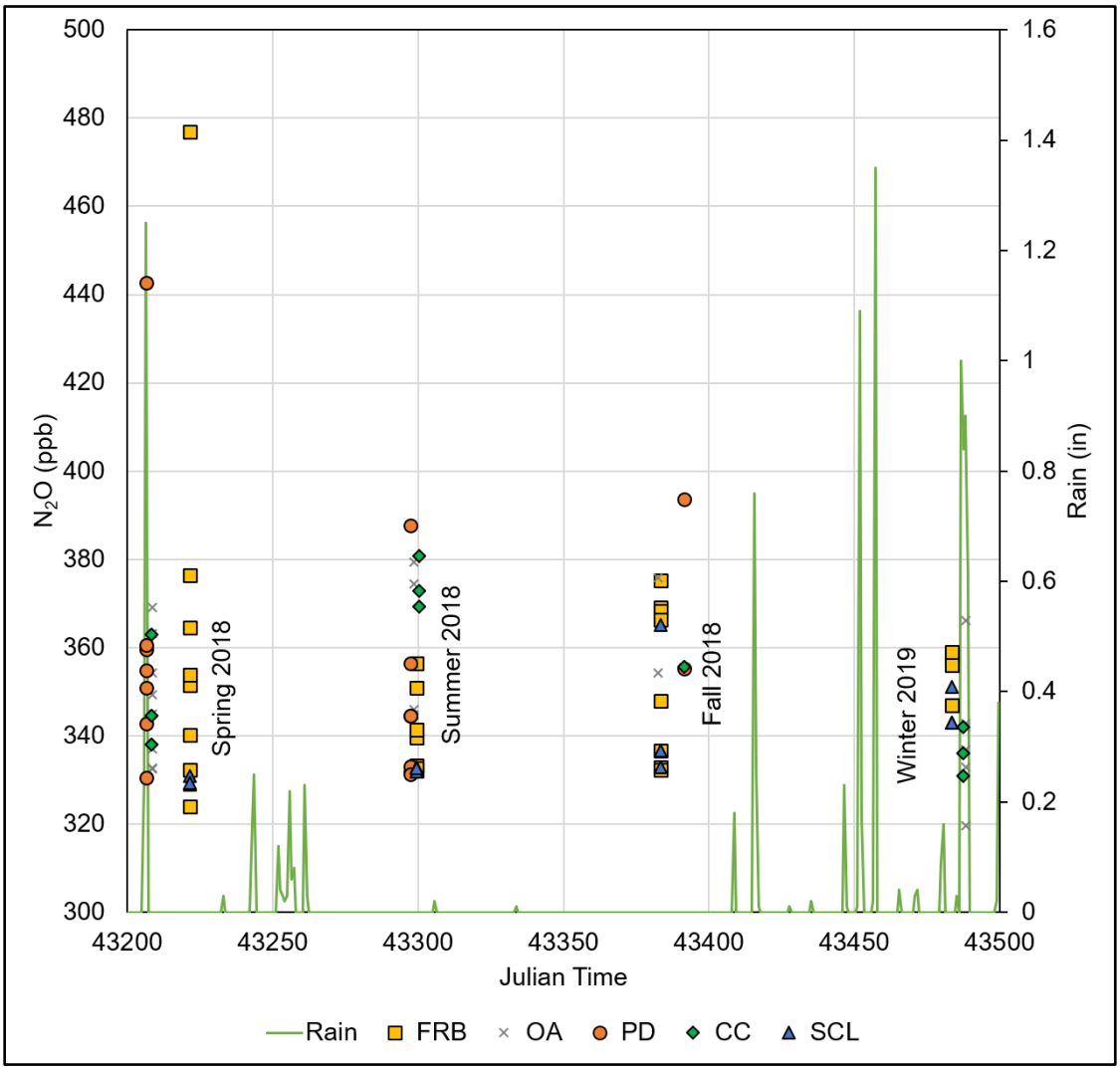


**Figure 7.4** The $N_2O$ mixing ratios (ppb) in samples collected at active landfills (Prima Deshecha "PD," Olinda Alpha "OA," and Frank R. Bowerman "FRB") and closed landfills (Santiago Canyon "SCL" and Coyote Canyon "CC"). Rainfall for Orange County during the same period is also shown. The global background of $N_2O$ was 331 ppb.

Annual rainfall for Orange County for 2018 and 2019 (University of California Agricultural and Natural Resources, 2021) was also included in Figure 7.4 because precipitation can increase anaerobic pockets conducive to $N_2O$ formation as well as form leachate. Leachate (i.e., the

contaminated liquid that seeps out of decomposing trash) can increase after rain and can create favorable conditions for $N_2O$ formation. The largest concern regarding $N_2O$ formation at landfills historically has been from this leachate because it contains a variety of organic and inorganic species and available space for nitrification and denitrification processes (Li et al., 2018). This is especially relevant for landfills with limited or outdated infrastructure, as the leachate can accumulate, release gases, and contaminate groundwater.

Orange County landfills have a dedicated leachate collection system to trap, enclose, and treat the water once it moves underground. Therefore, any emissions of $N_2O$ from collected leachate would not easily reach the atmosphere because the leachate is contained. However, contaminated water after a rainstorm could potentially generate $N_2O$ from leachate in the active dumping area when the water is still on the landfill surface, which is why the rainfall data are also shown. As shown in Figure 7.4, Summer 2018 followed a dry spell with little precipitation and Fall 2018 followed a very dry summer with little-to-no rainfall, while Spring 2018 and Winter 2019 followed periods of light rain. Figure 7.4 shows the nitrous oxide mixing ratios at Orange County landfills did not exhibit an obvious seasonal dependence. The average and standard deviation of $N_2O$ for Winter and Summer, which are considered “opposite” seasons, were very similar: 343±12 ppb in Winter 2019 and 346 ±16 ppb in Summer 2018 regardless of the difference in rainfall.

The values in Figure 7.4 are discussed separately for the active and closed landfills, starting with the active landfills below. The minimum, median, average, and maximum $N_2O$ mixing ratios at the active landfills (Prima Deshecha, Frank R. Bowerman, and Olinda Alpha) across all four seasons are shown in Table 7.2. The overall average and standard deviation of $N_2O$ at the active Orange County landfills was 351±24 ppb, a little higher than the global average of 331 ppb (Prinn et al., 2018). The active landfill $N_2O$ average was slightly lower than the dairy farm average (356±16 ppb), but the $N_2O$ at the active landfills had a higher standard deviation and more variability.

**Table 7.2** Minimum, median, average, and maximum $N_2O$ mixing ratios (ppb) at active Orange County landfills by season

| Season | $N_2O$ (ppb) | | | |
|---|---|---|---|---|
| | Minimum | Median | Average | Maximum |
| Spring 2018 | 320 | 347 | 355 | 477 |
| Summer 2018 | 331 | 341 | 344 | 388 |
| Fall 2018 | 332 | 361 | 360 | 394 |
| Winter 2019 | 327 | 341 | 344 | 374 |

Nitrous oxide at active landfills was elevated near active dumping areas for Spring 2018, Summer 2018, and Fall 2018. Unsurprisingly, the sample containing the maximum $N_2O$ in Winter 2019 (341 ppb) was collected right next to a sludge pile at Prima Deshecha landfill, which likely had the right combination of aerobic and anaerobic conditions for $N_2O$ formation. Sludge has already been established as an $N_2O$ emitter (Ahn et al., 2010; Massara et al., 2017) and it was not surprising that $N_2O$ was elevated nearby. Perhaps more interesting were the locations representing the minimum mixing ratios, as these imply what areas were *not* contributing $N_2O$.

The minimum for Spring 2018, 320 ppb, was collected at an area of the Olinda Alpha landfill that had not received waste since October 2017, six months before the sample was collected. The ground was covered with at least one foot of intermediate cover material. As $N_2O$ was more *depleted* over the old waste area than anywhere else at any active landfill during Spring 2018, it may be that $N_2O$ is not emitted in high quantities from deep within the Orange County landfills during the long decomposition process. This agrees with the information presented in Table 1.3 in Chapter 1.4.1, which showed that although the initial decomposition processes (Stages I – III) generate large quantities of gases including $CO_2$, acids, alcohols, $H_2$, and $CH_4$, the long-term underground process (Stage IV) generates primarily $CH_4$ and $CO_2$ and not necessarily $N_2O$ (Lisk, 1991; Crawford & Smith, 2016; Farquhar & Rovers, 1973). Additionally, as $N_2O$ requires pockets of aerobic conditions to form directly, it seems unlikely that the overwhelmingly anaerobic conditions deep within the landfill would be conducive to $N_2O$ formation. The

intermediate cover material and LFG extraction infrastructure likely also play a role in preventing rogue $N_2O$ emissions from outgassing from the surface of the landfill.

During Summer 2018, the minimum $N_2O$ mixing ratio, 331 ppb, was found at the weather station on the grounds of Prima Deshecha landfill, but upwind of the waste collection zone. This could imply that the air entering Prima Deshecha landfill was depleted in $N_2O$, and that certain locations at the landfill emitted small quantities of the gas. However, strangely enough, the *maximum* $N_2O$ mixing ratio during Summer 2018 at the active landfills was *also* found upwind of Prima Deshecha. This again implies that there were likely small contributors of $N_2O$ nearby, but no obvious emitters like the manure management system at the dairy farm.

During Fall 2018, the minimum value of $N_2O$, 332 ppb, was collected seven feet above the ground at Frank R. Bowerman landfill, in an area where at least a foot of intermediate cover material covered the landfill so that no trash was exposed. This area would lay dormant for a few months before trash would be piled on it once again. The lack of $N_2O$ at that location supports the idea that $N_2O$ is likely not part of the long-term waste decomposition process or that, if it is a minute part of the process (i.e., a “trace gas” constituent in Stage IV decomposition, constituting between 0 and 9% LFG), it was well-blocked by the cover materials and well-extracted by the LFG collection system.

Lastly, during Winter 2019, the minimum mixing ratio of $N_2O$, 327 ppb, was collected at a mulch pile at Olinda Alpha that the landfill engineers were going to use for alternative daily cover. This implies that using mulch has an added benefit—it likely does not emit high levels of $N_2O$, unlike sludge, which is also approved as a daily cover material and was responsible for the maximum $N_2O$ mixing ratio in Winter 2019.

The minimum, median, average, and maximum mixing ratios of $N_2O$ were also determined for the closed landfills (Coyote Canyon and Santiago Canyon) across all four seasons. These are shown in Table 7.3. Overall, the average and standard deviation of $N_2O$ at the closed landfills was

345±16 ppb, slightly lower than the active landfills with slightly less variability, and a little lower than the dairy farm $N_2O$ average. The $N_2O$ average at the closed landfills was closer to the AGAGE average of 331 ppb (Prinn et al., 2018), but still slightly enhanced.

**Table 7.3** Minimum, median, average, and maximum $N_2O$ mixing ratios (ppb) at closed Orange County landfills by season

| Season | $N_2O$ (ppb) | | | |
|---|---|---|---|---|
| | **Minimum** | **Median** | **Average** | **Maximum** |
| Spring 2018 | 329 | 334 | 339 | 363 |
| Summer 2018 | 332 | 351 | 353 | 381 |
| Fall 2018 | 333 | 346 | 348 | 365 |
| Winter 2019 | 331 | 343 | 341 | 351 |

For these closed landfills in Table 7.3, the minimum $N_2O$ mixing ratios during Spring 2018, Summer 2018, Fall 2018, and Winter 2019 were similar to each other and to the global $N_2O$ average from AGAGE. Although Summer 2018 had the highest median, average, and maximum mixing $N_2O$ ratios at the closed landfills, no clear seasonal trends were noted and again the lack of $N_2O$ could simply be the result of a lack of obvious sources. The lack of leachate, which can produce $N_2O$ but was not commonly found above ground at the Orange County landfills. The $N_2O$ in all cases was not much higher than the global background mixing ratio likely because of the modern landfill infrastructure, namely the underground leachate extraction system and LFG collection system. It is recommended that $N_2O$ from the leachate life cycle be further examined, but the amount of $N_2O$ emitted at Orange County landfills appears trivial compared to other sources globally.

### 7.3 Summary and Conclusion

Nitrous oxide is a very important GHG with a GWP of 298 times that of $CO_2$ on the 100-year scale. Understanding all its sources, even the small ones, is important when designing climate mitigation strategies. The Visalia dairy farm had an average mixing ratio of 356±16 ppb $N_2O$, a little higher than the global average of 331 ppb (Prinn et al., 2018). Nitrous oxide was not enhanced near areas of enteric fermentation, but it was enhanced near the manure management

system when specific ideal anaerobic and aerobic conditions were properly met. Mixing ratios of $N_2O$ at the dairy farm were the most enhanced near the manure management system, with a maximum of 448 ppb $N_2O$ collected downwind of the two lagoons. The EPA (2020c) and IPCC (Eggleston et al., 2006; Buendia et al., 2019) assume that the lagoons do not emit $N_2O$ because they do not contain enough waste solids to create the heterogenous crust needed to bridge the nitrification and denitrification processes. However, this study and previous literature (Owen & Silver, 2015) suggest otherwise. Therefore, it is recommended that lagoons are included in future inventories and an emission factor for lagoons is developed, as the scale up across all lagoons in the SJV would lead to a nontrivial amount of $N_2O$ emissions from manure management systems.

Orange County active landfills (Prima Deshecha, Olinda Alpha, and Frank R. Bowerman) and closed landfills (Coyote Canyon and Santiago Canyon) had an average of 349±22 ppb $N_2O$ overall. Active landfills had an average of 351±24 ppb $N_2O$ and closed landfills had an average of 346±16 ppb $N_2O$. This study supported that $N_2O$ production from underground decomposition, although likely minimal, is well-blocked by the intermediate and final cover materials because of the low mixing ratios found near the older waste areas at Olinda Alpha and Frank R. Bowerman and at the closed landfills. Leachate remains the primary concern for $N_2O$ formation, but Orange County landfills collect and trap leachate formed underground so that it does not easily leak or outgas into the atmosphere. This infrastructure combined with Orange County's minimal rainfall could have led to the low surface-level leachate formation and the corresponding low mixing ratios of $N_2O$ at the landfills.

Overall, it is recommended that $N_2O$ be monitored, particularly at landfills without the modern infrastructure of Orange County, especially if leachate is stored in open-air containers rather than in closed tanks. If emissions are low even with outdated or open waste management

strategies, it is not necessary to include $N_2O$ from landfills in future GHG inventories as the amount is trivial compared to other GHGs, like $CH_4$ and $CO_2$, that are released in large quantities.

## 7.4 References


Ahn, J. H., Kim, S., Park, H., Rahm, B., Pagilla, K., & Chandran, K. (2010). N2O emissions from activated sludge processes, 2008− 2009: results of a national monitoring survey in the United States. *Environmental Science & Technology*, *44*(12), 4505-4511.

Buendia, E., Tanabe, K., Kranjc, A., Baasansuren, J., Fukuda, M., Ngarize, S., ... & Federici, S. (2019). refinement to the 2006 IPCC guidelines for national greenhouse gas inventories. *IPCC: Geneva, Switzerland*.

Crawford, J. F., & Smith, P. G. (2016). *Landfill technology*. Elsevier.

Eggleston, S., Buendia, L., Miwa, K., Ngara, T., & Tanabe, K. (Eds.). (2006). *2006 IPCC guidelines for national greenhouse gas inventories* (Vol. 5). Hayama, Japan: Institute for Global Environmental Strategies.

Environmental Protection Agency (EPA). (2020c). Inventory of U.S. Greenhouse Gas Emissions and Sinks: 1990-2018. Retrieved from https://www.epa.gov/sites/production/files/2020-04/documents/us-ghg-inventory-2020-main-text.pdf

Farquhar, G. J., & Rovers, F. A. (1973). Gas production during refuse decomposition. *Water, Air, and Soil Pollution*, 2(4), 483-495.

Jiang, X., Ku, W. L., Shia, R. L., Li, Q., Elkins, J. W., Prinn, R. G., & Yung, Y. L. (2007). Seasonal cycle of $N_2O$: Analysis of data. *Global biogeochemical cycles*, *21*(1).

Levin, I., Ciais, P., Langenfelds, R., Schmidt, M., Ramonet, M., Sidorov, K., ... & Lloyd, J. (2002). Three years of trace gas observations over the EuroSiberian domain derived from aircraft sampling—a concerted action. *Tellus B: Chemical and Physical Meteorology*, *54*(5), 696-712.

Li, W., Sun, Y., Wang, H., & Wang, Y. N. (2018). Improving leachate quality and optimizing $CH_4$ and $N_2O$ emissions from a pre-aerated semi-aerobic bioreactor landfill using different pre-aeration strategies. *Chemosphere*, *209*, 839-847.

Lisk, D. J. (1991). Environmental effects of landfills. *Science of the total environment*, 100, 415-468.

Massara, T. M., Malamis, S., Guisasola, A., Baeza, J. A., Noutsopoulos, C., & Katsou, E. (2017). A review on nitrous oxide (N2O) emissions during biological nutrient removal from municipal wastewater and sludge reject water. *Science of the Total Environment*, *596*, 106-123.

Minschwaner, K., Salawitch, R. J., & McElroy, M. B. (1993). Absorption of solar radiation by $O_2$: Implications for $O_3$ and lifetimes of $N_2O$, $CFCl_3$, and $CF_2Cl_2$. *Journal of Geophysical Research: Atmospheres*, *98*(D6), 10543-10561.

Owen, J. J., & Silver, W. L. (2015). Greenhouse gas emissions from dairy manure management: a review of field-based studies. *Global change biology, 21*(2), 550-565.

Petersen, S. O., & Sommer, S. G. (2011). Ammonia and nitrous oxide interactions: roles of manure organic matter management. *Animal Feed Science and Technology, 166*, 503-513.

Prinn, R. G., Weiss, R. F., Arduini, J., Arnold, T., DeWitt, H. L., Fraser, P. J., ... & Zhou, L. (2018). History of chemically and radiatively important atmospheric gases from the Advanced Global Atmospheric Gases Experiment (AGAGE). *Earth System Science Data*, *10*(2), 985-1018.

Rinne, J., Pihlatie, M., Lohila, A., Thum, T., Aurela, M., Tuovinen, J. P., ... & Vesala, T. (2005). Nitrous oxide emissions from a municipal landfill. *Environmental science & technology, 39*(20), 7790-7793.

University of California Agricultural and Natural Resources. (2021). UCCE Orange County Weather: Irvine Monthly Totals. Retrieved from http://ceorange.ucanr.edu/about/weather/?weather=station&station=75

# 8. Air Pollution and Disadvantaged Communities

This work has examined the traces gases from dairy farms and landfills in California. Although landfills in Orange County are not necessarily built near disadvantaged communities, this is not the case for dairy farms. As shown in Chapter 1.3.3, dairy farms in the SJV are primarily located near or within disadvantaged communities. This means that these communities are affected by the trace gases emitted at these facilities in addition to their low socioeconomic status and exposure to other types of air pollution.

Although Orange County does not include as many disadvantaged communities as the SJV, it is also often a nonattainment area for $PM_{2.5}$ and ozone, meaning that the residents in the Los Angeles Air Basin still deal with a lot of pollution. Emissions at landfills and dairy farms are relatively easy to measure and target for reduction strategies in California because they are large and non-moving point sources. Other sources of emissions, such as vehicles, are more difficult to target for reduction strategies because they emit less per unit and do not remain in one place. This is important to consider when trying to implement statewide regulations.

On top of trying to clean up their local air quality, all counties in California must decrease GHG emissions to meet various state reduction requirements discussed in Chapter 1.2. This study confirmed that GHGs, particularly methane, are emitted in large quantities at landfills and dairy farms, with a large contribution from manure and enteric sources. The highest concentration of dairy farms in California is in the SJV, which is densely packed with disadvantaged communities. Excessive methane emissions pose a financial problem for farmers in these communities because they will need to decrease their emissions or face fines starting in 2024.

Overall, landfills in this study released smaller amounts of GHGs and other gases than dairy farms because of their modern engineering infrastructure, monitoring, and regulations. The biggest problem facing landfills is the evaporation and decomposition of chemicals in the actively dumped waste as well as the biogenic emissions from the daily cover material, which has the

potential to create ozone. Historically, dairy farms have not had the same incentives as landfills to clean up their emissions. Many of them are inherited family businesses that cannot always afford, or may not be receptive to, large infrastructural changes with high initial cost. However, there are still options—even state funding—for dairy farms to reduce their emissions. These are discussed in Chapter 8.5.1 and Chapter 8.5.2.

Out of the criteria pollutants listed with NAAQS in Table 1.1, California counties are most often nonattainment zones for PM and $O_3$ rather than for the other compounds. This chapter examines how the dairy farm and landfills contribute to this issue as well as odor. Air movement in the SJV was also determined. Following these discussions, potential solutions that could be implemented to decrease emissions at dairies and landfills are proposed.

## 8.1 Wind Direction in the San Joaquin Valley

As mentioned, the SJV contains the highest number of disadvantaged communities in the state. The direction of air flow through the SJV determines how heavily these communities are hit by gases from strong emitters, like landfills, dairy farms, vehicles, and other industries. If the wind direction blows *away* from most disadvantaged communities, that would not be as concerning as the wind blowing *through* the disadvantaged communities. Unfortunately, however, previous literature states that the typical wind direction is from the northwest (Western Regional Climate Center, 2008), so that was expected. For this study, the wind direction through the SJV was determined 1) by using a forward trajectory model and the Visalia dairy farm as a reference, and 2) using SARP data collected over the SJV.

### 8.1.1 Wind Direction from Forward Trajectories

To examine the forward trajectories of trace gases during the campaigns at the dairy site, 24-hour, 3-dimensional forward trajectories were run using the NOAA Air Resources Laboratory's Hybrid Single-Particle Lagrangian Integrated Trajectory (HYSPLIT) model (Stein et al., 2015). Global Data Assimilation System 0.5-degree meteorological data were used to compute forward

trajectories for the September 2018 and March 2019 campaigns. Global Forecast System 0.25-degree meteorological data were used to compute forward trajectories for the June 2019, September 2019, January 2020 campaigns.

All trajectories were computed at 100 m above ground level each hour, every hour for each campaign to determine the average movement of air from the Visalia dairy. Figure 8.1 shows example forward trajectories from January 14, 2020, during the most recent dairy campaign as a function of longitude, latitude, and altitude through the SJV, with disadvantaged communities marked according to the CalEnviroScreen 3.0 designation. Manually identified bovine-containing areas described in Chapter 2.4.1 were also marked for reference. The forward trajectories for the other campaigns looked similar, with air predominantly moving from the northwest. Starting at the northern region in the SJV, the air can pick up pollutants as it travels, spreading pollution through the disadvantaged communities downwind. According to Figure 8.1, air travels through highly concentrated farmland as it works its way through the SJV.

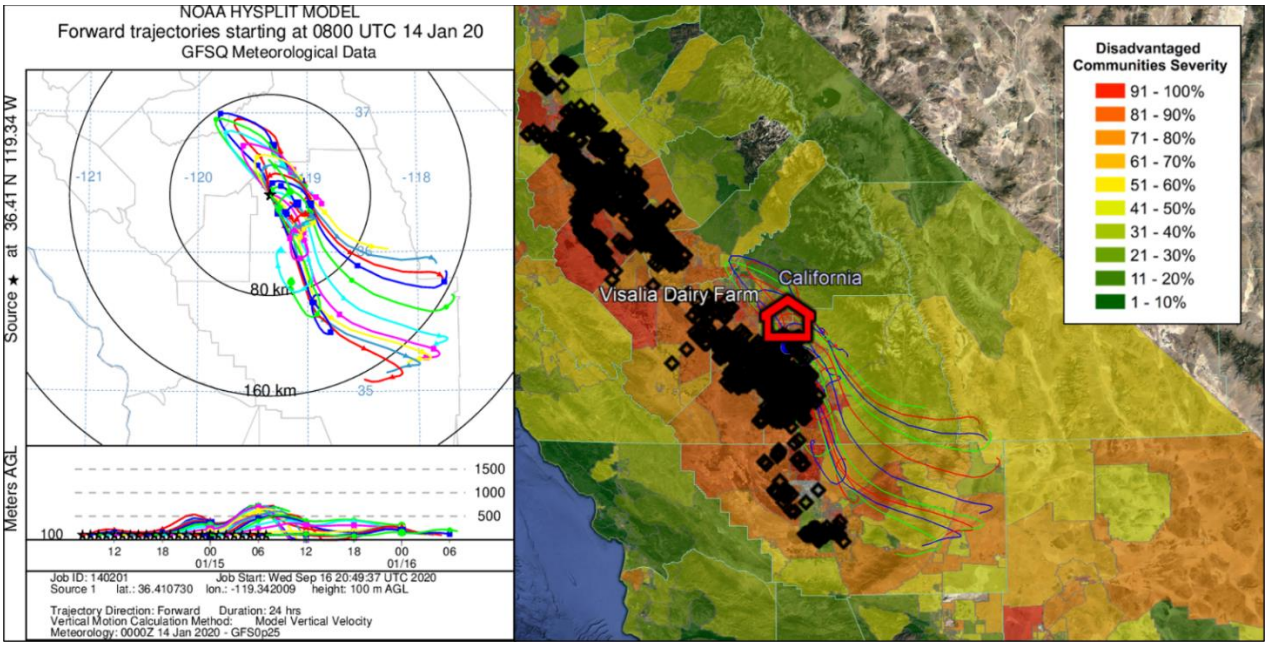


**Figure 8.1** HYSPLIT forward trajectories over 24 hours throughout the disadvantaged communities through the SJV from the dairy site in Visalia, CA on January 14, 2020 for the January 2020 campaign. Bovine-containing areas are also shown as black diamonds and the dairy farm is marked with a red building.

According to the HYSPLIT forward trajectories, the air from dairies, roadways, and other industries likely traveled through the surrounding disadvantaged communities throughout the SJV and other areas of California. For example, the HYSPLIT forward trajectory indicates that the air sampled in Visalia during the January 2020 campaign may have traveled south all the way to Kern County over a 24-hour period.

### 8.1.2 Wind Direction from Airborne Data

The wind direction and speed during all the SARP flights were also measured at a frequency of 1 $s^{-1}$ by the navigation software on the plane. These data were matched up to the middle of the sample duration for air samples collected by the Rowland-Blake lab's WAS instrument. The overall wind speed and direction for all SARP flights through the SJV is shown in Figure 8.2.

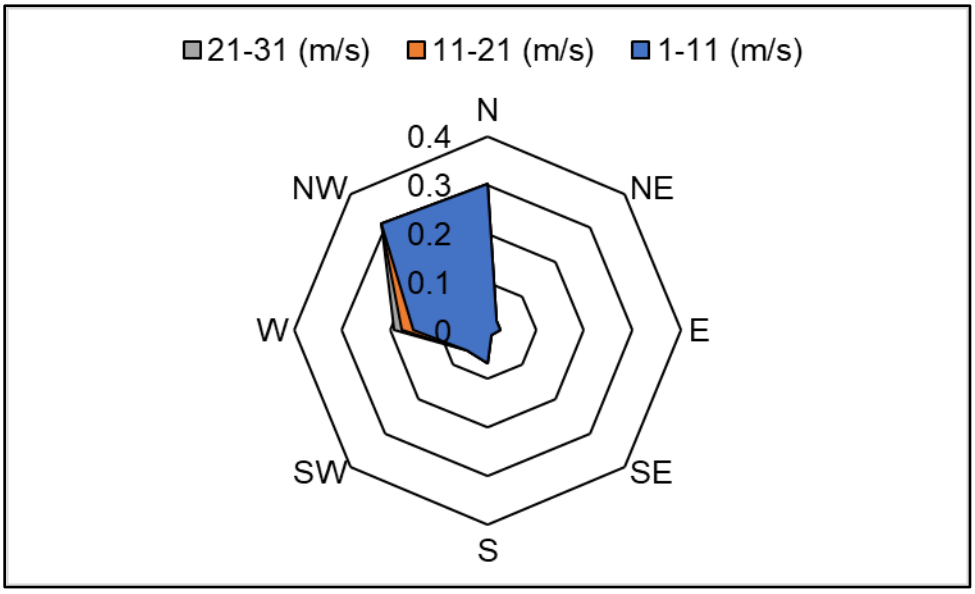


**Figure 8.2** Wind speed and direction for all SARP flights through the SJV used in this analysis.

Overall, the wind was mostly coming from the north, northwest, or west during the duration of the SARP flights. This implies that air traveled down the Valley over and through the disadvantaged communities at speeds ranging from 1–31 m/s depending on the flight. Figure 8.2 matched the expected wind directions for the SJV; previous literature has shown that the wind in

that area moves predominantly from the northwest (Western Regional Climate Center, 2008). There is not just the Visalia dairy farm the SJV. Thousands of other cow-containing areas share the space with bustling roadways, landfills, agricultural land, and oil and natural gas operations. This air mixes together and can travel long distances, affecting the people living in the area.

Using SARP data, the wind direction was confirmed to be predominantly from the northwest through the SJV. Therefore, the wind direction 1) shown in the HYSPLIT forward trajectories, 2) the data from the plane during SARP flights, and 3) reported in the literature all agreed: the wind primarily comes from the northwest and travels through the San Joaquin Valley. This implies that all the pollutants from dairy farms, oil and natural gas, agriculture, and transportation travel through disadvantaged communities where people work, live, and play. These communities are disproportionately burdened by high levels of pollution and often have low socioeconomic status.

**8.2 Ozone Formation Potential**

Ozone is a GHG and major pollutant in the troposphere. Blacet (1952) showed that it can be formed by the photolysis of $NO_2$ in Reaction 8-1 and subsequent reaction with oxygen in Reaction 8-2:

$$NO_2 + hv\ (\lambda \leq 420\ nm) \rightarrow NO + O(^3P) \qquad \text{Reaction 8-1}$$

$$O(^3P) + O_2 + M \rightarrow O_3 + M \qquad \text{Reaction 8-2}$$

However, ozone can also be formed from reactions of oxidized VOCs. Volatile organic compounds are commonly oxidized by hydroxyl radicals, which are formed mostly during the day by the photolysis of ozone, as shown in Reaction 8-3 and Reaction 8-4 (DeMore & Raper, 1966; Paraskevopoulos & Cvetanović, 1971; Vaghjiani & Ravishankara, 1991; Finlayson-Pitts & Pitts, 1999):

$$O_3 + hv\ (\lambda \leq 310\ nm) \rightarrow O_2 + O(^1D) \qquad \text{Reaction 8-3}$$

$$O(^1D) + H_2O \rightarrow 2\bullet OH \qquad \text{Reaction 8-4}$$

A hydroxyl radical can oxidize VOCs and eventually create an alkyl peroxy radical (Levy II, 1971; Atkinson, 2000; Finlayson-Pitts & Pitts, 1999; Heicklen, 1968). An example of this is shown for methane in Reaction 8-5 and Reaction 8-6.

$$CH_4 + \bullet OH \rightarrow \bullet CH_3 + H_2O \qquad \text{Reaction 8-5}$$

$$\bullet CH_3 + O_2 + M \rightarrow CH_3OO\bullet + M \qquad \text{Reaction 8-6}$$

In areas with motor vehicles, such as in Orange County or the SJV, $NO_x$ is a commonly found pollutant (Haagen-Smit, 1952; Calvert, 1976). This $NO_x$, as NO, can react with the alkyl peroxy radical to form $NO_2$ (Heicklen, 1968; Nicolet, 1970; Atkinson, 2000; Finlayson-Pitts & Pitts, 1999). This is shown in Reactions 8-7 through 8-9.

$$CH_3OO\bullet + NO \rightarrow CH_3O\bullet + NO_2 \qquad \text{Reaction 8-7}$$

$$CH_3O\bullet + O_2 \rightarrow HCHO + HOO\bullet \qquad \text{Reaction 8-8}$$

$$HOO\bullet + NO \rightarrow \bullet OH + NO_2 \qquad \text{Reaction 8-9}$$

The $NO_2$ formed in Reaction 8-9 can go on to make $O_3$ through the steps shown in Reaction 8-1 and Reaction 8-2. These steps can occur for various molecules at different rates. Alkenes and other molecules go through similar steps as Reaction 8-5 and Reaction 8-6 to become oxidized to an $RO_2$ radical, which can form $O_3$ when $NO_x$ is present. The potential production of ozone was determined from a variety of VOCs at the dairy farm and Orange County landfills.

As shown above, the concentration of VOCs and $NO_x$ are important for ozone formation in areas such as the SJV and Orange County. Two different methods were considered for calculating the ozone creation potential of VOCs released at the landfills and dairy farm: maximum incremental reactivity (MIR) (Carter et al., 1995) and photochemical ozone creation potential (POCP) (Derwent & Jenkin, 1991). Carter et al. (1995) introduced the MIR method to determine the maximum reactive conditions of VOCs in high $NO_x$ conditions when ozone formation is most sensitive to the VOC concentration. Carter (2009) updated the original MIR values. Derwent and Jenkin (1991) introduced the POCP method by simulating the ozone formation by various VOCs

using a photochemical trajectory model under European atmospheric conditions. Derwent et al. (2007) revised and added some POCP values. To determine whether the MIR or POCP paradigm should be used for the calculations in this study, it was first considered whether the study areas were more likely $NO_x$-limited or VOC-limited.

At high VOC/$NO_x$ ratios, decreasing the VOC concentration barely alters the $O_3$ concentration, while decreasing the $NO_x$ concentration more easily decreases the $O_3$ concentration. These areas tend to be rural, suburban, or downwind and are known as "$NO_x$-limited." On the contrary, at low VOC/$NO_x$ ratios, decreasing the VOC concentration more easily decreases the $O_3$ concentration, while decreasing the $NO_x$ concentration does not quickly decrease the $O_3$ concentration. Areas like these, which tend to be major city centers like downtown Los Angeles, are known as "VOC-limited" (Finlayson-Pitts & Pitts, 1999). The study areas of the SJV and Orange County may be thought of as "$NO_x$-limited" because they are not primarily major urban city centers. After combining this reasoning with the fact that the SJV counties and Orange County are consistently attainment areas for $NO_2$ (meaning they likely do not have an excess of $NO_x$), it was decided that the region is more likely "$NO_x$-limited," but the POCP approach and the MIR approach were both used for this analysis.

Derwent et al. (2007) listed POCP values for a variety of alkanes, alkenes, aromatics, cycloalkanes, oxygenates, and halocarbons. To calculate the ozone formation potential using Derwent's POCP values, Equation 8-1 from Shin et al. (2013) was used:

$$\text{Ozone formation potential (OFP)}\left(\frac{\mu g}{m^3}\right) = \text{VOC (ppb)} * \frac{\text{molecular weight}\left(\frac{g}{mol}\right)}{22.4\ \text{mol}^{-1}} * \text{POCP} \qquad \text{Equation 8-1}$$

This formula calculates the ozone formation potential (OFP) by multiplying the VOC mixing ratio by its molecular weight and the POCP value found in Derwent et al. (2007), all divided by a constant. The biggest limitation to using the POCP scale for this study was that Derwent et al. (2007) originally intended it to be used under European atmospheric conditions, which would likely be different than those in California. However, using the POCP values for this study allows readers

to compare relative contributions of gases at the landfill and dairy farm to determine which VOCs may contribute significant quantities of ozone to those areas.

This study also used the updated MIR values found in Carter (2009) to calculate the OFP using the concentration of forty-three VOCs. This was calculated using Equation 8-2:

$$\text{Ozone formation potential (OFP)} = [\text{VOC}] * \frac{\text{MW}}{\text{NA}} * \text{MIR} \qquad \text{Equation 8-2}$$

where

OFP = ozone formation potential, in (μg $O^3/m^3$)

[VOC] = VOC concentration, in (molecules VOC/$m^3$)

MW = molecular weight, in (μg VOC/mol VOC)

NA = Avogadro's number, $6.022 \times 10^{23}$ molecules VOC/mol VOC

MIR = μg $O^3$/ μg VOC

Carter (2009) calculated these MIR values based on the Los Angeles Air Basin, a likely VOC-limited region, and not necessarily for use in the SJV. However, they are used in this study for the dairy and the landfills to compare the relative contributions from VOCs.

### 8.2.1 Ozone Formation Potential at the Dairy Farm

The OFP was calculated using the POCP values found in Derwent et al. (2007) for forty different VOCs found at the dairy farm during the March 2019, June 2019, September 2019, and January 2020 campaigns. The September 2018 campaign was missing data for a handful of the forty compounds and was not used for the analysis in Chapter 8.2.1. The OFP was calculated using the median and maximum mixing ratios of each gas found at the dairy farm during each campaign to determine potential amounts of ozone that could be created using Equation 8-1 with POCP values from Derwent et al. (2007). These data are shown organized by compound class in Table 8.1. Red, bolded text indicates $O_3$ concentrations that exceeded the eight-hour standard in NAAQS, 0.070 ppm $O_3$, or 137 μg $O_3$ $m^{-3}$.

**Table 8.1** Ozone formation potential at the dairy farm by season calculated from the median (med) and maximum (max) mixing ratios of various VOCs and POCP values (Derwent et al., 2007). Red, bolded values indicate $O_3$ > NAAQS (0.070 ppm).

| Class | Compound | Ozone Formation Potential (μg/m³) | | | | | | | |
|---|---|---|---|---|---|---|---|---|---|
| | | March 2019 | | June 2019 | | Sept. 2019 | | Jan. 2020 | |
| | | Med | Max | Med | Max | Med | Max | Med | Max |
| Alkane | Ethane | 29 | 72 | 10 | 18 | 14 | 89 | 36 | 49 |
| Alkane | i-Butane | 10 | 34 | 6 | 14 | 4 | 45 | 23 | 42 |
| Alkane | i-Pentane | 11 | 92 | 9 | 20 | 5 | **181** | 22 | 51 |
| Alkane | n-Butane | 19 | 79 | 8 | 9 | 4 | 32 | 43 | 89 |
| Alkane | n-Heptane | 6 | 9 | 3 | 7 | 3 | 9 | 4 | 13 |
| Alkane | n-Hexane | 6 | 98 | 4 | 95 | 5 | **386** | 20 | **741** |
| Alkane | n-Pentane | 11 | 59 | 9 | 25 | 7 | 119 | 32 | 157 |
| Alkane | Propane | 32 | **161** | 16 | 46 | 14 | 60 | 58 | 124 |
| Alkene | 1-Butene | 16 | 28 | 7 | 38 | 6 | 135 | 9 | 59 |
| Alkene | 1-Pentene | 5 | 7 | 5 | 12 | 7 | 35 | 6 | 26 |
| Alkene | cis-2-Butene | < LOD | 0 | 4 | 4 | 4 | 39 | 6 | 12 |
| Alkene | Ethene | 31 | **220** | 21 | **280** | 21 | **371** | 87 | **302** |
| Alkene | i-Butene | 8 | 37 | 8 | 25 | 8 | 74 | 7 | 128 |
| Alkene | Isoprene | 8 | 90 | 99 | **187** | 34 | **151** | 10 | **182** |
| Alkene | Limonene | **418** | **6683** | **272653** | **2172322** | **197** | **2016** | 47 | **13311** |
| Alkene | Propene | 12 | 133 | 11 | 114 | 11 | **440** | 22 | 110 |
| Alkene | trans-2-Butene | 5 | 8 | 4 | 8 | 5 | 53 | 5 | 19 |
| Alkyne | Ethyne | 4 | 10 | 1 | 10 | 1 | 3 | 4 | 9 |
| Aromatic | 2-Ethyltoluene | 7 | 14 | 5 | 7 | 4 | 8 | 5 | 16 |
| Aromatic | 3-Ethyltoluene | 9 | 25 | 5 | 10 | 6 | 25 | 7 | 17 |
| Aromatic | 4-Ethyltoluene | 6 | 16 | 4 | 7 | 5 | 11 | 4 | 14 |
| Aromatic | Benzene | 3 | 10 | 1 | 4 | 2 | 13 | 4 | 10 |
| Aromatic | Ethylbenzene | 9 | 20 | 3 | 6 | 3 | 19 | 5 | 17 |
| Aromatic | o-Xylene | 14 | 31 | 4 | 8 | 7 | 24 | 7 | 20 |
| Aromatic | Toluene | 12 | **403** | 22 | 92 | 12 | 119 | 25 | 56 |
| Halocarbon | 1,2-DCE | 11 | 19 | 4 | 6 | 4 | 6 | 7 | 8 |
| Halocarbon | $C_2Cl_4$ | 0 | 0 | 0 | 0 | 0 | 0 | 0 | 0 |
| Halocarbon | $C_2HCl_3$ | 0 | 0 | 0 | 1 | 0 | 0 | 1 | 69 |
| Halocarbon | $CH_2Cl_2$ | 1 | 3 | 1 | 1 | 1 | 2 | 1 | 2 |
| Halocarbon | $CH_3CH_2Cl$ | 0 | 1 | 0 | 0 | 0 | 1 | 0 | 0 |
| Halocarbon | $CH_3Cl$ | 1 | 2 | 1 | 2 | 1 | 2 | 1 | 2 |
| Oxygenate | 2-Butanol | **163** | **777** | 17 | **4373** | 8 | **1414** | 30 | **813** |
| Oxygenate | Acetaldehyde | **137** | **4610** | **267** | **5607** | **274** | **2204** | **298** | **4251** |
| Oxygenate | Acetone | 116 | **557** | **175** | **944** | **190** | **1491** | **208** | **924** |
| Oxygenate | Butanal | 11 | **503** | 15 | **146** | 26 | **487** | 17 | **392** |
| Oxygenate | Butanone | 22 | **1450** | 21 | 96 | 32 | **411** | 44 | **438** |
| Oxygenate | Ethanol | **260** | **493897** | **1983** | **225716** | **437** | **55373** | **3115** | **92037** |
| Oxygenate | Methanol | **299** | **5256** | **1021** | **6656** | **591** | **3551** | **633** | **6233** |
| Oxygenate | Methyl isobutyl ketone | < LOD | 0 | 6 | 29 | 7 | 45 | 5 | 34 |
| **Total** | | 1713 | 515413 | 276433 | 2416946 | 1959 | 69442 | 4862 | 120778 |

The OFP in Table 8.1 was calculated using the median and maximum mixing ratios to determine the “typical” ozone concentrations that would be produced compared to the absolute maximum. As shown in Table 8.1, limonene, acetaldehyde, methanol, ethanol and occasionally acetone and 2-butanol likely form significant ozone concentrations at the dairy farm out of the VOCs measured during those four campaigns.

Chapter 5.1 showed that methanol, ethanol, and acetaldehyde were enhanced near various locations at the dairy farm. For example, methanol was enhanced near cow breath, free stalls, outdoor cows (i.e., dry cows and heifers), and lagoons. Ethanol was enhanced near the cow breath, free stalls, outdoor cows, and silage. Lastly, acetaldehyde was enhanced near the lagoons and the outdoor cows. Acetone, although not previously discussed, was similar to methanol and was enhanced near cow breath and free stall areas. Limonene was largely enhanced near outdoor cows, the free stalls, and silage. It seemed likely that limonene was coming from the feed directly. Finally, 2-butanol was also enhanced greatly near silage. Overall, the high mixing ratios of oxygenates and alkenes found near the cows and their feed were likely responsible for much of the dairy farm contribution to $O_3$ formation from the VOCs in Table 8.1.

The OFP was also calculated using the median and maximum mixing ratios of forty-one VOCs found at the dairy farm during each campaign and the MIR values presented in Carter (2009) to determine potential amounts of ozone that could be created using Equation 8-2. These data are shown organized by compound class in Table 8.2. Red, bolded text indicates $O_3$ concentrations that exceeded the NAAQS, 0.070 ppm $O_3$, or 137 μg $O_3$ $m^{-3}$. Although Carter (2009) included an MIR value for methane, its contribution to ozone was not considered because of its long lifetime.

**Table 8.2** Ozone formation potential at the dairy farm by season calculated from the median (med) and maximum (max) mixing ratios of various VOCs and MIR values (Carter, 2009). Red, bolded values indicate $O_3$ > NAAQS (0.070 ppm).

| Class | Compound | Ozone Formation Potential (µg/m³) | | | | | | | |
|---|---|---|---|---|---|---|---|---|---|
| | | March 2019 | | June 2019 | | Sept. 2019 | | Jan. 2020 | |
| | | Med | Max | Med | Max | Med | Max | Med | Max |
| Alkane | Ethane | 1 | 2 | 0 | 1 | 0 | 3 | 1 | 2 |
| Alkane | i-Butane | 0 | 1 | 0 | 1 | 0 | 2 | 1 | 2 |
| Alkane | i-Pentane | 0 | 4 | 0 | 1 | 0 | 7 | 1 | 2 |
| Alkane | n-Butane | 1 | 3 | 0 | 0 | 0 | 1 | 1 | 3 |
| Alkane | n-Heptane | 0 | 0 | 0 | 0 | 0 | 0 | 0 | 0 |
| Alkane | n-Hexane | 0 | 3 | 0 | 3 | 0 | 11 | 1 | 21 |
| Alkane | n-Pentane | 0 | 2 | 0 | 1 | 0 | 4 | 1 | 5 |
| Alkane | Propane | 1 | 5 | 1 | 1 | 0 | 2 | 2 | 4 |
| Alkene | 1-Butene | 1 | 2 | 0 | 2 | 0 | 8 | 1 | 3 |
| Alkene | 1-Pentene | 0 | 1 | 0 | 1 | 1 | 2 | 0 | 2 |
| Alkene | cis-2-Butene | 0 | 0 | 0 | 0 | 0 | 5 | 1 | 1 |
| Alkene | Ethene | 3 | 18 | 2 | 23 | 2 | 31 | 7 | 25 |
| Alkene | i-Butene | 1 | 5 | 1 | 3 | 1 | 10 | 1 | 18 |
| Alkene | Isoprene | 1 | 8 | 8 | 16 | 3 | 13 | 1 | 16 |
| Alkene | Limonene | 25 | **392** | **15987** | **127376** | 12 | 118 | 3 | **781** |
| Alkene | Propene | 1 | 12 | 1 | 10 | 1 | 40 | 2 | 10 |
| Alkyne | Ethyne | 1 | 1 | 0 | 1 | 0 | 0 | 0 | 1 |
| Alkene | trans-2-Butene | 1 | 1 | 0 | 1 | 1 | 6 | 1 | 2 |
| Aromatic | 2-Ethyltoluene | 1 | 1 | 0 | 0 | 0 | 1 | 0 | 1 |
| Aromatic | 3-Ethyltoluene | 1 | 2 | 0 | 1 | 1 | 2 | 1 | 1 |
| Aromatic | 4-Ethyltoluene | 0 | 1 | 0 | 0 | 0 | 1 | 0 | 1 |
| Aromatic | Benzene | 0 | 1 | 0 | 0 | 0 | 1 | 0 | 1 |
| Aromatic | Ethylbenzene | 19 | 42 | 7 | 13 | 7 | 41 | 11 | 36 |
| Aromatic | o-Xylene | 1 | 3 | 0 | 1 | 1 | 2 | 1 | 2 |
| Aromatic | Toluene | 1 | 33 | 2 | 8 | 1 | 10 | 2 | 5 |
| Halocarbon | 1,2-DCE | 0 | 1 | 0 | 0 | 0 | 0 | 0 | 0 |
| Halocarbon | $C_2Cl_4$ | 0 | 0 | 0 | 0 | 0 | 0 | 0 | 0 |
| Halocarbon | $C_2HCl_3$ | 0 | 0 | 0 | 0 | 0 | 0 | 0 | 1 |
| Halocarbon | $CCl_4$ | 0 | 0 | 0 | 0 | 0 | 0 | 0 | 0 |
| Halocarbon | $CH_2C_{l2}$ | 0 | 0 | 0 | 0 | 0 | 0 | 0 | 0 |
| Halocarbon | $CH_3Br$ | 0 | 0 | 0 | 0 | 0 | 0 | 0 | 0 |
| Halocarbon | $CHCl_3$ | 0 | 0 | 0 | 0 | 0 | 0 | 0 | 0 |
| Other | CO | 10 | 19 | 7 | 14 | 9 | 18 | 11 | 25 |
| Oxygenate | 2-Butanol | 5 | 24 | 1 | 136 | 0 | 44 | 1 | 25 |
| Oxygenate | Acetaldehyde | 15 | **502** | 29 | **610** | 30 | **240** | 32 | **463** |
| Oxygenate | Acetone | 6 | 31 | 10 | 52 | 10 | 82 | 11 | 51 |
| Oxygenate | Butanal | 1 | 39 | 1 | 11 | 2 | 38 | 1 | 31 |
| Oxygenate | Butanone | 1 | 61 | 1 | 4 | 1 | 17 | 2 | 19 |
| Oxygenate | Ethanol | 11 | **20337** | 82 | **9294** | 18 | **2280** | 128 | **3790** |
| Oxygenate | Methanol | 14 | **248** | 48 | **314** | 28 | **167** | 30 | 294 |
| Oxygenate | Methyl isobutyl ketone | 0 | 0 | 0 | 2 | 0 | 2 | 0 | 2 |
| **Total** | | 196 | 22425 | 16223 | 141973 | 170 | 4344 | 348 | 9492 |

Using the MIR values presented in Carter (2009) led to OFP values that were lower overall than those presented in Table 8.1. However, the overall trend was the same: the oxygenates and alkenes dominated the potential ozone formation, with small contribution from the aromatic compounds.

In the future, more studies should be performed to determine the contribution of ozone from all dairy farms in the SJV. It is important to consider these farms as potential point sources of ozone in a region that is usually a nonattainment zone. Communities downwind of the dairy farms suffer the consequences of VOC emissions and subsequent ozone formation, which is correlated with negative human health effects and environmental impacts.

### 8.2.2 Ozone Formation Potential at the Orange County Landfills

Although the OFP in Chapter 8.2 was calculated for gases measured at the landfills and dairy farms, one must first applaud the incredible engineering of California landfills, particularly in Orange County. Based on the near-background levels of many trace gases at the closed Orange County landfills, it is evident that the infrastructure successfully prevents many rogue emissions from escaping. This is at least partly because of California's thick final cover material requirements. Overall, landfills in the state of California have some of the strictest requirements in the country and are even stricter than other states on the West Coast. As a reminder, California requires 6 inches of daily cover, 12 inches of intermediate cover, and a total of at least 4 feet of final cover (Closure and Post-Closure Maintenance Requirements for Solid Waste Landfills, 1997). For example, although the state of Oregon also requires 6 inches of daily cover material and 12 inches of intermediate cover material, their requirements for final cover are less strict. Oregon landfills need 18 inches of earthen material plus 6 inches on top to promote plant growth, for a total of only 2 feet of final cover (Criteria for Municipal Solid Waste Landfills, 1997). As another example, Washington state's landfills only need 0.76 millimeters of geomembrane, plus 2 feet of compacted soil, and finally 1 foot of anti-erosion vegetative layer for a total of about 3

feet of final cover material (Criteria for Municipal Solid Waste Landfills, 1993). Although California appears to lead the West Coast in landfill innovation and upkeep, this chapter shows that improvements could still be made, including reducing emissions from ADC and increasing waste enforcement.

Although landfills are emitting much less than they would have been decades ago, there is still room for improvement, particularly around the potential creation of secondary pollutants like ozone. The OFP at the Orange County landfills during the Spring 2018 and Summer 2018 campaigns was calculated for fifty-seven different VOCs using the POCP values from Derwent et al. (2007) for Equation 8-1. These data are shown in Table 8.3. Red, bolded text indicates $O_3$ concentrations that exceeded the NAAQS for ozone, 0.070 ppm $O_3$, or 137 µg $O_3$ $m^{-3}$.

**Table 8.3** Ozone formation potential at the Orange County landfills by season calculated from the median (med) and maximum (max) mixing ratios of various VOCs and the POCP values in Derwent et al. (2007). Red, bold values indicate $O_3$ > NAAQS (0.070 ppm).

| Class | Compound | Ozone Formation Potential (µg/m$^3$) | | | |
|---|---|---|---|---|---|
| | | Spring 2018 | | Summer 2018 | |
| | | Med | Max | Med | Max |
| Alkane | 2,2-Dimethylbutane | 3 | 70 | 7 | **267** |
| Alkane | Ethane | 30 | 58 | 13 | 60 |
| Alkane | i-Butane | 23 | **2421** | 22 | **2639** |
| Alkane | i-Pentane | 52 | **3203** | 31 | **4197** |
| Alkane | n-Butane | 35 | **1073** | 20 | **2248** |
| Alkane | n-Decane | 3 | 109 | 5 | **1350** |
| Alkane | n-Heptane | 4 | 48 | 4 | 105 |
| Alkane | n-Hexane | 6 | 91 | 6 | 90 |
| Alkane | n-Nonane | 5 | **173** | 3 | **771** |
| Alkane | n-Octane | 2 | 44 | 3 | **184** |
| Alkane | n-Pentane | 17 | **484** | 13 | **704** |
| Alkane | n-Undecane | 3 | **277** | 3 | **725** |
| Alkane | Propane | 33 | **635** | 34 | **896** |
| Alkene | 1-Butene | 9 | **166** | 11 | **218** |
| Alkene | 1-Pentene | 1 | 55 | 2 | 34 |
| Alkene | α-Pinene | 6 | **19738** | 11 | **6713** |
| Alkene | β-Pinene | 3 | **6801** | 2 | **1416** |
| Alkene | cis-2-Butene | 1 | 13 | 1 | 15 |
| Alkene | cis-2-Pentene | 0 | 14 | 0 | 12 |

| | | | | | |
|---|---|---|---|---|---|
| Alkene | Ethene | 36 | 120 | 36 | **264** |
| Alkene | i-Butene | 9 | 70 | 6 | 40 |
| Alkene | Isoprene | 9 | 65 | 20 | 123 |
| Alkene | Limonene | 3 | **7212** | 8 | **13354** |
| Alkene | Propene | 22 | **208** | 25 | **411** |
| Alkene | trans-2-Butene | 1 | 20 | 1 | 9 |
| Alkene | trans-2-Pentene | 1 | **441** | 0 | 30 |
| Alkyne | Ethyne | 4 | 24 | 3 | 7 |
| Aromatic | 1,2,3-Trimethylbenzene | 5 | **4299** | 6 | **1528** |
| Aromatic | 1,2,4-Trimethylbenzene | 11 | **153** | 11 | **2033** |
| Aromatic | 1,3,5-Trimethylbenzene | 3 | 41 | 3 | **587** |
| Aromatic | 2-Ethyltoluene | 3 | 25 | 2 | **342** |
| Aromatic | 4-Ethyltoluene | 2 | 25 | 2 | **327** |
| Aromatic | Benzene | 3 | 5 | 2 | 9 |
| Aromatic | Ethylbenzene | 3 | 62 | 4 | **833** |
| Aromatic | i-Propylbenzene | 0 | 5 | 0 | **338** |
| Aromatic | m-Ethyltoluene | 5 | 78 | 6 | **871** |
| Aromatic | n-Propylbenzene | 1 | 12 | 1 | 135 |
| Aromatic | o-Xylene | 6 | 104 | 7 | **1782** |
| Aromatic | Toluene | 16 | **260** | 23 | **2059** |
| Cycloalkane | Cyclohexane | 2 | 25 | 3 | 73 |
| Cycloalkane | Methylcyclohexane | 2 | 25 | 8 | **404** |
| Cycloalkane | Methylcyclopentane | 8 | 48 | 8 | 104 |
| Halocarbon | 1,2-DCE | 10 | 71 | 6 | 131 |
| Halocarbon | $C_2Cl_4$ | 0 | 0 | 0 | 18 |
| Halocarbon | $C_2HCl_3$ | 0 | 9 | 0 | 53 |
| Halocarbon | $CH_2Cl_2$ | 1 | 19 | 1 | 26 |
| Halocarbon | $CH_3CH_2Cl$ | 0 | 2 | 0 | 1 |
| Halocarbon | $CH_3Cl$ | 1 | 2 | 1 | 2 |
| Oxygenate | 2-Butanol | 4 | 33 | 5 | 102 |
| Oxygenate | Acetaldehyde | **273** | **1217** | **230** | **6406** |
| Oxygenate | Acetone | **213** | **1388** | 79 | **2827** |
| Oxygenate | Butanal | 71 | **1749** | **168** | **61733** |
| Oxygenate | Butanone | 29 | **8847** | 68 | **22462** |
| Oxygenate | Ethanol | 125 | **59992** | **240** | **177000** |
| Oxygenate | Isopropanol | 7 | **965** | 23 | **15345** |
| Oxygenate | Methanol | 60 | **16942** | 98 | **29448** |
| Oxygenate | Methyl isobutyl ketone | 4 | 29 | 5 | **476** |
| **Total** | | 1192 | 140066 | 1299 | 364337 |

Again, like at the dairy farm, the alkenes and oxygenates dominated potential ozone formation with some contribution from alkanes and aromatics. During Spring 2018, maximum ethanol, α-pinene, methanol, and butanone mixing ratios could have produced significant ozone concentrations. Also, during Spring 2018, the median acetaldehyde, acetone, ethanol, and butanal could have produced the highest "typical" ozone concentrations (calculated with the median VOC mixing ratios).

During Summer 2018, maximum ozone concentrations could have been produced by ethanol, butanal, methanol, and butanone, while the "typical" ozone concentrations (calculated with the median VOC mixing ratios) could have been produced by ethanol, acetaldehyde, butanal, and methanol. Acetone, isopropanol, β-pinene, and limonene were often big contributors to OFP as well. These are all gases that could be produced biogenically *and* during waste decomposition, so it is likely that they originated from the organic daily cover material, on-site compost, and active dumping. More information about the green organic material in the form of cover and compost is discussed more in Chapter 8.5.3. Table 8.4 shows the OFP of eighty VOCs at the Orange County landfills using the MIR values from Carter (2009) and the formula in Equation 8-2. Although Carter (2009) included an MIR value for methane, its contribution to ozone was excluded because of its long lifetime.

**Table 8.4** Ozone formation potential at the Orange County landfills by season calculated from the median (med) and maximum (max) mixing ratios of various VOCs and MIR values (Carter, 2009). Red, bolded values indicate $O_3$ > NAAQS (0.070 ppm).

| Class | Compound | Spring 2018 | | Summer 2018 | |
|---|---|---|---|---|---|
| | | Med | Max | Med | Max |
| Alkane | 2,2,4-Trimethylpentane | 0 | 2 | n/a | n/a |
| Alkane | 2,2-Dimethylbutane | 0 | 3 | 0 | 4 |
| Alkane | 2,3-Dimethylpentane | 0 | 1 | 0 | 2 |
| Alkane | 2,4-Dimethylpentane | 0 | 2 | n/a | n/a |
| Alkane | 2-Methylhexane | 0 | 5 | n/a | n/a |
| Alkane | 3-Methylhexane | 1 | 8 | n/a | n/a |
| Alkane | 3-Methylpentane | 0 | 2 | n/a | n/a |
| Alkane | Ethane | 1 | 2 | 0 | 2 |

| | | | | | |
|---|---|---|---|---|---|
| Alkane | i-Butane | 1 | 97 | 1 | 106 |
| Alkane | i-Pentane | 2 | 125 | 1 | **164** |
| Alkane | n-Butane | 1 | 36 | 1 | 76 |
| Alkane | n-Decane | 0 | 2 | 0 | 23 |
| Alkane | n-Heptane | 0 | 1 | 0 | 3 |
| Alkane | n-Hexane | 0 | 3 | 0 | 3 |
| Alkane | n-Nonane | 0 | 4 | 0 | 16 |
| Alkane | n-Octane | 0 | 1 | 0 | 4 |
| Alkane | n-Pentane | 1 | 15 | 0 | 21 |
| Alkane | n-Undecane | 0 | 4 | 0 | 11 |
| Alkane | Propane | 1 | 20 | 1 | 29 |
| Alkene | 1-Butene | 1 | 9 | 1 | 12 |
| Alkene | 1-Pentene | 0 | 4 | 0 | 2 |
| Alkene | 2-Methyl-1-butene | 0 | 1 | 0 | 1 |
| Alkene | 2-Methyl-2-butene | 0 | **145** | n/a | n/a |
| Alkene | 3-Carene | 0 | **161** | 0 | 15 |
| Alkene | 3-Methyl-1-butene | 0 | 1 | 0 | 1 |
| Alkene | alpha-Pinene | 0 | **1198** | 1 | **407** |
| Alkene | alpha-Terpinene | 0 | 32 | n/a | n/a |
| Alkene | beta-Phellandrene | 0 | 103 | 0 | 18 |
| Alkene | beta-Pinene | 0 | **664** | 0 | **138** |
| Alkene | Camphene | 0 | 9 | 0 | 9 |
| Alkene | cis-2-Butene | 0 | 2 | 0 | 2 |
| Alkene | cis-2-Pentene | 0 | 1 | 0 | 1 |
| Alkene | Ethene | 3 | 10 | 3 | 22 |
| Alkene | gamma-Terpinene | 0 | **192** | 0 | 64 |
| Alkene | i-Butene | 1 | 10 | 1 | 6 |
| Alkene | Isoprene | 1 | 6 | 2 | 10 |
| Alkene | Limonene | 0 | **423** | 0 | **783** |
| Alkene | Myrcene | 0 | **209** | 0 | 45 |
| Alkene | Propene | 2 | 19 | 2 | 37 |
| Alkene | Styrene | n/a | n/a | 1 | 28 |
| Alkene | trans-2-Butene | 0 | 2 | 0 | 1 |
| Alkene | trans-2-Pentene | 0 | 38 | 0 | 3 |
| Alkyne | Ethyne | 1 | 3 | 0 | 1 |
| Aromatic | 1,2,3-Trimethylbenzene | 1 | **448** | 1 | **159** |
| Aromatic | 1,2,4-Trimethylbenzene | 1 | 11 | 1 | **150** |
| Aromatic | 1,3,5-Trimethylbenzene | 0 | 4 | 0 | 61 |
| Aromatic | Benzene | 0 | 0 | 0 | 1 |
| Aromatic | Ethylbenzene | 7 | 131 | 9 | **1759** |

| | | | | | |
|---|---|---|---|---|---|
| Aromatic | i-Propylbenzene | 0 | 0 | 0 | 24 |
| Aromatic | Methylcyclohexane | 0 | 1 | 0 | 10 |
| Aromatic | m-Ethyltoluene | 0 | 7 | 0 | 76 |
| Aromatic | n-Propylbenzene | 0 | 1 | 0 | 7 |
| Aromatic | o-ethyltoluene | 0 | 2 | 0 | 24 |
| Aromatic | o-Xylene | 1 | 9 | 1 | **160** |
| Aromatic | p-Ethyltoluene | 0 | 2 | 0 | 21 |
| Aromatic | Toluene | 1 | 22 | 2 | **171** |
| Cycloalkane | Cyclohexane | 0 | 1 | 0 | 3 |
| Cycloalkane | Cyclopentane | 0 | 4 | 0 | 57 |
| Cycloalkane | Methylcyclopentane | 0 | 2 | 0 | 4 |
| Halocarbon | 1,2-DCE | 0 | 2 | 0 | 4 |
| Halocarbon | $C_2Cl_4$ | 0 | 0 | 0 | 0 |
| Halocarbon | $C_2HCl_3$ | 0 | 0 | 0 | 1 |
| Halocarbon | $CCl_4$ | 0 | 0 | 0 | 0 |
| Halocarbon | $CH_2Cl_2$ | 0 | 0 | 0 | 0 |
| Halocarbon | $CH_3Br$ | 0 | 0 | 0 | 0 |
| Halocarbon | $CH_3CCl_3$ | 0 | 0 | 0 | 0 |
| Halocarbon | $CH_3CH_2Cl$ | 0 | 0 | 0 | 0 |
| Halocarbon | $CHCl_3$ | 0 | 0 | 0 | 0 |
| Other | CO | 12 | 23 | 10 | 14 |
| Oxygenate | 2-Butanol | 0 | 1 | 0 | 5 |
| Oxygenate | Acetaldehyde | 30 | 132 | 25 | **697** |
| Oxygenate | Acetone | 12 | 76 | 4 | **155** |
| Oxygenate | Butanal | 6 | 136 | 13 | **4818** |
| Oxygenate | Butanone | 1 | **374** | 3 | **951** |
| Oxygenate | Ethanol | 5 | **2470** | 10 | **7288** |
| Oxygenate | Isopropanol | 0 | 30 | 1 | **476** |
| Oxygenate | Methanol | 3 | **799** | 5 | **1389** |
| Oxygenate | Methyl isobutyl ketone | 0 | 2 | 0 | 26 |
| Sulfur Species | $CS_2$ | 0 | 7 | 0 | 2 |
| **Total** | | 122 | 8330 | 131 | 20762 |

Overall, using Equation 8-2 to calculate OFP resulted in lower values overall despite more VOCs contributing to the total. However, similar trends were seen: oxygenates and alkenes again dominated the OFP. Interestingly, aromatics (e.g., 1,2,3-trimethylbenzene, 1,2,4-trimethylbenzene, 1,3,5-trimethylbenzene, 2-ethyltoluene, 4-ethyltoluene, ethylbenzene, i-propylbenzene, m-ethyltoluene, o-xylene, and toluene) were also enhanced at the landfills using

either Equation 8-1 or Equation 8-2, especially during Summer 2018, and often had $O_3$ > NAAQS. Chapter 8.3 examines the VOC contribution to secondary aerosol formation from landfills, for which aromatics also contributed. Previous studies have shown that these aromatic VOCs are often elevated in paints. Mo et al. (2015) showed that aromatics constituted between 79 – 99% VOCs from various paint industries in the Yangtze River Delta. Additionally, other sources like vehicles and MSW containing rubber, pesticides, paints, cosmetics, and glues also emit aromatics (Zdeb & Lebiocka, 2016). All the landfills used in this study have a Class III designation, meaning they are not supposed to accept paint. However, paint emissions may have been a source of enhanced aromatics found at Orange County landfills.

To narrow down possible aromatic sources for Spring 2018 and Summer 2018, the ratio of toluene to benzene was calculated. A low T/B ratio, T/B ≤ 2, indicated possible vehicular sources. A high T/B ratio, T/B > 2, indicated possible industrial sources. A mix of both types of sources were expected for the Orange County landfills. The T/B ratio was calculated for twenty-six whole air samples collected directly next to the active dumping areas across all landfill campaigns. The T/B ratio ranged from 1 to 91 with an average and standard deviation of 8±17. Eight samples had T/B < 2, likely indicating the influence of emissions from vehicles working on the landfill surface, and fifteen samples had T/B > 2, indicating that other sources of aromatics were likely (e.g., industrial emissions from paints, inks, or adhesives) (Bretón et al., 2017). For all samples with T/B > 2 and T/B <2, the m/p-xylene mixing ratios were plotted against ethylbenzene mixing ratios to determine a correlation. Samples that were exactly T/B = 2 (n = 3 samples) were not included. The higher the correlation ($R^2$ = 1), the more likely that the source was paint volatilization.

For the samples collected near active dumping with T/B > 2, Figure 8.3A shows that ethylbenzene and m/p-xylene were well correlated with an $R^2$ = 0.97 whereas Figure 8.3B shows that samples collected near active dumping with T/B < 2 were not as well correlated with an $R^2$ =

0.69. Overall, this indicated that aromatic surface-sources may have included paint volatilization and other industrial emissions.

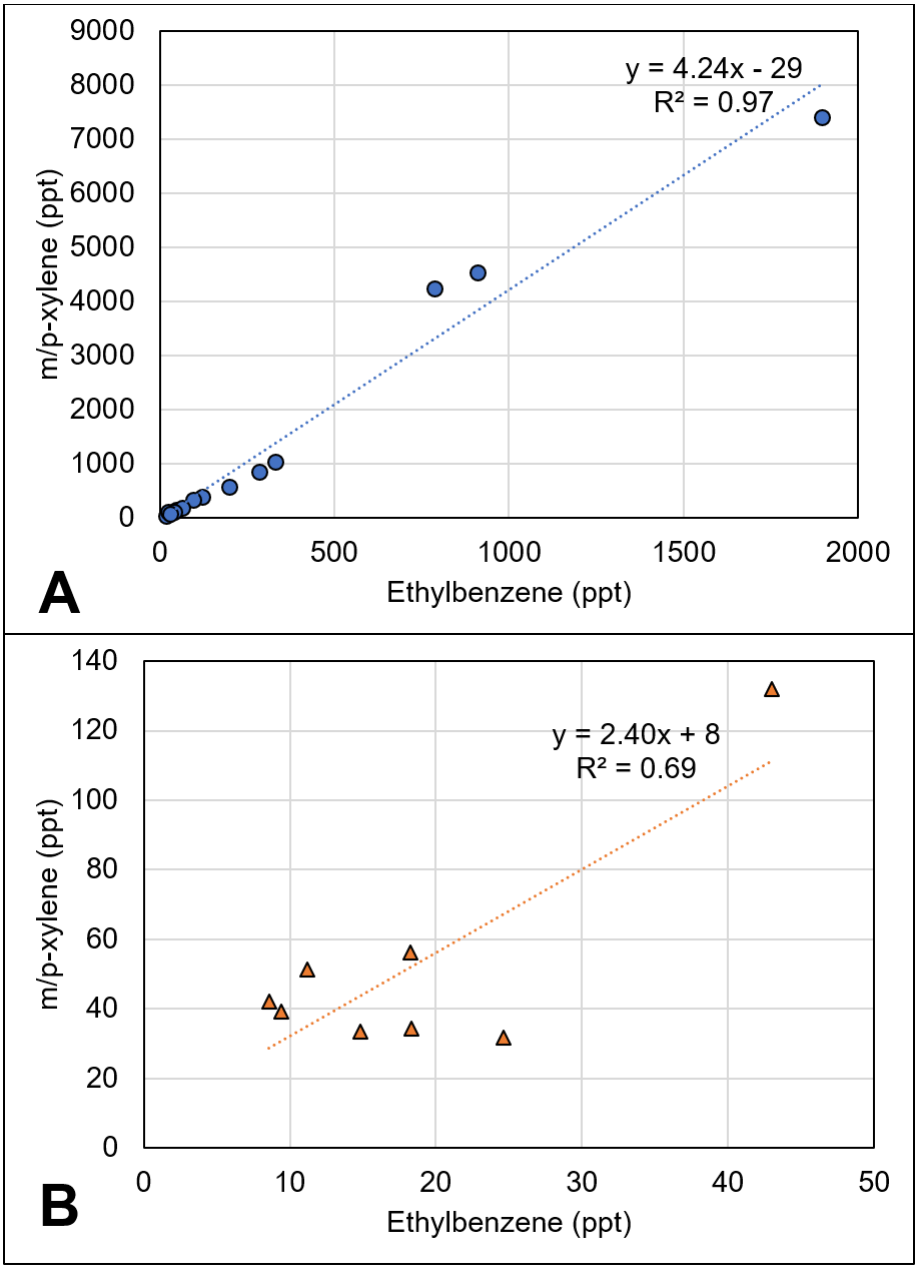


**Figure 8.3** Correlation plots of ethylbenzene versus m/p-xylene for samples collected near active dumping A) with a toluene to benzene ratio of T/B > 2 and B) with a toluene to benzene ratio of T/B < 2 for all Orange County landfill campaigns. The correlation coefficient was $R^2$ = 0.97 for T/B >2 and $R^2$ = 0.69 for T/B < 2. Samples with T/B = 2 were not included.

It appeared that industrial emissions (e.g., paint volatilization) may have contributed to these above-surface aromatic enhancements along with some likely vehicular contributions from

landfill machinery. This is important because these gases have a high OFP and can create poor air quality and pollution for people living downwind of the landfills. It is encouraged to continue to strongly enforce disposal of waste at these landfills to decrease possible toxic gases that also contribute to environmental issues.

Regardless of on-site source, landfills and dairy farms have the capability of forming ozone with the surprisingly high amount of oxygenates and alkenes they both produce. While on-site landfill engineers and dairy farm employees are exposed to these gases directly, residents living downwind of these sites are exposed to their reaction byproducts, leading to potential negative health effects, environmental damage, and nonattainment days. Ozone formation is not the only outcome of VOC emissions; secondary organic aerosols (SOAs) can also potentially form, as discussed below in Chapter 8.3.

**8.3 Secondary Organic Aerosol and Particulate Matter Formation**

To form secondary organic aerosols (SOAs), anthropogenic or biogenic VOCs are first oxidized by OH, $O_3$, or $NO_3$, creating products with decreased vapor pressure. Those products then can condense and evaporate and eventually stick to a particle to participate in heterogenous chemistry. Otherwise, if the vapor pressure is not sufficiently lowered, the first-generation product can become oxidized further into second or third-generation products, which have even lower vapor pressures. Eventually, the vapor pressure is low enough that the compound is even more likely to participate in heterogenous chemistry. Generally, the presence of more functional groups and larger molar mass will lead to more particle formation by decreasing volatility, while more branching leads to a higher fragmentation rate and a lower SOA yield.

Secondary organic aerosols are estimated to constitute up to 80% of the total organic particulate matter in the ambient air (Turpin & Huntzicker, 1995). This makes SOAs extremely important in the SJV, which is consistently a nonattainment zone for $PM_{2.5}$ and sometimes $PM_{10}$. These particles can harm the cardiovascular, mental, and reproductive health of humans; they

can also harm the environment (e.g., by weakening tree bark) and decrease visibility. However, particles are also assumed to cool down the earth by scattering light or forming clouds (Finlayson-Pitts & Pitts, 1999). The SJV is full of already-known sources that contribute to its elevated PM. For example, the burning of fossil fuels at industrial facilities can emit $SO_2$, which later forms $H_2SO_4$ in particles. Additionally, $NO_x$, which is produced during combustion of fossil fuels, can generate $HNO_3$ gas. When this gas mixes with ammonia, a common emission from agricultural regions, it can create $NH_4NO_3$ in particles. The SJV contains a lot of industrial factories, motor vehicles, and farmland, which explains why there are so many particles. This section explores the dairy farm's potential contribution. Additionally, Orange County is also a nonattainment area for $PM_{2.5}$, which could be a result of the notorious traffic in the Los Angeles Air Basin combined with the agricultural emissions from more rural areas like Chino, California. The Orange County landfills' potential contribution to SOA formation at the regional scale is also assessed here.

Shin et al. (2013) presented SOA yields for a variety of compounds including alkanes, alkenes, and aromatics. These values from Shin et al. (2013) were chosen for this analysis because they considered various experimental conditions from previous studies and relayed average SOA yield values. To calculate the SOA formation potential using SOA yields from Shin et al. (2013), Equation 8-3 was used:

$$\text{SOA formation potential } \left(\frac{\text{ng}}{\text{m}^3}\right) = \text{VOC (ppb)} * \text{SOA yield } \left(\frac{\mu\text{g}}{\text{ppm m}^3}\right) * \frac{1\text{ ppm}}{1000\text{ ppb}} * \frac{1000\text{ ng}}{1\ \mu\text{g}} \qquad \text{Equation 8-3}$$

This formula calculates SOA formation potentials by multiplying the VOC mixing ratios determined from whole air samples and the SOA yield values presented in Shin et al. (2013). Although SOA yields are different under different atmospheric conditions, calculating relative SOA formation potentials for this study allows readers to compare relative contributions of VOCs at the landfill and dairy farm and determine which ones would most likely contribute to particle formation at those locations. As previously mentioned, ideal molecules for SOA formation have a high molar mass and a low vapor pressure. Lighter alkanes ($C_2$ to $C_6$) do not have an SOA yield associated

with them. Even for Shin et al. (2013), although they measured fifty-five VOCs, only about half of them could form SOA. Candidates were typically aromatics and heavier alkanes ($C_7$ to $C_{11}$). As shown in Chapter 6.2.2, DMS also contributes to SOA in the SJV. Although Shin et al. (2013) did not present the values for SOA yields from DMS, DMS is still considered a source of SOA.

### 8.3.1 Secondary Organic Aerosol Formation at the Dairy Farm

The SOA formation potential of nine different VOCs at the dairy farm was calculated using the SOA yields presented in Shin et al. (2013) for the March 2019, June 2019, September 2019, and January 2020 campaigns. The SOA formation potential was calculated using the median and maximum mixing ratios of each VOC found at the dairy farm during each campaign to determine the amount of SOA that could be created. These data are shown organized by compound class in Table 8.5.

**Table 8.5** SOA formation potential at the dairy farm by season calculated from the median (med) and maximum (max) mixing ratios of various VOCs and the SOA yields in Shin et al. (2013).

| Class | Compound | SOA Formation Potential (ng/m$^3$) | | | | | | | |
|---|---|---|---|---|---|---|---|---|---|
| | | March 2019 | | June 2019 | | Sept 2019 | | Jan 2020 | |
| | | Med | Max | Med | Max | Med | Max | Med | Max |
| Alkene | Isoprene | 4 | 48 | 53 | 100 | 18 | 80 | 5 | 97 |
| Alkyne | Ethyne | 24 | 58 | 6 | 61 | 7 | 18 | 23 | 52 |
| Aromatic | 2-Ethyltoluene | 6 | 12 | 5 | 6 | 4 | 7 | 4 | 13 |
| Aromatic | 3-Ethyltoluene | 6 | 16 | 3 | 6 | 4 | 16 | 4 | 11 |
| Aromatic | 4-Ethyltoluene | 5 | 14 | 3 | 6 | 4 | 10 | 4 | 12 |
| Aromatic | Benzene | 129 | 371 | 46 | 146 | 62 | 471 | 165 | 372 |
| Aromatic | Ethylbenzene | 17 | 37 | 7 | 12 | 6 | 36 | 9 | 32 |
| Aromatic | o-Xylene | 5 | 10 | 1 | 3 | 2 | 8 | 2 | 7 |
| Aromatic | Toluene | 30 | 976 | 54 | 223 | 28 | 288 | 61 | 136 |
| **Total** | | 226 | 1542 | 178 | 562 | 135 | 934 | 278 | 732 |

The SOA formation potential was calculated using the median and maximum mixing ratios to determine what the “typical” SOA concentrations would be compared to the absolute maximum. The gases with significant SOA formation potential were similar between the maximum and the median calculations. Benzene, toluene, isoprene and ethyne likely contributed the most SOA from the dairy farm. According to the NAAQS in Table 1.1, $PM_{2.5}$ has a 24-hour limit of 35 μg $m^{-3}$ and

a 1-year primary pollutant average limit of 12.0 μg $m^{-3}$. As Turpin and Huntzicker (1995) showed, organic particulate matter in the atmosphere is up to 80% SOA. For this study, it is assumed that 80% of the SOA becomes particles. If the NAAQS for $PM_{2.5}$ is then rewritten in SOA and converted to nanograms, the 24-hour limit would be 28,000 ng SOA $m^{-3}$ and the 1-year limit would be 9,600 ng SOA $m^{-3}$. None of the SOA formation potentials in Table 8.5 approach these values. While there is likely SOA and particle formation occurring from VOCs released at the Visalia dairy farm, the contribution from the VOCs in Table 8.5 does not exceed the standards set forth by NAAQS.

It is also likely that other compounds that were not measured or not included in Shin et al. (2013), such as amines or DMS, contribute to particle formation as well. It was shown in Chapter 6.2.2 that DMS contributes up to 1.86 kg aerosols $hd^{-1}$ $yr^{-1}$ at the Visalia dairy farm based on Chen and Jang (2012), which may be as high as a 5% total contribution to the submicron particle formation in the SJV. Other than the DMS, the enteric and manure sources at the dairy farm were likely not responsible for much of the SOA formation in Table 8.5, which was still well below the NAAQS limit. Instead, SOA formation and the large concentration of particles in the SJV are more likely caused by a combination of traffic and agriculture along with these dairy farm emissions and are not exclusively from dairy farms themselves.

### 8.3.2 Secondary Organic Aerosol Formation at the Orange County Landfills

The SOA formation potential of 22 different VOCs at the Orange County landfills was calculated using the SOA yields from Shin et al. (2013) for the Spring 2018 and Summer 2018 campaigns. The SOA formation potential was calculated using the median and maximum mixing ratios of each gas found at the landfills during each campaign to determine the amount of SOA that could be created. These data are shown organized by compound class in Table 8.6.

**Table 8.6** SOA formation potential at the Orange County landfills by season calculated from the median (med) and maximum (max) mixing ratios of various VOCs and the SOA yields in Shin et al. (2013).

| Class | Compound | SOA Formation Potential (ng/m$^3$) | | | |
|---|---|---|---|---|---|
| | | Spring 2018 | | Summer 2018 | |
| | | Med | Max | Med | Max |
| Alkane | n-Decane | 13 | 443 | 20 | 5468 |
| Alkane | n-Heptane | 1 | 12 | 1 | 27 |
| Alkane | n-Nonane | 12 | 385 | 8 | 1719 |
| Alkane | n-Octane | 1 | 25 | 1 | 104 |
| Alkane | n-Undecane | 21 | 2073 | 24 | 5424 |
| Alkene | Isoprene | 5 | 35 | 11 | 65 |
| Alkyne | Ethyne | 25 | 145 | 15 | 40 |
| Aromatic | 1,2,3-Trimethylbenzene | 4 | 3785 | 5 | 1346 |
| Aromatic | 1,2,4-Trimethylbenzene | 6 | 82 | 6 | 1089 |
| Aromatic | 1,3,5-Trimethylbenzene | 2 | 21 | 2 | 299 |
| Aromatic | Benzene | 119 | 194 | 75 | 349 |
| Aromatic | Ethylbenzene | 6 | 116 | 8 | 1555 |
| Aromatic | i-Propylbenzene | 1 | 10 | 1 | 658 |
| Aromatic | m-Ethyltoluene | 3 | 49 | 3 | 547 |
| Aromatic | n-Propylbenzene | 2 | 15 | 1 | 175 |
| Aromatic | o-Ethyltoluene | 2 | 21 | 2 | 290 |
| Aromatic | o-Xylene | 2 | 35 | 2 | 593 |
| Aromatic | p-Ethyltoluene | 2 | 22 | 2 | 280 |
| Aromatic | Toluene | 39 | 630 | 56 | 4994 |
| Cycloalkane | Cyclohexane | 3 | 35 | 4 | 105 |
| Cycloalkane | Methylcyclohexane | 1 | 10 | 3 | 170 |
| Cycloalkane | Methylcyclopentane | 1 | 4 | 1 | 10 |
| **Total** | | 269 | 8148 | 252 | 25305 |

More trace gases that could contribute to SOA formation (i.e., heavy alkanes) were measured for the landfill campaigns than for the dairy farm campaigns. Aromatics and heavy alkanes dominated the formation of SOA at the landfill from the VOCs presented in Table 8.6. Trace gases like n-decane, n-undecane, toluene, n-nonane, and occasionally 1,2,3-trimethylbenzene and ethyne are potentially large contributors of SOA from landfills.

The values in Table 8.6 were compared to the 24-hour $PM_{2.5}$ NAAQS limit expressed as SOA formation (i.e., 28,000 ng SOA $m^{-3}$) and the 1-year NAAQS limit expressed as SOA formation

(i.e., 9,600 ng SOA $m^{-3}$), calculated by assuming that organic particulate matter in the SJV is 80% SOA (Turpin & Huntzicker, 1995). Fortunately, the $PM_{2.5}$ that could form as a result of maximum SOA conversion is under the NAAQS limit. However, some gases (i.e., n-decane, n-undecane, and toluene) were about halfway to the yearlong NAAQS limit. Although they were still below it, these gases are not negligible, and they can accumulate with gases emitted from other sources and cause pollution.

The SOA formation potentials were much higher at the landfills overall than they were at the dairy farm, by an order of magnitude or more depending on the compound. This is likely caused by a combination of evaporation during active dumping and emissions from landfill vehicles (e.g., commercial dump trucks, personal vehicles, construction equipment). These VOC emissions at the landfill could be contributing to SOA and particle formation downwind of the landfill. Compounded with road and industry emissions, this leads to nonattainment days for the county and poor air quality for the locals.

### 8.4 Odorous Compounds and the Effect on Human Well-Being

The dairy industry and the waste management industry are generally considered to be quite odorous. Persistent odors, while often not a direct threat to human health, are an occupational nuisance and can be overwhelming to nearby communities. For example, Shusterman (1992) reported that health symptoms related to odor exposure often occur even when the odors are non-toxic. Lorig et al. (1990, 1991) reported that odorous compounds at concentrations lower than what the nose can perceive *still* produce brain responses noted by electroencephalogram tests, later identified by Zald and Pardo (1997) as responses tied to the amygdala, a part of the brain involved in feeling emotions. The hedonic qualities (i.e., pleasantness or unpleasantness) of an odor can affect mood because the olfactory and emotion systems in the human brain overlap (Schiffman et al., 1974), and unpleasant odors can cause stress (Schiffman, 1998).

The most common complaints of people living in odorous areas are irritated eyes, nose, or throat, headache, and drowsiness (Schiffman, 1998). Just like how the GHG emissions from dairy farms and landfills are important for the environment, unpleasant odors are important for communities living near these operations. To determine the contribution of trace gases at the Visalia dairy farm and Orange County landfills to odor, the minimum odor thresholds presented in Nagata and Takeuchi (2003), Hellman and Small (1974), Leonardos et al. (1974), Abraham et al. (2002), and Murnane et al. (2013) were compared to the mixing ratios for gases detected. These values represent the lowest mixing ratio necessary for a sensitive human olfactory system to detect the associated smell. It is important to reiterate that when gases are present, but below the odor threshold, they are not perceived but can still cause stress and other mental health concerns. The odor thresholds are introduced in subsequent sections Chapter 8.4.1 and Chapter 8.4.2.

### 8.4.1 Odorous Compounds at the Visalia Dairy Farm

At dairy farms, odor can be caused by ammonia, $H_2S$, VOCs, aromatics, volatile fatty acids, nitrogen-containing compounds, and sulfur-containing compounds (Hammond et al., 1989; Hartung, 1985; O'Neill & Phillips, 1992). The effect of animal odors on human well-being has been studied before. Schiffman et al. (1995) examined the potential effects of livestock odors on the health of communities living near a large swine farm. The forty-four people living near the operation reported higher levels of tension, depression, anger, fatigue, and confusion after experiencing the associated odors than the people in the control group. Schiffman (1998) noted that 68% of "more-sensitive" people experiencing animal odors reported that the odors would make them ill after only thirty minutes. "Less-sensitive" people reported similarly, with 62% stating the odors would make them sick after thirty minutes. Both groups complained of symptoms including teary eyes, headaches, congestion, dry eyes, and nasal irritation (Schiffman, 1998). It is important to note that many of the compounds that make up animal odor are fortunately not

toxic or were below the toxicity level at the Visalia dairy farm. The human response to odor in this case is often emotional, but still very real and impactful for those affected by it.

At the dairy farm in Visalia, CA, the following compounds were measured and compared to their associated odor thresholds to determine which could be contributing to odor. Table 8.7 lists the compounds with their minimum odor thresholds.

**Table 8.7** Odorous VOCs measured at the Visalia dairy farm with their associated minimum odor thresholds (ppb)

| Compound | Odor Threshold (ppb) | Source |
|---|---|---|
| $CH_4$ | 2.90E+09 | Murnane et al. (2013) |
| $CO_2$ | 3.90E+07 | Murnane et al. (2013) |
| DMS | 3 | Nagata and Takeuchi (2003) |
| OCS | 55 | Nagata and Takeuchi (2003) |
| $CHCl_3$ | 102 | Murnane et al. (2013) |
| $CH_3CH_2Cl$ | 3800 | Murnane et al. (2013) |
| $CH_2Cl_2$ | 1200 | Murnane et al. (2013) |
| $CHBr_3$ | 190 | Murnane et al. (2013) |
| $CCl_4$ | 1680 | Murnane et al. (2013) |
| $C_2Cl_4$ | 767 | Murnane et al. (2013) |
| $CH_3Cl$ | 1.00E+04 | Murnane et al. (2013) |
| $C_2HCl_3$ | 500 | Murnane et al. (2013) |
| 1,2-DCE | 4300 | Murnane et al. (2013) |
| Methylisobutylketone | 30 | Murnane et al. (2013) |
| Ethane | 2.03E+07 | Murnane et al. (2013) |
| Ethene | 1.70E+04 | Murnane et al. (2013) |
| Ethyne | 2.26E+05 | Murnane et al. (2013) |
| Propane | 1.50E+06 | Murnane et al. (2013) |
| Propene | 1.01E+04 | Murnane et al. (2013) |
| i-Butane | 421 | Murnane et al. (2013) |
| n-Butane | 421 | Murnane et al. (2013) |
| 1-Butene | 362 | Murnane et al. (2013) |
| i-Butene | 362 | Murnane et al. (2013) |
| trans-2-Butene | 362 | Murnane et al. (2013) |
| cis-2-Butene | 362 | Murnane et al. (2013) |
| i-Pentane | 1290 | Murnane et al. (2013) |
| n-Pentane | 1290 | Murnane et al. (2013) |
| 1-Pentene | 100 | Nagata and Takeuchi (2003) |
| Isoprene | 48 | Nagata and Takeuchi (2003) |
| n-Hexane | 1500 | Murnane et al. (2013) |

| | | |
|---|---|---|
| n-Heptane | 410 | Murnane et al. (2013) |
| Benzene | 2700 | Nagata and Takeuchi (2003) |
| Toluene | 170 | Hellman and Small (1974) |
| Ethylbenzene | 170 | Nagata and Takeuchi (2003) |
| m+p-xylene | 80 | Hellman and Small (1974) |
| o-Xylene | 80 | Hellman and Small (1974) |
| 3-Ethyltoluene | 18 | Nagata and Takeuchi (2003) |
| 4-Ethyltoluene | 8.3 | Nagata and Takeuchi (2003) |
| 2-Ethyltoluene | 74 | Nagata and Takeuchi (2003) |
| Methanol | 3.30E+04 | Nagata and Takeuchi (2003) |
| Ethanol | 520 | Nagata and Takeuchi (2003) |
| Limonene | 38 | Nagata and Takeuchi (2003) |
| Butanal | 0.3 | Murnane et al. (2013) |
| Butanone | 70 | Murnane et al. (2013) |
| 2-Butanol | 120 | Hellman and Small (1974) |
| Acetone | 4.20E+04 | Nagata and Takeuchi (2003) |
| Acetaldehyde | 210 | Leonardos et al. (1974) |

A reduction factor was calculated to determine how much a maximum mixing ratio at the dairy farm would need to be reduced to bring the odor below the perceptible threshold. This reduction factor was defined according to Equation 8-4.

$$\mathrm{RF} = \frac{\text{maximum mixing ratio (ppb)}}{\text{odor threshold (ppb)}} \quad \text{Equation 8-4}$$

Gases that exceeded their odor thresholds at the dairy farm included limonene, butanal, ethanol, and DMS. The RFs for these trace gases are shown in Table 8.8, and their odor thresholds are listed at the bottom of the table. The “Upwind” category included samples collected upwind of the dairy. These still likely include emissions from the surrounding croplands and the city of Visalia in general. The processing pit had no detectable odor from the compounds measured in this study and is not included in Table 8.8. “Regional” samples were collected within a few miles around the dairy farm, and the “Landfill” samples were collected downwind of Visalia landfill.

**Table 8.8** Trace gases exceeding the odor threshold at the Visalia dairy farm and their associated RFs

| RF | Limonene | Butanal | Ethanol | DMS |
|---|---|---|---|---|
| Upwind | 15 | 2 | | |
| Silage | 54 | 4 | 14 | |
| Region | 4 | | 2 | |
| Processing Pit | | | | |
| Office | | | | 3 |
| Landfill | 2 | 4 | | |
| Lagoons | 132 | 7 | 4 | 26 |
| Free Stalls | 69 | 7 | 3 | |
| Flush Water | | | | 20 |
| Crops | | 6 | | |
| Cows | 84 | 6 | 6 | 6 |
| Cow Breath | | 2 | 3 | 25 |
| Bedding | | 2 | | |
| **Odor Threshold** | **38** | **0.3** | **520** | **3** |

Butanal, DMS, and ethanol are thought to have unpleasant smells. Ruth (1986), in an analysis of hundreds of scents, noted that butanal smells sweet and rancid, DMS smells like decayed cabbage, and ethanol smells sweet and alcoholic. Although limonene was not included in Ruth (1986), other studies have emphasized its importance as a contributor to the odor of citrus fruits (Rodríguez et al., 2017).

Limonene was above the odor threshold upwind, near the silage, regionally, at the Visalia landfill, and near the lagoons, free stalls, and outdoor cows. Limonene odor was most prominent near the lagoons, outdoor cows, and free stalls. Given that limonene is a biogenic emission, and that it was also above the odor threshold near the silage, it is likely that the cow's feed as well as the surrounding croplands contributed to its prevalent odor. Limonene was not initially expected to exceed the odor threshold near the lagoons. However, it seems that it may be a product of decomposition of the cows' waste, which contains undigested parts of the cows' feed. As discussed in Chapter 4.2.2, dairy cows that consume corn silage have the highest undigestible

fraction of feed compared to other types of cows, so it is expected that a large percentage of the feed will be passed as undigested waste, which will emit trace gases as it enters the lagoons.

Butanal was above the odor threshold upwind and near silage, the Visalia landfill, lagoons, free stalls, crops, outdoor cows, cow breath, and bedding. Butanal would need to be reduced by a factor of seven near the lagoons and free stalls to be brought below the odor threshold. Butanal had the lowest odor threshold out of the four trace gases in Table 8.8, at only 0.3 ppb, but it has a notoriously pungent and acrid odor (Hall & Oser, 1965; Murnane et al., 2013).

Ethanol was above the odor threshold near silage, lagoons, free stalls, cows, cow breath, and regionally. Ethanol would need to be reduced by a factor of fourteen near the silage to bring it below a perceptible odor level. As shown in Chapter 5.1, ethanol is an important oxygenate that is emitted by silage in all its forms—as raw feed, from the cows during rumination, and from the undigested waste. Ethanol exceeded the odor threshold in the general Visalia region likely because of the other dairy farms in the area, which all contribute their silage, enteric, and manure emissions simultaneously.

Lastly, DMS exceeded the odor threshold near the office (which also contained the milk parlor), lagoons, flush water, cows, and cow breath. Dimethyl sulfide would need to be reduced over twenty times near the lagoons, flush water, and cow breath to bring it below the odor threshold. Although the RF was high near the lagoons, Chapter 6.2.2 showed that DMS was more consistently enhanced near the cows and particularly in their breath, showing that it is likely emitted during enteric fermentation. Cow breath had a much higher median DMS mixing ratio than lagoons, meaning enteric emissions of DMS may be more consistent than manure emissions of DMS. Reducing the amount of DMS coming from the cows would a large priority in reducing the odor from the VOCs in Table 8.8. Although limonene, butanal, ethanol, and DMS were the only measured compounds that exceeded the odor threshold, that does not imply that odors from other trace gases were not subconsciously processed. Odor from these gases, although

imperceptible, can still affect those living near the dairy farm (i.e., disadvantaged communities), which is why their odor thresholds were still included in Table 8.7. Lastly, this is by no means a comprehensive list of odorous compounds at the dairy farm, merely an exploration. Additional compounds that were not measured in this study, like amines or extra sulfur-containing gases, were likely also present and may have contributed to the odor.

### 8.4.2 Odorous Compounds at the Orange County Landfills

According to the literature, LFG odor at landfills (if it was not reduced by cover material) is primarily produced by esters, sulfur compounds, solvents, alkyl benzenes, and limonene (Giess et al., 1999). Studies have shown that raw LFG under the landfill surface can require over a 100-fold dilution to bring gases below the odor threshold (Young & Parker, 1983). Odorous trace gas mixing ratios at three active landfills (Frank R. Bowerman, Olinda Alpha, and Prima Deshecha) and two closed landfills (Coyote Canyon and Santiago Canyon) in Orange County were compared to the odor thresholds presented in Nagata and Takeuchi (2003), Hellman and Small (1974), Leonardos et al. (1974), Abraham et al. (2002), Ruth (1986) and Murnane et al. (2013). Surprisingly, the odor at these landfills as samples were collected seemed highly variable during the campaigns. Occasional odors were perceptible, particularly near the active dumping area, but often the Orange County landfills did not express odor over much of the working face. More compounds were measured for the landfill campaign than the dairy study. Odor thresholds presented in Table 8.9 were used for the landfills in addition to the odor thresholds already presented in Table 8.7.

**Table 8.9** Additional odorous compounds measured at Orange County landfills with their associated minimum odor thresholds

| Compound | Odor Threshold (ppb) | Reference |
|---|---|---|
| i-Propylbenzene | 8 | Hellman and Small (1974) |
| n-Propylbenzene | 3.8 | Nagata and Takeuchi (2003) |
| 1,3,5-Trimethylbenzene | 170 | Nagata and Takeuchi (2003) |
| 1,2,4-Trimethylbenzene | 120 | Nagata and Takeuchi (2003) |
| α-Pinene | 18 | Nagata and Takeuchi (2003) |
| β-Pinene | 33 | Nagata and Takeuchi (2003) |
| DMDS | 2.2 | Nagata and Takeuchi (2003) |
| $CS_2$ | 210 | Nagata and Takeuchi (2003) |
| Isopropanol | 3190 | Ruth (1986) |
| α-Terpinene | 1430 | Abraham et al. (2002) |
| γ-terpinene | 9817 | Abraham et al. (2002) |
| Myrcene | 12.98 | Ruth (1986) |
| Methyl Chloroform | 970 | Murnane et al. (2013) |
| CFC-12 | 2E+08 | Murnane et al. (2013) |
| CFC-11 | 5000 | Murnane et al. (2013) |
| HCFC-22 | 2E+08 | Murnane et al. (2013) |
| 1,2-DBE | 1E+04 | Murnane et al. (2013) |
| n-Octane | 660 | Murnane et al. (2013) |
| n-Nonane | 2300 | Murnane et al. (2013) |
| 2,3-Dimethylbutane | 426 | Murnane et al. (2013) |
| 3-Methylpentane | 426 | Murnane et al. (2013) |
| 2,4-Dimethylpentane | 660 | Murnane et al. (2013) |
| Methylcyclopentane | 426 | Murnane et al. (2013) |
| Cyclohexane | 520 | Murnane et al. (2013) |
| Methylcylohexane | 149 | Murnane et al. (2013) |
| 2,2-Dimethylbutane | 426 | Murnane et al. (2013) |
| 2-Methylhexane | 410 | Murnane et al. (2013) |
| 3-Methylhexane | 410 | Murnane et al. (2013) |
| 2,2,4-Trimethylpentane | 660 | Murnane et al. (2013) |

The trace gases listed in Table 8.7 and Table 8.9 were measured at the Orange County landfills during Spring 2018 and Summer 2018 and compared to their associated odor thresholds to determine whether any of them contributed to the landfill smell. Most of these compounds were lower than the odor thresholds presented in the tables, and many of the gases that had RF > 1 at the dairy farm also had RF > 1 at the landfills. This supports the idea of variability in the landfill

smell, which seemed to depend on time and location. Table 8.10 shows the RFs for the compounds that exceeded the odor threshold at the active and closed landfills.

**Table 8.10** Trace gases exceeding the odor threshold at Orange County landfills during Spring and Summer 2018 and their associated RFs

| **Landfill** | **Spring 2018 (Compound \| RF)** | | **Summer 2018 (Compound \| RF)** | |
|---|---|---|---|---|
| Frank R. Bowerman | Butanal | 26 | Butanal | 913 |
| | | | Ethanol | 5 |
| | | | Butanone | 3 |
| Olinda Alpha | α-Pinene | 3 | Butanal | 166 |
| | Ethanol | 2 | | |
| | Butanone | 1.2 | | |
| Prima Deshecha | Butanal | 8 | Butanal | 21 |
| Coyote Canyon | Butanal | 2 | Butanal | 8 |
| Santiago Canyon | Butanal | 7 | N/A | |

Similar to the dairy farms, butanal was a large component of odor. The samples with the highest mixing ratios (and therefore the largest RFs) were typically collected near the active dumping area or near the LFG collection pumps, indicating potentially leaky infrastructure. Ethanol was also above the odor threshold at Olinda Alpha in Spring 2018 and Frank R. Bowerman during Summer 2018. Butanone had RF > 1 during Spring 2018 at Olinda Alpha and during Summer 2018 at Frank R. Bowerman. Lastly, α-pinene had RF > 1 during Spring 2018 at Olinda Alpha. Although not shown here, β-pinene also had an RF very slightly over 1. Both α-pinene and β-pinene were predominately elevated near the active dumping area, the mulch used for daily cover, and the MSW compost pile at Olinda Alpha. Overall, the active dumping area, LFG pumps, and on-site mulch and compost contributed the highest amount of odor.

This agrees with an odor study done at Frank R. Bowerman landfill in 2017 (SCS Engineers, 2017). In the study, engineers determined an odor rate for different areas around Frank R. Bowerman landfill in units of D/T*$m^3$/s, where D/T is dilutions per threshold, the number of dilutions needed so that a volume of odorous air would no longer be detected by 50% of the population. Odors are typically a nuisance around 7 D/T.

SCS Engineers (2017) determined that the working face (i.e., where active dumping occurs) of Frank R. Bowerman landfill emits odor at a rate of 4,286 D/T*$m^3$/s, the highest out of all sources. They determined that the second highest odor rate came from processed green material (PGM) at 3,211 D/T*$m^3$/s (SCS Engineers, 2017). All other odor rates from SCS Engineers (2017) were an order of magnitude smaller. This study shows that odor at all active Orange County landfills may match this trend, as odor likely came from the same sources—the active dumping area, the green waste, and the compost, and that major contributors to odor include ethanol, butanal, α-pinene, and butanone. Although butanal, α-pinene, ethanol, and butanone were the most odorous compounds measured for this study at the Orange County landfills, that does not imply that other compounds are not subconsciously processed and can affect landfill engineers and people living nearby. It is also expected that additional compounds not measured for this work also contribute to odor. After reviewing Chapter 8.2.2, 8.3.2, and 8.4.2, it seems that mulch and compost at Orange County landfills contribute many gases to OFP, SOA formation, and odor. Mulch and compost at these landfills are discussed further in Chapter 8.5.3.

## 8.5 Proposed Solutions to Reduce Emissions at Dairy Farms and Landfills

Previous chapters have examined specific gases ($CH_4$, $CO_2$, methanol, ethanol, acetaldehyde, DMS, OCS, and $N_2O$) and Chapter 8 has explored trace gas contribution to ozone formation, SOA formation, and odor at the dairy farm and Orange County landfills. The accumulation of trace gases affects people living near and downwind of these sources, particularly in communities of disadvantage. Many of the gases are also harmful for the environment. This section explores some potential solutions to reduce enteric and manure emissions and looks further at the benefits and drawbacks of using mulch and compost at Orange County landfills.

### 8.5.1 Reducing Enteric Emissions: Changes to Cow Feed

Chapter 4.2.2 showed that enteric emissions from cows release a large amount of methane. Governor Brown's SB-1383, passed in 2016, requires that methane emissions, regardless of source, be reduced to 40% below 2013 levels by 2030. Per SB-1383, California will adopt regulations to reduce methane emissions from dairy farms starting on January 1, 2024 (S.B. 1383, 2016). Dairy farm owners and employees, who primarily reside in disadvantaged communities, will be greatly affected by this because they will be responsible for either reducing their methane emissions or paying fines if they do not remain on track towards methane mitigation.

Additionally, Chapter 8.2.1, 8.3.1, and 8.4.1 showed that dairy cow feed may release VOCs that contribute to ozone, SOA formation, and odor downwind of the dairy. This also greatly affects people, particularly disadvantaged communities, who work or live in the proximity. Although ammonia was not measured in this study, it is often elevated at dairy farms and can lead to high levels of odor, toxicity, pollution, and water eutrophication. Elevated ammonia also contributes to particle formation when mixed with $NO_x$ from vehicles.

One of the most obvious proposed solutions to changing enteric emissions is to change the cows' diets. This could potentially decrease GHG and other trace gas emissions. Previous studies have shown that decreasing the amount of crude protein in the dairy cow feed also decreases levels of ammonia. Changing their diets also impacted how much methane the cows emitted (Liu et al., 2012). High levels of protein in dairy cow feed have been associated with elevated DMS (Hobbs & Mottram, 2000), which was also reported for this study in Chapter 6.2. By decreasing the amount of protein in the feed overall, emissions of these gases could potentially be decreased. This chapter explores this idea and its major drawbacks.

One popular "cure-all" idea that has been proposed has been to substitute part of the cows' diets with seaweed to decrease GHG emissions. Studies as early as the 1950s have explored this idea. Initially, though, seaweed was tested to try to increase the production of

butterfat from cows rather than to decrease their emissions. Diets containing 10% of brown seaweeds, *Ascophyllum nodosum* and *Laminaria Clouston*, were fed to cows in Scotland. The authors concluded that the possibility of feeding seaweed to cows was limited because of its low nutritional value, low palatability, and high cost (Burt et al., 1954).

However, in 2019, researchers fed post-lactating cows increasing levels of *Asparagopsis armata*, a type of red algae that grows primarily in temperate seas. After replacing only 0.5% of the cows' diets with the algae, they found that enteric methane emissions decreased by over 26%. After replacing their diets with 1% of the algae, they found that methane levels decreased by over 67% (Roque et al., 2019a). Similar studies were done by incorporating up to 5% *Asparagopsis taxiformis*, a red seaweed that grows in tropical waters, into diets of Holstein and Jersey cows. Methane reductions of 95% were reported after substituting 5% of the organic matter in their feed with the seaweed because of the anti-methanogenic effects of its brominated components (Roque et al., 2019b). A study in Australia confirmed that out of 20 different types of seaweed, *Asparagopsis taxiformis* was the most efficient at decreasing methane emissions from cows (Machado et al., 2014). A switch to a diet including 5% *Asparagopsis taxiformis* for cows at the Visalia dairy farm and in the entire SJV is considered below.

During the most recent dairy campaign (January 2020), the dairy site housed a total of 6,610 cows. Out of these, 3,239 were Holstein milk cows and the rest were dry cows and heifers. An adult cow needs to eat, on average, about 3% of her body weight per day to stay healthy. Adult Holstein milk cows weigh about 1,500 pounds on average. This means that a single cow at the dairy farm consumes, on average, 45 pounds of food every day. To replace 5% of their typical diet with *Asparagopsis taxiformis*, over 2 pounds of seaweed would be necessary, per cow daily. This amounts to 7,300 pounds of seaweed needed to sustain only the milk cows at the Visalia dairy farm daily. This does not include the heifers or dry cows. If all 1,505,000 milk cows in the SJV switched to the same diet, over $1 \times 10^{10}$ pounds of seaweed would be needed to sustain the

entire SJV population of milk cows *daily*. This calculation does not include heifers, dry cows, or beef cattle. Not only is this an immense amount of seaweed, but the SJV is not geographically located at the coastline, and the cold Pacific Ocean would not support the growth of *Asparagopsis taxiformis*, although it might support large-scale growth of *Asparagopsis armata*. However, the cost—both monetarily and environmentally—of hauling the seaweed to the Valley are nontrivial.

Though the results from seaweed feed are promising, dairy farmers are unlikely to integrate changes right away—if at all. Currently, there is a lack of infrastructure to support commercial and affordable large-scale aquafarming efforts, although some organizations are making a global effort to change that. Additionally, more long-term studies should be completed to determine the biochemistry surrounding anti-methanogenesis and the passage of additional minerals from the seaweed into the cow's milk, which is eventually consumed by humans. Finally, there is currently no strong incentive program to persuade farmers to switch the cows' feed. Although the seaweed diet is a popular idea, it is not currently feasible or advised for the Visalia dairy farm or other dairies in the SJV.

Instead of focusing on enteric emissions, it is suggested that dairy farms focus on manure emissions for methane reduction. As shown in Chapter 4.2.1, methane also is emitted in large quantities from manure management systems. Dairy farmers may choose to target these first because there are stronger incentives in place, as discussed further below in Chapter 8.5.2.

### 8.5.2 Reducing Manure Emissions: Install Anaerobic Digesters

SB-1383 will begin to regulate methane emissions more strictly from big industries like oil, natural gas, waste management, and dairies starting in 2024 (S.B. 1383, 2016). What makes SB-1383 different from previous regulations is that it has economic support backing it, particularly in the form of grants. Government outreach and large grants make it more feasible for dairy farmers in the SJV to begin decreasing their methane emissions before the stricter regulations begin.

According to the Science and Technology Advisor at CARB, manure management is easier to target for methane reduction than the cows themselves (Barringer & McGhee, 2018). This is likely because manure management systems are inanimate point sources. The most impactful SB-1383 grant can be used for the installation of anerobic digesters, which cover and seal open-air lagoons, like those at the dairy site in this study (and most dairies in the SJV). A mixture of mostly methane and carbon dioxide, known as biogas, is then produced during the anaerobic bacterial decomposition of the manure's organic material. Biogas typically contains around 50 to 70% methane, 30 to 40% carbon dioxide, and small amounts of trace gases such as hydrogen sulfide, hydrogen, nitrogen, and siloxanes (U.S. Department of Agriculture, 2014). This gas has a similar composition to the LFG produced at landfills. Methane can then be extracted and captured for electricity or transportation fuel. Biogas can be conditioned to meet SoCalGas standards and be transported using the pre-existing natural gas pipeline infrastructure.

Using a digester not only improves the air quality, but it also offers water quality benefits and can generate cow bedding and fertilizer as byproducts. Currently, the waste management industry, namely landfills, have progressed at a much faster rate than dairy farms over the last few decades when it comes to energy generation from waste. According to the EPA's Landfill Methane Outreach Program, there were already nearly 600 landfill gas-to-energy projects in the United States as of August 2020, while the total number of manure-based digesters in the country is less than half of that (EPA, 2020b).

The biggest drawbacks to their installation at dairy farms include their cost and the trust of the dairy community (CoBank, 2020; Barringer & McGhee, 2018). Some pilot digesters in the past did not work as planned, and it will take time to rebuild the trust of the dairy industry before installing better digesters (Barringer & McGhee, 2018). Most dairy farms that can afford anaerobic digesters are large, typically containing 2,000 cows or more. An anaerobic digester costs around $3 million for a dairy farm with 2,500 cows, and each additional 1,000 cows decreases the cost

per cow by 15 to 20% (CoBank, 2020). Analyzing the raw data shared by the CDFA's Dairy Digester Research and Development Program (DDRDP) revealed that dairy farms typically monetarily match the financial support they receive from grants related to SB-1383 (CDFA, 2020). Often, this costs hundreds of thousands (if not millions) of dollars.

While this is feasible for large dairy farms, many farms contain an average of less than 2,000 cows. The average number of cows per dairy from 2004 through 2017 was shown in Figure 2.16. The average number of cows per dairy using the most recent completed agricultural report from 2017 is shown below in Figure 8.4 (CDFA, 2018).

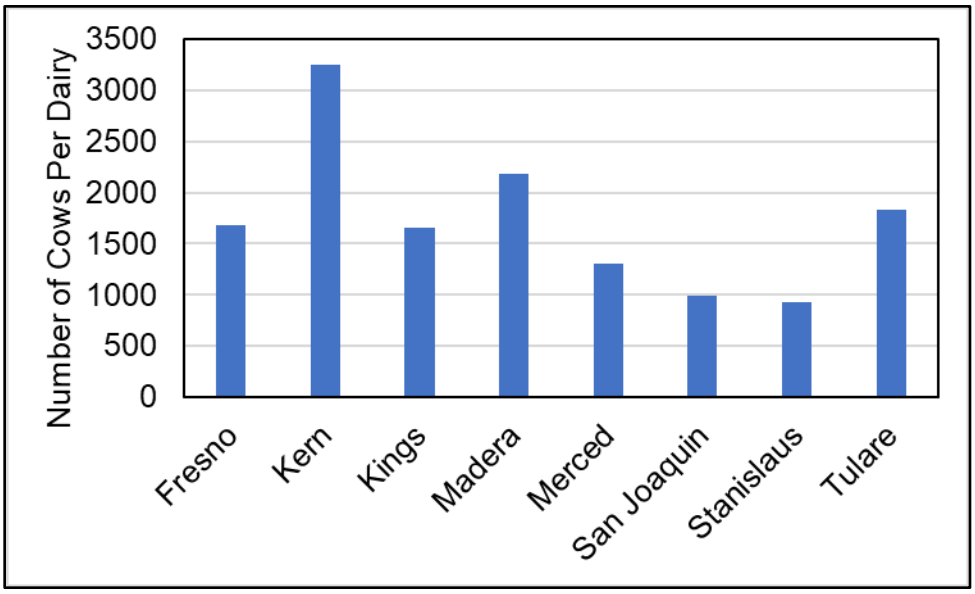


**Figure 8.4** Average number of cows per dairy in 2017 for SJV counties. Data obtained from CDFA (2018).

Counties with more cows per dairy, such as Kern, Madera, and Tulare, may be more likely to purchase an anaerobic digester. However, for smaller dairies with fewer cows, such as those in Merced, San Joaquin, and Stanislaus, this solution may not be as monetarily feasible. Instead, these counties could consider the Alternative Manure Management Program (AMMP), discussed further below. Additionally, counties with less cows per dairy may also consider flaring the methane generated during manure management to convert it to carbon dioxide, which has a lower GWP. This is similar to what the Orange County landfills do during their LFG recovery process.

Each county's number of approved anaerobic digesters was determined from the data provided by the CDFA DDRDP and is shown in Figure 8.5.

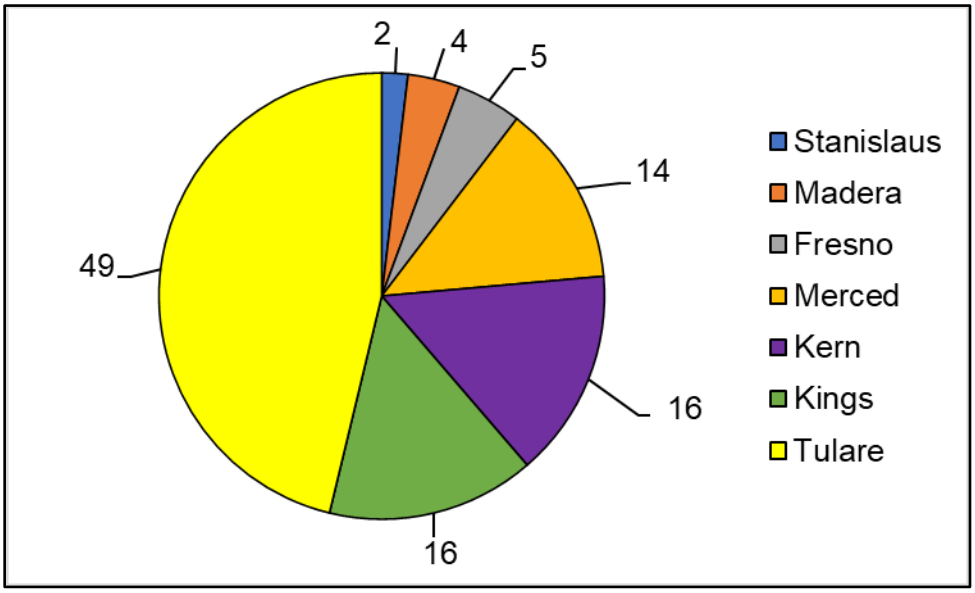


**Figure 8.5** Number of anaerobic digester projects in SJV counties. Data obtained from the CDFA DDRDP (CDFA, 2020).

The CDFA DDRDP reported that 109 anaerobic digester projects have been approved as of the end of 2019. Out of these approved projects, 2 have been cancelled, 13 have been completed, and 93 are still in progress. Tulare County contains nearly half of the approved anaerobic digester projects in the SJV. This could be the result of the combination of having a high average number of cows per dairy and a high total number of dairies compared to the rest of the SJV. The projects presented in Figure 8.5 all create biogas, but the biogas has a range of end uses. Figure 8.6 shows the approved projects separated by the end use of the biogas that will be generated by their anaerobic digesters.

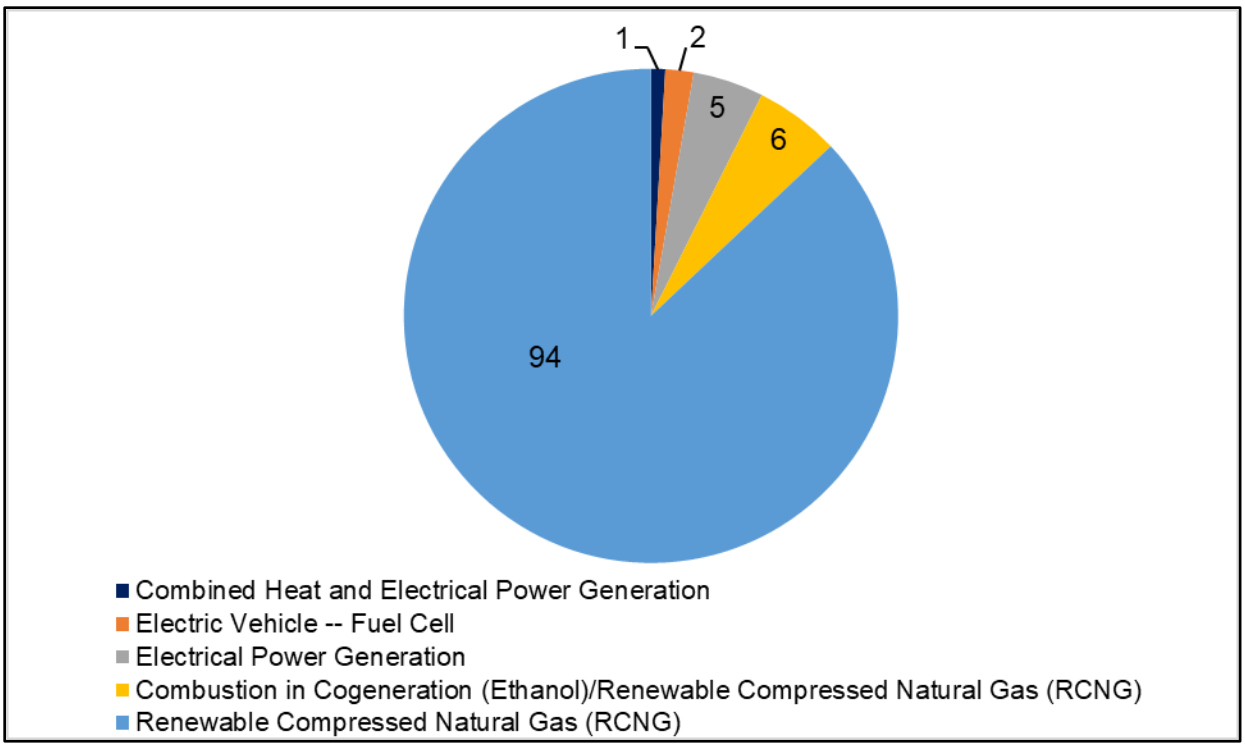


**Figure 8.6** Approved anaerobic digester projects in the SJV separated by biogas end use. Data was obtained from the CDFA DDRDP (CDFA, 2020).

Overwhelmingly, the biogas for most of the approved projects will be used as a source of Renewable Compressed Natural Gas (RCNG). Other projects will be used to create cogeneration products, produce electric vehicle fuel cell fuel, or combined heat and electrical power generation. Projects typically range from $1.7 million dollars to nearly $17 million dollars, with an average total cost of around $5 million dollars and a median cost of around $4 million dollars. The most expensive projects generate biogas for electrical vehicle fuel cells; these cost at least $16 million dollars.

While creating electricity from biogas projects will likely not drastically change the energy market in California, it can benefit individual farms and the communities living nearby. Generating on-site electricity can lower the electric bill for farmers and allow them to sell energy to pay for the installation of the digester. When combined with other anaerobic digesters installed for the wastewater and waste treatment industries, digesters could provide between 4 and 10% of the current natural gas demand in the United States—without relying on fracking (Sustainable

Business, 2013). The Environmental Protection Agency (EPA) claims that installing digesters can also increase the resilience of an individual community (U.S. Department of Agriculture, 2014). This is extremely important for residents and workers in the SJV, which is home to most of the state's designated disadvantaged communities. The EPA claims that biogas-producing anaerobic digesters can better prepare these communities for climate change by securing their sources of electricity, transportation, and food in case the power grid fails (U.S. Department of Agriculture, 2014).

Recently, the Visalia dairy site presented in this study was approved to install a digester, with installation beginning in 2021. They received $1.7 million from CDFA DDRDP and contributed $3.4 million in matching funds, bringing the total cost to just over $5 million. It is estimated that the installation will reduce GHG emissions by nearly 200,000 metric tons of $CO_2$ equivalent (MT $CO_2e$) over a 10-year period (CDFA, 2020). The biogas generated will be conditioned to meet SoCalGas standards for vehicle fuel. As more dairies around the country adopt anaerobic digesters, the energy potential from biogas sources becomes more significant. The EPA estimates that the energy potential from livestock manure biogas in the U.S. is 257 billion $ft^3$/yr. This amounts to an annual energy production of 142,000,000 MMBtu/yr, or an electricity potential of 13.1 billion kWh/yr (U.S. Department of Agriculture, 2014). This is enough electricity to power over one million homes for a year.

The CDFA funds not only the DDRDP program, but also the AMMP. The AMMP funds non-digester manure management practices in California to reduce GHG emissions. These projects often remove solids from the manure before it enters the lagoons. As shown in Chapter 4.2.1, extra solids in the manure management system may result in much higher mixing ratios of methane. The removed solids are often composted (CDFA, 2020). These AMMP projects are less expensive alternative for dairy farms that are interested in decreasing their GHG emissions but cannot afford to purchase a digester. Overall, regardless of project choice, decreasing emissions

from manure management currently seems more feasible than changing the dairy cows' feed. These projects will have positive long-term outcomes such as increased community resilience, better air quality, and cleaner electricity generation.

### 8.5.3 Reducing Landfill Emissions: Compost at Orange County Landfills

As part of AB-1594, which started in 2020, using green material as ADC at landfills now constitutes "disposal" instead of "diversion." If landfills choose to continue to receive green waste, the waste now counts toward their daily waste limit. This means that landfills may choose to find an alternative strategy to get rid of the green waste they receive so that they can continue to dispose waste at the same rate. One seemingly attractive option for landfill operators is to compost the green waste. Compost can be used as ADC, and it still counts as "diversion," meaning that it is not counted towards the total waste collected.

Although many see this as a clean alternative, the composting process releases GHGs and reactive biogenic hydrocarbons (i.e., isoprene, limonene, α-pinene, etc.) into the troposphere. These biogenic compounds react quickly with nitrate radicals ($k \sim 10^{-11}$ $cm^3$/molec-s) during the nighttime (Atkinson, 1997c), $O_3$ molecules ($k \sim 10^{-16}$ $cm^3$/molec-s) during the night and day (Atkinson, 1997c; Khamaganov & Hites, 2001; Ceacero-Vega et al., 2011), or hydroxyl radicals ($k \sim 10^{-10}$ $cm^3$/molec-s) during the day to form a variety of products (Kim et al., 2010; Howard & Evenson, 1976; Atkinson, 1997c). As discussed in Chapter 8.2, these reactions can create ozone after the oxidized hydrocarbons react with anthropogenic $NO_x$, not uncommon near Orange County landfills (Brosseau & Heitz, 1994; Atkinson, 1997c; Ceacero-Vega et al., 2011). Chapter 8.3.2 and 8.4.2 showed that the gases found in mulch and compost also likely contribute to SOA formation and odor nearby—and downwind of—the Orange County landfills. Although composting mulch at the landfill to use as ADC is attractive, there are several drawbacks, which are explored here.

It was shown in Chapter 8.3.2 that the cover material and the compost programs at Orange County landfills might be contributing to ozone formation downwind. Mulch was used as daily cover material during the time of sampling, and all active landfills had on-site composting programs to explore the use of compost as potential cover material (or for recycling purposes) after AB-1594 began. To explore the potential biogenic gases released from this future cover material, samples were collected inside and outside an indoor composting facility in Orange, California. Composting was done off-site, but the facility had a variety of composts ready for distribution, mostly for landscaping purposes. Although considered a much higher quality material than the MSW compost found at the Orange County landfills, their finished product still produced biogenic compounds.

Figure 8.7 compares enhancements of various biogenic compounds and methane at the composting facility to the compost pile at Frank R. Bowerman landfill in order of reaction rate with the hydroxyl radical, which is loosely related to how much ozone they can create (Kim et al., 2010; Howard & Evenson, 1976; Atkinson, 1997c; Gill & Hites, 2002; Kerr & Sheppard, 1981; Corchnoy & Atkinson, 1990; Atkinson et al., 1990; Atkinson & Aschmann, 1984). The y-axis uses a logarithmic scale so that the mixing ratios between gases are more comparable. The POCP values for some of these compounds (e.g., 3-carene, myrcene, ocimene, camphene) were not included in Derwent et al. (2007), but they likely still contribute to ozone formation because of their reactivity with the hydroxyl radical.

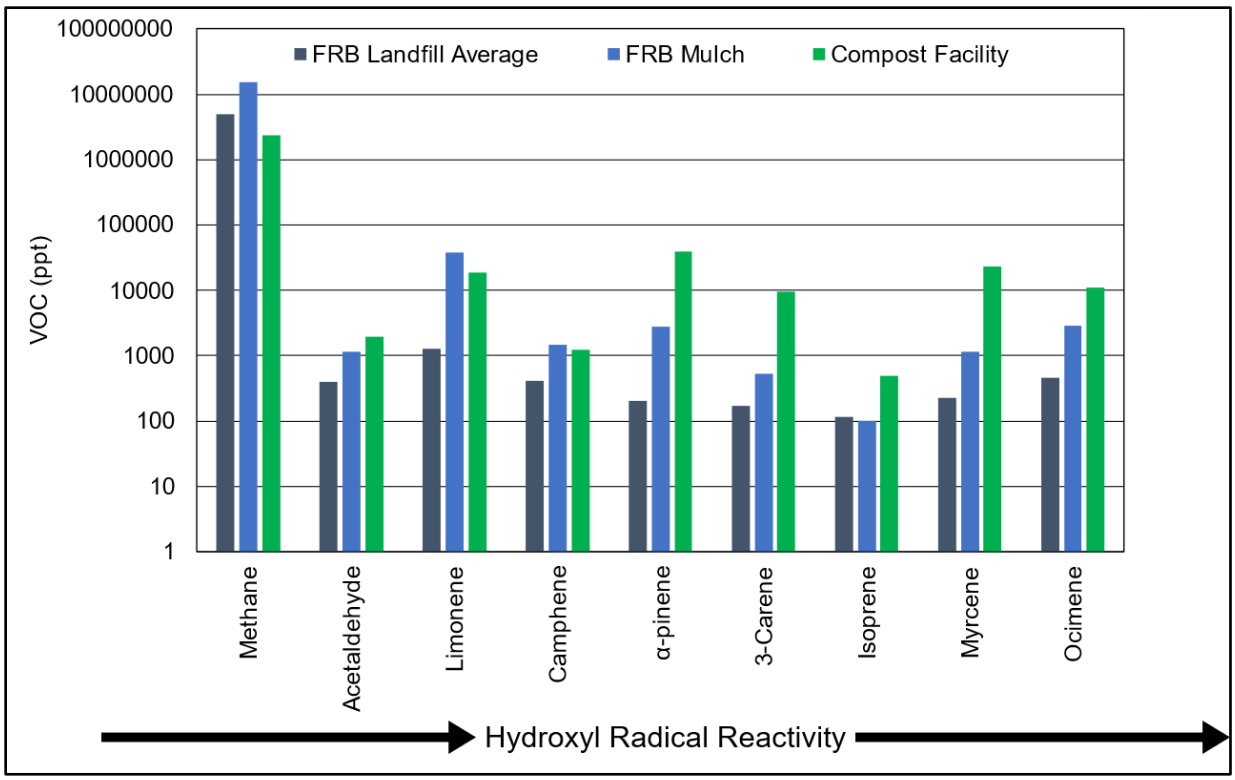


**Figure 8.7** Log-scale emissions ordered by reaction rate with hydroxyl radicals ($k_{CH4+OH}$ ~ $10^{-14}$ to $k_{ocimene+OH}$ ~$10^{-10}$ $cm^3$/molec-s) (Kim et al., 2010; Howard & Evenson, 1976). Biogenic alkenes were more enhanced at the composting facility and in Frank R. Bowerman (FRB) composting mulch than overall at the Frank R. Bowerman landfill. Alkenes were elevated by Frank R. Bowerman mulch daily cover material (limonene was 38 ppb) and inside the composting facility (α-pinene was 67 ppb).

The biogenic emissions from the compositing facility's compost were more enhanced than Frank R. Bowerman's pile of mulch ADC in every case except limonene, which was higher in Frank R. Bowerman's mulch pile. It is expected that more biogenic compounds were emitted than what is reported here because of their fast oxidation. Overall, the finished compost piles at the composting facility had higher mixing ratios of these select biogenic VOCs than the mulch at the landfill. This suggests that using compost as landfill cover would release compounds that lead to ozone formation even if the cover material prevented rogue LFG emissions from escaping the landfill.

Composted MSW is lower quality than the "organic" compost that was sampled at the compost facility due to plastic and glass contamination (Farrell & Jones, 2009). Regardless of if

MSW decomposes in a landfill or as compost, it still releases leachate into the ground (and emissions into the air) and would require an aftercare period like a landfill (Hurst et al., 2005). Literature shows that completely composting MSW can reduce biogas (i.e., mostly $CH_4$ and $CO_2$) emissions by over 80% versus leaving the MSW to decay in a landfill (Farrell & Jones, 2009; Adani et al., 2004). If composting is stopped early, GHG emissions are not reduced. This waiting period and necessary space for large-scale composting are not lucrative for landfill operators. Therefore, it is not recommended that landfill operators use compost as ADC. As there are other approved ADC materials that landfills could select, it appears that burying the green waste and counting it as disposal rather than composting it might be a better way to control emissions, $O_3$ formation, and odor. The landfill is designed to capture emissions that are generated below the surface rather than from the top, so these rogue emissions would be better prevented if the green material were stored underground rather than decomposing freely. This way, communities living downwind would not be exposed to as many secondary pollutants as they would be otherwise.

Although this is the suggestion based on research presented here, Frank R. Bowerman landfill has recently proposed to build Bee Canyon Greenery, a 30-acre composting operation that will receive a maximum of 437 tons per day of PGM and agricultural waste (OCWR, 2019). As this operation will occur outdoors, it is likely that VOCs will continue to be emitted that can create ozone, and odor. For the future, it is important to monitor emissions at Bee Canyon Greenery and determine whether fewer VOCs (not just methane) are emitted by composting or by burying the green material. It is also important that the landfills statewide determine whether the additional biogenic emissions are worth maintaining the waste disposal rate by diverting the green material rather than burying it.

### 8.6 Summary and Conclusion

This chapter has shown that the expected and confirmed wind direction in the SJV were similar. Based on SARP airborne data, HYSPLIT forward trajectories, and previous literature

(Western Regional Climate Center, 2008), wind came from the northwest. This means that the wind can transport harmful pollutants from the dairy farms in the SJV through the disadvantaged communities in the area. This is particularly important for $O_3$ and SOA formation, as the SJV is frequently in nonattainment for $O_3$ and PM.

The OFP was determined using the POCP method presented in Derwent et al. (2007) and the MIR method (Carter et al., 1995; Carter, 2009). The POCP method claims to be more accurate in a $NO_x$-limited regime, meaning that the VOC to $NO_x$ ratio is high, and that changing the $NO_x$ has more of an effect on the $O_3$ concentration than change the VOCs. This is applicable for suburban and rural areas, which include much of the SJV and Orange County. The MIR method tends to be more accurate in a VOC-limited regime, meaning that the $NO_x$ to VOC ratio is high, and that changing the VOCs has more of an effect on the $O_3$ concentration than changing the $NO_x$. This is more applicable for urban areas like the city of Los Angeles.

The dairy farm OFP was calculated for March 2019, June 2019, September 2019, and January 2020 using Equation 8-1 and Equation 8-2 to determine the amount of $O_3$ that could form based on the median and maximum VOC mixing ratios at the Visalia dairy farm. These OFP values were compared to the 8-hour NAAQS standard from Table 1.1, 137 μg $O_3/m^3$. Equation 8-1 and Equation 8-2 predicted different OFP values for the dairy farm VOCs, but the trends between the two were similar: alkenes and oxygenates dominated the potential to form $O_3$. Contributing VOCs were found to be most enhanced near the cows and their feed, so those may be large sources of $O_3$ from the dairy farm and other SJV dairies. These dairies should be considered possible point sources of $O_3$ in a region that is frequently a nonattainment area.

The Orange County landfill OFPs were calculated for Spring 2018 and Summer 2018 using Equation 8-1 and Equation 8-2, and then they were compared to the 8-hour NAAQS from Table 1.1. Again, the alkenes and oxygenates dominated both calculations, with Equation 8-2 predicting lower OFP values overall. This biogenic contribution was likely from the mulch used as

ADC and the on-site composting programs. There was some contribution from aromatics as well, which may have originated from a combination of vehicular emissions (with a toluene to benzene ratio of T/B < 2) and paint or industrial emissions (with a ratio of T/B > 2). Landfills should continue to strongly enforce disposal to ensure that the types of industrial waste being dumped are allowed at Class III landfills to better prevent $O_3$ formation in communities downwind.

Ozone is not the only pollution-related issue in California; particle formation is also a concern. Turpin and Huntzicker (1995) showed that 80% of the total organic PM is made of SOA. The SOA formation potential of VOCs at the dairy farm and Orange County landfills were determined using the SOA yields from Shin et al. (2013) and the formula in Equation 8-3. These were compared to the NAAQS $PM_{2.5}$ standard from Table 1.1, written as SOA: 28,000 ng SOA/$m^3$ for the 24-hour limit and 9,600 ng SOA/$m^3$ for the 1-year limit.

At the dairy farm, aromatics and DMS were likely large SOA contributors. Dimethyl sulfide may account for up to 5% of the total submicron particle count in the SJV. The calculation for this was shown in Chapter 6.2.2. The other VOCs measured at the Visalia dairy farm were likely not large regional contributors compared to the influence of traffic and agriculture from the whole SJV.

The SOA yields from Shin et al. (2013) and Equation 8-3 also were used to calculate the SOA formation at the Orange County landfills during Spring 2018 and Summer 2018. Heavy alkanes (> $C_9$) and aromatics were likely significant contributors, however, the $PM_{2.5}$ resulting from these VOCs was smaller than the NAAQS limit. The SOA formation potential from Orange County landfills was much higher than the dairy farms, likely a result of the combination of vehicular emissions and active dumping.

The contribution to odor at the Visalia dairy farm and Orange County landfills was also explored. Reduction factors were calculated to determine how much a VOC would need to be reduced to bring it below the odor threshold. Although many odors may not be at a perceptible level, they can still affect the mental health of residents and workers nearby. At the dairy farm,

limonene, butanal, ethanol, and DMS had RF > 1 and likely originated from a variety of sources including cows, silage, and waste, with RFs ranging from 2 to 132. At the Orange County landfills, butanal, ethanol, α-pinene, and butanone exceeded the odor thresholds with RFs ranging from 1.2 to 913. The odor likely originated from the active dumping and green material used for mulch ADC and compost. This agrees with a previous odor study at Frank R. Bowerman landfill (SCS Engineers, 2017).

Green material as mulch and compost was shown to be a likely issue for OFP and odor at Orange County landfills because of the release of highly reactive biogenic VOCs. To lower the ozone and odor, landfill engineers may consider counting green material towards their disposal rate rather than trying to divert it as compost and use it as ADC because of the biogenic compounds that will be released during composting and afterwards. Additionally, composting costs time and space. The process requires a large surface area, which many landfills do not have, and months of waiting for the compost to mature. Although Frank R. Bowerman is implementing an outdoor composting program, it is not recommended that other landfills follow their example. Instead, it may be better for the environment and residents downwind if the green material decomposed underground where the LFG and leachate collection systems will prevent harmful rogue emissions that will easily escape if the material is left to compost on the surface.

Proposed solutions to enteric and manure emissions at dairy farms and the biogenic emissions at landfills were also explored. For enteric dairy farm emissions, seaweed has been shown to be a promising solution with $CH_4$ reductions of 95% reported for *Asparagopsis taxiformis* (Roque et al., 2019b). To replace cows' feed with 5% of this seaweed, 7,300 pounds of seaweed would be necessary to support just the milk cow population at the Visalia dairy farm daily. In the SJV, $1x10^{10}$ pounds of seaweed would be needed to sustain the milk cows daily. There is not currently enough aquafarming infrastructure to support this endeavor, nor does *Asparagopsis taxiformis* grow in the Pacific Ocean, which is also sufficiently far away from the dairies in the SJV

anyway. Instead, it is suggested that dairy farmers focus on reducing manure emissions rather than enteric emissions.

For dairies with approximately 2,000 cows or more (e.g., Kern, Madera, and Tulare Counties), it may be financially feasible to install manure digesters that could convert waste to energy, reducing emissions in the process. The Visalia dairy in this study will be installing a digester in 2021 along with many other dairies with support from SB-1383 funding. Most projects are generating RCNG. Smaller dairies with less than 2,000 cows may consider the AMMP to fund non-digester practices that may be more appropriate financially, but still reduce emissions.

This research has shown that dairy farms in the SJV and landfills in Orange County emit various VOCs and GHGs. However, there are feasible improvements they could make to provide a cleaner future for their communities. Dairy farmers may consider installing anaerobic digesters to prevent methane emissions from their manure management systems and covering their silage piles to prevent emissions of reactive oxygenates. At landfills, engineers may consider the drawbacks of using compost as ADC, as it can contribute to air quality concerns and odor for the surrounding area. Although GHG reductions are extremely important, the waste management and dairy industries must also begin to think beyond those reductions. By decreasing the amounts of other reactive VOCs, they can make California a better place to live for all residents—regardless of their zip code.

## 8.7 References


Abraham, M. H., Gola, J. M., Cometto-Muniz, J. E., & Cain, W. S. (2002). A model for odour thresholds. *Chemical Senses*, *27*(2), 95-104.

Adani, F., Tambone, F., & Gotti, A. (2004). Biostabilization of municipal solid waste. *Waste Management*, *24*(8), 775-783.

Atkinson, R. (1997c). Gas-phase tropospheric chemistry of volatile organic compounds: 1. Alkanes and alkenes. *Journal of Physical and Chemical Reference Data, 26*(2), 215-290.

Atkinson, R. (2000). Atmospheric chemistry of VOCs and NOx. *Atmospheric environment*, *34*(12-14), 2063-2101.

Atkinson, R., & Aschmann, S. M. (1984). Rate constants for the reaction of OH radicals with a series of alkenes and dialkenes at 295±1 K. *International journal of chemical kinetics, 16*(10), 1175-1186.

Atkinson, R., Aschmann, S. M., & Arey, J. (1990). Rate constants for the gas-phase reactions of OH and $NO_3$ radicals and $O_3$ with sabinene and camphene at 296±2 K. *Atmospheric Environment. Part A. General Topics, 24*(10), 2647-2654.

Barringer, F., & McGhee, G. (2018). Under New Pollution Regulations, Milk Producers Seek Profit in Dairy Air. *…& the West.* Retrieved from https://west.stanford.edu/news/blogs/and-the-west-blog/2018/california-methane-dairy-farms

Blacet, F. E. (1952). Photochemistry in the lower atmosphere. *Industrial & Engineering Chemistry*, *44*(6), 1339-1342.

Bretón, J. G. C., Bretón, R. M. C., Ucan, F. V., Baeza, C. B., Fuentes, M. D. L. L. E., Lara, E. R., ... & Chi, M. P. U. (2017). Characterization and sources of Aromatic Hydrocarbons (BTEX) in the atmosphere of two urban sites located in Yucatan Peninsula in Mexico. *Atmosphere, 8(*6), 107.

Brosseau, J., & Heitz, M. (1994). Trace gas compound emissions from municipal landfill sanitary sites. *Atmospheric Environment, 28*(2), 285-293.

Burt, A. W. A., Bartlett, S., & Rowland, S. J. (1954). The use of seaweed meals in concentrate mixtures for dairy cows. *Journal of Dairy Research*, *21*(3), 299-304.

California Department of Food and Agriculture (CDFA). (2018). California Agricultural Statistics Review 2017–2018. Retrieved from https://www.cdfa.ca.gov/Statistics/PDFs/2017-18AgReport.pdf

California Department of Food and Agriculture (CDFA). (2020). Dairy Digester Research and Development Program: Report of Projects Funded (2015 – 2019). Retrieved from https://www.cdfa.ca.gov/oefi/ddrdp/docs/DDRDP_Report_April2020.pdf

Calvert, J. G. (1976). Test of the theory of ozone generation in Los Angeles atmosphere. *Environmental science & technology*, *10*(3), 248-256.

Carter, W. P. (2009). Updated maximum incremental reactivity scale and hydrocarbon bin reactivities for regulatory applications. *California Air Resources Board Contract*, *2009*, 339.

Carter, W. P., Pierce, J. A., Luo, D., & Malkina, I. L. (1995). Environmental chamber study of maximum incremental reactivities of volatile organic compounds. *Atmospheric Environment*, *29*(18), 2499-2511.

Ceacero-Vega, A. A., Ballesteros, B., Bejan, I., Barnes, I., & Albaladejo, J. (2011). Daytime Reactions of 1, 8-Cineole in the Troposphere. *ChemPhysChem, 12*(11), 2145-2154.

Chen, T., & Jang, M. (2012). Secondary organic aerosol formation from photooxidation of a mixture of dimethyl sulfide and isoprene. *Atmospheric environment*, *46*, 271-278.

Closure and Post-Closure Maintenance Requirements for Solid Waste Landfills, 27 C.C.R. § 21090 (1997).

CoBank. (2020). California Incentives Spur Dairy Manure Methane Digester Developments. *Globe Newswire*. Retrieved from https://www.globenewswire.com/news-release/2020/08/05/2073733/0/en/California-Incentives-Spur-Dairy-Manure-Methane-Digester-Developments.html

Corchnoy, S. B., & Atkinson, R. (1990). Kinetics of the gas-phase reactions of hydroxyl and nitrogen oxide ($NO_3$) radicals with 2-carene, 1, 8-cineole, p-cymene, and terpinolene. *Environmental Science & Technology, 24*(10), 1497-1502.

Criteria for Municipal Solid Waste Landfills (1993). 173 W.A.C. § 351.

Criteria for Municipal Solid Waste Landfills (1997). 40 C.F.R. § 258.

DeMore, W. B., & Raper, O. F. (1966). Primary processes in ozone photolysis. *The Journal of Chemical Physics*, *44*(5), 1780-1783.

Derwent, R. G., & Jenkin, M. E. (1991). Hydrocarbons and the long-range transport of ozone and PAN across Europe. *Atmospheric Environment. Part A. General Topics*, *25*(8), 1661-1678.

Derwent, R. G., Jenkin, M. E., Passant, N. R., & Pilling, M. J. (2007). Reactivity-based strategies for photochemical ozone control in Europe. *Environmental science & policy*, *10*(5), 445-453.

Environmental Protection Agency (EPA). (2020b). Landfill Methane Outreach Program (LMOP). Retrieved from https://www.epa.gov/lmop

Farrell, M., & Jones, D. L. (2009). Critical evaluation of municipal solid waste composting and potential compost markets. *Bioresource technology, 100*(19), 4301-4310.

Finlayson-Pitts, B. J., & Pitts, J. N. (1999). *Chemistry of the upper and lower atmosphere: theory, experiments, and applications*. Elsevier.

Giess, P., Bush, A., & Dye, M. (1999). Trace gas measurements in landfill gas from closed landfill sites. *International Journal of Environmental Studies*, *57*(1), 65-77.

Gill, K. J., & Hites, R. A. (2002). Rate constants for the gas-phase reactions of the hydroxyl radical with isoprene, α-and β-pinene, and limonene as a function of temperature. *The Journal of Physical Chemistry A, 106*(11), 2538-2544.

Haagen-Smit, A. J. (1952). Chemistry and physiology of Los Angeles smog. *Industrial & Engineering Chemistry*, *44*(6), 1342-1346.

Hall, R. L., & Oser, B. L. (1965). Recent Progress in Consideration of Flavoring Ingredients Under Food Additives Amendment. 3. Gras Substances. *Food Technology, 19*(2 P 2), 151.

Hammond, E. G., Heppner, C., & Smith, R. (1989). Odors of swine waste lagoons. *Agriculture, ecosystems & environment*, *25*(2-3), 103-110.

Hartung, J. (1985). Gas chromatographic analysis of volatile fatty acids and phenolic/indolic compounds in pig house dust after ethanolic extraction. *Environmental Technology*, *6*(1-11), 21-30.

Heicklen, J. (1968). Gas-phase reactions of alkylperoxy and alkoxy radicals.

Hellman, T. M., & Small, F. H. (1974). Characterization of the odor properties of 101 petrochemicals using sensory methods. *Journal of the Air Pollution Control Association*, *24*(10), 979-982.

Hobbs, P., & Mottram, T. (2000). New directions: Significant contributions of dimethyl sulphide from livestock to the atmosphere. *Atmospheric Environment*, *34*(21), 3649-3650.

Howard, C. J., & Evenson, K. M. (1976). Rate constants for the reactions of OH with CH4 and fluorine, chlorine, and bromine substituted methanes at 296 K. *The Journal of Chemical Physics, 64*(1), 197-202.

Hurst, C., Longhurst, P., Pollard, S., Smith, R., Jefferson, B., & Gronow, J. (2005). Assessment of municipal waste compost as a daily cover material for odour control at landfill sites. *Environmental pollution, 135*(1), 171-177.

Kerr, J. A., & Sheppard, D. W. (1981). Kinetics of the reactions of hydroxyl radicals with aldehydes studied under atmospheric conditions. *Environmental science & technology, 15*(8), 960-963.

Khamaganov, V. G., & Hites, R. A. (2001). Rate constants for the gas-phase reactions of ozone with isoprene, α-and β-pinene, and limonene as a function of temperature. *The Journal of Physical Chemistry A, 105*(5), 815-822.

Kim, D., Stevens, P. S., & Hites, R. A. (2010). Rate Constants for the Gas-Phase Reactions of OH and O3 with β-Ocimene, β-Myrcene, and α-and β-Farnesene as a Function of Temperature. *The Journal of Physical Chemistry A, 115*(4), 500-506.

Leonardos, G., Kendall, D., & Barnard, N. (1974). Odor threshold determination of 53 odorant chemicals. *Journal of Environmental Conservation Engineering*, *3*(8), 579-585.

Levy II, H. (1971). Normal atmosphere: Large radical and formaldehyde concentrations predicted. *Science*, *173*(3992), 141-143.

Liu, Z., Powers, W., Oldick, B., Davidson, J., & Meyer, D. (2012). Gas emissions from dairy cows fed typical diets of Midwest, South, and West regions of the United States. *Journal of environmental quality*, *41*(4), 1228-1237.

Lorig, T. S., Herman, K. B., Schwartz, G. E., & Cain, W. S. (1990). EEG activity during administration of low-concentration odors. *Bulletin of the Psychonomic Society*, *28*(5), 405-408.

Lorig, T. S., Huffman, E., DeMartino, A., & DeMarco, J. (1991). The effects of low concentration odors on EEG activity and behavior. *Journal of Psychophysiology*.

Machado, L., Magnusson, M., Paul, N. A., de Nys, R., & Tomkins, N. (2014). Effects of marine and freshwater macroalgae on in vitro total gas and methane production. *PLoS One, 9*(1), e85289.

Mo, Z. W., Niu, H., Lu, S. H., Shao, M., & Gou, B. (2015). Process-based emission characteristics of volatile organic compounds (VOCs) from paint industry in the yangtze river delta, china. *Huan jing ke xue= Huanjing kexue*, *36*(6), 1944-1951.

Murnane, S. S., Lehocky, A. H., & Owens, P. D. (Eds.). (2013). *Odor thresholds for chemicals with established health standards*. AIHA.

Nagata, Y., & Takeuchi, N. (2003). Measurement of odor threshold by triangle odor bag method. *Odor measurement review*, *118*, 118-127.

Nicolet, M. (1970). Ozone and hydrogen reactions. *Annales de Geophysique, 26*, 531-546

O'Neill, D. H., & Phillips, V. R. (1992). A review of the control of odour nuisance from livestock buildings: Part 3, properties of the odorous substances which have been identified in livestock wastes or in the air around them. *Journal of Agricultural Engineering Research*, *53*, 23-50.

Orange County Waste and Recycling (OCWR). (2019). Bee Canyon Greenery Composting Operation at FRB Landfill. Retrieved from https://ceqanet.opr.ca.gov/2019099059/2

Paraskevopoulos, G., & Cvetanović, R. J. (1971). Relative rate of reaction of O (1D2) with H2O. *Chemical Physics Letters, 9*(6), 603-605.

Rodríguez, A., Peris, J. E., Redondo, A., Shimada, T., Costell, E., Carbonell, I., ... & Peña, L. (2017). Impact of D-limonene synthase up-or down-regulation on sweet orange fruit and juice odor perception. *Food chemistry*, *217*, 139-150.

Roque, B. M., Salwen, J. K., Kinley, R., & Kebreab, E. (2019a). Inclusion of *Asparagopsis armata* in lactating dairy cows' diet reduces enteric methane emission by over 50 percent. *Journal of Cleaner Production*, *234*, 132-138.

Roque, B. M., Brooke, C. G., Ladau, J., Polley, T., Marsh, L. J., Najafi, N., ... & Eloe-Fadrosh, E. (2019b). Effect of the macroalgae *Asparagopsis taxiformis* on methane production and rumen microbiome assemblage. *Animal Microbiome, 1*(1), 3.

Ruth, J. H. (1986). Odor thresholds and irritation levels of several chemical substances: a review. *American Industrial Hygiene Association Journal*, *47*(3), A-142.

S.B. 1383, 2015-2016 Biennium, 2016 Reg. Sess. (Cal. 2016).

Schiffman, S. S. (1974). Physicochemical correlates of olfactory quality. *Science*, 112-117.

Schiffman, S. S. (1998). Livestock odors: implications for human health and well-being. *Journal of animal Science*, *76*(5), 1343-1355.

Schiffman, S. S., Miller, E. A. S., Suggs, M. S., & Graham, B. G. (1995). The effect of environmental odors emanating from commercial swine operations on the mood of nearby residents. *Brain research bulletin*, *37*(4), 369-375.

SCS Engineers (2017). Franklin R. Bowerman Landfill Quantitative Odor Analysis. *SES Engineers.*

Shin, H. J., Kim, J. C., Lee, S. J., & Kim, Y. P. (2013). Evaluation of the optimum volatile organic compounds control strategy considering the formation of ozone and secondary organic aerosol in Seoul, Korea. *Environmental Science and Pollution Research*, *20*(3), 1468-1481.

Shusterman, D. (1992). Critical review: the health significance of environmental odor pollution. *Archives of Environmental Health: An International Journal*, *47*(1), 76-87.

Stein, A. F., Draxler, R. R., Rolph, G. D., Stunder, B. J., Cohen, M. D., & Ngan, F. (2015). NOAA's HYSPLIT atmospheric transport and dispersion modeling system. *Bulletin of the American Meteorological Society*, *96*(12), 2059-2077.

Sustainable Business. (2013). U.S. dairy industry signs onto roadmap for biogas. *GreenBiz*. Retrieved from https://www.greenbiz.com/article/us-dairy-industry-signs-roadmap-biogas

Turpin, B. J., & Huntzicker, J. J. (1995). Identification of secondary organic aerosol episodes and quantitation of primary and secondary organic aerosol concentrations during SCAQS. *Atmospheric Environment*, *29*(23), 3527-3544.

U.S. Department of Agriculture, U.S. Environmental Protection Agency, U.S. Department of

Energy. (2014). Biogas Opportunities Roadmap. Retrieved from https://www.epa.gov/sites/production/files/2015-12/documents/biogas-roadmap.pdf

Vaghjiani, G. L., & Ravishankara, A. R. (1991). New measurement of the rate coefficient for the reaction of OH with methane. *Nature*, *350*(6317), 406-409.

Western Regional Climate Center (2008). Climate of California. Retrieved from https://wrcc.dri.edu/Climate/narrative_ca.php, accessed May 20th, 2009.

Young, P. J., & Parker, A. (1983). The identification and possible environmental impact of trace gases and vapours in landfill gas. *Waste Management & Research*, *1*(3), 213-226.

Zald, D. H., & Pardo, J. V. (1997). Emotion, olfaction, and the human amygdala: amygdala activation during aversive olfactory stimulation. *Proceedings of the National Academy of Sciences*, *94*(8), 4119-4124.

Zdeb, M., & Lebiocka, M. (2016). Microbial removal of selected volatile organic compounds from the model landfill gas. *Ecological Chemistry and Engineering S, 23*(2), 215-228.